

A FINITE DIFFERENCE ALGORITHM FOR TWO-DIMENSIONAL INVERSION OF GEOELECTROMAGNETIC DATA

A THESIS

*submitted in fulfilment of the
requirements for the award of the degree*

of

DOCTOR OF PHILOSOPHY

in

EARTH SCIENCES

By

ANUPMA RASTOGI



**DEPARTMENT OF EARTH SCIENCES
UNIVERSITY OF ROORKEE
ROORKEE-247 667 (INDIA)**

FEBRUARY, 1997

Gratis

2011/11/22

18-5-81

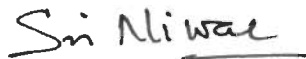
CANDIDATE'S DECLARATION

I hereby certify that the work which is being presented in the thesis entitled " A FINITE DIFFERENCE ALGORITHM FOR TWO-DIMENSIONAL INVERSION OF GEOELECTROMAGNETIC DATA " in fulfillment of the requirement for the award of the Degree of Doctor of Philosophy, submitted in the **Department of Earth Sciences, University of Roorkee**, is an authentic record of my own work carried out during the period from July, 1993 to February, 1997 under the supervision of Dr. Sri Niwas and Dr. P.K. Gupta.

The matter embodied in this thesis has not been submitted by me for the award of any other degree.


(ANUPMA RASTOGI)

This is to certify that the above statement made by the candidate is correct to the best of our knowledge.



(Dr. Sri Niwas)
Professor
Dept. of Earth Sciences
University of Roorkee
Roorkee, India



(Dr. P.K. Gupta)
Asst. Professor
Dept. of Earth Sciences
University of Roorkee
Roorkee, India


Date: 18. 2. 97

The Ph.D Viva-Voce of Ms. Anupma Rastogi, Research Scholar has been held on

20.9.97



Signature of Supervisor(s)


Signature of H.O.D. 20/9/97



Signature of External Examiner

ACKNOWLEDGEMENT

At the outset, I express my deep sense of gratitude to my supervisors, Dr. P.K. Gupta and Prof. Sri Niwas, for their meticulous and inspiring guidance. It was Dr. Gupta who exposed me to the field of 'modelling and inversion', presented the problem, and rendered advice on both academic and personal matters, besides inculcating me with his brilliant ideas. The thesis would not have taken its present form, but for the critical appraisal of the manuscript by Prof. Sri Niwas.

I wish to thank Prof. A.K. Jain and Prof. S.K. Updhyay, who, during their terms as Heads of the Department, provided the necessary facilities to execute this work and for the many courtesies extended to me while this thesis was in progress.

I benefitted from the encouragement received from Prof. Ramesh Chander, Prof. V.N. Singh and Dr. R.G.S. Sastry, for which I express my sincere thanks..

My seniors Drs. Sudhir Kumar, H.N. Sinha and Sandeep Singh advised me and assisted me in various ways.

Financial support provided by Council of Scientific Research, New Delhi, is acknowledged.

The help extended by the technical and non-technical staff of the Department is duly appreciated.

I especially thank Ajay, Puspita, Thomas, Misra, Pujari, Basir and Sundaram for generating oxygen rich atmosphere, full of love and humour that proved, to be indispensable. But for their patience and calm efficiency, this thesis would not have been completed. Others who cooperated are Mukherjee, Binayak, Siva, Pushpendra, Shweta, Karki, Dr. Vineet, Dr. Kalpna, Dr. Anupma. I am also thankful to Meenakshi, Khurana, Manisha, Pallavi, Raju, Kalpna, Ajay, Surabhi and Sajla for their constant support.

The wonderful times spent with Mrs. Mamta Gupta, Manasi and Poorva will always be long cherished.

YP always kept me on my toes by his persistent reassurance and has made me believe where there is will, there is way.

Love, inspiration and encouragement was never lacking with Mummy, Papa, Rachna, Dinku, Meenu, Deepak and Sanjay around which helped me achieve a long cherished goal.


ANUPMA RASTOGI

ABSTRACT

Data inversion is an interplay of physico-mathematical operators devised to extract meaningful information about a system from an observed data set and to appraise the quality of an inverse solution. In geoelectromagnetic methods, where sources are natural electromagnetic (EM) fields, the earth is parameterized in terms of electrical resistivity which is of special significance as it carries information about the lithology, pore fluid, temperature and chemical variations. The present study is an effort to improve the data inversion capabilities of EM data. For this purpose an efficient 2-D inversion algorithm, **EM2INV**, for geoelectromagnetic data has been developed.

The EM field is a non-linear function of subsurface resistivity distribution. As a result the inverse problem is quasi-linearized and solved iteratively. For each inversion iteration, a new forward problem, yielding the response of current resistivity model, has to be solved. Therefore, the forward algorithm is a prerequisite for an inversion algorithm. For generation of EM response, a boundary value problem is solved analytically or numerically. However, for the problems involving complex geometries one has to seek numerical solutions only. Due to its simple mathematics and easy implementation, finite difference method has been chosen over other numerical techniques for solving the EM boundary value problem.

The research work was initiated with the implementation of finite difference formulation of the forward EM problem (Brewitt-Taylor & Weaver, 1976). Since the use of Dirichlet boundary conditions results in a large study domain, special finite domain, integral and asymptotic boundary conditions are implemented. In the present work, an integrated formulation of these boundary conditions has been developed.

The quasi-linearization of non-linear problem results in a matrix equation which is solved using Bi-Conjugate Gradient Method (BCGM), a semi-iterative matrix solver that dispenses with the necessity of explicit computation of Jacobian matrix. To fix the

number of unknown block resistivities for all frequencies and throughout the inversion process, a superblock notion has been developed. The initial guess is made on the basis of observed anomaly and other *a priori* information.

The inversion algorithm **EM2INV** is the culmination of research that started with the development of a primitive algorithm. The algorithm has been written in FORTRAN 77 and implemented on an IBM compatible EISA based PC-486 machine with 32 MB RAM and 383 MB hard disk, using the SVR 4.0 version of Unix operating system and F78 FORTRAN compiler. For a typical model, having 31 x 15 nodes, the algorithm takes about 3 minutes for 10 inversion iterations.

EM2INV comprises 6120 lines, 42 subroutines and 3 function subprograms. The main program has two basic modules - Forward and Inverse. Its special efficiency features which result in cost effectiveness are - (i) Optimal grid generation based on grid design thumb rules, (ii) Finite domain boundary conditions, (iii) Interpolation matrix that permits generation of response at observation points, (iv) Gaussian elimination, the forward matrix solver, which enables reuse of already decomposed coefficient matrix, (v) Use of logarithm of resistivity to ensure positive values of estimated parameters, (vi) Superblock notion that reduces the number of blocks with unknown resistivities and, in turn, the size of Jacobian matrix and (vii) BCGM matrix solver for inverse problem. Besides being efficient, **EM2INV** is versatile on account of its features like - (i) Inversion with field/synthetic data, (ii) Error free/erroneous synthetic data, (iii) Inversion of MT/GDS data and (iv) Inversion of profiling/sounding data.

The algorithm has been rigorously tested by setting up exercises of diverse nature and practical significance. For establishing the validity of forward computations, the published results of various models have been reproduced after carrying out the no contrast and mesh convergence studies. Similarly, for checking validity of inversion computations, the synthetic anomalies have been inverted and compared with those of the true model. The stability of the algorithm has been established by inverting the synthetic response corrupted with Gaussian noise.

EM2INV has been employed in two different sets of experiments designed to study the nature of forward and inverse problems. The forward experiments aim at studying the impact of parameters like depth of burial, resistivity contrast, separation between two bodies on model responses. Although a preliminary quantitative discriminant analysis was attempted to design thumb rules for estimating size and

resistivity of target yet it did not succeed. However, qualitative inferences have been drawn.

The inversion experiments performed are aimed at gauging - (i) Relative performances of response functions, (ii) Inversion quality for two modes of polarization, (iii) Efficacy of single and multifrequency inversions and (iv) Minimum number of frequencies and observation points needed for successful data inversion. The inversion of MT data provides better estimates of vertical position of the target, whereas the inversion of GDS data deciphers the horizontal variations better. It has been observed that the conductive and resistive bodies are better resolved by inversion of E- and B-polarization data respectively. The results of multifrequency inversion imply that increase in number of frequencies does not necessarily enhance the inversion quality especially when the spread of observation points is sufficiently large to sense the target. The study of minimum number of observation points highlights the importance of single point inversion which furnishes useful information about the inhomogeneity.

After the design exercises, **EM2INV** has been exhaustively tested by inverting synthetic data, field data, as well as data derived from models based on field studies. Few geologically significant models are picked up from the literature for generation of synthetic data. For these models, initially 1-D inversion is carried out at each point of the profile which is then stacked to get the starting model for 2-D inversion. The comparison of inverted model with the 1-D stacked model leads us to conclude that 2-D inversion substantially improves the quality of the inverted model.

Next, a study has been carried out on models derived from GDS or MT field studies. The reliability of the estimates of resistivity is evident in the goodness of fit of the computed and observed responses. Lastly, the algorithm **EM2INV** is tested on Trans Himalayan conductor and COPROD2, GDS and MT field data respectively. The inverted models are in broad agreement with the published results. This supported the confidence in the utility of the algorithm.

The results of various experiments and those of inversion of synthetic/field geoelectromagnetic data in terms of resistivity model have established the veracity of the algorithm and also amply displayed the capabilities of the inversion algorithm. Also discussed, is the possible scope of future work in various directions for its upgradation and extension to 3-D environment.

CONTENTS

Abbreviations
List of Figures
List of Tables

PAGE NO:

CHAPTER 1

INTRODUCTION

1.1 Motivation	1
1.2 Why geoelectromagnetic methods	5
1.3 State of art	8
1.3.1 Developments in numerical techniques	9
1.3.2 Developments in inversion techniques	11
1.4 Scope of the present work	12
1.5 Organisation of chapters	14

CHAPTER 2

FORMULATION OF EM FORWARD PROBLEM

2.1 General	16
2.2 Electromagnetic theory	17
2.3 Electrical properties of earth	18
2.4 The EM boundary value problem	20
2.4.1 Governing partial differential equations	21
2.4.1.1 Modes of polarization	22
2.4.1.2 Two-dimensional Equations	22
2.4.1.3 One-dimensional Equations	24
2.4.2 Partitioning of fields	26
2.5 The boundary conditions	27
2.5.1 Interface boundary conditions	28
2.5.2 Domain boundary conditions	29
2.5.2.1 The finite domain integrated boundary conditions - Integral form	31
2.5.2.2 The finite domain integrated boundary conditions - Series form	34
2.5.2.3 Asymptotic boundary conditions	36
2.6 Solution of EM boundary value problem	39
2.6.1 One-dimensional EM problem	40
2.7 The response functions	44
2.7.1 MT response function	45

2.7.2	GDS response function	47
2.7.3	Transformation matrices	48
2.8	Closure	48
CHAPTER 3		
FORMULATION OF EM INVERSE PROBLEM		49
3.1	General	49
3.2	Alleviation of ill-posedness	50
3.2.1	Inconsistency	51
3.2.2	Non-uniqueness	51
3.2.3	Instability	52
3.3	Classification of inverse problems	52
3.3.1	Least square inverse	53
3.3.2	Minimum norm inverse	54
3.3.3	Regularised inverse	54
3.3.4	Weighted inverses	56
3.4	Appraisal of solution	57
3.4.1	Measures of misfit	57
3.4.2	System characteristics matrices	58
3.4.2.1	Information density matrix	58
3.4.2.2	Resolution density matrix	58
3.4.2.3	Dirichlet spread function	58
3.5	Experiment design	59
3.6	Solution of EM inverse problem	59
3.6.1	Different methodologies	59
3.6.1.1	Trial and error method	60
3.6.1.2	Non-linear methods	60
3.6.1.3	Direct and quasi-linearized methods	60
3.6.2	SIS algorithm for 1-D inversion	61
3.6.3	EM21NV algorithm for 2-D inversion	64
3.7	Closure	67
CHAPTER 4		
EM PROBLEMS - IMPLEMENTATION OF FINITE DIFFERENCE METHOD		68
4.1	General	68
4.2	Finite difference implementation	69
4.2.1	Discrete governing equations	73
4.2.1.1	B-polarization	74
4.2.1.2	E-polarization	74
4.2.2	Discrete boundary conditions	75
4.2.2.1	Asymptotic boundary conditions	75
4.2.2.2	Integral boundary conditions	76
4.3	Structure of coefficient matrix	80
4.3.1	Transformation matrices for derived responses	83

4.3.1.1 B-polarization	83
4.3.1.2 E-polarization	84
4.4 Inverse formulation	85
4.4.1 Derivative of coefficient matrix	86
4.4.2 Computation of Jacobian/derived Jacobians	88
4.5 Choice of matrix solver	89
4.5.1 Forward matrix solver	90
4.5.2 Inverse matrix solver	91
4.6 Solution of the inverse problem	94
4.7 Closure	94

CHAPTER 5

DEVELOPMENT OF ALGORITHM - EM2INV	95
5.1 General	95
5.2 Background	95
5.3 Sequence of development	96
5.3.1 Version I	96
5.3.2 Version II	97
5.3.3 Version III	97
5.3.4 Version IV	98
5.3.5 Version V	99
5.3.6 Version VI	100
5.4 Salient features	101
5.4.1 Versatility features	101
5.4.1.1 Response functions	101
5.4.1.2 Sounding data	101
5.4.1.3 Source term	102
5.4.1.4 Gaussian noise	102
5.4.1.5 Field and synthetic data	102
5.4.2 Efficiency features	102
5.4.2.1 Superblock	102
5.4.2.2 Grid generator	104
5.4.2.3 Logarithm of resistivity	104
5.4.2.4 Interpolation matrix	104
5.4.2.5 Bi-conjugate gradient method	104
5.4.2.6 Finite domain boundary condition	104
5.5 Description of algorithm	105
5.5.1 Structure	105
5.5.2 Subprograms of EM21NV	108
5.5.2.1 Forward subprograms	109
5.5.2.2 Inversion subprograms	118
5.6 Computing environment	134
5.6.1 Hardware limitations	134
5.6.2 Software limitations	134
5.7 Closure	134

CHAPTER 6	
ALGORITHM TESTING AND EXPERIMENT DESIGN EXERCISES	135
6.1 General	135
6.2 Validation of EM2INV	135
6.2.1 Forward algorithm	135
6.2.1.1 Mesh convergence test	136
6.2.1.2 No contrast study	137
6.2.1.3 Reproduction of published results	137
6.2.2 Inversion algorithm	139
6.2.2.1 Inversion of synthetic responses	139
6.2.2.2 Check on stability	139
6.3 Experiment design exercises	142
6.3.1 Experiments on forward algorithm	143
6.3.1.1 Effect of resistivity contrast	143
6.3.1.2 Impact of depth of burial	146
6.3.1.3 Effect of separation between two bodies	146
6.3.2 Experiments on inversion algorithm	146
6.3.2.1 Relative performances of response functions	158
6.3.2.2 Inversion quality for B- and E-polarizations	159
6.3.2.3 Efficacy of single and multifrequency inversion	160
6.3.2.4 Minimum number of observation points	160
6.4 Closure	165
 CHAPTER 7	
RESULTS AND DISCUSSION	167
7.1 General	167
7.2 Inversion of synthetic data	168
7.2.1 Horst model	169
7.2.2 Resistive block model	170
7.2.3 Conductive block model	173
7.2.4 Conductive and resistive block pair model	173
7.2.5 Sedimentary basin model	174
7.3 Inversion of data derived from field studies based models	174
7.3.1 Transverse conductive structure	178
7.3.2 Trans Himalayan conductor	179
7.3.3 Graben structure	181
7.4 Inversion of field data	182
7.4.1 Trans Himalayan conductor data	182
7.4.2 COPROD2 data	185
7.5 Closure	187

CHAPTER 8	
CONCLUSIONS AND SUGGESTIONS	190
8.1 Concluding remarks	190
8.1.1 Achievements of the algorithm	190
8.1.2 Limitations of the algorithm	191
8.2 Suggestions for future work	191
References	193
Appendix 1 Derivation of recurrence relation (2.88)	211
Appendix 2 Basic steps of Bi-conjugate gradient method to solve matrix equation $\mathbf{Ax} = \mathbf{b}$	213
Appendix 3 Documentation on input requirements of the inverse algorithm ' EM2INV '	214

ABBREVIATIONS

Although all the abbreviations and symbols used in this thesis have been defined in the local context, we have compiled them here also for convenience:

BCGM	Bi-Conjugate Gradient Method
BVP	Boundary Value Problem
CGM	Conjugate Gradient Method
DEM	Differential Equation Method
EM	Electro-Magnetic
EMSLAB	Electro-Magnetic Sounding of Lithosphere And Beyond
FDM	Finite Difference Method
FEM	Finite Element Method
GDS	Geomagnetic Depth Sounding
HM	Hybrid Method
IEM	Integral Equation Method
LU	Lower triangular Upper triangular
MT	Magneto-Tellurics
MVP	Magneto Variational Profiling
NACP	North American Central Plains
rms	root mean square
SIS	Straightforward Inversion Scheme
TOBE	Thompson Belt

LIST OF FIGURES

	PAGE NO.
Fig. 1.1 Functional diagram for (a) forward problem and (b) inverse problem.	2
Fig. 1.2 Logic diagram for obtaining numerical solution of forward problem.	4
Fig.1.3 Typical earth models (a) 1-D and (b) 2-D. Also shown is the coordinate system.	23
Fig. 2.2 Buried target in a layered earth model.	26
Fig. 2.3 The interface S between two regions with different material properties.	28
Fig. 2.4 The three different choices of the modelling domain for boundary value problem. Domain boundaries (a) at infinity, (b) right over the target and (c) at optimal finite distances.	30
Fig. 2.5 Position of vertical boundaries when asymptotic boundary conditions are used.	39
Fig. 4.1 A typical finite difference grid.	72
Fig. 4.2 The parameters of the four blocks surrounding the node (m,n) in the 2-D finite difference grid.	72
Fig. 4.3 The structure of FDM coefficient matrix when integral and asymptotic boundary conditions are employed. Here the submatrices β_1 and β_n are full; β_i , $i = 2, n-1$ are tridiagonal and α_i , γ_i , $i = 1, n-1$ are diagonal.	81
Fig. 5.1 Finite difference grid and nodes to demonstrate superblock notion. Thick lines represent boundaries of superblocks formed by merging four subblocks.	103
Fig. 5.2 EM2INV , the inversion algorithm at a glance.	106

Fig. 5.3 Flow chart of the main program of algorithm EM2INV .	107
Fig. 5.4 Flow chart of subroutine FWDSOL .	110
Fig. 5.5 Tree of subprograms called in subroutine FWDSOL .	111
Fig. 5.6 Flow chart of subroutine RESPONSE .	116
Fig. 5.7 Flow chart of subroutine FDSOLVE .	118
Fig. 5.8 Flow chart of subroutine INVSOL .	122
Fig. 5.9 Tree of subprograms called in subroutine INVSOL .	124
Fig. 5.10 Flow chart of subroutine RHSMAT .	125
Fig. 5.11 Flow chart of subroutine RESMAT .	127
Fig. 5.12 Flow chart of subroutine CGINV .	129
Fig. 5.13 Flow chart of subroutine JDELT .	132
Fig. 5.14 Flow chart of subroutine JHDELR .	133
Fig. 6.1 The BW model (a) the real (b) and imaginary (c) components of electric field for E-polarization.	136
Fig. 6.2 Mesh convergence test: The real (a) and imaginary (b) components of electric field of BW model computed using five different grids 11 x 11, 21 x 21, 41 x 41 (BW), 81 x 81 and 31 x 12 (optimal grid) nodes.	137
Fig. 6.3 The two models chosen from report of Zhdanov et al., (1990) (a,d). Comparison of EM2INV results with some of the results given in report (b,c) and (e, f) are plots of real parts of E_x and H_x for the two models respectively.	138
Fig. 6.4 The models studied - (a) the conductive block model, (b) the resistive block model and (c) the model having both conductive and resistive blocks.	140
Fig. 6.5 Inversion of Z_{xy} response of the conductive block model - (a) the comparison of responses of true and inverted models, (b) convergence of rms error in inversion and (c) resistivity contour plots over the inversion domain.	141
Fig. 6.6 Inversion of synthetic Z_{xy} data for conductive block model with increasing random noise. The comparisons of true and inverted model responses for (a) noise free, (b) 2% noise and (c) 5% noise. Parts (d) - (f) show the contours of resistivity	

(in ohm-m) within inversion domain while (g) - (i) show the convergence of rms error in inversion for noise free, 2% and 5% noise respectively.	144
Fig. 6.7 Impact of resistivity contrast on ρ_{yx} of model 1 for a given depth of burial. Plots (a), (b), (c), (d) and (e) correspond to 0, 10, 30, 40 and 50 km burial depth respectively.	147
Fig. 6.8 Same as Fig. 6.7 but for ρ_{xy} .	148
Fig. 6.9 Same as Fig. 6.7 but for model 2.	149
Fig. 6.10 Same as Fig. 6.9 but for ρ_{xy} plots.	150
Fig. 6.11 Impact of resistivity contrast on ρ_{yx} of model 3 for a given separation value. Plots (a), (b), (c), (d) and (e) correspond to 0, 10, 20, 30 and 40 km separation.	151
Fig. 6.12 Same as Fig. 6.11 but for ρ_{xy} .	152
Fig. 6.13 Variation in ρ_{yx} of model 1 with change in depth of burial for a given resistivity contrast ratio. Plots (a), (b), (c), (d) and (e) are for resistivity contrasts 2, 5, 10, 100 and 1000 respectively.	153
Fig. 6.14 Same as Fig. 6.13 but for ρ_{xy} .	154
Fig. 6.15 Variation in ρ_{yx} (a,b,c) and ρ_{xy} (d,e,f) for model 2 for resistivity contrast ratio 10, 50 and 100.	155
Fig. 6.16 Effect of variation in separation between the two blocks of model 3 on ρ_{yx} for resistivity contrast ratios 1, 2, 5, 10, 100 and 1000 shown respectively in (a), (b), (c), (d), (e) and (f).	156
Fig. 6.17 Same as Fig. 6.16 but for ρ_{xy} .	157
Fig. 6.18 The inversion quality of MT and GDS responses. The comparison of true and inverted model responses for (a) MT and (b) GDS responses; (c) and (d) present the obtained resistivity contours (in ohm-m); (e) the % rms errors during inversion.	161
Fig. 6.19 Inversion quality for two modes of polarization for model 1. The Z_{yx} and Z_{xy} responses of true and inverted model are shown in (a) and (b) respectively; the resistivity contours of inverted model for the two polarizations are contoured in (c) and (d); (e) shows the % rms errors during inversion.	162
Fig. 6.20 Same as Fig. 6.19 but for model 2.	163

- Fig. 6.21 The results of inversion performed using 1, 3 and 6 frequencies - (a) the % rms errors during inversion, (b) the CPU run time of algorithm for the three cases, (c), (d) and (e) show the obtained resistivity contours (in ohm-m) within the inversion domain for 1, 3 and 6 frequencies. 164
- Fig. 6.22 Impact of spread of observation points on inversion quality - (a), (b), (c) and (d) show the inverted resistivity contours when 31, 19, 5 and 1 points were used for inversion. 166
- Fig. 7.1 (a) Horst model with positions of observation points marked on the horizontal axis by arrows; (b) and (c) the pseudosections obtained from SIS for the B and E- polarizations; (d) and (e) resistivity contour plots of model obtained from **EM2INV** for both B and E- polarizations. 171
- Fig. 7.2 As in Fig. 7.1 but for the resistive block model. 172
- Fig. 7.3 As in Fig. 7.1 but for the conductive block model. 175
- Fig. 7.4 As in Fig. 7.1 but for the conductive and resistive block model. 176
- Fig. 7.5 (a) Sedimentary basin model with 2:1 vertical exaggeration (after Madden & Mackie, 1989). (b) Comparison of true and computed Z_{xy} response. (c) Resistivity contour plots of inverted models obtained from inversion of Z_{xy} response. (d) Convergence of the inversion iterations for inverted model. 177
- Fig. 7.6 (a) Proposed model for the conductor striking across the Himalayas (after Arora & Mahashabde, 1987). (b) The real and imaginary parts of the observed GDS response. (c) and (d) The real and imaginary parts of GDS responses for two cases are compared with the computed model response. (e) and (f) The resistivity contours of inverted model within the inversion domain for the two cases. 180
- Fig. 7.7 (a) Proposed geoelectrical model for the Trans-Himalayan conductor (after Arora, 1990). (b) % rms error plot representing convergence. (c) Resistivity contours of the real part of GDS response of the inverted model within inversion domain. (d) Comparison of the real part of GDS response of the true model with the computed one for three periods. 183
- Fig. 7.8 (a) Proposed graben model based on the MT field study (after Peeples & Rankin, 1973). (b) Comparison of convergence of % rms error for Z_{yx} and Z_{xy} inversions. (c) and (d) Resistivity contour plots within the inversion domain for Z_{yx} and Z_{xy} responses respectively. 184

- Fig. 7.9 (a) Comparison of the real part of inverted response of Trans Himalayan conductor model with the observations for three periods. (b) Convergence plot of % rms error of inversion. (c) The resistivity contours of real part of GDS response of the inverted model within the inversion domain. 186
- Fig. 7.10 (a) The pseudosection obtained from 1-D SIS inversions of the Z_{xy} responses at the 4 sites of the COPROD2R data. (b) The 2-D starting model, obtained from the pseudosection, the sites are indicated by the arrows. 188
- Fig. 7.11 Resistivity contours of Z_{xy} response within domain of inversion of the NACP model, obtained after 2-D inversion, for; (a) complete inversion domain ranging from -113 to 118 km in horizontal and 3 to 60 km in vertical direction, (b) top portion of domain extending from 3 to 20 km in vertical direction and (c) a section of domain extending from -84 to 118 km in horizontal and 20 to 60 km in vertical direction. 189

LIST OF TABLES

	PAGE NO.
Table 5.1 Description of EM2INV control parameters.	108
Table 5.2 Brief description of grid parameters used in EM2INV .	109
Table 5.3 Various forward subprograms and their purpose(s).	112
Table 5.4 Various inversion subprograms and their purpose(s).	119
Table 5.5 Description and values of dimension control parameters.	134
Table 7.1 Various models chosen for testing of EM2INV .	167

INTRODUCTION

1.1 Motivation

Deciphering the right messages from the signals is data interpretation. This activity, which pervades all walks of life is something that we humans are particularly good at. For example, most of us can recall faces even when we have not seen the person for many years, we recognize voices over poor telephone lines, identify thousands of species of plants and so on. However, insufficient and inaccurate information can lead to misinterpretation. A classic example of such gross misinterpretation is the story of five blind men who were trying to identify an elephant by each feeling a different part of the elephant body.

Many interesting questions, concerning the properties of the physical world, can be answered by analysing the indirectly measured or experimental observations. The answers to these questions are stated in terms of numerical values/statistics of the specific properties, termed as 'model parameters'. We assume that there is a specific physico-mathematical theory that relates the model parameters to the data. The prediction of results based on some general principles, a model and a set of specific conditions relevant to the problem is termed as 'direct' or 'forward problem'. In contrast, the estimation of model parameters from given data and general principles is termed as 'inverse problem' (Fig. 1.1). Thus, quantitative interpretation of data is an inverse problem and its solution is obtained through inverse theory.

Inverse theory is an organized set of mathematical procedures for reducing data to obtain meaningful information about the physical world. Geophysicists term this procedure as 'parameter estimation'. The model parameters can either be continuous functions of one or more variables or discrete numerical quantities. Though discrete

parametrization of continuous functions is approximate and it introduces error yet it allows use of theory of vectors and matrices rather than the complicated theory of continuous functions and operators. Therefore, discrete inverse theory provides a good starting point.

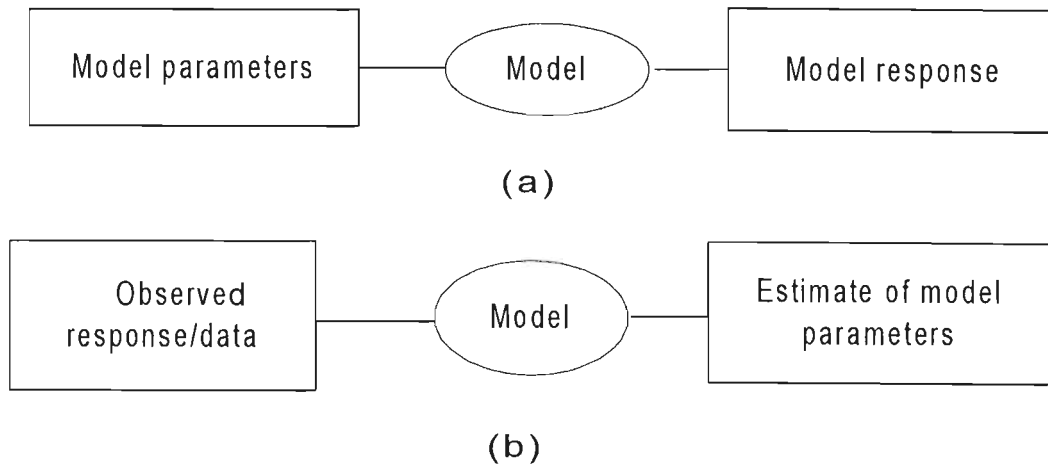


Fig. 1.1 Functional diagram for (a) forward problem and (b) inverse problem.

The aim of geophysics is to obtain information about the subsurface of the earth. Since it is impossible to take direct samples of the object of interest, the fields such as elastic wave, potential, electromagnetic are employed to probe the unknown object. These physical fields are generated by variations in the subsurface material properties and measured at the surface. In this context, the mapping of model to measured fields is known as forward problem while mapping of measured fields to the model is known as inverse problem. Typical model parameters are the geometry, orientation and physical properties of the target.

With reference to geophysics, the data interpretation is a two step procedure. The first step involves quantitative interpretation where physical earth parameters are estimated from observed data. This is followed by the second step, wherein, the obtained geophysical model is translated in terms of meaningful geology. Thus, the whole process of retrieving a reasonable geological structure from observations is called geophysical data interpretation. The present study, however, deals only with the first step, i.e. quantitative interpretation.

The earliest method used for quantitative interpretation can be described as trial and error exercise. Starting with a model, with parameters chosen subjectively, the

fit between the observed and the computed responses is resorted. In case of good agreement the model is accepted otherwise an inference is drawn and the model is modified accordingly. In contrast to this, data inversion is a guided search method where model selection at each step is based on certain criteria. Besides this, the trial and error method neither provides the confidence interval for the estimated model parameters nor any measure for quality of interpretation. It is absolutely necessary to evaluate the quality, as an interpretation unqualified by its quality index would be doubtful. Further, all the elements of uncertainty must be resolved before attempting to make a sensible interpretation of the observed data. We may often have to contend with uncertainties about which we have no control or information. Even in such cases it is essential to estimate and quantify these uncertainties before venturing in to interpretation. Thus, data inversion which appraises quality of solution and assesses reliability of interpretation is more objective than the ordinary quantitative interpretation. It can be viewed as an attempt to obtain a representative solution of the inverse problem with its level of confidence.

One form of data inversion is pattern recognition, which deals with techniques assigning patterns to their respective classes. Here, pattern is a qualitative or quantitative description of an entity of interest (Duda & Hart, 1973; Ripley, 1996). This process is performed through statistical approaches like discriminant analysis (Prelat, 1977; Aminzadeh, 1987) or machine learning approaches like knowledge based expert system (Devijver & Kittler, 1987; Raiche, 1991; Poulton et al., 1992) and artificial intelligence (Palaz, 1986). For any one of these approaches, two types of methods can be used: (i) Non-Parametric and (ii) Parametric methods. In non-parametric methods, the models used are totally flexible, whereas in parametric methods these belong to a specific family of models with a small number of parameters. In this study only parametric inversion has been carried out.

In order to understand the physical behaviour of the system with simplified assumptions, well established laws of physics and mathematics are translated into governing partial differential equations. A pre-condition for the existence of an inverse solution is that the forward solution must exist. The analytical solution of a forward problem, comprising the governing equations, is either unique or, at most, a whole class of solutions can be derived from it. Unfortunately, analytical solutions to many

problems of interest either do not exist, or are restricted to idealized situations or are too complex to evaluate. Therefore, one has to seek recourse to numerical methods such as integral equation or differential equation method to obtain solution of the forward problem (Fig. 1.2).

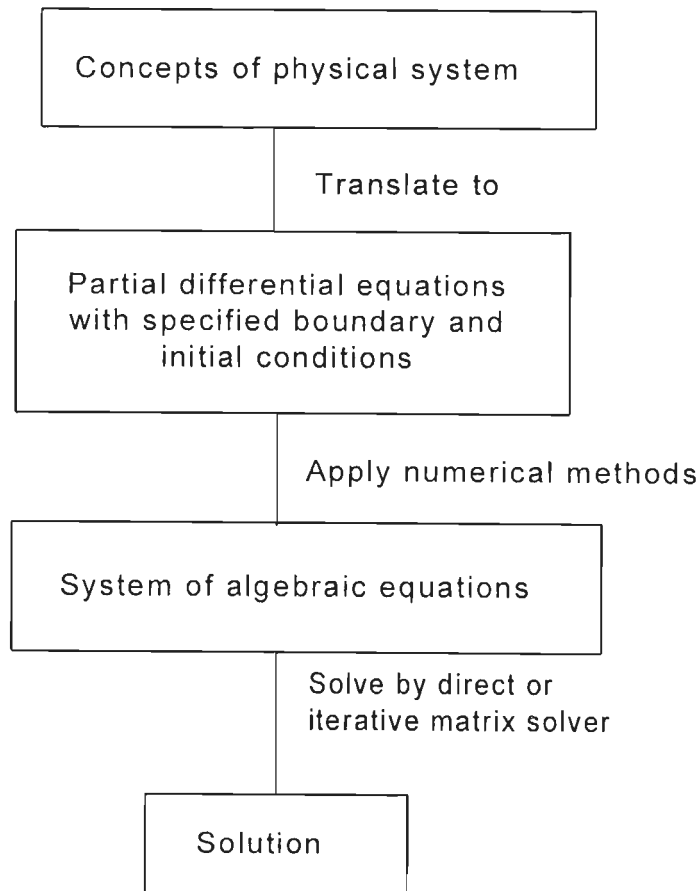


Fig. 1.2 Logic diagram for obtaining numerical solution of forward problem.

Geophysical inverse problems are usually ill-posed and as such their solutions are inherently non-unique (Backus & Gilbert, 1967; Tikhonov & Arsenin, 1977). The ill-posedness is caused by inadequate and insufficient data or sometimes by invalid assumptions used in defining the solution space of possible models while non-uniqueness arises due to the existence of an infinite number of models which may explain the data within the limits set by the accuracy of measurements. In addition, ill-conditioned system having erroneous data lead to instability that is prone to getting amplified during inversion. The problem is further compounded by non-linearity that

is inherent in the mathematical relations describing the physical experiment. These problems are regularized by replacing the ill-posed problem by an equivalent well-posed problem. This replacement yields a stable, albeit approximate solution possessing essential features of the exact solution.

For illustration of limitations and possible sources of error, the basic characteristics of the numerical solution to a geophysical problem need to be emphasized. Since a numerical solution depends upon the strategy and parameters of discretization of the domain under study, unlike the analytical solution, it may not be, and, in general, is not unique. Due to quantification of input data, coefficients and intermediate computational results, the finite length register effects render the results machine-dependent. Therefore, the resolution of inversion depends on inaccuracy of model, insufficient and erroneous data, parameter coupling, the computational methodology and numerical software employed in solving the inverse problem.

The geophysical data, observed to understand the processes taking place in the earth's crust and mantle, have to be interpreted to retrieve the desired information. Although the 1990s have witnessed an incredible growth in the power of technologies available to the geophysicist to probe the earth's interior, many geophysical methods are handicapped on account of their existing data inversion capabilities. The development of more general and powerful data inversion algorithms is, therefore, the need of the time. This is particularly true for two-dimensional (2-D) or three-dimensional (3-D) inversion algorithms for electromagnetic (EM) data because even today very few efficient and high precision numerical softwares are available. The present study was taken up with this goal in mind to develop an economically viable and efficient 2-D inversion algorithm for geoelectromagnetic studies of the geosphere.

1.2 Why geoelectromagnetic methods?

The electromagnetic methods provide estimates of electrical resistivity as a function of depth and lateral distance. A wide range of these methods has been successfully employed in the fields of mineral, hydrocarbon and geothermal explorations, aeronomy, archaeology, oceanography, environment, engineering and solid earth geophysics. Applications can be at any scale - exploration of ground water in arid/semi-arid terrain, investigation of geothermal resources, estimation of basement

depth for foundation works, mapping of industrial hazardous waste dump containing heavy metals, study of deep geology of regional tectonic structures. In the last one decade, the EMSLAB (Electro-Magnetic Sounding of Lithosphere And Beyond) experiment, the largest EM study to date has played a significant role in popularizing the applicability of these methods (EMSLAB, 1988).

The parametrization of earth in terms of electrical resistivity has special significance due to its dependence on chemical composition and thermal state. Resistivity is a good indicator of distinctive character of materials and a knowledge of its spatial distribution provides a clue to the way different kinds of materials are present in the deeper regions.

Depending upon the source, which can be natural or artificial, the electromagnetic methods can be classified either as natural/passive source or as artificial/active source methods. The natural source methods are also termed as geoelectromagnetic methods. In contrast to the depth of investigation of few tens of kilometres in artificial source methods, the geoelectromagnetic methods, where the source is located in the earth's magnetosphere and ionosphere, can measure electrical properties even up to hundreds of kilometres in the mantle. This is achieved by selecting proper frequency range from the wide range of natural EM fields.

Such deep probing greatly facilitates not only the studies on the earth's internal constitution, but also in understanding the physical and geological processes such as the convection currents, temperature induced phase changes in the deeper crust, the presence of radioactive material, hot chambers, geothermal resources, extensive conductive mineral deposits and of stress changes as a possible precursor to earthquake prediction study. Moreover these methods are particularly useful in remote areas where it would be difficult to transport the heavy source equipment, necessary in artificial source electromagnetic methods. The two most popular geoelectromagnetic methods are Magneto-Tellurics (MT) and Geomagnetic Depth Sounding (GDS) also known as Magneto Variational Profiling (MVP) in East European literature. The recent success of MT for hydrocarbon exploration in volcanic regions, where seismic reflection methods failed, has provided a new impetus to research in geoelectromagnetics. The choice of geoelectromagnetic methods was further motivated

by the widespread applications of MT and GDS methods in diverse fields of earth investigations, notably:

1. For mapping:
 - (i) Large and deep seated features of the earth's interior (Reddy & Rankin, 1972; Peeples & Rankin, 1973; Jones & Hutton, 1979; Adam et al., 1982; EMSLAB, 1989; Roy et al., 1989; Jones & Craven, 1990; ERCEUGT Group, 1992; Gupta et al., 1993; Hjelt & Korja, 1993; Jones & Haak, 1993; Ingham, 1996).
 - (ii) Sedimentary basins in hydrocarbon exploration (Vozoff, 1972; Stanley et al., 1985; Christopherson, 1990; Constable et al., 1994).
 - (iii) Small scale structures for mineral exploration (Strangway et al., 1973; Lakanen, 1986; Livelybrooks et al., 1996).
 - (iv) Structures beneath surface volcanics and metamorphic areas which are difficult to explore using conventional seismic techniques (Orange, 1989; Singh et al., 1992; Jones & Dumas, 1993; Rao et al., 1996).
 - (v) Ground water zones (Vozoff et al., 1982; Bernard et al., 1990; McNeill, 1990).
 - (vi) Convergent and divergent plate margins (Kurtz et al., 1986; Wannamaker et al., 1989a; Heinson et al., 1993; Jones, 1993; Ingham, 1994).
2. In seismo-electromagnetic studies as a precursor to earthquake (Rikitake, 1976; Honkura et al., 1977; Arora & Singh, 1992; Ernst et al., 1993; Park et al., 1993; Parrot & Johnston, 1993; Rozluski & Yukutake, 1993; Honkura et al., 1994; Park, 1994).
3. For detection of geothermal pockets (Hoover et al., 1978; Wright et al., 1985; Pellerin et al., 1996).
4. For estimation of thickness of the permafrost by audio magnetotellurics (Koziar & Strangway, 1978).
5. In oceanic studies (Filloux, 1981; Mackie et al., 1988; Palshin, 1988; Chave, 1990; Constable, 1990; Heinson et al., 1993; Lilley, 1993; Palshin, 1994).
6. To study coast effect (Rikitake, 1961; Fainberg, 1980; Chave & Cox, 1983; Kuvshinov et al., 1990; Vanyan & Palshin, 1990; Takeda, 1991; Tarits, 1992).

7. To detect large scale horizontal inhomogeneities of resistivity in crust and upper mantle (Hutton, 1976; Singh, 1980; Beamish & Banks, 1983; Chamalaun et al., 1987; Hjelt, 1988; EMSLAB, 1989; Arora & Singh, 1992; Gough, 1992; Arora, 1993; Chamalaun & McKnight, 1993; Reddy & Arora, 1993; Brown, 1994).
8. Environmental applications (Bazinet & Legault, 1985; Chouteau et al., 1994).

1.3 STATE OF ART

The EM phenomenon in earth is of induction type. The observed EM field variations are inverted to estimate the subsurface resistivity distribution. In general, one never gets the true resistivity distribution from the data, as the problem is ill-posed due to infinite number of parameters and finite number of observations. Therefore, a simple model like layered earth or regular shaped body having finite number of parameters is employed to obtain a meaningful solution to this problem.

The real earth can be represented by 3-D geometries. But the current status of EM data inversion is such that even when the target being investigated is 3-D, the inversion is carried out using one-dimensional(1-D) or sometimes 2-D approximation of the true model. The reason for this is that inversion methodologies have been adequately developed only for the 1-D case. Now 2-D inversion algorithms are also being used (Weidelt, 1975b; Jupp & Vozoff, 1977; Pek, 1985; Sasaki, 1989; deGroot-Hedlin & Constable, 1990; Smith & Booker, 1991; Oldenburg & Ellis, 1993; Yamane et al., 1996), but for 3-D inversion of EM data only isolated attempt has been made (Mackie and Madden, 1993b). However, with the lately achieved success of 3-D EM forward modelling algorithms now serious attempts are afoot to develop viable 3-D inversion algorithms. Limitations in computing power have been the principal barrier to invert EM data using 2-D or 3-D models. With the advent of powerful workstations, the 2-D inversion has now become tractable. Progress on 3-D inversion, however, is still slow. Although the first endeavours in 2-D EM inversion started around 1975, it gained momentum in nineties only, as the review of literature conducted in the next section illustrates.

When the present study was launched in 1993, the bulk of quantitative data interpretation of EM data was carried out using trial and error methods or 1-D inversion

yielding stacked model (Wannamaker et al., 1989b; Jones & Craven, 1990; Agarwal et al., 1993). For EMSLAB, the quantitative interpretation of 3-D data was performed using either the trial and error method of 2-D forward modelling (Wannamaker et al., 1989b) or the 2-D inversion (Jiracek et al., 1989). Although many results obtained using 2-D inversion algorithms were published in literature, yet these algorithms were not in public domain. The critical assessment of all the existing algorithms led to the conclusion that there still exists scope for further development in 2-D EM inversion. When the 3-D data inversion algorithm comes in use, the 2-D inversion algorithm would still be used to get the best possible initial guess model. A good 2-D inversion algorithm is thus a prerequisite for an efficient 3-D inversion algorithm. Due to simple mathematical formulation of EM theory in frequency domain, the inversion algorithm in this study has been developed for frequency domain.

The literature of electromagnetic modelling can be classified into two categories - (i) developments in numerical techniques and (ii) developments in inversion techniques. A brief review of literature for these two classes is presented here. The review is constrained because of the limited library resources available.

1.3.1 Developments in numerical techniques

The simplest earth models are the one-dimensional ones, where resistivity is assumed to vary only with depth. More realistic models of earth are the 2-D ones, where the resistivity is allowed to vary in one horizontal direction as well. Two-dimensional forward modelling can be performed analytically only for few idealized models, but accurate numerical solutions are now provided by many efficient computer programs in widespread use. The numerical methods employed for 2-D EM modelling, are Integral Equation Method (IEM), Differential Equation Method (DEM) and Hybrid Methods (HM).

IEM, where the anomalous region is discretized, results in a small but full coefficient matrix. In fact, it is the most widely used method in EM modelling (Hohmann, 1971; Raiche, 1974; Reddy et al., 1977; Ting & Hohmann, 1981; Wannamaker et al., 1984a; Wannamaker, 1991; Xiong, 1992; Zhdanov & Fang, 1996). Due to non-availability of efficient algorithms for computation of Green's functions in other cases, the use of IEM is limited to confined targets buried in layered earth. The

DEMs are popular for modelling of complex geometries. The two popular DEMs, Finite Difference Method (FDM) and Finite Element Method (FEM), give rise to large but grossly sparse coefficient matrices as the whole study domain is discretized. The recent advances in iterative solution techniques have made these methods more popular (Sarkar, 1991). The simple mathematics and easy implementation of FDM have led to its preference over FEM, particularly for geophysical problems (Jones & Pascoe, 1971; Brewitt-Taylor & Weaver, 1976; Mackie & Madden, 1993a; Smith, 1996b; Weaver et al., 1996). HMs which are amalgamation of IEM and DEM are again suited only for the confined bodies (Lee et al., 1981). For the present study the FDM has been preferred. Although Weaver (1994) has compiled the chronological development of 2-D EM modelling using FDM yet it is reviewed here for completeness.

The results of 2-D induction problem for quarter-space model, given by Jones & Price (1970), had provided a foundation for all future works in this field. They had extended their work for different types of models (Jones & Price, 1971). The first 2-D FDM algorithm was given by Jones & Pascoe (1971) for a general structure buried in layered earth. Besides theoretical development, the computer program was also available in this paper. The method included a provision for variable grid size but could not be used for models having non-uniform surrounding region. This algorithm was further modified by Pascoe & Jones (1972) for a more general case where the models could be different at the two ends. Williamson et al. (1974) discovered an error in FDM representation of second derivatives as given by Jones & Pascoe (1971) for variable grid spacings. In this context, Jones & Thomson (1974) explained that this error could be reduced when grid spacings were not too irregular.

The 2-D induction problem had been reexamined and modified by Brewitt-Taylor & Weaver (1976). They not only replaced the one-sided difference formula of Jones & Pascoe (1971) by the central difference one but also modified the simple average of conductivities by taking its weighted average. Here, an improved version of 2-D EM forward formulation was proposed that became a landmark in the field of FDM modelling. Weaver & Brewitt-Taylor (1978) formulated an asymptotic expansion for greater accuracy of E-polarization boundary conditions. Chen & Fung (1989) tested the discretization criterion of FDM mesh. In recent years, with the advancement in iterative methods, significant progress has also been made in 3-D FDM forward

modelling (Madden & Mackie, 1989; Xinghua et al., 1991; Mackie et al., 1993; Weaver, 1994; Smith, 1996a, 1996b). However, in 3-D grid it is difficult to define field and resistivity values at the nodes. To overcome these difficulties, recently staggered grids have been used in modelling where the separate nodes are assigned to each field component (Mackie et al., 1993; Weaver, 1994; Smith, 1996a). On the other hand, Weaver et al. (1996) have claimed that even fixed grids can be used with accuracy comparable to that yielded by staggered grids.

Apart from the conventional ones, few alternative approaches are also discussed in literature, e.g. analogy with equations for voltage and current in a transmission surface (Madden & Swift, 1969), integration of differential equations over rectangular domains surrounding each node (Doucet & Pham Van Ngoc, 1984). An extension of finite difference to triangular elements has been developed by Aprea et al. (1990) and Weaver (1994). There has been some work exclusively on the development of appropriate boundary conditions at domain boundaries, e.g. Williamson et al. (1974), Jones (1974), Weaver & Brewitt-Taylor (1978), Zhdanov et al. (1982) and Weaver (1994). The work of Zhdanov et al. (1982) is important on account of its discussion on quantitative analysis of model validity.

1.3.2 Developments in inversion techniques

In general, the 'inverse problem' is much more difficult to solve than the corresponding 'forward problem'. This is particularly true for non-linear EM inverse problem.

The solution of a non-linear inverse problem can be obtained using three different approaches: (i) transformation of non-linear problem to a linear one, (ii) quasi-linearization of the non-linear problem and (iii) use of non-linear methods. In the first approach, which is a direct approach, the problem can be solved using any linear method and, unlike the other two approaches it does not require an initial guess model. The problem is solved iteratively for the other two indirect approaches.

Being the simplest approximation, 1-D model is still widely used. Most of the EM literature is devoted to the modelling of layered earth model. Even today the 3-D resistivity anomalies are mostly inverted using 1-D inversion algorithms. Although 1-D inversion is well understood, yet it is beset with difficulties because no unique solution

exists for the incomplete data sets available in practice. Several efficient 1-D inversion algorithms such as Patrick & Bostick (1969), Weidelt (1972), Parker (1977), Oldenburg (1979), Fischer et al. (1981), Parker & Whaler (1981), Whittall & Oldenburg (1992), Weaver & Agarwal (1993), Gupta et al. (1996) provide specified one-dimensional models that are consistent with the data.

The methodology for solving 2-D/3-D EM inverse problem is still not fully developed. The available 2-D inversion algorithms - Weidelt (1975b), Jupp & Vozoff (1977), Rodi et al. (1984), Pek (1985), Sasaki (1989), deGroot-Hedlin & Constable (1990), Oldenburg (1990), Smith & Booker (1991), Oldenburg & Ellis (1993), Yamane et al. (1996) - are still developing and yet to be rigorously tested on real earth data. The 3-D inverse problem is still in its infancy (Mackie & Madden, 1993b). Therefore, the geophysical community has been striving to develop versatile and economically viable EM data inversion algorithms that can provide meaningful information about the resistivity variations in the earth. Scarcity of such an algorithm motivated us to develop our own 2-D inversion algorithm. Due to limitations of available computational resources we could not undertake the 3-D problem and restricted ourselves to 2-D inversion. Moreover, after gaining confidence in 2-D problems it would be easier to handle the 3-D ones. The present work has resulted in the development of an efficient finite difference based 2-D algorithm for inversion of geoelectromagnetic data and it is christened as **EM2INV**.

1.4 Scope of the present work

Since direct formulation of 2-D inverse problem is not available, this non-linear problem can be solved either through quasi-linearization or using non-linear methods. However, the usage of non-linear methods, like simulated annealing or genetic algorithm, is limited on account of their economic viability which is poor even for 1-D problems (Dosso & Oldenburg, 1991; Schultz et al., 1994). Therefore, the inverse problem is solved using an indirect quasi-linearization approach.

The literature survey revealed that 2-D inversion is mostly carried out using 1-D inversion or its stacked results. However, there are few instances when 2-D inversion algorithms have also been employed (Jiracek et al., 1989). Some available 2-D inversion algorithms, like Rapid Relaxation Inversion (RRI) (Smith & Booker, 1991),

Generalized Rapid Relaxation Inversion (GRRRI) (Yamane et al., 1996), are basically 1-D exploiting the slow resistivity variation in horizontal direction and taking its care only through 2-D forward modelling. A comprehensive algorithm is needed to carry out numerical modelling of geoelectromagnetic data. For the algorithm to be useful in any meaningful study, it should be able to solve the forward and also the inverse problems. This means that it should be able to (i) simulate MT/GDS response for a given model and (ii) invert the observed response in terms of resistivity values.

The inversion algorithm **EM2INV**, based on FDM, is the outcome of a thorough and extensive research during which various versions of the algorithm were developed. These versions were critically appraised and the derived inferences were incorporated in the subsequent algorithms. This led to the development of **EM2INV** where the same algorithm can be used for inverting synthetic or field data.

Initially, to start the research work, the FDM formulation of the forward problem given by Brewitt-Taylor & Weaver (1976) was implemented. The final forward algorithm includes features such as automatic grid design, integral boundary conditions at both top and bottom boundaries of the grid and asymptotic boundary conditions at the vertical boundaries of the grid. For quasi-linearization, the response vector is expressed in Taylor series and only the linear terms of the series are retained. Thus, the non-linear problem becomes linear in perturbations and is solved iteratively. The economic viability of the algorithm highly depends on how efficiently one can solve the inverse matrix equation obtained after quasi-linearization. Bi-conjugate gradient matrix solver, which dispenses with the necessity of explicit computation of Jacobian matrix, is used for this purpose. The current model is successively improved until the error measure is within preassigned limit and the parameters are stable. A superblock notion, to fix the number of unknown block resistivities for all frequencies and throughout the inversion process, has been developed.

The developed algorithm is validated and rigorously checked. Its accuracy and efficacy are established through few theoretical experiment design exercises. These experiments of diverse nature are performed on certain features of forward and inversion algorithm. The results of these exercises provide useful information, necessary for successful planning of data procurement and for inversion of field data. Lastly, the data inversion of synthetic and field data has been carried out.

It may be alluded here that standard units, symbols and terminologies recommended by Hobbs (1992) are used in the present work.

1.5 Organisation of chapters

The objectives of this study are fulfilled with the development of the software package **EM2INV** which is capable of carrying out both forward modelling and data inversion for geoelectromagnetic studies. The thesis has been organised into 8 chapters. A brief account of the contents in subsequent chapters of the thesis follows.

The mathematical formulation of forward problem is presented in Chapter 2 which covers a brief description of EM theory and ranges of electrical properties within the earth. It also formulates a boundary value problem comprising the governing partial differential equations and requisite boundary conditions. An integrated formulation of special finite domain integral and asymptotic boundary conditions has been developed. MT and GDS methods and their response functions are also summarized in the end.

The characteristics of ill-posed EM inverse problem and some techniques for its alleviation are presented in Chapter 3. Besides the different methodologies for solving inverse problem, the direct Straightforward Inversion Scheme (SIS) algorithm for 1-D inverse problem and quasi-linearized scheme for 2-D inverse problem are also presented.

In order to successfully implement the FDM for solving forward and inverse problems, the discrete governing equations, discrete boundary conditions, transformation matrices derived for response functions and the implicit computation of Jacobian matrix are discussed in Chapter 4. Finally a discussion regarding the choice of suitable matrix solvers for forward and inverse matrix equations is given.

Chapter 5 presents the sequence of development with a critical review of various primitive versions of the algorithm. Description of salient efficiency and versatility features, structure, control and grid parameters, important subprograms of the algorithm and various hardware/software limitations of the computing environment is also included.

The developed algorithm was tested and validated using synthetic models. Several theoretical experiments, which were designed and performed to set up guidelines for better data procurement and inversion quality, and their results are

discussed in Chapter 6.

Chapter 7 presents the inversion results of data sets derived from synthetic and field studies based models and also from field data.

Chapter 8 summarizes the achievements and limitations of the algorithm developed in this thesis and suggests possible lines along on which the work can be extended.

Appendix 1 contains derivation of recurrence relations for SIS algorithm. The basic steps of bi-conjugate gradient method are given in Appendix 2. Appendix 3 contains documentation on input requirements of the inversion algorithm **EM2INV**.

FORMULATION OF EM FORWARD PROBLEM

2.1 General

The geoelectromagnetic methods deal with the observation and analysis of EM fields with a view to derive pertinent information about the geoelectric structure of subsurface. The observed field can be viewed as a superposition of the primary and secondary fields. Primary fields, generated by an external source, induce secondary currents in the earth which, in turn, give rise to the secondary fields. If the earth model is a uniform half-space, then the induced currents and the resulting secondary fields follow a regular pattern. Inhomogeneities present in the real earth invariably disturb this regular pattern of secondary currents and fields leading to perturbation of the total EM fields. These perturbed fields, measured on the earth's surface, provide an insight into the resistivity distribution within the earth. This helps in deciphering the structure of the earth and also in understanding the ongoing physical processes.

The mechanism of perturbed fields can be understood only when the capability of generating responses of arbitrary resistivity distributions is fully developed. The computation of EM response of a given earth model, with prescribed resistivities, is known as the forward problem of EM induction.

An exhaustive knowledge of EM theory, based on the fundamental Maxwell's equations, is essential for solving the forward problem. In literature there exist a vast number of texts on EM theory differing in their emphasis on mathematical background, computational aspects and applications. One can refer to Stratton (1941), Smythe (1950), Morse & Feshbach (1953) and Jackson (1975) for fundamentals, to

Mitra (1973, 1975), Morgan (1990), Zhou (1993) and Taflove (1995) for computational aspects and to Grant & West (1965), Rikitake (1966), Ward (1967), Porstendorfer (1975), Rokityansky (1982), Wait (1982), Kaufman & Keller (1983), Berdichevsky & Zhdanov (1984) and Nabighian (1988, 1991) for geophysical applications. For completeness, a brief account of electromagnetic theory is presented here. Since the foundation of the present study is the work of Brewitt-Taylor & Weaver (1976), the $e^{i\omega t}$ time dependence used by them has been followed here also.

2.2 Electromagnetic theory

The EM phenomenon is governed by the Biot-Savart law for magnetic induction due to current, Faraday's law of induction, Coulomb's law of electric fields due to charges and the law of non-existence of magnetic monopole. Maxwell's equations are the concise mathematical statements of these laws that, assuming linear, isotropic medium and an $e^{i\omega t}$ time-dependence, can be written as the following first order partial differential equations

$$\nabla \times \mathbf{B} = \mu \mathbf{J} + i \omega \mu \mathbf{D}, \quad \dots(2.1)$$

$$\nabla \times \mathbf{E} = -i \omega \mathbf{B}, \quad \dots(2.2)$$

$$\nabla \cdot \mathbf{D} = q_e, \quad \dots(2.3)$$

$$\nabla \cdot \mathbf{B} = 0, \quad \dots(2.4)$$

$$\text{where } \nabla = \frac{\partial}{\partial x} \hat{i} + \frac{\partial}{\partial y} \hat{j} + \frac{\partial}{\partial z} \hat{k}.$$

Here \mathbf{B} , \mathbf{E} , \mathbf{D} and \mathbf{J} are the vectors representing the magnetic induction in Tesla, the electric field in Volts/metre(m), the electric displacement in Coulombs/m² and the electric current density in Amperes/m² respectively. Similarly, q_e , ω and μ are the scalars representing free electric charge density in Coulombs/m³, the spectral angular frequency in Hertz and the magnetic permeability in Henry/m. It can be easily established that, for \mathbf{B} and \mathbf{D} having continuous first and second derivatives, equation (2.4) can be derived from equation (2.2), while equation (2.3) can be derived from equation (2.1). The equation of continuity which states the law of conservation of

electric charge can be written as

$$\nabla \cdot \mathbf{J} = -i\omega q_e \quad \dots(2.5)$$

The two vector equations (2.1) and (2.2) involve four vectors. Therefore, the constitutive relations are employed to express these equations in terms of two independent EM vectors. These relations state the dependence of various vectors on the gross material properties, the electrical conductivity, σ , and the dielectric permittivity, ϵ , as

$$\mathbf{J} = \sigma \mathbf{E} \quad \dots(2.6)$$

and

$$\mathbf{D} = \epsilon \mathbf{E} \quad \dots(2.7)$$

Here, σ in Siemens/m and ϵ in Farad/m are the second order tensors which may be functions of position vector \mathbf{r} and spectral angular frequency ω . A third relation defines the magnetic field intensity vector \mathbf{H} , commonly mentioned in literature, as

$$\mathbf{B} = \mu \mathbf{H} \quad \dots(2.8)$$

where \mathbf{H} is in Amperes/m. The constitutive relations are not always linear or single-valued. For example, σ and ϵ may be functions of \mathbf{E} . The constitutive relation (2.6), in the linear case, may be recognised as a statement of Ohm's law. In order to ascertain which of these functional dependencies are of relevance in the context of the various EM methods, a discussion of geoelectromagnetic properties follows.

2.3 Electrical properties of earth

For an isotropic earth, the parameter tensors σ , ϵ and μ reduce to scalars and are, in general, functions of position only. The only other functional dependence of importance is with respect to frequency. In some studies, the dependence of resistivity on temperature has been used to gather information about the thermal gradient in earth. Several texts have discussed the electrical properties of rocks and minerals, notable amongst these being Grant & West (1965), Keller & Frischknecht (1966) and Ward & Fraser (1967). Here, a brief account of the ranges of σ , ϵ and μ widely encountered in the earth, is presented.

The parameter electrical conductivity σ or its inverse, the electrical resistivity ρ which is more popular in geophysical literature, has the widest range of all physical parameters of earth. The resistivity varies in the range 10^{-8} - 10^{13} ohm-m for different rocks and minerals. A resistivity value less than 10^{-5} ohm-m relates to a conductor while one greater than 10^8 ohm-m relates to insulators. The intermediate values correspond to semi-conductors. This wide range results from the diverse physical phenomena that contribute to the resistivity of rocks. In the upper crust, the ionic conduction of electrolytes in the pores of rocks is the primary contributor to resistivity of rocks, while in the lower crust and upper mantle the electronic mode of conduction is the primary contributor. In the former case, if it is desired to account for electrode and membrane polarization through a change in resistivity, it becomes frequency dependent and complex in nature. For surface rocks, water present in pore spaces is the most important factor controlling the resistivity. It has been shown that the anomaly caused by a target, buried in a conducting host medium, gets enhanced as the contrast in the resistivity values of the target and host medium increases. However, it asymptotically reaches a maximum value, rendering the cases, where the resistivity contrast is greater than 1000, indiscernible from each other. Hence, such cases can be modelled as if the target is suspended in free space.

The free space value of electric permittivity is $\epsilon_0 = 10^{-9}/36\pi$ Farad/m. With the exception of water ($\epsilon/\epsilon_0 \approx 80$), electric permittivity rarely vary by more than an order of magnitude. For most rocks and earth materials the typical value is $\epsilon \approx 9\epsilon_0$. The primary contributions to ϵ are only due to the microscopic phenomena like the lengthening of bonds between the atoms and the preferred orientation of molecules along the direction of the field. However, if the macroscopic phenomena, like electrode and membrane polarization, are accounted through permittivity, ϵ attains large values and becomes frequency dependent.

The magnetic permeability μ in most geophysical situations equals its free space value $\mu_0 = 4\pi \times 10^{-7}$ Henry/m. Only for the ferromagnetic minerals it goes upto $6\mu_0$. In the case of remanent magnetization studies, μ becomes non-linear and multivalued due to the phenomenon of hysteresis.

2.4 The EM boundary value problem

The geoelectromagnetic field variations can be studied by solving the Maxwell's equations (2.1) and (2.2). The solution can be achieved by transforming these equations into a well posed EM Boundary Value Problem (BVP) in any one of the field vectors \mathbf{B} or \mathbf{E} . For this purpose a right-handed cartesian coordinate system, with z -positive downward and air-earth interface at $z = 0$, is used here. Besides the assumption of a plane wave propagating vertically downwards along the z -axis, following assumptions are also made about the physical nature of earth:

- (1) Earth is a linear and isotropic medium so that the change in output is proportional to the change in input field and the physical variables σ , ϵ and μ are scalars. In particular μ is assumed to be equal to μ_0 , its free space value, throughout.
- (2) Earth is a source free and passive medium.
- (3) The flat earth model is appropriate as only the EM fields with periods less than 1 day are to be studied.
- (4) Since the frequencies used are less than 10^5 Hz and the resistivities commonly encountered in earth are less than 10^4 ohm-m, the free charge decays instantaneously.

In view of the assumption (4), equations (2.3) and (2.5) respectively get simplified as

$$\nabla \cdot \mathbf{D} = 0 \quad \dots(2.9)$$

and

$$\nabla \cdot \mathbf{J} = 0. \quad \dots(2.10)$$

These equations imply that for an isotropic medium the decay of charge is faster than the propagation of electromagnetic wave and the charge density will reach equilibrium in practically no time. The surface charges may, however, accumulate at the interface of two homogeneous regions.

Further, for frequencies less than 10^5 Hz, the displacement current term in equation (2.1) is negligibly smaller than the conduction current term and can, therefore, be neglected. After using Ohm's law, the equation (2.1) gets simplified as

$$\nabla \times \mathbf{B} = \mu \sigma \mathbf{E} \quad \dots(2.11)$$

while equation (2.2) is restated here for continuity as

$$\nabla \times \mathbf{E} = -j \omega \mathbf{B}. \quad \dots(2.12)$$

The fields governed by these equations are termed quasi-static because in spite of the field being time dependent, its variation is very slow and at any given instant of time it behaves like a static field. Thus, for the quasi-static case, the two equations (2.11) and (2.12) are sufficient to describe the complete behaviour of EM fields.

The two steps for defining a BVP comprise development of the governing partial differential equations and of the requisite boundary conditions for each of the field vector \mathbf{B} and \mathbf{E} .

2.4.1 Governing partial differential equations

To eliminate \mathbf{E} , from equations (2.11) and (2.12), take **curl** of the equation, obtained after dividing equation (2.11) by σ , and then use equation (2.12) along with the following identity

$$\nabla \times (\nabla \times \mathbf{v}) = \nabla (\nabla \cdot \mathbf{v}) - \nabla^2 \mathbf{v}$$

$$\text{where } \nabla^2 = \frac{\partial^2}{\partial x^2} + \frac{\partial^2}{\partial y^2} + \frac{\partial^2}{\partial z^2}.$$

The resulting equation satisfied by vector \mathbf{B} is

$$\nabla^2 \mathbf{B} + k^2 \mathbf{B} + \frac{\nabla \sigma}{\sigma} \times (\nabla \times \mathbf{B}) = 0, \quad \dots(2.13)$$

where, k , the wave number or propagation constant, is defined as

$$k^2 = -j \omega \mu \sigma. \quad \dots(2.14)$$

For a homogeneous region this equation reduces to the Helmholtz equation as

$$\nabla^2 \mathbf{B} + k^2 \mathbf{B} = 0. \quad \dots(2.15)$$

Similarly, \mathbf{B} can be eliminated from equations (2.11) and (2.12) by switching the roles of equations (2.11) and (2.12) to get the equation satisfied by \mathbf{E} as the following Helmholtz equation

$$\nabla^2 \mathbf{E} + k^2 \mathbf{E} = 0. \quad \dots(2.16)$$

The wave number k is related to skin depth δ (in metres), as

$$k = \frac{1+i}{\delta} \quad \dots(2.17)$$

with $i = \sqrt{-1}$ and δ as

$$\delta = \sqrt{\frac{2}{\omega \mu \sigma}} \quad \dots(2.18)$$

The skin depth is defined as the depth at which the amplitude of EM field is attenuated by a factor of e . It is a useful guide to the depth of penetration of the field at a given frequency. It may be alluded here that since the wave number k is a complex quantity, the electromagnetic phenomenon in earth is a diffusion process. The induction fields, therefore, do not propagate as EM waves, rather these diffuse through the electrical conductor much like the heat flows through a thermal conductor.

2.4.1.1 Modes of polarization

The EM fields of an induction problem can be partitioned, depending upon the direction of propagation of the electric and magnetic fields, into two modes of polarization. In Transverse Electric (TE) or E-polarization mode, the electric field is transverse to the z -axis while in Transverse Magnetic (TM) or B-polarization mode the magnetic field is transverse to the z -axis. Since the EM wave is a transverse wave, the vertical component of field, E_z or B_z for respective polarization, does not exist. Thus, for a 3-D problem the non-vanishing electric and magnetic field components can be expressed as sets for two polarizations. For E-polarization the five scalar components are E_x , E_y , B_x , B_y and B_z while for the B-polarization these are E_x , E_y , E_z , B_x and B_y .

2.4.1.2 Two-dimensional equations

For 2-D problems, the model parameters, the field vectors and the source characteristics are chosen to be independent of the horizontal coordinate, x -, corresponding to the strike direction (Fig. 2.1b). The vector equations (2.11) and (2.12) reduce to the following six scalar equations

$$\frac{\partial B_z}{\partial y} - \frac{\partial B_y}{\partial z} = \mu \sigma E_x \quad \dots(2.19a)$$

$$\frac{\partial B_x}{\partial z} = \mu \sigma E_y \quad \dots(2.19b)$$

$$\frac{\partial B_x}{\partial y} = -\mu \sigma E_z \quad \dots(2.19c)$$

$$\frac{\partial E_z}{\partial y} - \frac{\partial E_y}{\partial z} = -i\omega B_x \quad \dots(2.19d)$$

$$\frac{\partial E_x}{\partial z} = -i\omega B_y \quad \dots(2.19e)$$

$$\frac{\partial E_x}{\partial y} = i\omega B_z \quad \dots(2.19f)$$

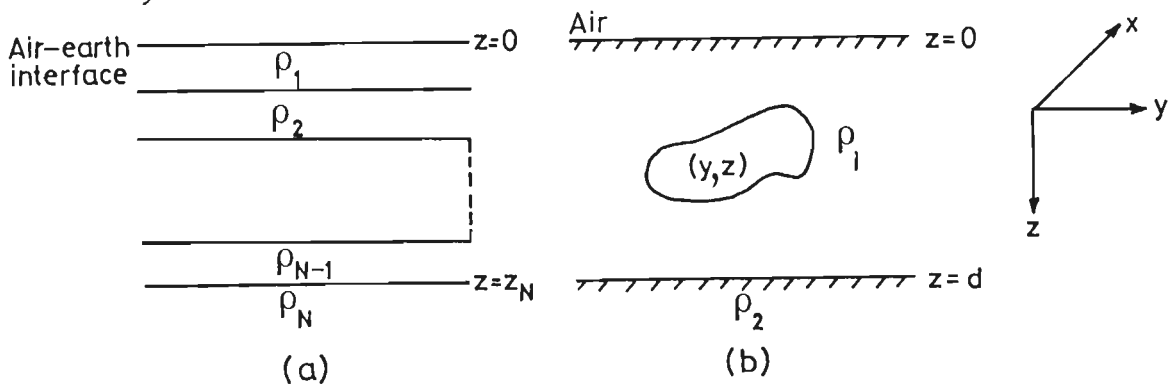


Fig. 2.1 Typical earth models (a) 1-D and (b) 2-D. Also shown is the coordinate system.

These equations can be grouped on the basis of their dependence on B_x or E_x , as B- and E- polarizations, respectively, as

B-polarization

$$\frac{\partial B_x}{\partial z} = \mu \sigma E_y \quad \dots(2.20a)$$

$$\frac{\partial B_x}{\partial y} = -\mu \sigma E_z \quad \dots(2.20b)$$

$$\frac{\partial E_z}{\partial y} - \frac{\partial E_y}{\partial z} = -i\omega B_x \quad \dots(2.20c)$$

E-polarization

$$\frac{\partial E_x}{\partial z} = -i \omega B_y \quad \dots(2.21.a)$$

$$\frac{\partial E_x}{\partial y} = i \omega B_z \quad \dots(2.21.b)$$

$$\frac{\partial B_z}{\partial y} - \frac{\partial B_y}{\partial z} = \mu \sigma E_x \quad \dots(2.21.c)$$

The only non-vanishing magnetic field component in the B-polarization and the electric field component in the E-polarization is parallel to strike of the 2-D structure. The field component sets for the two polarizations are distinct and independent.

The x- component of the magnetic and electric fields in the two polarizations, respectively satisfy the following partial differential equations

$$[L_1(k)] B_x = \left[\frac{\partial^2}{\partial y^2} + \frac{\partial^2}{\partial z^2} - \frac{1}{\sigma} \frac{\partial \sigma}{\partial y} \frac{\partial}{\partial y} - \frac{1}{\sigma} \frac{\partial \sigma}{\partial z} \frac{\partial}{\partial z} + k^2 \right] B_x = 0 \quad \dots(2.22)$$

and

$$[L_2(k)] E_x = \left[\frac{\partial^2}{\partial y^2} + \frac{\partial^2}{\partial z^2} + k^2 \right] E_x = 0. \quad \dots(2.23)$$

2.4.1.3 One-dimensional equations

In case of a 1-D earth model, where there is no lateral variation in material properties, the field components vary only with depth (Fig. 2.1 a). The equations for the B- and E- polarizations reduce to following equations

$$\frac{\partial^2 B_x}{\partial z^2} - \frac{1}{\sigma} \frac{\partial \sigma}{\partial z} \frac{\partial B_x}{\partial z} + k^2 B_x = 0 \quad \dots(2.24)$$

and

$$\frac{\partial^2 E_x}{\partial z^2} + k^2 E_x = 0. \quad \dots(2.25)$$

Let, for simplification of notation, the suffix x be dropped so that

$$E = E_x \text{ and } B = B_x \quad \dots(2.26)$$

Generally, it is simpler to solve the EM partial differential equations in terms of the scalar or vector potential rather than in terms of the vector field. But in the case of a 2-D problem there is no advantage in introducing potentials as the field can be partitioned into two independent modes governed by two scalar equations.

For air, the non-conducting region where $\sigma = 0$, the basic equation (2.11) simplifies to

$$\nabla \times B = 0. \quad \dots(2.27)$$

Thus \mathbf{B} becomes irrotational and is derivable from a magnetic scalar potential Ω , defined as

$$B = -\nabla \Omega. \quad \dots(2.28)$$

By virtue of (2.4), it follows that

$$\nabla^2 \Omega = 0. \quad \dots(2.29)$$

It serves as the governing differential equation for the magnetic field in air. The equations (2.19b) and (2.19c) reduce to

$$\frac{\partial B_x}{\partial z} = \frac{\partial B_x}{\partial y} = 0,$$

Implying that

$$B = B_0. \quad \dots(2.30)$$

B_0 being the constant primary magnetic field in air due to the source. Thus, the primary B-polarized field is constant in air.

2.4.2 Partitioning of fields

In order to solve the governing equations (2.22) or (2.23) one of the options is to view the total EM fields as a superposition of the normal and anomalous fields as

$$F = F_n + F_a \quad \dots(2.31)$$

Here, F stands for any one of the electric or magnetic field components and the subscripts 'n' and 'a' denote normal and anomalous fields respectively. The normal field is the response of a simplified model while the anomalous field is the response of the anomalous bodies or inhomogeneities present in the simplified model. For example, as shown in Fig. 2.2, the 2-D model consisting of a buried body in a layered earth can be viewed as if a body of anomalous conductivity is superimposed over the normal layered earth model.

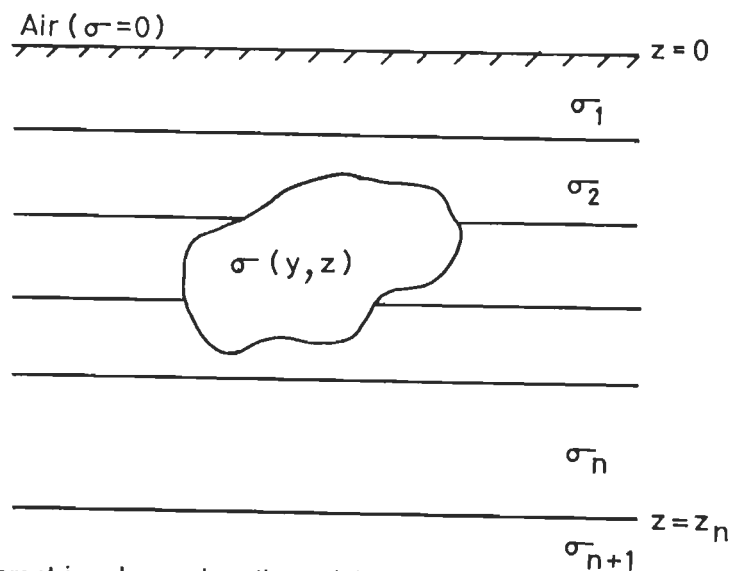


Fig. 2.2 Buried target in a layered earth model.

The conductivity at a point, σ , is the sum of the layer conductivity, σ_n , and the anomalous conductivity, σ_a , which is non-zero only in the body. Thus

$$\sigma = \sigma_n + \sigma_a \quad \dots(2.32)$$

This conductivity relation corresponds to the wave number relation

$$k^2 = k_n^2 + k_a^2 \quad \dots(2.33)$$

On substituting these superposition relations in equations (2.22) and (2.23), the equation gets partitioned into following two sets of equations for the magnetic and electric fields respectively

$$[L_1(k_n)](B_n) = 0, \quad \dots(2.34 a)$$

$$[L_1(k)](B_a) = -[L_1(k_a)] B_n + (\sigma_n k_a^2 + \sigma_a k_n^2) (B_n + B_a) \quad \dots(2.34 b)$$

and

$$[L_2(k_n)](E_n) = 0, \quad \dots(2.35 a)$$

$$[L_2(k)](E_a) = k_a^2 E_n \quad \dots(2.35 b)$$

The anomalous magnetic field in air will become

$$B - B_0 = -\nabla \Omega \quad \dots(2.36)$$

It may be emphasized here that as the sources are natural EM fields, the use of homogeneous Helmholtz equations is justified in geoelectromagnetics. The primary source fields have their origin in the electric currents blowing in and beyond the ionosphere which, in turn, arise from the complex interactions of solar radiations and plasma flux with the earth's magnetosphere and ionosphere. The primary field, the external inducing field due to source, is horizontal and laterally uniform. Being a natural source, the signals can be treated as plane wave incident normally on the earth. Therefore, the domain of study can be treated as source free and the effect of source is accounted through the boundary conditions.

In order to complete the statement of a well posed EM boundary value problem, the necessary and sufficient boundary conditions for the equations (2.22), (2.23), (2.24) or (2.25) must be identified.

2.5 The boundary conditions

There are two types of boundary conditions, first defined on any interface of discontinuity and the second defined on domain boundaries. The former are either

explicitly imposed or used to derive appropriate smooth resistivity function at a point situated at the interface of different regions. The domain boundary conditions define the asymptotic behaviour of field or its integrated effect on a boundary.

2.5.1 Interface boundary conditions

The necessary boundary conditions to be imposed on an interface, separating two media, 1 and 2, with different physical properties (Fig. 2.3), may be obtained by simply replacing the differential operator ∇ by the unit normal vector \mathbf{n} and by setting the $i\omega$ term to zero in equations (2.1) - (2.4). The resulting boundary conditions are

- (1) The tangential components of \mathbf{H} are discontinuous, the discontinuity being equal to the surface current density \mathbf{J}_s , i.e.

$$\mathbf{n} \times (\mathbf{H}_2 - \mathbf{H}_1) = \mathbf{J}_s \quad \dots(2.37)$$

- (2) The tangential components of \mathbf{E} are continuous, i.e.

$$\mathbf{n} \times (\mathbf{E}_2 - \mathbf{E}_1) = 0. \quad \dots(2.38)$$

- (3) The normal components of \mathbf{B} are continuous, i.e.

$$\mathbf{n} \cdot (\mathbf{B}_2 - \mathbf{B}_1) = 0. \quad \dots(2.39)$$

- (4) The normal components of \mathbf{D} are discontinuous, the discontinuity being equal to the surface charge density q_s , i.e.

$$\mathbf{n} \cdot (\mathbf{D}_2 - \mathbf{D}_1) = q_s \quad \dots(2.40)$$

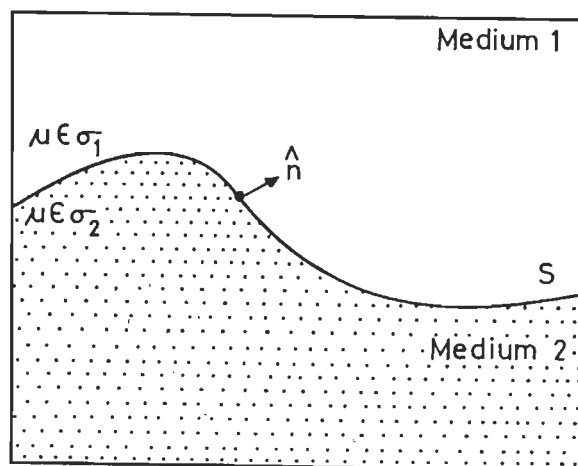


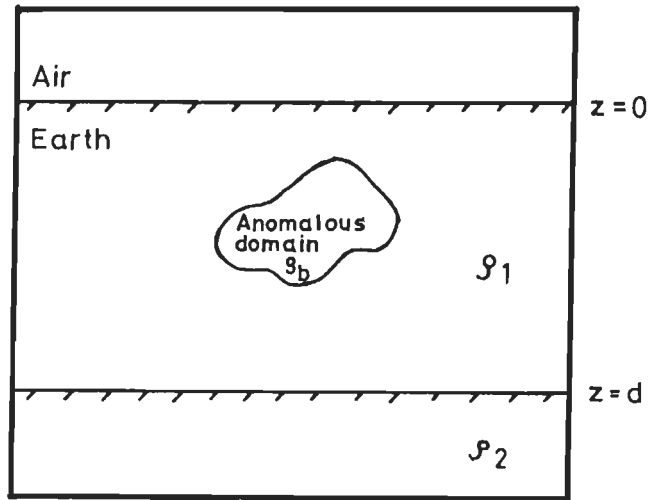
Fig. 2.3 The interface S between two regions with different material properties.

2.5.2 Domain boundary conditions

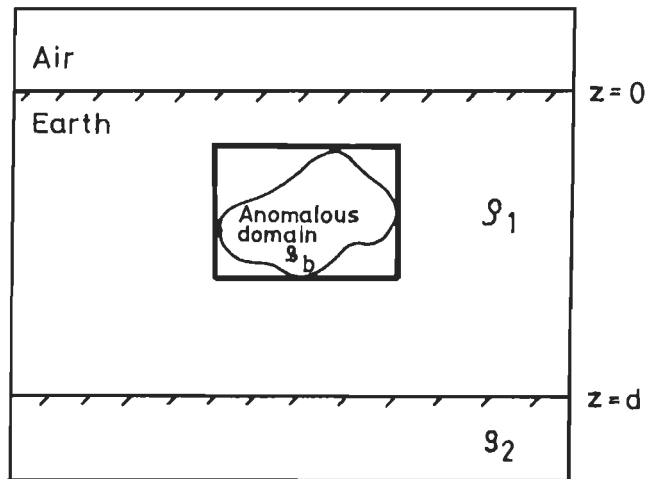
Apart from the interface boundary conditions, the boundary conditions have to be applied on the domain boundaries. These may either be Dirichlet or Neumann or Mixed boundary conditions, which, respectively, specify either the field, or its normal derivative or a linear superposition of the two. Since in geoelectromagnetics, the source is of infinite extent, the primary field due to the source will remain constant within the domain. However, due to attenuation in the conducting earth, the field does tend to zero as $z \rightarrow \infty$. The anomalous field, on the other hand, tends to zero as one moves away from the anomalous target, i.e. as z or $y \rightarrow \pm \infty$. The boundary conditions are imposed on all the four sides of the domain. For B-polarization the magnetic field is already known at air-earth interface (vide equation 2.30). In E-polarization, to account for slow attenuation of anomalous field in air, a thick subregion must be introduced above the earth's surface. Dirichlet boundary conditions on all the domain boundaries are the simplest choice.

The EM boundary value problem, in its generality, possessed very few analytic solutions and that too for idealized conditions only. Hence, the general boundary value problem has to be solved using some numerical method which means that the domain boundaries must be placed at finite, albeit large, distances. However, one is never certain whether the domain is large enough to justify the use of Dirichlet boundary conditions defined for boundaries at infinity (Fig. 2.4a). Further, if the domain size is too large, then it becomes too demanding on the computing resources. Therefore, special boundary conditions have to be designed for placing domain boundaries at optimal distances.

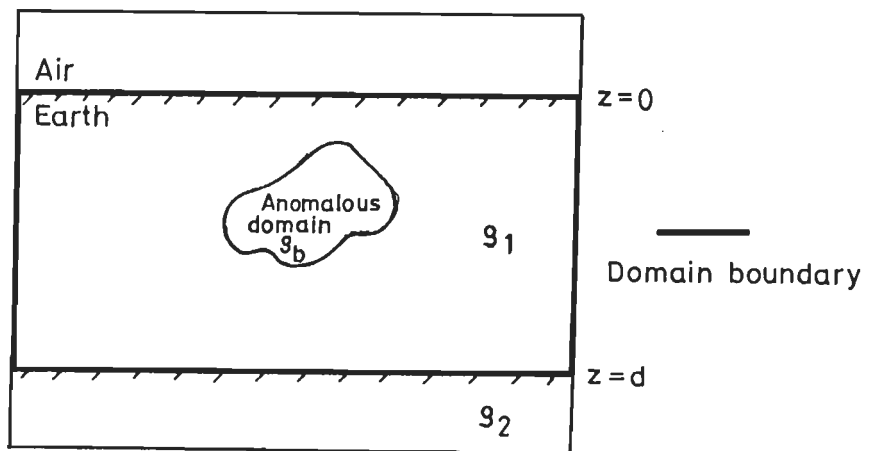
A numerical technique when applied for solving the EM boundary value problem reduces it to a matrix equation. Bigger the domain, larger the coefficient matrix size. The minimum possible domain size is the one when the domain boundaries are placed right over the anomalous target (Fig. 2.4b). Besides the gradual reduction in the matrix size, there results a reduction in sparsity structure of the coefficient matrix as the domain size is reduced. The two extremes, the boundaries at infinity and the boundaries at target surface, exhibit the trade-off between the domain size and sparsity structure of the coefficient matrix. For the two cases, the coefficient matrices are banded and full respectively.



(a)



(b)



(c)

Fig. 2.4 The three different choices of the modelling domain for boundary value problem. Domain boundaries (a) at infinity, (b) right over the target and (c) at optimal finite distances.

In the present work, we have followed an approach which is in between the two extremes. The boundaries are placed at finite distances by placing the top boundary at air-earth interface and the bottom one at an optimal vertical distance from the basement (Fig. 2.4c). This results in both numerical accuracy and optimization of the domain size. At the same time the banded structure of matrix is not significantly disturbed. The integrated effect of the region lying outside the domain is accounted through the designed boundary conditions.

2.5.2.1 The finite domain integrated boundary conditions - Integral form

Following Weaver (1994), the boundary conditions are designed for both the pairs of horizontal and vertical boundaries of the finite domain. For the horizontal boundaries, when the Helmholtz equation is solved in the overlying or the underlying half-space, it results in integral boundary conditions. Whereas an asymptotic expression for the integrals has been derived for the vertical boundaries.

The boundary condition, for a given horizontal interface $z = s$, has been derived here, in a generalized form, by solving the following governing differential equation in the overlying or underlying half-space

$$(\nabla^2 + k^2)F = 0. \quad \dots(2.41)$$

Here, F is either electric or magnetic field component. It may be alluded here that in air, $z < 0$, $k = 0$.

Since no lateral variations are present in the overlying/underlying domain, the equation (2.41) is solved in Fourier domain. The Fourier transform pair used, is defined as

$$\hat{F}(\eta) = \int_{-\infty}^{\infty} F(y) e^{i\eta y} dy \quad \dots(2.42a)$$

and

$$F(y) = \frac{1}{2\pi} \int_{-\infty}^{\infty} \hat{F}(\eta) e^{-i\eta y} d\eta. \quad \dots(2.42b)$$

Formulation of forward problem

source is present in air at $z = -\infty$, its effect has to be added to the field. The equation (2.53) should, therefore, be modified as

$$F'(y,0^-) = -i\omega B_0 - \frac{1}{\pi} \int_{-\infty}^{\infty} [F(v,0) - F(y,0)] \frac{1}{(v-y)^2} dv. \quad \dots(2.55)$$

In E-polarization these boundary conditions, termed as 'integral boundary conditions', are imposed on both top and bottom boundaries of the domain. However, in B-polarization these are applied only on the bottom boundary. On the top boundary placed at air-earth interface, the magnetic field being constant, Dirichlet boundary conditions are imposed. The integral boundary conditions are evaluated at the point lying just outside the study domain, 0^- or d^+ , and these are migrated to the corresponding points within the domain by invoking the interface boundary conditions on the tangential components of the fields. Unlike the tangential electric field which remains continuous, the tangential components of magnetic field are discontinuous across the interface whenever the surface currents are present.

2.5.2.2 The finite domain integrated boundary conditions - Series form

Brewitt-Taylor & Weaver (1976) derived the top integral boundary condition equation (2.55) using the anomalous magnetic scalar potential and the convolution theorem which led to Hilbert transform integral of the vertical magnetic field.

Another alternative derivation of these boundary conditions which in addition leads to the asymptotic boundary conditions on the vertical boundaries is presented here. In this approach, the field $\hat{F}(\eta,s)$ appearing in the integral of equation (2.47) is expanded in Maclaurin series.

Taking cue from Brewitt-Taylor & Weaver (1976), the field $\hat{F}(\eta,s)$ in equation (2.47), is expressed in terms of two well behaved functions $\hat{f}_1(\eta,s)$ and $\hat{f}_2(\eta,s)$ as,

$$\hat{F}(\eta,s) = -\left[\frac{\hat{f}_1(\eta,s)}{\eta} + \frac{\hat{f}_2(\eta,s)}{|\eta|} \right]. \quad \dots(2.56)$$

The equation (2.47) can now be rewritten as

$$F(y,z) = -\frac{1}{2\pi} \int_{-\infty}^{\infty} \left[\frac{\hat{f}_1(\eta,s)}{\eta} + \frac{\hat{f}_2(\eta,s)}{|\eta|} \right] \hat{P}(\eta,z-s) e^{-i\eta y} d\eta. \quad \dots(2.57)$$

The functions $\hat{f}_1(\eta,s)$ and $\hat{f}_2(\eta,s)$, being well behaved functions, can be expanded in Maclaurin series and thereby the equation (2.57) can be expressed as

$$F(y,z) = -\frac{1}{2\pi} \int_{-\infty}^{\infty} \left[\frac{1}{\eta} \sum_{j=0}^{\infty} \eta^j \frac{\hat{f}_1^{(j)}(0,s)}{j!} + \frac{1}{|\eta|} \sum_{j=0}^{\infty} \eta^j \frac{\hat{f}_2^{(j)}(0,s)}{j!} \right] \hat{P}(\eta,z-s) e^{-i\eta y} d\eta \dots(2.58)$$

On interchanging integration and summation operations in this equation, one gets

$$F(y,z) = -\frac{1}{2\pi} \sum_{j=0}^{\infty} \frac{\eta^j}{j!} \left[\frac{\hat{f}_1^{(j)}(0,s)}{\eta} + \frac{\hat{f}_2^{(j)}(0,s)}{|\eta|} \right] \int_{-\infty}^{\infty} \hat{P}(\eta,z-s) e^{-i\eta y} d\eta. \quad \dots(2.59)$$

The above series is integrated term by term and the integral T_j , in the general term of the series, can be expressed as

$$T_j = -(-i)^{j-1} \left[\hat{f}_1^{(j)} \frac{\partial^{j-1} p}{\partial y^{j-1}} + \hat{f}_2^{(j)} \frac{\partial^{j-1} q}{\partial y^{j-1}} \right] \quad \dots(2.60a)$$

where the functions p and q , related to the functions \hat{f}_1 and \hat{f}_2 respectively, are defined as

$$p(y,z) = \frac{1}{2\pi} \int_{-\infty}^{\infty} \hat{P}(\eta,z) e^{-i\eta y} d\eta \quad \dots(2.60b)$$

and

$$q(y,z) = \frac{1}{2\pi} \int_{-\infty}^{\infty} \text{sgn} \eta \hat{P}(\eta,z) e^{-i\eta y} d\eta. \quad \dots(2.60c)$$

The equation (2.59) is the desired boundary condition which can be imposed at any horizontal or vertical interface.

2.5.2.3 Asymptotic boundary conditions

In order to validate this formulation and to establish its utility, the boundary conditions are derived for the vertical boundaries and the results are matched with the asymptotic boundary conditions of Weaver & Brewitt-Taylor (1978). For a given polarization, the vertical boundaries are chosen with respect to the decay of anomalous field within the domain. In B-polarization these boundaries are close as the attenuation of anomalous field is rapid in the conducting earth. The position of these boundaries is crucial for E-polarization as the domain extends up in the air where the decay of anomalous field is very slow. This implies that the vertical boundaries valid for the conducting domain are to be pushed farther in air and this may lead to a very large domain of study. Therefore, the integral equation (2.59) is solved in air for E-polarization with E replacing F. From equation (2.21a), the vertical component of electric field, in air, is

$$\frac{\partial E}{\partial z} = -i \omega B_0. \quad \dots(2.61)$$

The integration of the above equation with respect to z gives

$$E = -i \omega B_0 z + C_1, \quad \dots(2.62)$$

where C_1 is the constant of integration. On taking care of the source field, from equation (2.59), the electric field in air is modified as

$$E(y,z) = C_1 - i \omega B_0 z - \frac{1}{2\pi} \sum_{j=0}^{\infty} \frac{\eta^j}{j!} \left[\frac{\hat{f}_1^{(j)}(0,s)}{\eta} + \frac{\hat{f}_2^{(j)}(0,s)}{|\eta|} \right] \int_{-\infty}^{\infty} e^{z|\eta|} e^{-i\eta y} d\eta. \quad \dots(2.63)$$

The term by term integration leads to the result

$$E(y,z) = C_1 - i \omega B_0 z - \frac{i}{\pi} f_1(0,0) \tan^{-1} \frac{y}{|z|} - \frac{f_2(0,0)}{2\pi} \log r^2 - \frac{1}{\pi} \frac{(zf_1' + iy f_2'(0,0))}{r^2} + O\left(\frac{1}{r^2}\right). \quad \dots(2.64)$$

This expression converges for large r, where $r = (y^2 + z^2)^{1/2}$ and thus, the higher order terms can be neglected. Here, a trade-off exists between accuracy and the number of higher order terms retained in the asymptotic approximation. The truncated expression is termed as asymptotic boundary condition (Brewitt-Taylor & Weaver, 1976) and can

be used for any horizontal interface, s . The generalized boundary condition valid with accuracy $O(1/r^n)$ was given by Zhdanov et al. (1982). At air-earth interface, $z = 0$, the equation (2.64) reduces to

$$E(y,0) = C_1 - \frac{i}{\pi} f_1(0,0) \frac{\pi}{2} \operatorname{sgn} y - \frac{i}{\pi} \frac{f_2'(0,0)}{y} + O\left(\frac{1}{r^2}\right). \quad \dots(2.65)$$

Using the condition that $E(y,0) \rightarrow E_{\pm}(0)$, when $y \rightarrow \pm \infty$, the constant and the coefficients are evaluated to be

$$C_1 = \frac{E_+(0) + E_-(0)}{2} = \bar{E}(0)$$

$$\text{and } f_1(0,0) = i[E_+(0) - E_-(0)] = i\Delta E(0),$$

where $E_-(0)$ and $E_+(0)$ are the 1-D fields at the left and right boundaries respectively. Substituting these values in equation (2.64) and neglecting terms of order higher than $(1/r)$, one gets

$$E(y,z) = \bar{E}(0) - i\omega B_0 z + \frac{\Delta E(0)}{\pi} \arctan \frac{y}{|z|}. \quad \dots(2.66)$$

This is the same asymptotic boundary condition as derived by Brewitt-Taylor & Weaver (1976). The first term becomes dominant as $z \rightarrow -\infty$ and for $y \rightarrow \pm \infty$ it reduces into the boundary condition for 1-D fields,

$$E(\pm\infty, z) = E_{\pm}(0) - i\omega B_0 z. \quad \dots(2.67)$$

A scrutiny of equation (2.64) suggests that by adding the derivatives of field in vertical and horizontal directions the terms of order $(1/r)$ will cancel out automatically. Therefore, the vertical and horizontal components of the electric field are computed by differentiating equation (2.64) with respect to z and y respectively as

$$\frac{\partial E}{\partial z} = -i\omega B_0 + \frac{i}{\pi} \frac{y}{r^2} f_1(0,0) + \frac{1}{\pi} \frac{f_2'(0,0)}{r^2} + O\left(\frac{1}{r^4}\right) \quad \dots(2.68a)$$

Fourier transform of equation (2.41) with respect to y is

$$\tilde{F}''(\eta, z) = c^2 \tilde{F}(\eta, z) \quad \dots(2.43)$$

where the prime (') indicates z derivative and the constant c^2 is given by

$$c^2 = (\eta^2 + i\alpha^2) \quad \dots(2.44)$$

$$\text{with } \alpha^2 = \omega \mu \sigma. \quad \dots(2.45)$$

It may be emphasized here that in air, where α is zero, c^2 reduces to η^2 . The solution of equation (2.43) is

$$\tilde{F}(\eta, z) = \tilde{F}(\eta, s) \hat{P}(\eta, z-s), \quad \dots(2.46a)$$

where $\hat{P}(\eta, z-s)$ is the solution defined as follows

$$\hat{P}(\eta, z-s) = e^{-(z-s) \gamma_0(\eta)} \quad \dots(2.46b)$$

with $\gamma_0(\eta) = c^2$.

The inverse Fourier transform of equation (2.46a) may be written as

$$F(y, z) = \frac{1}{2\pi} \int_{-\infty}^{\infty} \tilde{F}(\eta, s) \hat{P}(\eta, z-s) e^{i\eta y} d\eta. \quad \dots(2.47)$$

From the tabulated Fourier transforms (Erdelyi, 1954), the inverse Fourier transform $P(y, z)$ of $\hat{P}(\eta, z)$ is

$$P(y, z) = \frac{K_1[(y^2 + z^2)^{1/2} \alpha_0 \sqrt{i}]}{(y^2 + z^2)^{1/2}} \quad \dots(2.48)$$

where K_1 is the modified Bessel function of order 1. However, in air the equation (2.48) reduces to

$$P(y, z) = -\frac{1}{\pi} \frac{z}{y^2 + z^2}. \quad \dots(2.49)$$

Using the convolution theorem, equation (2.47) can be written as

$$F(y,z) = \frac{1}{2\pi} \int_{-\infty}^{\infty} F(v,s) P(y-v, z-s) dv. \quad \dots(2.50)$$

This equation provides the field value at interface $z = s$. However, the integral appearing in equation (2.50) becomes singular at $v = y$ when $z = s$. To circumvent this singularity, constant function $F(y,s)$ is subtracted from both the sides and, after using the fact that the integral of function $P(y,z)$ with respect to y is unity, one gets

$$F(y,z) - F(y,s) \int_{-\infty}^{\infty} P(y-v, z-s) dv = \frac{1}{2\pi} \int_{-\infty}^{\infty} [F(v,s) - F(y,s)] P(y-v, z-s) dv. \quad \dots(2.51)$$

Now at $z = s$, the left hand side of the above equation becomes indeterminate. This difficulty is overcome by differentiating the equation (2.51) with respect to z to get

$$F'(y,z) - \frac{\partial}{\partial z} [F(y,s) \int_{-\infty}^{\infty} P(y-v, z-s) dv] = \frac{1}{2\pi} \int_{-\infty}^{\infty} \frac{\partial}{\partial z} \{ [F(v,s) - F(y,s)] P(y-v, z-s) \} dv \quad \dots(2.52)$$

The differentiation in equation (2.52) gets simplified as the factor $(z-s)$ ensures that the term involving the derivative of integral vanishes when $z = s$ and the integral on right hand side is interpreted as Cauchy Principal value. This Neumann boundary condition can be imposed on any horizontal interface at the vertical level $z = s$. In particular, at $s = 0^-$, the air-earth interface, the equation (2.52) reduces to

$$F'(y,0^-) = \frac{1}{\pi} \int_{-\infty}^{\infty} [F(v,0) - F(y,0)] \frac{1}{(y-v)^2} dv. \quad \dots(2.53)$$

Similarly, at $s = d^+$, the bottom interface within the lower half-space, equation (2.52) becomes

$$F'(y,d^+) + \alpha_0 \sqrt{i} F(y,d^+) = \frac{\alpha_0 \sqrt{i}}{\pi} \int_{-\infty}^{\infty} [F(v,d^+) - F(y,d^+)] \frac{K_1(|y-v| \alpha_0 \sqrt{i})}{|y-v|} dv. \quad \dots(2.54)$$

These equations are valid only in the absence of sources. Since we assume that the

and

$$\frac{\partial E}{\partial y} = -\frac{i}{\pi} \frac{z f_1(0,0)}{r^2} - \frac{i}{\pi} \frac{f_2'(0,0)}{r^2} + O\left(\frac{1}{r^4}\right). \quad \dots(2.68b)$$

Multiplying equation (2.68a) by z and equation (2.68b) by y and adding the products into equation (2.64), one gets the following more accurate mixed boundary condition

$$\left(1 + y \frac{\partial}{\partial y} + z \frac{\partial}{\partial z}\right) E(y,z) \sim \bar{E}(0) - 2i\omega B_0 z + \frac{\Delta E(0)}{\pi} \arctan \frac{y}{|z|}. \quad \dots(2.69)$$

Here, the terms $O(1/r)$ get cancelled while the terms of $O(1/r^2)$ have been neglected. This is more precise as the error is $O(1/r^2)$. On the air-earth interface ($z = 0$) the equation (2.69) simplifies to

$$\left(1 + y \frac{\partial}{\partial y}\right) E(y,0) = E_x(0). \quad \dots(2.70)$$

The field decay is very rapid within the conductor, hence its second order derivative with respect to y can be neglected for large but finite y . In that case the governing E-polarization Helmholtz equation, for large y , becomes

$$E''(y,z) = -i\omega\mu\sigma E(y,z). \quad \dots(2.71)$$

The solution of this equation is

$$E(y,z) = E(y,0) e^{+kz} \quad \dots(2.72)$$

where $E(y,0)$ is the surface field. At large horizontal distances, the field behaves like that in a layered earth and becomes one-dimensional. The solution of equation (2.71), for $y = \pm\infty$, reduces to

$$E_x(z) = E_x(0) e^{+kz} \quad \dots(2.73)$$

where $E(\infty, z) = E_x(z)$ and $E(\infty, 0) = E_x(0)$.

Here, $E_{\pm}(0)$ and $E_{\pm}(z)$ are the 1-D field values at the surface and within the subsurface respectively. Inside the conductor, the field becomes near zero well before the domain boundaries. When the boundary is placed at infinity, the surface field values are $E_{\pm}(0)$ while for boundaries at finite distance these are $E(y,0)$ (Fig. 2.5). Therefore, the field within the conductor is scaled in terms of the modified surface field values as

$$E(y,z) = E(y,0) \frac{E_{\pm}(z)}{E_{\pm}(0)} \quad \dots(2.74)$$

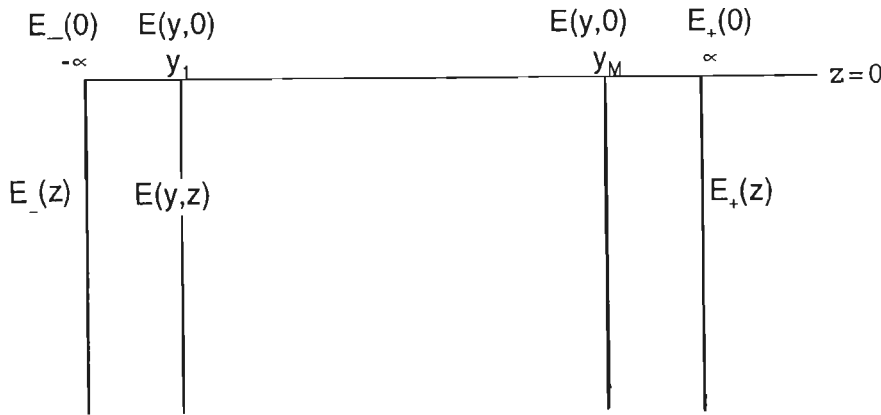


Fig. 2.5 Position of vertical boundaries when asymptotic boundary conditions are used.

This equation governs the field behaviour on the side boundaries of the domain. The equations, (2.69) and (2.74), constitute the asymptotic boundary conditions and result in reduction of the horizontal extent of the domain for E-polarization.

2.6 Solution of EM boundary value problem

The partial differential equation (2.22) or (2.23) together with the integral boundary conditions (2.54) and (2.55) and the asymptotic boundary conditions (2.69) and (2.74) define the complete EM boundary value problem. Analytic solutions of 2-D problem exist only for idealized situations, the non-idealized problems are solved, in general, using numerical methods. The implementation of a numerical method is discussed in detail in Chapter 4.

Any numerical method reduces the BVP to a matrix equation such as

$$CF = S, \quad \dots(2.75)$$

where \mathbf{C} is the coefficient matrix depending on the resistivity distribution, \mathbf{F} is the unknown field component vector and \mathbf{S} is the known right hand side vector depending upon the known boundary/1-D fields. For computation of right hand side vector \mathbf{S} , the 1-D solution at the side nodes should be known. Therefore, first the solution of 1-D EM problem must be obtained.

2.6.1 One-dimensional EM problem

The 1-D layered earth model is shown in Fig. 2.1a where resistivity is a function of only z . The layer resistivities are ρ_l 's, l being the layer index ranging from 1 to N .

The 1-D EM problem can be solved analytically. Several texts have presented alternative formulations of 1-D solutions, e.g. Keller & Frischknecht (1966), Wait (1982), Ward & Hohmann (1988) and Weaver (1994). Weaver (1994), in Appendix A of his book, has discussed the 1-D solution in compact form.

The basic steps of all these variations involve the development of a recurrence relation for computation of the response function at the layer interfaces. The values evaluated at the air-earth interface are scaled with respect to the constant magnetic field in air. Once the field is evaluated at the surface, it is computed at the other interfaces using the already developed recurrence relation in reverse sequence.

The derivation of the response function, in terms of a power series expansion, is presented here. It is the basis of the Straightforward Inversion Scheme (SIS) of Gupta et al. (1996), which is used in the present study for 1-D data inversion, discussed in Chapter 3.

The surface impedance of an N -layered Earth, resting on a half-space, is obtained by solving the appropriate 1-D Helmholtz equation, (2.24) or (2.25), subject to the boundary constraints of continuity of the tangential components of EM field at each interface. One can write the downward looking impedance Z_l (Pedersen & Hermance, 1986), defined as the ratio of horizontal orthogonal electric and magnetic field components, at the top of the l -th layer, in terms of the following recurrence relation

$$Z_l = z_{ol} \frac{1 + R_l e^{-2k_l d_l}}{1 - R_l e^{-2k_l d_l}}, \quad l = 1, 2, \dots, N-1 \quad \dots(2.76)$$

where R_l , the reflection function, is

$$R_l = \frac{z_{0l} - Z_{l+1}}{z_{0l} + Z_{l+1}} \quad \dots(2.77)$$

Here d_l is thickness of the l -th layer. The intrinsic impedance z_{0l} and the propagation constant k_l are defined as

$$z_{0l} = \sqrt{\frac{i \omega \mu}{\sigma_l}} \quad \dots(2.78)$$

and

$$k_l = \sqrt{i \omega \mu \sigma_l} \quad \dots(2.79)$$

The impedance at the surface of the deepest half-space is given by

$$Z_N = z_{0N} \quad \dots(2.80)$$

Let the thickness d_l of each layer be chosen in accordance with the equal penetration depth criterion introduced by Kunetz (1972) and Loewenthal (1975) and subsequently used by Parker (1980) to define his proxy parameter 'P' in H^+ formulation. This choice would result in $d_l/\delta_l = \alpha$, a constant. Here δ_l , the unit frequency skin depth of the l -th layer, is

$$\delta_l = \sqrt{\frac{\rho_l}{\pi \mu}} \quad \dots(2.81)$$

Now, let us define a parameter u as

$$u = e^{-2(1+i)\alpha\sqrt{f}}, \quad \omega = 2\pi f. \quad \dots(2.82)$$

where f is the linear frequency in Hertz. The two fold relations between impedance and reflection function, equations (2.76) and (2.77), can be reexpressed, after some algebraic steps, as the following recurrence relation for reflection function

$$R_{l-1} = \frac{R_l(u) + r_{l-1}}{1 + R_l(u) r_{l-1}} u \quad \dots(2.83)$$

$$\text{with } R_{N-1}(u) = 0, \quad R_N(u) = r_N u$$

$$\text{and } R_{N-1}(u) = \frac{r_N u + r_{N-1}}{1 + r_{N-1} r_N u} u. \quad \dots(2.84)$$

Here, r_l , the reflection coefficient at the l -th interface between the l -th and the $(l+1)$ -th layers, is given by

$$r_l = \frac{Z_{0l} - Z_{0,l+1}}{Z_{0l} + Z_{0,l+1}} = \frac{\sqrt{\rho_{l+1}} - \sqrt{\rho_l}}{\sqrt{\rho_{l+1}} + \sqrt{\rho_l}}. \quad \dots(2.85)$$

Now, since

$$|u| \leq 1 \quad \text{and} \quad |R_l| < 1$$

the reflection function $R_l(u)$ can be expressed in terms of a power series in u (Appendix 1) as

$$R_l(u) = \sum_{m=1}^{\infty} R_{lm} u^m. \quad \dots(2.86)$$

Using this expression for $R_l(u)$ and $R_{l-1}(u)$ in equation (2.83) and performing some simple algebraic steps (Appendix 1), the following recurrence relation between the coefficients of same powers of u in the power series of R_{l-1} and R_l is obtained

$$R_{l-1,1} = r_{l-1}, \quad \dots(2.87)$$

$$R_{l-1,m} = r_{l-1}^* R_{l,m-1} - r_{l-1} \sum_{k=2}^{m-1} R_{l,m-k} R_{l-1,k} \quad \dots(2.88)$$

$$\text{with } r_{l-1}^* = 1 - r_{l-1}^2.$$

The expression for $Z_l(u)$ at the top of the l -th layer can also be written as the following

power series

$$Z_l(u) = \sqrt{i\omega\mu} \sum_{m=0}^{\infty} c_{lm} u^m. \quad \dots(2.89)$$

For $m > 0$, the coefficients, c_{lm} , would be related to $R_{l,m}$ as

$$c_{lm} = \sum_{j=0}^{m-1} R_{l,m-j} C_{lj} \quad \dots(2.90)$$

whereas

$$c_{l0} = \sqrt{\rho_l} \quad \dots(2.91)$$

Equations (2.85) to (2.91) can be employed to compute the impedance at the air-earth interface corresponding to $l = 1$.

Since the coefficients c_{lm} 's are real, both the real and imaginary components of impedance can be obtained simply by retaining the real and imaginary parts of the term $\sqrt{(i\omega\mu)}u^m$ in the series. These can be respectively expressed as

$$[(i\omega\mu)^{1/2} u^m]_{Re} = \sqrt{\omega\mu/2} e^{-m\beta} [\cos m\beta + \sin m\beta] \quad \dots(2.92a)$$

and

$$[(i\omega\mu)^{1/2} u^m]_{Im} = -\sqrt{\omega\mu/2} e^{-m\beta} [\cos m\beta - \sin m\beta] \quad \dots(2.92b)$$

where $\beta = 2\alpha\sqrt{f}$.

Once Z_l 's are evaluated, the magnetic field at the air-earth interface can be computed by $F_1 = 2B_0$, where B_0 is the constant primary magnetic field in air. This magnetic field value can be used to compute orthogonal electric field component using Z_1 . These EM field components can be continued downward using Z_l 's in reverse sequence.

2.7 The response functions

The solution of EM boundary value problem provides the field values. The obtained field values can be transformed into other field components by using appropriate Maxwell's equations. These values measured at the surface of the earth are the observations/data for the EM inverse problem. Since observations do not evince any direct information about the physical property, i.e. electrical resistivity, derived observables (response functions) are obtained from these. Although these observables do not present a direct functional relationship with the subsurface resistivity, yet these do reflect the bulk information about the resistivity distribution. Such information is very helpful in designing the initial guess model for inversion. The explicit relations between several response functions and the field component values have been developed in literature (Cagniard, 1953; Schmucker, 1970).

The choice of response function is governed by the goal of study, whether the interest lies in lateral or vertical variation of resistivity. The spatial variation of resistivity can be studied in two modes. First is profiling, where, for a given frequency, the observations are taken at points along a profile. Second is sounding, where, for different frequencies the observations are taken at a single point. Profiling helps in delineating lateral variations while sounding deciphers the vertical variations of resistivity. To discover lateral variations at different depth levels, soundings must be performed at several points along a profile or alternatively profiling must be carried out at different frequencies. The Magneto-Tellurics (MT) uses sounding mode while Geomagnetic Depth Sounding (GDS) uses profiling mode for studying the subsurface resistivity distribution.

The details about these methods and their applications are available in standard references like Kaufman & Keller (1981), Rokityansky (1982), Berdichevsky & Zhdanov (1984), Nabighian (1988,1991) and Vozoff (1990, 1991).

The geoelectromagnetic methods use the natural earth's magnetic field with time periods ranging from fraction of a second to several years or the frequency ranging from 10^{-4} Hz to 10^4 Hz. The variations in the period ranging from 10 min to 24 hour are particularly suited for mapping electrical inhomogeneities in earth's crust and upper mantle. The MT and GDS methods employ the ratio of different field components as response functions. These functions are independent of strength of the

primary signal and are dependent only on the electrical properties of the earth. In MT, the response function, impedance, is the ratio of horizontal and mutually perpendicular electric and magnetic field components whereas in GDS it is the ratio of vertical to horizontal magnetic field components.

The definitions of these response functions, based on linearity of Maxwell's field equations, present the linear relationships between the different field components as

$$E_x = \alpha_x B_x + \beta_x B_y, \quad \dots(2.93a)$$

$$E_y = \alpha_y B_y + \beta_y B_x, \quad \dots(2.93b)$$

$$\text{and } E_z = \alpha_z B_x + \beta_z B_y. \quad \dots(2.93c)$$

where α 's and β 's are complex constants. The first two relations, equations (2.93a) and (2.93b), are used to derive the MT response function, whereas the third one, equation (2.93c), is used to define the GDS response function. The response functions used and their relations with resistivity are outlined here.

2.7.1 MT response function

The MT method was first described independently by Tikhonov (1950) and Cagniard (1953). Under the plane wave assumption, the ratio of the observed horizontal electric field (E_x or E_y) and the orthogonal horizontal magnetic field (B_y or B_x) at the surface of the layered earth is called the impedance

$$Z = \mu \frac{E_x}{B_y} = -\mu \frac{E_y}{B_x}. \quad \dots(2.94)$$

The impedance values are used to define the commonly used MT response function, apparent resistivity, as the resistivity of an equivalent half-space that gives rise to same impedance value. The apparent resistivity, ρ_a , and the impedance phase, ϕ , are respectively given by the relations

$$\rho_a = \frac{1}{\omega \mu} |Z|^2 \quad \dots(2.95)$$

and

$$\phi = \tan^{-1} \left[\frac{\text{Im}(Z)}{\text{Re}(Z)} \right]. \quad \dots(2.96)$$

with $0^\circ \leq \phi \leq 90^\circ$. For a homogeneous half-space, the phase of impedance will always be 45° . Further, the phase is more sensitive to change in frequency than the apparent resistivity.

The earth rarely behaves as a one-dimensional and isotropic model, therefore, the apparent resistivity and phase defined above have only limited utility. To describe anisotropy or higher dimensionality, Cantwell (1960) introduced a rank 2 impedance tensor Z as

$$\begin{pmatrix} E_x \\ E_y \end{pmatrix} = \frac{1}{\mu} \begin{pmatrix} Z_{xx} & Z_{xy} \\ Z_{yx} & Z_{yy} \end{pmatrix} \begin{pmatrix} B_x \\ B_y \end{pmatrix}, \quad \dots(2.97)$$

or

$$E = \frac{1}{\mu} [Z][B] \quad \dots(2.98)$$

where Z_{xy} , Z_{yx} are the principal and Z_{xx} , Z_{yy} are the additional impedances. For this definition to be compatible, in case of 1-D earth, with the formulation of Cagniard (1953)

$$Z_{xx} = Z_{yy} = 0$$

and

$$Z_{xy} = Z_{yx}$$

For 2-D model, the coordinate system is so chosen that the x- axis coincide with the strike direction of the model. In such cases, it is required to calculate apparent resistivity in two orthogonal directions (Reddy & Rankin, 1973),

$$\rho_{xy} = \frac{1}{\omega \mu} \left| \frac{E_x}{H_y} \right|^2 = \frac{\mu}{\omega} \left| \frac{E_x}{B_y} \right|^2 \quad \dots(2.99)$$

and

$$\rho_{yx} = \frac{1}{\omega \mu} \left| \frac{E_y}{H_x} \right|^2 = \frac{\mu}{\omega} \left| \frac{E_y}{B_x} \right|^2 \quad \dots(2.100)$$

Normally, the measurement axes are laid out in some predetermined directions so that the measurement coordinate axes will be at some arbitrary angle to the regional geologic strike. Therefore, it will be necessary to mathematically rotate, by seeking the minimum of additional impedances, the impedance tensor to the principal directions. In case of a perfectly two-dimensional model, Z_{xx} and Z_{yy} will be zero. Thus,

$$Z = \begin{pmatrix} 0 & Z_{xy} \\ Z_{yx} & 0 \end{pmatrix} \quad \dots(2.101)$$

2.7.2 GDS response function

The variations in geomagnetic field recorded on the surface are the sum of fields due to external and internal origins. The GDS method utilizes the temporal variations in internal field which consists of a normal and anomalous part, the latter being interpreted in terms of resistivity signatures. However, the anomalies observed in the variation studies may be due to either external or internal sources. This forms the basis and objective of GDS (Rokityansky, 1982).

In 1-D earth, where lateral variations are not present, the observed fields are the vector sum of external and internal fields and referred to as normal field components (Schmucker, 1970). In the most simple form the effect of local resistivity anomalies shows up in vertical component as distortion effects are superimposed on the near vanishing 'normal' B_z field. Although anomalies of comparable magnitude are produced in x and y components, yet these are small in proportion to the background normal fields and hence cannot be easily seen. B_z is a totally anomalous field being zero for 1-D models. For 2-D structures, since the B_x component does not exist for E-polarization, the equation (2.93c) gets simplified as

$$B_z = \beta_z B_y \quad \dots(2.102)$$

This equation defines the two-dimensional GDS response function known as Induction

vector, given by

$$I_{zy} = -\frac{B_z}{B_y} \quad \dots(2.103)$$

For 3-D models the real and imaginary parts of the complex constants α and β are combined to form 2-D vectors called the magnetic response function. These vectors, termed as 'induction arrows' or 'perturbation vectors', are drawn as lines on geographic maps and contain information about the depth and lateral extent of the conductive structure.

2.7.3 Transformation matrices

It may be added here that the derived response functions can be written in matrix notation as

$$R = TF, \quad \dots(2.104)$$

where R is the derived response function vector, T is the transformation matrix derived from the relationship between the response function and the respective field components and F is the corresponding field component vector.

2.8 Closure

The governing Helmholtz equations and the requisite boundary conditions define an EM boundary value problem which is solved using some numerical technique. The solution in the form of field values/components do not contain direct information about the resistivity, therefore, response functions are derived from these. The derived response functions will be used as data for inversion as discussed in Chapter 3.

**FORMULATION OF
EM INVERSE PROBLEM**

3.1 General

Data inversion is an educated interpretation exercise. It is more objective than the simple quantitative data interpretation where one is only interested in a model whose computed response fits the observed response. The aim of geophysical data inversion is not only to infer, from a given set of observations, as much information about the earth system as possible, but also to appraise the quality of inference together with its level of confidence. For undertaking parametric inversion, the system is defined in terms of the data and an operator. The latter is characterized by physics of the problem and distribution of physical parameters of the model. The interrelationship of data and operator governs the system characteristics.

In EM data inversion, the observed field values are interpreted to estimate the unknown subsurface spatial variation of resistivity. The resistivity within the earth is a continuously varying function $\rho(x,y,z)$. Since it can vary arbitrarily, in general, infinite parameters are needed to describe it precisely (Parker, 1977). The retrieval of general 3-D variation of resistivity, from the 2-D data procured over the air-earth surface, is not feasible. According to Bailey (1970) and Weidelt (1972), only 1-D EM problem can theoretically have a unique solution under idealized conditions and that too when the data is defined as an exact distribution. However, the observations will always be finite in number. As a result, the EM inverse problem becomes a grossly underdetermined one. This implies that there may exist an infinity of models whose response will match the observed data equally well. Such an eventuality is termed as 'non-uniqueness'.

The observations are, in practice, corrupted with natural, observational and instrumental noise. These erroneous observations may lead to inconsistency and instability in the system. The inconsistency arises as a result of incompatibility of the chosen model with the noisy data set. For an inconsistent system, the exact solution does not exist. The instability is a characteristic of the operator which gets highlighted in the presence of erroneous data. Due to instability, small errors in data may lead to large errors in estimated parameters. Therefore, the non-uniqueness, inconsistency and instability of the inverse problem suggest that the system under study is a degenerate one.

On every count, postulated by Hadamard (1932) to define a well-posed problem, the EM inverse problem is an ill-posed one due to insufficient and inaccurate data (Jackson, 1972). The goal of data inversion is to design algorithms which can alleviate this ill-posedness and yield approximate solution of such problems. Some of the techniques, used for this purpose, are discussed here.

3.2 Alleviation of ill-posedness

The exact solution of an ill-posed EM inverse problem may not exist. If it is so, the next best step is to look for schemes which can provide an approximate solution having essential features of the exact solution. In such schemes an attempt is made to regularize the problem. For regularization the ill-posed problem is replaced by an equivalent well-posed one which possesses a solution that can be treated as an approximate but reasonable solution of the original problem. Techniques used for the regularization are widely discussed in literature, particularly in the standard references like Backus & Gilbert (1967,1970), Sabatier (1974), Parker (1983), Tikhonov & Arsenin (1977), Twomey (1977), Parker & Whaler (1981), Menke (1984), Oldenburg (1984), Tarantola (1987), Hohmann & Raiche (1988), Hjelt (1992), Treitel et al. (1993), Meju (1994) and Oldenburg (1994). A good review of the techniques used for solving EM inverse problem is given by Sarkar et al. (1981b).

Various schemes developed for solving ill-posed problem are, in general, introduced in matrix notations. For a given problem, let m and n be the number of observations and unknown parameters respectively. The inverse problem can be expressed in matrix form as

$$Ax = b.$$

...(3.1)



247427

Here, \mathbf{A} is the $m \times n$ coefficient matrix which simulates physics of the problem, \mathbf{x} is the $n \times 1$ unknown parameter vector and \mathbf{b} is the $m \times 1$ known observation vector. The equation (3.1) can be interpreted as the mapping, by the matrix operator \mathbf{A} , of an n -dimensional vector \mathbf{x} to the m -dimensional vector \mathbf{b} . The solution of this problem seeks the operator which would map the right hand side vector \mathbf{b} to an n -dimensional vector \mathbf{x} .

The inverse problem can be solved when its inconsistency, non-uniqueness and instability are controlled. These negative characteristics of the system may exist either concurrently or one at a time. The means that can be employed to handle these features are discussed one by one.

3.2.1 Inconsistency

The inconsistency present in a system is basically an interplay of the coefficient matrix \mathbf{A} and the data vector \mathbf{b} . If the vector \mathbf{b} can not be expressed as a linear superposition of the column vectors of the matrix \mathbf{A} then inconsistency arises. To handle it, all one can do is to lower the acceptance level or quality of acceptable solution.

3.2.2 Non-uniqueness

The quality of inversion largely depends on parametrization that is on the choice of model parameters and the derived data needed to represent the model. The choice of model is always made on the basis of *a priori* information. The *a priori* knowledge in EM data inversion is derived from the geological information or from the results of other geophysical methods. This helps in better approximation of real earth models and, in turn, in improved interpretation (Jackson, 1979; Whittall, 1986). The non-uniqueness of EM inverse problem can be rendered by restricting the complexity of earth models. A class of simplified models, like a layered earth or the regular well shaped body, can be used as an approximation of the real structures. A 3-D model can be approximated by a 2-D or 1-D model depending upon the variation of physical parameters and the source characteristics. The reduction in dimensionality of the model results in smaller parameter space. The parametrization of real earth in terms of finite dimensional models helps in reducing the non-uniqueness.

3.2.3 Instability

The instability in a system implies that small changes in data may lead to large changes in parameter values. Basically, the root cause of instability is ill-conditioning of the coefficient matrix. An ill-conditioned matrix has a large condition number, defined as the ratio of the largest to smallest eigenvalue. It may be emphasized here that although instability is inherent in the system, yet it is reflected only in the presence of errors in computations and/or data.

In geoelectromagnetics, the equivalence is a commonly encountered problem for layered earth models. Under equivalence, one can not determine the layer resistivity and thickness independently, however, their product can accurately be estimated. Due to this layer parameter coupling, the poor resolvability of individual parameters leads to instability. However, the resolution of product itself, which represents a bulk parameter, reduces both the non-uniqueness and instability.

Some of these measures of alleviating ill-posedness of the inverse problem have been employed in the formulations of the 1-D/2-D EM inverse problem presented here.

3.3 Classification of inverse problems

The system defined by equation (3.1) can be classified on the basis of rank of the matrix **A**. The rank, p , is defined as the maximum number of independent rows or columns of the matrix. If the rank is equal to the minimum of m and n , the system is called 'full ranked', else it is termed 'rank deficient'. In simplified form, it can be stated that for

full ranked system $p = \min (m,n)$

while for

rank deficient system $p < \min (m,n)$.

An alternative classification of the system (3.1) can be given in terms of the relative values of m and n . The categorisation can be listed as

- (1) Evendetermined for $m = n$,
- (2) Overdetermined for $m > n$ and
- (3) Underdetermined for $m < n$.

For a full ranked system the evendetermined, overdetermined and underdetermined

cases are termed as 'perfectly even-determined', 'perfectly over-determined' and 'perfectly under-determined' respectively. Since the exact solution exists only for the perfectly even-determined case, one has to look for approximate solutions for the remaining cases. For the perfectly over-determined and under-determined cases, operationally one has to look for operators which can transform the rectangular coefficient matrix to a full ranked square one. Instead of listing the operational steps of various inverses, the logical sequence of obtaining these inverses is presented here.

3.3.1 Least square inverse

A perfectly over-determined system may suffer from inconsistency. The inconsistency may be ascertained by determining the rank of augmented matrix $[A|b]$. If it is smaller than the rank of original matrix A then the system is inconsistent. In such a case, instead of looking for zero misfit, a minimum error solution is sought. The model parameter vector, which minimizes the misfit between the model response and the observations, is accepted as the desired solution. For this purpose, the norm, ϕ , of the residual vector, e , is minimized. The minimization problem can be stated as

$$\text{minimize } \phi_1 = e^T e, \quad \dots(3.2)$$

$$\text{where } e = b - Ax. \quad \dots(3.3)$$

The least square solution of equation (3.1), obtained by minimization of ϕ_1 with respect to the components of the unknown vector x , can be written as

$$x = A_i^{-1} b, \quad \dots(3.4)$$

$$\text{where } A_i^{-1} = (A^T A)^{-1} A^T \quad \dots(3.5)$$

is termed as 'least square inverse' of matrix A (Lawson & Hanson, 1974). Here, the superscript T and -1 stand for the matrix transpose and inverse operations respectively. Generally the L_2 norm is used as it results in a linear system of equations. Further, it yields the best estimate when the error follows Gaussian distribution. It may be emphasized again that the least square solution is a result of lowering the acceptable level of accuracy of the solution.

3.3.2 Minimum norm inverse

For the perfectly underdetermined system, the observations do not provide enough information for unique determination of all the model parameters. As a result, an infinity of solutions will exist for such a system. Therefore, some extraneous constraints need be applied to seek a unique solution. For this purpose, the length of the solution vector \mathbf{x} is commonly minimized, subject to the constraint that the solution satisfies the matrix equation (3.1). This constrained minimization problem can be stated as

$$\text{minimize } \phi_m = \mathbf{x}^T \mathbf{x}, \quad \dots(3.6)$$

$$\text{subject to } \mathbf{Ax} = \mathbf{b}. \quad \dots(3.7)$$

The minimum norm solution is obtained as

$$\mathbf{x} = \mathbf{A}_m^{-1} \mathbf{b}, \quad \dots(3.8)$$

$$\text{where } \mathbf{A}_m^{-1} = \mathbf{A}^T (\mathbf{AA}^T)^{-1} \quad \dots(3.9)$$

is the minimum norm inverse of matrix \mathbf{A} . For the constrained minimization of the objective function, ϕ_m , the Lagrange's method of undetermined multipliers is used. The obtained solution is unique with respect to the chosen objective function.

3.3.3 Regularized inverses

The above two solutions exist only for the full ranked systems for which the respective coefficient matrix products, $\mathbf{A}^T \mathbf{A}$ and \mathbf{AA}^T , appearing in their definitions, are non-singular.

A rank deficient system is overdetermined or underdetermined, depending upon the values of m and n . However, inherently it is underdetermined as $p < n$. As a result, the inverse problem is neither completely overdetermined nor completely underdetermined. It may be termed as a 'mixed determined' problem for which one can neither seek the least square nor the minimum norm solution. For its solution, a new objective function, ϕ_r , which minimizes a combination of the norms of error and solution vectors, is defined as

$$\phi_r = \epsilon (\mathbf{e}^T \mathbf{e}) + (1 - \epsilon) \mathbf{x}^T \mathbf{x}. \quad \dots(3.10)$$

In equation (3.10), ϵ is a trade-off parameter that determines the relative importance being given to the minimization of error or solution vector norms. The value of ϵ can vary between 0 and 1, leading to the minimum norm and the least square solutions for these two extreme values. The objective function (3.10) can be written, in modified form, as

$$\phi_{rl} = \mathbf{e}^T \mathbf{e} + \lambda^2 \mathbf{x}^T \mathbf{x} \quad \dots(3.11)$$

or

$$\phi_{rm} = v \mathbf{e}^T \mathbf{e} + \mathbf{x}^T \mathbf{x}, \quad \dots(3.12)$$

$$\text{where } \lambda^2 = \frac{(1 - \epsilon)}{\epsilon} \text{ and } v^2 = \frac{1}{\lambda^2}.$$

Equation (3.1), when solved using this objective function, provides a solution analogous to the solution for perfectly overdetermined and perfectly underdetermined cases respectively, as

$$\mathbf{x} = (\mathbf{A}^T \mathbf{A} + \lambda^2 \mathbf{I})^{-1} \mathbf{A}^T \mathbf{b} \quad \dots(3.13)$$

and

$$\mathbf{x} = \mathbf{A}^T (\mathbf{A} \mathbf{A}^T + v^2 \mathbf{I})^{-1} \mathbf{b}. \quad \dots(3.14)$$

In the above expressions the parameter λ or v play the role of a damping factor which prevents the unbounded oscillations in the solution. Therefore, the method is also known as 'Damped least square' or 'Damped minimum norm' method. This method was independently developed by Tikhonov, Phillips, Twomey and Marquardt in early sixties and is popularly known as 'Ridge-regression' or 'Marquardt method' in geophysical literature with λ or v being termed 'Marquardt parameter' (Marquardt, 1970). As such, there is no precise criterion for choosing λ or v and, in general, the experimental experiences are used to determine it. Initially one starts with a large value of λ or v and keep on decreasing it till high oscillations set in the solution or the desired numerical accuracy is achieved. In the former case, the solution corresponding to the previous value of λ or v is accepted.

The ridge-regression method can also be used for full rank systems when the coefficient matrix is ill-conditioned. The impact of small eigenvalues gets reduced by

the addition of Marquardt parameter λ or ν to these. The enhanced eigenvalues result in improved stability. In a similar manner, a rank deficient system can also be solved using this method.

3.3.4 Weighted inverses

Some observations are, in general, more accurate than the others. This *a priori* knowledge can be used in assigning weights to scale the observations accordingly. The more accurate observations will be assigned higher weights in comparison to the less accurate ones. The model parameters can be obtained by introducing weighting matrices, \mathbf{W}_e for error vector and \mathbf{W}_m for solution vector respectively. The inverse of data error co-variance matrix, whenever available, is the most widely used weighting matrix \mathbf{W}_e . If not available, one may employ a diagonal matrix with inverse of data errors as the diagonal entries. The \mathbf{W}_m is constructed on the basis of the smoothness or other constraints imposed on the solution vector. The new objective functions, weighted residual or weighted length, are respectively defined as

$$\phi_{wl} = \mathbf{e}^T \mathbf{W}_e \mathbf{e} \quad \dots(3.15)$$

and

$$\phi_{wm} = \mathbf{x}^T \mathbf{W}_m \mathbf{x} \quad \dots(3.16)$$

The solution corresponding to these objective functions, termed as the 'weighted least square' and the 'weighted minimum norm' solutions, are

$$\mathbf{x} = (\mathbf{A}^T \mathbf{W}_e \mathbf{A})^{-1} \mathbf{A}^T \mathbf{W}_e \mathbf{b} \quad \dots(3.17)$$

and

$$\mathbf{x} = \mathbf{W}_m \mathbf{A}^T (\mathbf{A} \mathbf{W}_m \mathbf{A}^T)^{-1} \mathbf{b} \quad \dots(3.18)$$

Analogous to the weighted least square and weighted minimum norm solutions for the perfectly overdetermined and underdetermined cases, the weighting can also be applied to the ridge-regressed solutions. The solutions for these two cases, depending on the values of m and n , will be

$$\mathbf{x} = [\mathbf{A}^T \mathbf{W}_e \mathbf{A} + \lambda^2 \mathbf{W}_m]^{-1} \mathbf{A}^T \mathbf{W}_e \mathbf{b} \quad \dots(3.19)$$

and

$$\mathbf{x} = \mathbf{W}_m^{-1} \mathbf{A}^T [\mathbf{A} \mathbf{W}_m^{-1} \mathbf{A}^T + \lambda^2 \mathbf{W}_e^{-1}]^{-1} \mathbf{b} \quad \dots(3.20)$$

The special smoothness features desired in solution can be achieved by minimizing the norm of higher order differences of \mathbf{x} components. Higher the order of difference, smoother the solution. The trade-off then is between smoothness and finer details of the solution. Ridge-regression is having simplest smoothing function where norm of all the difference vectors of the unknown vector components is zero. In Occam's inversion, the norm of first order differences are minimized (Constable et al., 1987). Tikhonov regularization provides the flexibility that any *a priori* knowledge of system can also be translated in terms of a function and used as a constraint. All these inverses are one or the other kind of generalized inverses of matrix \mathbf{A} (Rao & Mitra, 1971).

3.4 Appraisal of solution

Apart from deciphering the information about the model parameters, one also wants to know about the resolving power of data, types of models that satisfy the data and the effect of inaccuracies present in data. The resolution and resolvability of a model provide its appraisal (Parker, 1980; Oldenburg, 1984; Hohmann & Raiche, 1988). Its main purpose is to find the unique properties of all acceptable solutions that fit the observations at an acceptable level of confidence.

3.4.1 Measures of misfit

The simplest and most popular measure of quality of inversion is the degree of misfit between the computed and the observed responses. Smaller the misfit, better the estimate. For estimation of misfit, the commonly used parameters are the absolute root mean square (rms) error and the relative rms error between the observed data and the computed data, respectively, defined as

$$\epsilon_a^2 = \sum_{i=1}^M [F_i^o - F_i^c]^2 / M \quad \dots(3.21)$$

and

$$\epsilon_r^2 = \sum_{i=1}^M [(F_i^o - F_i^c) / F_i^o]^2 / M. \quad \dots(3.22)$$

After computing this misfit, the quality of model is appraised by undertaking hypothesis testing, using the significance tests like the F-test, Chi-square test. Quality or effectiveness of the solution is determined by the variance of the parameters.

Generally, the model which yields the best fit with the observed response is accepted. But the mathematically best fit model may not ensure a geologically reasonable model. If the model is geologically irrelevant, the parameters extracted from it will be meaningless.

3.4.2 System characteristics matrices

The inherent characteristics of the system can be deciphered by studying the behaviour of information density and resolution matrices. The quality of solution, of an iterative method, largely depends on the choice of starting model. Thus, the behaviour of information and resolution density matrix can help in appraisal of the solution.

3.4.2.1 Information density matrix

The information density or data resolution matrix, \mathbf{S}_m , characterizes the m -dimensional data space and is defined as

$$\mathbf{S}_m = \mathbf{A} \mathbf{A}_g^{-1}. \quad \dots(3.23)$$

Here \mathbf{A}_g^{-1} is any one of the generalized inverses of the matrix \mathbf{A} . This $m \times m$ square matrix is a measure of independence of data. It describes the structure of misfit between the computed and the observed data. If $\mathbf{S}_m = \mathbf{I}_m$, \mathbf{I}_m being the $m \times m$ identity matrix, all data values are independently contributing and the misfit is zero. This implies the exact matching of computed response with the data.

3.4.2.2 Resolution density matrix

The model resolution matrix \mathbf{R}_n , characterizing the n -dimensional parameter space, is defined as

$$\mathbf{R}_n = \mathbf{A}_g^{-1} \mathbf{A}. \quad \dots(3.24)$$

The matrix \mathbf{R}_n is a measure of resolvability of parameter. When $\mathbf{R}_n = \mathbf{I}_n$, each model parameter is uniquely resolved. If \mathbf{R}_n is not an identity matrix, then estimates of model parameters are the weighted averages of a set of true parameters.

3.4.2.3 Dirichlet spread function

Another measure of quality is the spread of diagonals of resolution matrices. The resolution spread, based on the L_2 norm of differences between resolution matrix and the identity matrix, is termed as 'Dirichlet spread function'. For ideal case, when $\mathbf{R}_n = \mathbf{I}$, $\text{spread}(\mathbf{R}_n) = 0$.

3.5 Experiment designs

The matrices \mathbf{S}_m and \mathbf{R}_n highlight the characteristics of the system. Their deviation from corresponding identity matrices gives an idea as to how much confidence one can put in the system. If $\mathbf{S}_m(\mathbf{R}_n)$ is a diagonally dominant matrix with few adjacent off-diagonal elements being non-zero, then all the data values(parameters) are significantly(uniquely) contributing(resolved), but these are not entirely independent. If $\mathbf{S}_m(\mathbf{R}_n)$ is not diagonally dominant then the data(parameter) is not able to contribute(get resolved) significantly (uniquely) to(by) the interpretation based on current model and these are not independent also. The insignificant(unimportant) and the irrelevant data(parameters) result from ill-posedness of the inverse problem.

The information or the resolving power of data can be seen through these matrices without actually performing the experiment. Therefore, these matrices can be fruitfully used in experiment design exercises to improve the quality of resolution of procured data.

3.6 Solution of EM inverse problem

The EM forward problem comprises computation of the response of a known model with prescribed resistivities. The Helmholtz equation, which governs the EM phenomenon, is solved using finite difference method and the final matrix equation is

$$\mathbf{CF} = \mathbf{S}. \quad \dots(3.25)$$

Here, \mathbf{C} is the coefficient matrix depending on geometry and resistivity of the model, \mathbf{F} is the unknown field component and \mathbf{S} is the known right hand side vector derived from the boundary conditions. The field value, and therefore the response function derived from it, is a non-linear function of resistivity. Hence, the EM data inversion, which is evaluation of model resistivity parameters from a given set of observations, is a non-linear problem.

3.6.1 Different methodologies

The non-linear inverse problem can be solved using any one of the three approaches. First, transform the non-linear problem into a linear one and solve for the transformed parameters using a standard linear method. Second, quasi-linearize the non-linear problem to set up a linear problem in perturbations and solve it iteratively.

Lastly, use non-linear methods, like simulated annealing and genetic algorithm, for solving the non-linear inverse problem. The inversion of transformed linear problem is a single step procedure. For quasi-linearized and non-linear methods, however, the procedure becomes iterative as the current model is successively improved until the error measure is small and parameters are stable.

3.6.1.1 Trial and error method

The trial and error or curve matching method of quantitative data interpretation is not only one of the earliest ones but still the widely used one. Starting with a general model, the parameters are judiciously selected from a set of predetermined values. If the agreement between the computed and the observed response is good, then the model is accepted. In case of poor agreement the model is updated according to drawn conclusions. This process continues till one gets the good fit. Whereas in data inversion, the selection is based on certain criteria. The quasi-linearization method as well as the other non-linear methods which are used for inversion, can all be viewed as guided search methods.

3.6.1.2 Non-linear methods

The non-linear methods, i.e. simulated annealing, genetic algorithm (Goldberg, 1989), are still in developmental stage. Dosso & Oldenburg (1991) used simulated annealing for construction of extremal models for fitting 1-D models to MT data. Schultz et al. (1994) used genetic algorithm to explore the possibility of solution of 1-D MT problem. These algorithms can not gain popularity due to their poor economic viability.

3.6.1.3 Direct and quasi-linearized methods

The direct algorithm of transforming the non-linear problem to a linear one scores over the iterative ones, as it does not need an educated guess of the model parameters to start the inversion process. In iterative methods, closer the initial guess to the true model, faster is the convergence. Therefore all the available *a priori* information is used while choosing the initial guess model. In direct methods, however, the *a priori* information can not be incorporated directly. It has to be incorporated in the form of a constraint and this necessitates modification of the algorithm. Hence, choice of the inversion method, direct or iterative, is made keeping in view their respective merits and demerits. Since the initial guess model controls the quality of inversion in iterative algorithms, a proper choice of model and its parameter set will lead to a stable solution.

A 2-D inversion algorithm needs a good 1-D model for implementing boundary conditions. For generating initial models, a 1-D inversion algorithm Straightforward Inversion Scheme (SIS) (Gupta et al., 1996) has been adapted for the present work. In SIS, the non-linear problem is solved by transforming it to a linear one. The basic formulations of the two algorithms SIS and **EM2INV** are discussed here.

3.6.2 SIS algorithm for 1-D inversion

The SIS works with a layered earth model. It reduces the degree of non-uniqueness by choosing a model with layers of uniform thickness, thickness being expressed in units of skin depth. This way the layer thickness variable is eliminated. Further the elimination of layer thickness parameter, appearing in exponential term of the forward recurrence relation, alleviates the degree of non-linearity. The starting point of the algorithm is recurrence relation for the reflection function (vide equation 2.83) restated below

$$R_{l-1} = \frac{R_l(u) + r_{l-1}}{1 + R_l(u)r_{l-1}}u. \quad \dots(3.26)$$

Here, u , defined as

$$u = e^{-2(1+i)af}, \quad \dots(3.27)$$

is used as the variable of the following power series expression used in Chapter 2 to compute impedance at the air-earth interface,

$$Z_l(u) = \sqrt{i\omega\mu} \sum_{m=0}^{\infty} c_{lm} u^m. \quad \dots(3.28)$$

This relation can be rewritten in a matrix form as

$$Uc = Z_l, \quad \dots(3.29)$$

where the coefficient matrix,

$$U = \sqrt{i\omega\mu} \begin{bmatrix} 1 & u_1 & u_1^2 & \dots & u_1^j & \dots \\ 1 & u_2 & u_2^2 & \dots & u_2^j & \dots \\ \vdots & \vdots & \vdots & & \vdots & \dots \\ 1 & u_j & u_j^2 & \dots & u_j^j & \dots \\ \vdots & \vdots & \vdots & & \vdots & \dots \\ 1 & u_m & u_m^2 & \dots & u_m^j & \dots \end{bmatrix},$$

$$\text{or } U_{ij} = \sqrt{i \omega \mu} \cdot u_j^{i-1}$$

the unknown column vector,

$$\mathbf{c} = [c_{j0}, c_{j1}, c_{j2}, \dots, c_{jm}, \dots]^T$$

and the known impedance vector,

$$\mathbf{Z}_j = [Z_j(u_1), Z_j(u_2), \dots, Z_j(u_M)]^T.$$

The minimum norm solution of equation (3.29) can be written as

$$\hat{\mathbf{c}} = \mathbf{U}^T \mathbf{W} \quad \dots(3.30)$$

with

$$\mathbf{W} = [\mathbf{U} \mathbf{U}^T]^{-1} \mathbf{Z}_j \quad \dots(3.31)$$

The estimated solution vector \mathbf{c} is used to assess the quality of inverse solution by first computing the response vector

$$\hat{\mathbf{Z}}_j = \mathbf{U} \hat{\mathbf{c}} \quad \dots(3.32)$$

and then the misfit parameters absolute rms error ϵ_a and the relative rms error ϵ_r between the observed data Z_j and the predicted data \hat{Z}_j . The equation (3.30) will yield a unique solution only when equation (3.29) is consistent and the matrix \mathbf{U} is full rank. However, in the case of field data, where the inadequacy and the random errors of measurement make consistency impossible, one may seek a regularized minimum norm solution given by

$$\hat{\mathbf{c}} = \mathbf{U}^T (\mathbf{U} \mathbf{U}^T + \mathbf{E})^{-1} \mathbf{Z}_j \quad \dots(3.33)$$

where \mathbf{E} is the data error co-variance matrix. In case the error co-variance matrix is not available it can be approximated by $e^2 \mathbf{I}$, e being the average noise to signal ratio. Equation (3.30) provides that

$$c_{j0} = \sum_{l=1}^N \sqrt{i \omega \mu_l} w_l = \sqrt{\rho_l} \quad \dots(3.34)$$

and

$$c_{jm} = \sum_l U_{l,m+1} w_l, \quad m > 0. \quad \dots(3.35)$$

It may be added here that N is a sufficiently large number (between 1000-2000) so that the contribution of remainder terms of the power series is negligible. The forward recurrence relation between the coefficients of power series for two layers is rewritten as

$$c_{l,m} = R_{l,m} c_{l,0} + R_{l,m-1} c_{l,1} + R_{l,m-2} c_{l,2} + \dots + R_{l,2} c_{l,m-2} + R_{l,1} c_{l,m-1}. \quad \dots(3.36)$$

The coefficients R_{lm} can be related to c_{lm} from above equation as

$$2\sqrt{\rho_1} R_{l,m} = c_{l,m} R_{l,0} - c_{l,m-1} R_{l,1} - c_{l,m-2} R_{l,2} - \dots - c_{l,2} R_{l,m-2} - c_{l,1} R_{l,m-1}. \quad \dots(3.37)$$

Consequently, the following inverse recurrence relation is developed through equation (2.88)

$$R_{l,m-1} = \frac{1}{r_{l-1}^*} [R_{l-1,m} + r_{l-1} \sum_{k=2}^{m-1} R_{l,m-k} R_{l-1,k}]. \quad \dots(3.38)$$

The various reflection coefficients, r_l and the layer resistivities ρ_l , can be obtained as

$$r_l = R_{l,1} \quad \dots(3.39)$$

and

$$\rho_{l+1} = \left[\frac{1 + R_{l,1}}{1 - R_{l,1}} \right]^2 \rho_l. \quad \dots(3.40)$$

Once the resistivity of the l -th layer is obtained, its thickness can readily be computed through the expression

$$d_l = \alpha \delta_l = \alpha \sqrt{\rho_l / \pi \mu} \quad \dots(3.41)$$

where α is layer thickness unit parameter defined in Chapter 2 (vide equation 2.45). Thus, the solution of the inverse MT problem is completely obtained through equations (3.29) to (3.41), in a linear fashion, without any initial model. However, the value of α has to be judiciously chosen keeping in mind the expected thickness and resistivity of the target layer which ought to be resolved.

In order to estimate the quality of inverted resistivity model, the misfit ϵ_l between its response \hat{Z}_l and the observation Z_l is computed in a manner similar to that used for ϵ_r . The vector \mathbf{c} , obtained as the solution of equation (3.29) or (3.33), can be looked upon as the initial condition of an initial value problem. This means that as the

solution is continued downward, the error in \mathbf{c} will propagate and may get enhanced. This error propagation may sometimes lead to non-physical reflection coefficients lying outside the $(-1,1)$ interval. This should always be taken as a warning signal, that no further downward continuation of resistivity profile is possible. Such an eventuality will occur only when the regression parameter is not able to account for the error in data and/or the 1-D model is incompatible with the real resistivity distribution. A possible way out is to use higher regression parameter value. The higher regression parameter value will lead to the increased misfit and blurred resistivity profile. In addition to this, for smooth functioning of SIS algorithm, the inverted reflection coefficients should be approximated as zero whenever these lie within a prescribed infinitesimal interval. In the present study this interval is -0.01 to 0.01 .

The 1-D response, at vertical boundaries of 2-D model, computed through SIS, is used as boundary conditions. Further the stacked 1-D inversion results at different points of the profile provide a good initial guess for 2-D inversion algorithm.

For two-dimensional structures, a common question is how to choose between 1-D inversions of B- and E- polarizations as these may lead to different 1-D profiles. The E-polarization is simpler to interpret than the B-polarization since the latter gets more distorted by noise due to near-surface 2-D anomalies or 3-D structures (Wright, 1970; Reddy & Rankin, 1972; Jones & Hutton, 1979; Stanley, 1984). Unfortunately, any structural variation along strike contaminates the E-polarization which, in turn, disturbs the data interpretation. In contrast, the B-polarization is affected very little by such variations. Thus, while the B-polarization is more complicated, its two-dimensional quantitative interpretation is reliable even in the presence of substantial three-dimensional structures (Park et al. 1983; Wannamaker et al., 1984b).

3.6.3 EM2INV algorithm for 2-D inversion

The 2-D non-linear EM inverse problem is solved through quasi-linearization. Towards this end, the field/response vector is expressed in its Taylor series about an initial guess parameter vector \mathbf{P}^0 as

$$F_i(P) = F_i(P_j^0) + \sum_{j=1}^n \frac{\partial F_i}{\partial P_j} (P_j - P_j^0) + \frac{1}{2} \sum_{j=1}^n \sum_{k=1}^n \frac{\partial^2 F}{\partial P_j \partial P_k} (P_j - P_j^0) (P_k - P_k^0) + \dots, \quad i = 1, 2, \dots, m. \quad \dots(3.42)$$

The equation (3.42) can be written concisely as

$$F(P) = F(P_0) + J \Delta P + \frac{1}{2} \Delta P^T H \Delta P + \dots \quad \dots(3.43)$$

Here, **J** and **H** are the Jacobian and Hessian matrices respectively. For quasi-linearization, the guess model **P**⁰ is assumed to be sufficiently close to the unknown true parameter vector **P**, so that only the linear terms of the parameter correction vector need be retained in the series, which reduces to

$$F(P) = F(P^0) + J \Delta P. \quad \dots(3.44)$$

The above equation, in simplified form, can be written as

$$\Delta R = J \Delta P. \quad \dots(3.45)$$

Here, ΔR is the difference vector between the observed, **F(P)**, and the computed, **F(P**⁰), response vectors; ΔP is the unknown correction vector to be applied to the current resistivity parameter vector, **P**⁰, and **J** is the Jacobian matrix comprising partial derivatives of data with respect to resistivity parameters. The matrix **J** is a measure of how each data point would be affected by a change in a particular parameter and also termed as 'sensitivity matrix'.

The equation (3.45) can be solved for ΔP using the ridge-regressed least square or minimum norm estimators given below

$$\Delta P = (J^H J + \lambda^2 I)^{-1} J^H \Delta R \quad \dots(3.46)$$

and

$$\Delta P = J^H (J J^H + \lambda^2 I)^{-1} \Delta R. \quad \dots(3.47)$$

The solution of equation (3.45) is used to update the current resistivity parameter vector, **P**⁰, as

$$P = P^0 + \Delta P. \quad \dots(3.48)$$

This updated parameter vector **P** is used as initial guess for the next iteration. After each iteration, the solution is checked for convergence. The inversion process stops when either the convergence is achieved or the iteration number exceeds the given limit.

From the inverse problem formulation, it is clear that the basic steps of each inversion iteration are the solution of forward problem, the generation of Jacobian matrix and the solution of inverse equation (3.45). Hence, a saving in any of these steps can significantly reduce the total computation time.

The Jacobian matrix, appearing in equation (3.45), is obtained by differentiating equation (3.25) with respect to the unknown resistivity parameter, P_j , as

$$\mathbf{C} \frac{\partial F}{\partial P_j} + \frac{\partial \mathbf{C}}{\partial P_j} F = 0, \quad j = 1, 2, \dots, n. \quad \dots(3.49)$$

Since the right hand side of equation (3.25) does not depend on resistivity parameter, its derivative is set to zero.

Above equations can be combined into the following matrix equation

$$\mathbf{C} \mathbf{J} = \mathbf{Y} \quad \dots(3.50)$$

where the j^{th} columns of matrices \mathbf{J} and \mathbf{Y} are

$$J_j = \frac{\partial F}{\partial P_j} \quad \text{and} \quad Y_j = - \frac{\partial \mathbf{C}}{\partial P_j} F. \quad \dots(3.51)$$

The equation (3.25) and (3.50) have the same coefficient matrix \mathbf{C} , therefore in case of matrix solvers, based on direct methods, the already existing Lower and Upper triangular (LU) decomposition of matrix \mathbf{C} can be reused. Thus, each column of Jacobian matrix \mathbf{J} can be efficiently computed using equation (3.25) with corresponding column of matrix \mathbf{Y} as new right hand side. After obtaining the Jacobian matrix \mathbf{J} , the estimator given by equation (3.46) or (3.47) is used for inverse problem solution.

For each inversion iteration, the equation (3.25) is solved as many times as the number of unknown resistivity parameters. The Jacobian given by equation (3.51) is for the field component corresponding to the polarization. The Jacobians for the various response functions can be derived using the corresponding field components using equation (2.104) as

$$\frac{\partial R}{\partial P_j} = T \frac{\partial F}{\partial P_j} + \frac{\partial T}{\partial P_j} F. \quad \dots(3.52)$$

3.7 Closure

The solution of ill-posed EM inverse problem is obtained through regularization. The non-linear 2-D inverse problem is solved iteratively by quasi-linearization, whereas the 1-D inverse problem is solved directly. Numerical implementations of 2-D forward and inverse problems, based on finite difference method, are discussed next.

EM PROBLEMS - IMPLEMENTATION OF FINITE DIFFERENCE METHOD

4.1 General

The EM data inversion capabilities crucially depend upon the accuracy and efficiency with which one can solve the EM forward problem. This, in effect, means obtaining solution of the boundary value problem. The analytical methods for solving the partial differential equations, derived from Maxwell's equations, are restricted to models with simple geometries and resistivity variations like layered earth or targets such as sphere, cylinder or cuboid. Most of the available analytical solutions are either of integral type with complicated integrands or of the infinite series type. The exact evaluation of these solutions is not feasible. To overcome these limitations, the alternative approach like numerical methods are usually used for modelling of EM problems. An excellent review on computational electromagnetics is given by Miller (1988).

The complex real earth can be modelled using any one of the available numerical techniques that translate the integro - differential operator equation into a matrix equation. These numerical methods can be grouped into two broad classes - Integral Equation Methods (IEMs) and Differential Equation Methods (DEMs). Both these classes have identified merits and demerits in terms of their respective applicability. Preference of one method over the other is dictated by the complexity of the model and the available computational resources.

In IEM, the integral operator is transformed, through quadrature formulae, to a matrix operator. Here, only the anomalous region is modelled. This results in a small but full coefficient matrix. In fact much of the earlier work in 3-D modelling was done

using IEM only, e.g. Raiche (1974), Hohmann (1975), Weidelt (1975a), Wannamaker et al. (1984a, 1984b), Wannamaker (1991), Xiong (1992), Zhdanov & Fang (1996). However, in spite of these positive features the use of IEM is restricted to the modelling of confined bodies in a layered earth. It is so because this method is constrained by the necessity of efficient computation of Green's functions and the easily computable Green's functions exist only for the layered earth primary model.

The DEMs, Finite Difference Method (FDM) or Finite Element Method (FEM), are popular in simulating arbitrarily shaped geometries. In these methods the whole domain of study need be discretized. This results in a large but grossly sparse coefficient matrices. Earlier, their use was limited because of paucity of efficient large matrix solvers. Recent advances in iterative solution techniques have helped in establishing their superiority over IEM (Sarkar, 1991). The differential operator is reduced to a matrix operator through difference approximation in case of FDM. Whereas it is reduced through a functional minimization in case of FEM. The mathematics of FDM is much simpler and easier to implement than that of FEM. Further, FEM is very useful in solving problems with complex geometries having curved boundaries (Coggon, 1971; Reddy & Rankin, 1977; Wannamaker et al., 1987; Travis & Chave, 1989; Livelybrooks, 1993; Mogi, 1996). Now curved boundaries can be modelled using FDM too (Taflove, 1995). In geophysics, where the main emphasis is on the solution of inverse problem, any inversion method would have limited resolution because of erroneous observations. Therefore, it may not be economically viable to model refined curved boundaries instead of the simple linear boundaries. Moreover, the matrix solvers for FDM are more efficient than those commonly used for FEM.

Besides the methods belonging to the above two classes, there exist some Hybrid methods where positive features of IEM and DEM are amalgamated. But these methods are again applicable only to confined structures (Lee et al., 1981). Therefore, in the present work FDM is preferred.

4.2 Finite difference implementation

The first finite difference algorithm for 2-D EM modelling was given by Jones & Pascoe (1971). They solved the forward problem of geomagnetic perturbations due to inhomogeneity and subsequently extended their work to three-dimensional models

(Jones & Pascoe, 1972). Lines & Jones (1973a, 1973b) modified their algorithm to incorporate variable grid size and permit the vertical discontinuities to extend right up to grid boundaries. These algorithms employed Gauss-Seidel relaxation technique for solving the resulting large sparse system of equations. Although Gauss-Seidel or its relaxation variants are simple, these do not work satisfactorily when the coefficient matrix is ill-conditioned (Golub & Van Loan, 1983). As a result, the advanced semi-iterative methods, like Conjugate Gradient Method (CGM), have become more popular in case of indefinite coefficient matrices (Sarkar, 1991). In recent years, significant progress has been made in efficient use of CGM in the FDM algorithms for geoelectromagnetic modelling (Madden & Mackie, 1989; Xinghua et al., 1991; Mackie & Madden, 1993a; Mackie et al., 1993; Smith, 1996b).

Concurrent to the modelling work, there has been appreciable work on the development of appropriate boundary conditions that enable reduction in the domain of modelling (Williamson et al. 1974; Jones 1974; Engquist & Majda, 1977; Brewitt-Taylor & Weaver, 1976; Weaver & Brewitt-Taylor, 1978; Zhdanov et al., 1982; Weaver 1994). It may be stated here that bulk of the discussion of forward formulation presented in this chapter has been adapted from Weaver (1994).

In FDM, the derivatives are approximated by the appropriate difference formulae obtained by the Taylor series expansion. For detailed description of FDM, reference is made to the standard texts like Forsythe & Wasow (1964), Hildebrand (1974) and Mitchell & Griffiths (1980). A brief account of finite difference formulation of the EM problem is presented here.

For deriving the governing finite difference equation, the partial derivatives have to be translated to difference formulae. Let a smooth function $f(x)$ be expanded in Taylor series about x for small positive and negative increments, h , as

$$f(x+h) = f(x) + h f'(x) + \frac{h^2}{2} f''(x) + O(h^3) \quad \dots(4.1)$$

and

$$f(x-h) = f(x) - h f'(x) + \frac{h^2}{2} f''(x) + O(h^3). \quad \dots(4.2)$$

Ignoring the terms $O(h^2)$, multiplying equation (4.1) by α and (4.2) by β and adding,

one gets

$$f'(x) = \frac{\alpha f(x+h) + \beta f(x-h) - (\alpha+\beta)f(x)}{(\alpha-\beta)h} \quad \dots(4.3)$$

This equation represents a general expression of first difference which reduces to the following three difference formulae for the three sets of α and β values

$$f'_f(x) = \frac{f(x+h) - f(x)}{h} \quad \text{for } \alpha = 1, \beta = 0, \quad \dots(4.4)$$

$$f'_b(x) = \frac{f(x) - f(x-h)}{h} \quad \text{for } \alpha = 0, \beta = -1 \quad \dots(4.5)$$

and

$$f'_c(x) = \frac{f(x+h) - f(x-h)}{2h} \quad \text{for } \alpha = 1/2, \beta = -1/2. \quad \dots(4.6)$$

In literature $f'_f(x)$, $f'_b(x)$ and $f'_c(x)$ are known as the forward, backward and central first differences respectively. The central difference, having a round off error of order h^3 , is preferred over the other two differences having error of order h^2 . The difference formulae for the second differences can be derived in a similar manner. The following central difference formula for second order derivative again has less error in comparison to its forward and backward difference equivalents

$$f''_c(x) = \frac{f(x+h) - 2f(x) + f(x-h)}{h^2} \quad \dots(4.7)$$

The 2-D EM Boundary Value Problem (BVP) comprises the partial differential equations (2.22) or (2.23), the integral boundary conditions (2.54) or (2.55) and the asymptotic boundary conditions (2.69) and (2.74). In order to solve this BVP, using FDM, the domain of study is discretized in the yz - plane by laying a grid with the help of the horizontal lines, $z = z_n$, ($n=1,2,\dots,N$), and the vertical lines, $y = y_m$, ($m=1,2,\dots,M$) intersecting at nodes (m,n) . Here M and N are respectively the number of vertical and horizontal grid lines. Like any other numerical method, the accuracy of FDM depends on the grid spacing. Finer the mesh more accurate the results, albeit at a higher cost.

Proper care should be taken while discretizing near discontinuity. Whereas the step size can be coarse within a homogeneous region, it should be fine near discontinuity as shown in Fig. 4.1.

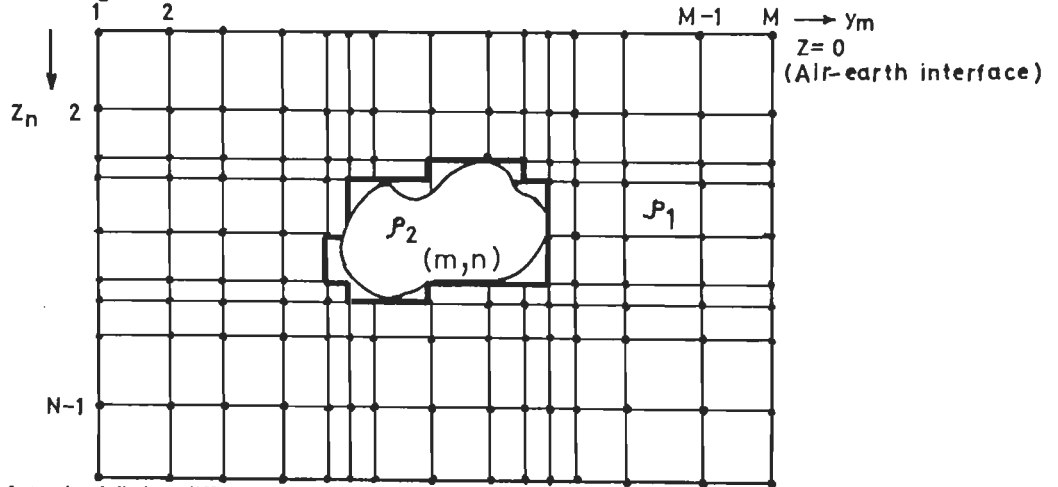


Fig. 4.1 A typical finite difference grid.

The cell's resistivity (or conductivity) is defined at the centre of cell $\rho_{m+1/2, n+1/2}$. A typical node of the 2-D grid with its four neighbouring cells is shown in Fig. 4.2. The top boundary of the grid is chosen at the air-earth interface at $z = z_1 = 0$ while the bottom boundary is at $z = z_N$, a minimal vertical level in the underlying half-space. The side boundaries of the grid are defined by the lines $y = y_1$ and $y = y_M$, on the left and right hand side of the model. The variable nodal spacings, in positive y - and z -directions, are given by

$$h_m = y_{m+1} - y_m, \quad d_n = z_{n+1} - z_n, \quad \text{where } 1 \leq m \leq M-1, \quad 1 \leq n \leq N-1.$$

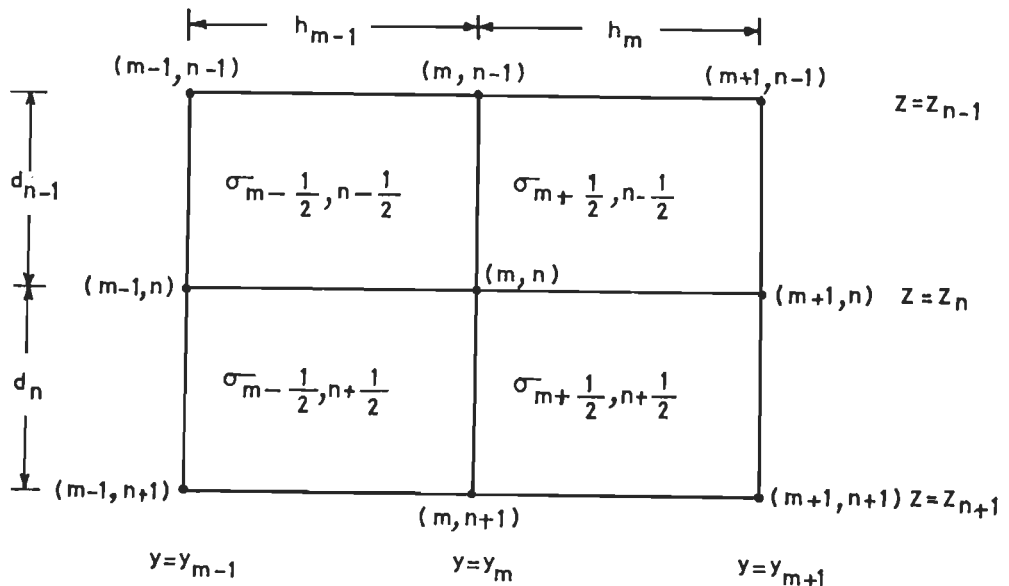


Fig. 4.2 The parameters of the four blocks surrounding the node (m,n) in the 2-D finite difference grid.

The finite difference equivalents of the governing partial differential equation and the requisite boundary conditions are discussed here. It may be added here that the choice of a particular difference formula is constrained by the location of the node. For the boundary nodes, either the forward or the backward difference formula is used, while for the internal nodes central difference formula is used.

4.2.1 Discrete governing equations

For internal nodes, the magnetic or electric field component is evaluated by solving the respective governing Helmholtz equations for B- and E- polarizations. The equations (2.22) and (2.23) are rewritten below

$$\rho \left(\frac{\partial^2 B}{\partial y^2} + \frac{\partial^2 B}{\partial z^2} \right) + \rho^* \frac{\partial B}{\partial y} + \rho' \frac{\partial B}{\partial z} = i \omega \mu B \quad \dots(4.8)$$

and

$$\frac{\partial^2 E}{\partial y^2} + \frac{\partial^2 E}{\partial z^2} - i \omega \mu E = 0. \quad \dots(4.9)$$

Here, superscripts * and ' denote partial differentiation with respect to y and z respectively. The governing differential equations are satisfied at all the internal nodes. To obtain the equivalent finite difference equation, the basic step is to identify the resistivity (conductivity) value to be assigned to a node surrounded by regions of different resistivities. Following Weaver (1994), a linear variation is assumed and the weighted average of resistivities (conductivities) is assigned as the resistivity (conductivity) value at the node. The discrete forms of these equations are distinct for the two modes of polarization. In order to describe these with clarity, the following constants are defined

$$\begin{aligned} h_m^+ &= h_m + h_{m-1}, & d_n^+ &= d_n + d_{n-1}, \\ h_m^- &= h_m - h_{m-1}, & d_n^- &= d_n - d_{n-1}, \\ h_m^p &= h_m h_{m-1}, & d_n^p &= d_n - d_{n-1}, \\ h_m^q &= h_m h_m^+, & d_n^q &= d_n d_n^+, \\ h_m^r &= h_{m-1} h_m^+, & d_n^r &= d_{n-1} d_n^+. \end{aligned} \quad \dots(4.10)$$

4.2.1.1 B-polarization

The resistivity at node (m,n) is defined to be the weighted average of resistivities of the four cells surrounding it, with cell areas being the weights, as

$$\rho_{m,n} = \frac{\beta_{m,n} + \beta_{m,n-1} + \beta_{m-1,n} + \beta_{m-1,n-1}}{h_m^* d_n^*}, \quad \dots(4.11)$$

where $\beta_{m,n} = h_m k_n \rho_{m+1/2, n+1/2}$. The derivatives of resistivity in the y- and z- directions are respectively defined as

$$\rho_{m,n}^* = \frac{\partial \rho}{\partial y} = \frac{\rho_{m+1/2,n} - \rho_{m-1/2,n}}{(h_m^*/2)} \quad \dots(4.12)$$

and

$$\rho_{m,n}' = \frac{\partial \rho}{\partial z} = \frac{\rho_{m,n+1/2} - \rho_{m,n-1/2}}{(d_n^*/2)}. \quad \dots(4.13)$$

At the top and bottom boundaries, it is assumed that

$$\rho_{m,1} = \rho_{m,3/2}, \quad \rho_{m,N} = \rho_{m,N-1/2} \quad \text{and} \quad \rho_{m,1}' = \rho_{m,N}' = 0. \quad \dots(4.14)$$

On approximating the derivatives by differences at internal node (m,n), equation (4.8) can be written in discrete form after some algebra as

$$\begin{aligned} & \frac{2\rho_{m,n} + h_{m-1} \dot{\rho}_{m,n}}{h_m^q} B_{m+1,n} + \frac{2\rho_{m,n} - h_m \dot{\rho}_{m,n}}{h_m^r} B_{m-1,n} + \frac{2\rho_{m,n} + d_{N-1} \rho_{m,n}'}{d_n^q} B_{m,n+1} + \frac{2\rho_{m,n} - d_n \rho_{m,n}'}{d_n^r} B_{m,n-1} \\ & = \left(\frac{2\rho_{m,n} - h_m \dot{\rho}_{m,n}}{h_m^p} + \frac{2\rho_{m,n} - d_n \rho_{m,n}'}{d_n^p} + i\omega\mu \right) B_{m,n}, \quad 2 \leq m \leq M-1, \quad 2 \leq n \leq N-1. \quad \dots(4.15) \end{aligned}$$

These (M-2)(N-2) internal nodes equations provide the coefficient matrix for the evaluation of magnetic field at internal nodes.

4.2.1.2 E-polarization

Analogous to the definition of resistivity at a node in B- polarization, for E- polarization also the weighted average of conductivity at node (m,n) is defined as

$$\sigma_{m,n} = \frac{\zeta_{m,n} + \zeta_{m,n-1} + \zeta_{m-1,n} + \zeta_{m-1,n-1}}{h_m^* d_n^*} \quad \dots(4.16)$$

where $\zeta_{m,n} = h_m k_n \sigma_{m+1/2, n+1/2}$. The equation (4.9) can be written in discrete form as

$$\frac{E_{m+1,n}}{h_m^q} + \frac{E_{m-1,n}}{h_m^r} + \frac{E_{m,n+1}}{d_n^q} + \frac{E_{m,n-1}}{d_n^r} = \left(\frac{1}{h_m^p} + \frac{1}{d_n^p} + \frac{1}{2} i \alpha_{m,n}^2 \right) E_{m,n} \quad \dots(4.17)$$

where $\alpha^2 = \omega \mu \sigma$, as defined in equation (2.45). Once the discrete governing equations are derived the supplementary discrete boundary condition equations are to be obtained next.

4.2.2 Discrete boundary conditions

As discussed in Chapter 2, the infinite domain can be modelled by imposing appropriate boundary conditions on the boundaries placed at finite distances. For horizontal boundaries, the Neumann boundary conditions given by equation (2.52) account for the integrated effect of the overlying and underlying half-spaces. The asymptotic boundary conditions, mixed in nature, are imposed for restricting the horizontal extent of the domain in E-polarization. The finite difference implementation of boundary conditions for both vertical and horizontal boundaries follows.

4.2.2.1 Asymptotic boundary conditions

For B-polarization, the magnetic field is constant at the surface (vide equation 2.30). Further, within earth the anomalous field decays exponentially as $y \rightarrow \pm\infty$. As a result, the field is 1-D at the side boundary nodes, i.e.

$$B_{1,n} = B_0, \quad B_{1,n} = B_-(z_n), \quad B_{M,n} = B_+(z_n), \quad 1 \leq m \leq M, \quad 2 \leq n \leq N. \quad \dots(4.18)$$

where $B_-(z_n)$ and $B_+(z_n)$ are 1-D magnetic fields at the left and right vertical boundaries.

For E-polarization from the asymptotic boundary conditions (2.74), the field at the left and right boundary nodes respectively are

$$E_{1,n} = E_{1,1} \left[\frac{E_-(z_n)}{E_-(0)} \right] \quad \dots(4.19)$$

and

$$E_{M,n} = E_{M,1} \left[\frac{E_+(z_n)}{E_+(0)} \right], \quad \dots(4.20)$$

for $2 \leq n \leq N$. Here $E_-(z_n)$ and $E_+(z_n)$ are 1-D electric fields at the left and right vertical boundaries. For top nodes on the side boundaries, the FDM implementation of

equation (2.70) led to the following expressions for the first and M^{th} node respectively (Weaver, 1994)

$$(1-\epsilon_1)E_{1,1} - E_{2,1} = -\epsilon_1 E_-(0) \quad \dots(4.21)$$

$$\text{where } \epsilon_1 = \frac{h_1(y_1 - 2h_1)}{y_1(y_1 - h_1)}$$

and

$$E_{M-1,1} - (1+\epsilon_M)E_{M,1} = -\epsilon_M E_+(0) \quad \dots(4.22)$$

$$\text{where } \epsilon_M = \frac{h_{M-1}(y_M + 2h_{M-1})}{y_M(y_M + h_{M-1})}$$

The equations (4.21) and (4.22) replace the infinite domain Dirichlet boundary conditions

$$E_1 = E_-(0) \quad \text{and} \quad E_M = E_+(0). \quad \dots(4.23)$$

4.2.2.2 Integral boundary conditions

The Neumann boundary conditions imposed on the horizontal boundaries are derived in Chapter 2 for homogeneous underlying half-space (vide equation 2.52). However, in the presence of layered substructure the boundary conditions get modified to accommodate the effect of layering which is written here, for any interface $z = s$, as

$$F'(y,z) + \frac{\partial}{\partial z} [F(y,s) \int_{-\infty}^{\infty} P(y-v, z-s) dv] = \frac{1}{2\pi} \int_{-\infty}^{\infty} \frac{\partial}{\partial z} [F(v,s) - F(y,s)] P(y-v, z-s) dv + \int_{-\infty}^{\infty} F(v,s) f'(y-v) dv. \quad \dots(4.24)$$

The integral boundary condition is imposed only on nodes from 2 to (M-1) as the fields at the first and the last node of the interface are already expressed in terms of vertical boundary condition. For this purpose, the first integral on the right hand side is solved semi-analytically. Whereas the second integral, correction term due to layering, is solved as discussed by Weaver (1994, p.175). Let the boundary condition be evaluated at node p with $y = y_p$ and the variable of integration v be represented by an arbitrary node m . Since the integrand becomes singular at node $m = p$, it is partitioned

into five integrals as

$$\int_{-\infty}^{\infty} = \int_{-\infty}^{y_1} + \int_{y_M}^{\infty} + \int_{y_{p-1}}^{y_{p+1}} + \left(\sum_{m=1}^{p-2} + \sum_{m=p+1}^{M-1} \right) \int_{y_m}^{y_{m+1}} \quad \dots(4.25)$$

The first two integrals, where y_1 and y_m are sufficiently far from the inhomogeneous region to justify the 1-D field approximation, are evaluated analytically. For evaluation of integrals under the summation signs, in the intervals $y_m < y < y_{m+1}$, $m = 1$ to $p-1$ or $p+1$ to M , the field variation is assumed to be linear and is represented as

$$F(y,s) = F_{m,1} + (y-y_m) \frac{F_{m+1,1} - F_{m,1}}{h_m} \quad \dots(4.26)$$

Here, F stands for either the magnetic or the electric field component. Lastly, around the singular point, y_p , the field is approximated by a quadratic variation using the parabola

$$F(y,s) = F_p + T_p^{(1)} (y - y_p) + T_p^{(2)} (y - y_p)^2, \quad \dots(4.27 a)$$

passing through the three points F_{p-1} , F_p and F_{p+1} . The coefficients $T_p^{(1)}$ and $T_p^{(2)}$ are given by

$$T_p^{(1)} = \frac{h_{p-1}}{h_p h_p^+} F_{p+1} + \frac{h_p^- F_p}{h_p h_{p-1}} - h_p F_{p-1} \quad \dots(4.27 b)$$

and

$$T_p^{(2)} = \frac{F_{p+1}}{h_p h_p^+} - \frac{F_p}{h_p h_{p-1}} + \frac{F_{p-1}}{h_{p-1} h_p^+} \quad \dots(4.27 c)$$

Here $h_p^\pm = h_p \pm h_{p-1}$. The equations (4.27b) and (4.27c) can be recognised as the finite difference expressions for the first and second order derivatives of F respectively, evaluated at $(p,1)$. On substituting these approximations, the integrals can be solved analytically.

For B-polarization, since the magnetic field is constant in air the Dirichlet boundary condition is applied on the air-earth interface and the integral boundary condition is imposed only at the bottom interface. As mentioned earlier, the tangential magnetic field is discontinuous in the presence of surface currents. Therefore, special

care must be taken while transferring the bottom integral boundary fields from d+ to d-. From equation (2.20a), the tangential electric field can be expressed in terms of the magnetic field as

$$B'_{m,z_N} = \frac{1}{\sigma_1 \rho_{m,N}} B'_{m,z_{N-1}} \quad \dots(4.28)$$

where σ_1 is the conductivity of the bottom half-space. Multiplying equation (2.54) by $\sigma_1 \rho_{m,N}$, it gets modified to

$$\begin{aligned} & (\alpha_1 \sqrt{i} + \frac{\sigma_1 \rho_{m,N}}{d_{N-1}} + \frac{id_{N-1} \alpha_1^2}{2}) B_{m,N} - \frac{\sigma_1 \rho_{m,N}}{d_{N-1}} B_{m,N-1} - \frac{d_{N-1} \sigma_1 \rho_{m,N}}{2} (\frac{\partial^2 B}{\partial y^2})_{m,N} \\ & - \frac{d_{N-1} \sigma_1 \rho_{m,N}}{2} (\frac{\partial B}{\partial y})_{m,N} = \frac{\alpha_1 \sqrt{i}}{\pi} \int_{-\infty}^{\infty} [B(v, z_N) - B_{m,N}] \frac{K_1(|y_m - v| \alpha_1 \sqrt{i})}{|y_m - v|} dv \\ & + \frac{1}{2\pi} \int_{-\infty}^{\infty} B(v, z_N) f^P(y - v) dv. \end{aligned} \quad \dots(4.29)$$

where $\rho'_{m,N} = 0$. This equation is the requisite boundary condition at d- for B-polarization where the vertical derivative is evaluated using backward difference form. On substituting the analytic values of integrals, the difference formula for derivatives and the 1-D values at the side boundary nodes, the discrete form of boundary conditions can be written as

$$\begin{aligned} & [\bar{D}_m^P + \frac{\pi \sigma_1 d_{N-1}}{h_m^r} (\dot{\rho}_{m,N} - \frac{1}{2} h_m \dot{\rho}_{m,N})] B_{m-1,N} + (\sum_{j=2}^{m-2} + \sum_{j=m-2}^{M-1}) (\bar{W}^P)_m^j B_{j,N} \\ & + [\bar{F}_m^P + \frac{\pi \sigma_1 d_{N-1}}{h_m^q} (\rho_{m,N} + \frac{1}{2} h_{m-1} \dot{\rho}_{m,N})] B_{m+1,N} + \\ & [\bar{M}_m^P - \pi \sigma_1 (\frac{\rho_{m,N}}{d_{N-1}} + \frac{d_{N-1}}{h_m^p} (\rho_{m,N} - \frac{1}{2} h_m \dot{\rho}_{m,N}) + \frac{i \omega \mu d_{N-1}}{2})] B_{m,N} \\ & = [(N_f^P)_m^1 - Q_m^1] B_-(z_N) + [(N_f^P)_m^M - Q_m^M] B_+(z_n), \quad 2 \leq m \leq M-1 \end{aligned} \quad \dots(4.30)$$

The coefficients Q_m^1 and Q_m^M are given by equation (5.21)-(5.22) of Weaver (1994, p.164) while other coefficients D_m^P , W_m^P , F_m^P , M_m^P and N_f^P by equation (5.84)-(5.90) of Weaver (1994, p.175) with his constant B_m^P being W_m^P here. The boundary conditions represented by the equations (4.18) and the (M-2) equations (4.30) along with the (M-2)(N-2) internal node equations (4.15) complete the linear system of equations to be solved for the (M-2)(N-1) unknowns $B_{m,n}$.

In E-polarization, the Neumann integral boundary conditions are applied on both top and bottom boundary interfaces. On substituting the difference formula and using the asymptotic boundary condition, the top boundary condition can be stated in the following discrete form

$$\begin{aligned} & \tilde{P}_m^1 E_{1,1} + \tilde{P}_m^M E_{M,1} + \left(\frac{\pi d_1}{h_m^r} + C_m\right) E_{m-1,1} + \left(\frac{\pi d_1}{h_m^q} + U_m\right) E_{m+1,1} \\ & + \left(\sum_{j=2}^{m-2} + \sum_{j=m+2}^{M-1}\right) A_m^j E_{j,1} + \left[L_m - \frac{\pi}{d_1} - \frac{\pi d_1}{h_m^p} - \frac{\pi i d_1 \alpha_{m,1}^2}{2}\right] E_{m,1} + \frac{\pi}{d_1} E_{m,2} \\ & = R_m^1 E_-(0) + R_m^M E_+(0) - \pi i \omega B_0, \quad 2 \leq m \leq M-1. \end{aligned} \quad \dots(4.31)$$

On the other hand, the discrete form of bottom boundary condition is

$$\begin{aligned} & \tilde{Q}_m^1 E_{1,N} + \tilde{Q}_m^M E_{M,N} + \left(\frac{\pi d_{N-1}}{h_m^r} + \tilde{D}_m\right) E_{m-1,N} + \left(\frac{\pi d_{N-1}}{h_m^q} + \tilde{F}_m\right) E_{m+1,N} \\ & + \left(\sum_{j=2}^{m-2} + \sum_{j=m+2}^{M-1}\right) B_m^j E_{j,N} + \left[\tilde{M}_m - \frac{\pi}{d_{N-1}} - \frac{\pi d_{N-1}}{h_m^p} - \frac{\pi i d_{N-1} \alpha_{m,N}^2}{2}\right] E_{m,N} \\ & + \frac{\pi}{d_{N-1}} E_{m,N-1} = \tilde{S}_m^1 E_-(z_n) + \tilde{S}_m^M E_+(z_n), \quad 2 \leq m \leq M-1. \end{aligned} \quad \dots(4.32)$$

The coefficients in equations (4.31) and (4.32) are defined in equations (5.11) - (5.18), (5.50) - (5.66) and (5.87) - (5.91) of Weaver (1994, p.163-164, 169-170, 175) with his constant U^M being E^M here. The (2N-2) asymptotic boundary condition equations (4.19) and (4.20), the two equations (4.21) and (4.22) on the top end nodes, (2M-4) equations (4.31) and (4.32) for the top and bottom interfaces, complete the boundary condition equations. This, together with the (M-2)(N-2) internal node equations (4.17), give a total of MN equations in unknowns $E_{m,n}$.

The linear system of equations for both modes of polarization can be compiled and written in matrix form as

$$CF = S, \quad \dots(4.33)$$

where C is the coefficient matrix comprising the terms from equations (4.15) and (4.30) or (4.17), (4.31) and (4.32), S is the known vector derived from boundary conditions and F is the unknown magnetic or electric field component vector. The size of coefficient matrix is $n_t \times n_t$ where n_t , the number of unknowns, is

$$n_t = \begin{cases} n_t + (M-2) & \text{for B-polarization} \\ n_t + 2(M-2) & \text{for E-polarization} \end{cases}$$

where $n_t = (M-2) \times (N-2)$, being the number of internal nodes.

4.3. Structure of coefficient matrix

The EM boundary value problem for a homogeneous region, with uniformly spaced grid and Dirichlet boundary conditions, results in the coefficient matrix having the following special structure

$$C = \begin{pmatrix} A & I & 0 & 0 & \dots \\ I & A & I & 0 & \dots \\ 0 & I & A & I & \dots \\ \dots & \dots & \dots & \dots & \dots \end{pmatrix}, \quad \dots(4.34a)$$

where **I** is a unit submatrix and **A** a tridiagonal submatrix written as

$$A = \begin{pmatrix} -4 & 1 & 0 & 0 & \dots \\ 1 & -4 & 1 & 0 & \dots \\ 0 & 1 & -4 & 1 & \dots \\ \dots & \dots & \dots & \dots & \dots \end{pmatrix}. \quad \dots(4.34b)$$

The order of matrix **C** is the total number of internal nodes, i.e. $n_i \times n_i$ while the order of **I** and **A** is the number of internal nodes in one direction, i.e. $(M-2) \times (M-2)$ or $(N-2) \times (N-2)$. The corresponding matrix equation can be solved using any special matrix solver.

The structure of coefficient matrix gets perturbed with the change in the nature of boundary. When the discrete Neumann boundary conditions are imposed on top and bottom boundaries, the field at a given node is related to all the nodes on the surface. This destroys the tridiagonal nature of the top/bottom diagonal block submatrix and becomes full. This loss in sparsity structure, however, is offset by the economy resulting from the enormously reduced grid size, provided special matrix solvers which optimally exploit the remaining structure are employed.

The coefficient matrix **C** of order $n_i \times n_i$ is a complex and banded matrix having the following special block tridiagonal structure

$$C = \begin{pmatrix} \beta_1 & \gamma_1 & \cdot & \cdot & \cdot \\ \alpha_1 & \beta_2 & \gamma_2 & \cdot & \cdot \\ \cdot & \alpha_2 & \beta_3 & \gamma_3 & \cdot \\ \cdot & \cdot & \cdot & \cdot & \cdot \\ \cdot & \cdot & \cdot & \alpha_{N-1} & \beta_N \end{pmatrix}. \quad \dots(4.35)$$

The top and bottom block rows correspond to the respective integral boundary conditions while the remaining rows correspond to rows of internal nodes. Here each block matrix is of size $(M-2) \times (M-2)$ corresponding to the internal nodes on any horizontal grid line. In particular, the submatrices α 's and γ 's are diagonal, β_1 and β_N are full and β_n 's, $1 < n < N$, are tridiagonal (Fig. 4.3).

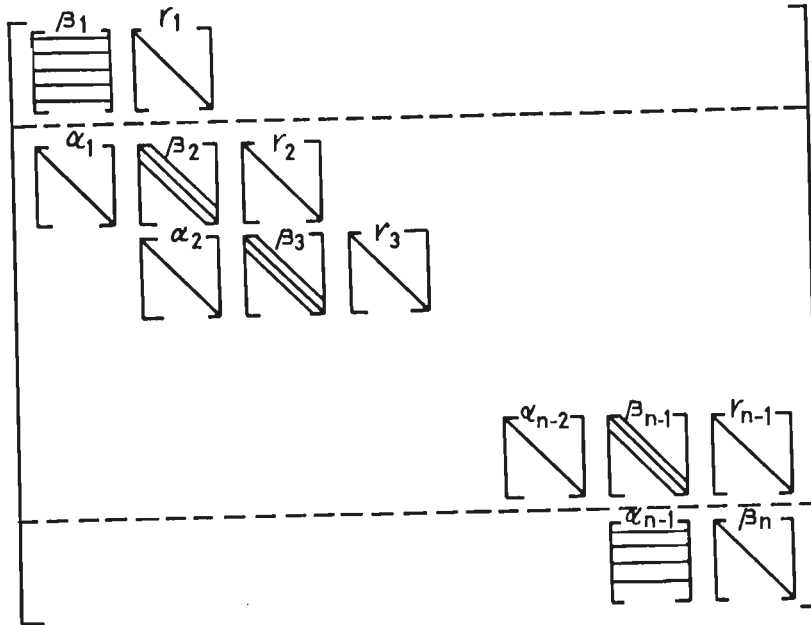


Fig. 4.3 The structure of FDM coefficient matrix when integral and asymptotic boundary conditions are employed. Here the submatrices β_1 and β_n are full; $\beta_i, i = 2, n-1$ are tridiagonal and $\alpha_i, \gamma_i, i = 1, n-1$ are diagonal.

The matrix C can be rewritten as

$$C = \begin{pmatrix} 1 & N-2 & 1 \\ M_1 & M_2 & 0 \\ M_3 & M_4 & M_5 \\ 0 & M_6 & M_7 \end{pmatrix} \quad \dots(4.36)$$

Here, M_1 and M_7 are full submatrices, M_2, M_3, M_5 and M_6 are diagonal and M_4 is a tridiagonal matrix. For retaining the pentadiagonal structure of middle blocks, it is essential to extend the asymptotic behaviour of fields, given by equations (4.21) and (4.22), to the second node on left and to the $(M-1)^{th}$ node on right for each horizontal level. If the field on these nodes were not computed analogous to those at boundary nodes, then due to their relation with four neighbouring points, the first and last nodes would have appeared as off diagonal elements in the diagonal block matrices α_1 and α_{n-1} . This would have spoilt the pentadiagonal structure and the complete banded

matrix would have to be considered. Here, we have traded in favour of economy. The elements of matrix \mathbf{C} are different for the two polarizations. For B-polarization, the p^{th} row for internal nodes of the coefficient matrix \mathbf{C} has the following five non-zero elements

$$\begin{aligned} C_{p,q1} &= (h_{p-1} \rho_{p-1,q3-1} + h_p \rho_{p,q3-1}) / d_{q3-1}, \\ C_{p,q2} &= (d_{q3} \rho_{p-1,q3} + d_{q3-1} \rho_{p-1,q3-1}) / h_{p-1}, \\ C_{p,q3} &= (C_{p,q1} + C_{p,q2} + C_{p,q4} + C_{p,q5}) + \frac{1}{2} \omega \mu h_p^* d_{q3}^* \end{aligned} \quad \dots(4.37)$$

$$C_{p,q4} = (d_{q3-1} \rho_{p,q3-1} + d_{q3} \rho_{p,q3}) / h_p$$

$$C_{p,q5} = (h_p \rho_{p,q3-1} + h_{p-1} \rho_{p-1,q3}) / d_{q3}$$

where $h_p^* = h_p + h_{p-1}$, $d_{q3}^* = d_{q3} + d_{q3-1}$.

The column numbers q 's are defined as

$$q1 = p - M + 2, \quad q2 = p - 1, \quad q3 = p, \quad q4 = p + 1 \quad \text{and} \quad q5 = p + M - 2. \quad \dots(4.38)$$

Similarly, for E-polarization the five non-zero elements of p^{th} row can be written as

$$\begin{aligned} C_{p,q1} &= \frac{h_p^*}{d_{q3-1}}, \\ C_{p,q2} &= -\frac{d_{q3}^*}{h_{p-1}}, \\ C_{p,q3} &= \left(\frac{h_p^*}{d_{q3-1}} + \frac{h_p^*}{d_{q3}} + \frac{d_{q3}^*}{h_p} + \frac{d_{q3}^*}{h_{p-1}} + \frac{1}{2} \omega \mu (h_{p-1} d_{q3-1} \sigma_{p-1,q3-1} + h_{p-1} d_{q3} \sigma_{p-1,q3} \right. \\ &\quad \left. + h_p d_{q3-1} \sigma_{p,q3-1} + h_p d_{q3} \sigma_{p,q3} \right) \end{aligned} \quad \dots(4.39)$$

$$C_{p,q4} = \frac{d_{q3}^*}{h_p}$$

$$C_{p,q5} = \frac{h_p^*}{d_{q3}}$$

where the column number q 's are given by equation (4.38). Once the main field

component, B_x or E_x , is computed the other field components can be derived from it by developing the requisite transformation matrices.

4.3.1 Transformation matrices for derived responses

4.3.1.1 B-polarization

For B-polarization only the horizontal electric field E_y is of practical interest, that too only at the surface of the earth. It is derived using equation (2.20a). However, if the node $(m,1)$ lies on a vertical boundary then E_y can not be defined uniquely at that node. In such situations, it is convenient to work with horizontal current density which is continuous across the interface and equation (2.20a) can be written as

$$\sigma E_y = \frac{1}{\mu} \frac{\partial B_x}{\partial z}. \quad \dots(4.40)$$

Substituting the difference formula for vertical derivative of B_x , the equation for E_y becomes

$$(E_y)_{m,1} = \omega \frac{\rho_{m,1}}{d_1} [B_{m,2} - B_0] - \frac{1}{2} i \omega d_1 B_0. \quad \dots(4.41)$$

It can be written in matrix notation as

$$E_y = (T_y^B) B. \quad \dots(4.42)$$

Here T_y^B is the transformation matrix of order $(M-2) \times n_1$. The non-zero elements of its p^{th} row are

$$(T_y^B)_{p,q3} = \omega \frac{r_{p1q}}{h_{p-1}} \left[-\frac{1}{d_1^2} - \frac{i}{2} d_1 \frac{h_p}{(r_{pq} + r_{p1q})} \right],$$

$$(T_y^E)_{p,q5} = \omega \frac{r_{p1q}}{h_{p-1}} \frac{1}{d_1^2}, \quad \dots(4.43)$$

$$\text{where } r_{pq} = h_p d_1 \frac{\rho_{p,1}}{\omega} \mu \quad \text{and} \quad r_{p1q} = h_{p-1} d_1 \frac{\rho_{p-1,1}}{\omega} \mu.$$

Once E_y is evaluated, the impedance Z_{yx} can be computed as

$$Z_{yx} = (T_y^B) B. \quad \dots(4.44)$$

The transformation matrix T_{yx} is given by

$$T_{yx} = [D_{B_x}]^{-1} T_y^B, \quad \dots(4.45)$$

where D_{B_x} is the diagonal matrix whose diagonal elements comprise the B_x values.

4.3.1.2 E-polarization

For E-polarization, the horizontal and vertical magnetic field components, B_y and B_z , can be derived from equations (2.21a) and (2.21b) by approximating the derivative by the corresponding difference formulas such as

$$(B_y)_{m,1} = \frac{i}{\omega} \left[\frac{1}{d_1} E_{m,2} + \frac{d_1}{h_m^q} E_{m+1,1} + \frac{d_1}{h_m^r} E_{m-1,1} - \left(\frac{1}{2} i d_1 \alpha_{m,1}^2 + \frac{1}{d_1} + \frac{d_1}{h_m^p} \right) E_{m,1} \right] \dots(4.46)$$

and

$$(B_z)_{m,1} = \frac{i}{\omega} \left[\frac{h_m}{h_m^r} E_{m+1,1} - \frac{h_m}{h_m^p} E_{m,1} - \frac{h_{m-1}}{h_m^q} E_{m-1,1} \right]. \quad \dots(4.47)$$

These field components, the impedance Z_{xy} and the induction vector I_{yz} can be written in matrix notation as

$$B_y = T_y^E E, \quad \dots(4.48)$$

$$B_z = T_z^E E, \quad \dots(4.49)$$

$$Z_{xy} = T_{xy} E, \quad \dots(4.50)$$

$$I_{zy} = T_{zy} E, \quad \dots(4.51)$$

where T_y^E , T_z^E , T_{xy} and T_{zy} are the $(M-2) \times n_1$ transformation matrices. The non-zero elements of the p^{th} row of different matrices are

$$(T_y^E)_{p,q1} = \frac{i}{\omega} \frac{d_1}{h_p^r},$$

$$(T_y^E)_{p,q3} = \frac{1}{2} \mu d_1 \frac{(h_p/\rho_{p,1} + h_{p-1}/\rho_{p-1,1})}{h_p^*} - \frac{i d_1}{\omega h_p^p} - \frac{i}{\omega d_1}, \quad \dots(4.52)$$

$$(T_y^E)_{p,q4} = -\frac{i}{\omega} \frac{d_1}{h_p^q},$$

$$(T_y^E)_{p,q5} = \frac{i}{\omega} \frac{1}{d_1},$$

and

$$(T_z^E)_{p,q2} = \frac{i}{\omega} \frac{h_p}{h_p^r},$$

$$(T_z^E)_{p,q3} = \frac{i}{\omega} \left[\frac{h_{p-1} - h_p}{h_p^p} + \frac{i}{2} \omega \mu \left(\frac{1}{\rho_{p,1}} - \frac{1}{\rho_{p-1,1}} \right) \frac{h_p^p}{h_p^*} \right], \quad \dots(4.53)$$

$$(T_z^E)_{p,q4} = -\frac{i}{\omega} \frac{h_p}{h_p^q}.$$

The transformation matrices for impedance and induction vector are given as

$$T_{xy} = [D_{B_y}]^{-1}, \quad \dots(4.54)$$

$$T_{zy} = [D_{B_y}]^{-1} [T_z^E] \quad \dots(4.55)$$

where \mathbf{D}_{B_y} , the diagonal matrix, comprises B_y values.

Thus, any field component, impedance or induction vector can be computed using above stated relations. It can then be inverted by computing the corresponding derived Jacobian.

4.4 Inverse formulation

The non-linear EM problem, after quasi-linearization, is solved iteratively starting with an initial guess model. In general, since a rough guess about the location and extent of the body can always be made from the observed response, there is no need to invert for resistivity of the whole finite difference modelling domain. The stacked 1-D inversions have proven to be very useful in providing accurate initial guess. The good initial guess results in faster convergence and a much smaller region encompassing the guessed body may be taken as the domain for inversion. The response at surface nodes is the observation vector, whereas the parameter vector \mathbf{P}

comprises resistivities of the blocks lying within the inversion domain. The initial guess values are the current estimates of ρ_j , the resistivity of the j^{th} block. For numerical accuracy, instead of ρ_j , its logarithm given below is used as parameter vector

$$P_j = \log \rho_j = -\log \sigma_j \quad \dots(4.56)$$

The derivative with respect to it is defined as

$$\frac{\partial}{\partial P_j} = \frac{1}{\rho_j} \frac{\partial}{\partial \rho_j} = -\frac{1}{\sigma_j} \frac{\partial}{\partial \sigma_j} \quad \dots(4.57)$$

It is more efficient to work with the logarithm of resistivity because of all the model parameters, the resistivity varies over the widest range. The logarithm operation not only properly scales this large variation but also guarantees that the resistivity has only positive values.

In order to solve the inverse problem matrix equation (3.45), the Jacobian matrix \mathbf{J} need be evaluated using equation (3.50) which is rewritten below

$$\mathbf{C}\mathbf{J} = \mathbf{Y}, \quad \dots(4.58)$$

where the j^{th} column of \mathbf{Y} is given by

$$Y_j = -\frac{\partial \mathbf{C}}{\partial P_j} \mathbf{F}.$$

The right hand side of equation (4.58) is computed by first differentiating the coefficient matrix \mathbf{C} with respect to the block resistivity parameter P_j and then multiplying it with the field vector \mathbf{F} .

4.4.1 Derivative of coefficient matrix

The derivative of a coefficient matrix element is zero unless its expression contains ρ_j . Since an internal node is associated with four regions, the elements of the row corresponding to this node contain only these four block resistivities. As a result, the matrix \mathbf{J} is grossly sparse with each row having at most four non-zero entries in column positions corresponding to the element whose resistivity is changed. For B-polarization, the derivatives of different entries in the p^{th} row of matrix \mathbf{C} are

$$\frac{\partial C_{p,q1}}{\partial P_j} = -\left(\frac{h_p^+}{d_{q1-1}}\right) \frac{1}{P_j},$$

$$\frac{\partial C_{p,q3}}{\partial P_j} = -(C_{p,q1} + C_{p,q2} + C_{p,q4} + C_{p,q5}) \frac{1}{P_j}, \quad \dots(4.59)$$

$$\frac{\partial C_{p,q4}}{\partial P_j} = -\left(\frac{h_p^+}{d_{q4}}\right) \frac{1}{P_j},$$

$$\frac{\partial C_{p,q5}}{\partial P_j} = -\left(\frac{d_{q5}^+}{h_{p-1}}\right) \frac{1}{P_j}$$

where q_i 's are given by equation (4.38).

For E-polarization, since the resistivity appears only in the imaginary term of the diagonal element, all the off diagonal terms will vanish. The p^{th} diagonal element of derivative matrix is

$$\frac{\partial C_{p,q3}}{\partial P_j} = -j\omega \frac{\mu}{2} h_{p-1} d_{q3-1} \frac{1}{P_j}. \quad \dots(4.60)$$

If the body is outcropping, in E-polarization, the top row block matrix, corresponding to the top integral boundary condition equation (4.31), is to be differentiated with respect to P_j . Since only the node at which the condition is being evaluated contains a resistivity term, all other entries in the full block will vanish. The derivative of the diagonal element of the top block is given by

$$\frac{\partial C_{p,q3}}{\partial P_j} = \frac{\pi j \omega \mu}{2} d_{q3} \frac{h_{p-1}}{h_p} \frac{1}{P_j}. \quad \dots(4.61)$$

Once the computation of derivative of the coefficient matrix \mathbf{C} is over, it is multiplied with the corresponding field vector \mathbf{F} to construct the j^{th} column of the right hand side matrix \mathbf{Y} of equation (4.58).

4.4.2 Computation of Jacobian/derived Jacobians

The Jacobian matrix \mathbf{J} can be computed explicitly by solving equation (4.58) using any standard matrix solver. The Jacobian $\mathbf{J}_x^{E,B}$, corresponding to the main field component, B_x or E_x , is used to derive the Jacobians for derived response functions.

For B-polarization, the j^{th} column of Jacobian, \mathbf{J}_{yx} , of impedance Z_{yx} can be written as

$$\frac{\partial Z_{yx}}{\partial P_j} = (J_{yx})_j = [D_{B_x}]^{-1} \frac{\partial E_y}{\partial P_j} - [D_{E_y}] [D_{B_x}]^{-2} \frac{\partial B_x}{\partial P_j}, \quad \dots(4.62)$$

where \mathbf{D}_{B_x} and \mathbf{D}_{E_y} are the diagonal matrices for B_x and E_y respectively. From equation (4.18), since the constant magnetic field does not depend on resistivity, the second term will vanish and above equation will reduce to the following equation as

$$(J_{yx})_j = [D_{B_x}]^{-1} [T_y \frac{\partial B_x}{\partial P_j} + \frac{\partial T_y}{\partial P_j} B_x]. \quad \dots(4.63)$$

For E-polarization, the Jacobians \mathbf{J}_{xy} for the impedance Z_{xy} can be derived as

$$\frac{\partial Z_{xy}}{\partial P_j} = (J_{xy})_j = [D_{B_y}]^{-1} \frac{\partial E_x}{\partial P_j} - [D_{E_x}] [D_{B_y}]^{-2} \frac{\partial B_y}{\partial P_j}. \quad \dots(4.64)$$

On using equation (4.48), it reduces to the following equation

$$(J_{xy})_j = [D_{B_y}]^{-1} [J_x^E - Z_{xy} T_y' J_x^E - Z_{xy} T_y' E_x]. \quad \dots(4.65)$$

Here T_y' is the derivative of transformation matrix T_y with respect to P_j .

For induction vector I_{zy} , the j^{th} column of the Jacobian \mathbf{J}_{zy} can be written as

$$\frac{\partial I_{zy}}{\partial P_j} = (J_{zy})_j = [D_{B_z}]^{-1} \frac{\partial B_z}{\partial P_j} - [D_{B_z}] [D_{B_y}]^{-2} \frac{\partial B_y}{\partial P_j}. \quad \dots(4.66)$$

Using the respective transformation matrices from equation (4.48) and (4.49), the above equation reduces to the following equation

$$(J_{zy})_j = [D_{B_z}]^{-1} [(T_z - I_{zy} T_y) J_x^E + (T_z' - I_{zy} T_y') E_x], \quad \dots(4.67)$$

where superscript (') indicates differentiation with respect to P_j . The different form of

Jacobian matrices can be written in a generalized form as

$$\mathbf{J}_R = \mathbf{T}' \mathbf{F} + \mathbf{T} \mathbf{J}_x \quad \dots(4.68)$$

Depending upon the response vector $\Delta \mathbf{R}$, the transformation matrices are developed and the derived Jacobians are computed. Once \mathbf{J} is evaluated, the inverse problem equation (3.45) can be solved using a suitable matrix solver. The criterion for choosing an appropriate matrix solver is discussed next.

4.5 Choice of matrix solver

From the inverse formulation, given in Chapter 3, it is clear that for each inversion iteration the solution of forward problem, generation of Jacobian matrix and solution of equation (3.45) account for the major share of computer time. Therefore, the total computation time can be reduced by saving it in any one of these steps. The forward problem matrix equation, being a well posed one, has an exact solution while the ill-posed inverse problem is to be regularised for obtaining a solution. The computation time can also be significantly reduced by making a judicious choice of an efficient matrix solver.

A variety of matrix solvers, direct, iterative and semi-iterative in nature, are used for matrix equations of EM problems (Sarkar et al., 1981a). For direct methods, where the complete banded matrix is stored, the solution is obtained in finite number of steps. The advantage of knowing number of steps *a priori* is, to a certain extent, offset by the build up of truncation and round-off errors in these methods. Whereas in the iterative methods, where a chosen initial guess is improved in a series of iterations, the procedure can be stopped in between whenever the approximate solution with prescribed accuracy is obtained. As a result, the round off error is limited. Further, since only the current row of the matrix is stored, these methods are preferred for sparse systems as these exploit the sparsity structures to the maximum (Jacobs, 1981a). Though iterative methods score on above grounds, yet their use is not recommended when diagonal dominance is not guaranteed *a priori*, or when the matrix is indefinite or when the matrix equation is to be solved for a number of right hand sides. For indefinite matrices, the semi-iterative method like conjugate gradient have proven to be useful. The conjugate gradient methods (Hestenes & Stiefel, 1952) are iterative methods but the maximum number of iterations needed for obtaining the solution is known *a priori*. Generally, the solution is obtained in at most Q_v iterations

where Q_v is the number of independent eigenvalues (Jennings, 1977). So it has positive features of both the direct as well as iterative methods. However, like iterative methods these are also constrained by the *a priori* knowledge of diagonal dominance. The CGMs are widely used for real matrices. The suitable matrix solver has been chosen according to matrix characteristics for the forward and inverse problems.

4.5.1 Forward matrix solver

The forward matrix equation has been solved using Gaussian elimination, a direct method. Special measures are taken to exploit the special block tridiagonal structure of the coefficient matrix. The FDM coefficient matrix \mathbf{C} is complex and has distributed eigenvalues. To exploit its special sparsity structure the iterative methods can be used. The early workers like Jones & Pascoe (1972), Hibbs & Jones (1976) did use relaxation methods but they did not address in detail to its accuracy. Apart from this, though the matrix is diagonally dominant, yet the off-diagonal elements, corresponding to second and $(M-1)^{\text{th}}$ nodes, are almost equal to the diagonal one restricting the use of iterative methods. Moreover, for solution of a matrix equation with different right hand sides, the direct methods may score over iterative ones inspite of the enormous sparsity of coefficient matrix.

Another alternative is to use the conjugate gradient method, a semi-iterative method. Due to distributed eigenvalues of matrix \mathbf{C} it will result in as many number of iterations as the order of matrix. Though number of iterations are less than needed in iterative methods, yet because of complexity of each conjugate gradient iteration it takes the same time as taken by iterative method. To overcome this inefficiency, preconditioning, an algebraic procedure to generate a transformed system of equations having a better eigenvalue spectrum, is used (Jacobs, 1981b). The widely used preconditioner, the incomplete Cholesky decomposition (Meijerink & van der Vorst, 1977; Kershaw, 1978), works satisfactorily only for a real and positive definite matrix. Another possible approach is to use augmented conjugate algorithm where the original complex system is augmented by its adjoint (Sarkar et al., 1988). But since the positive definiteness of the matrix is not known *a priori*, it can not be used. Mackie & Madden (1993a) and Mackie et al. (1994) have used minimum residual algorithm for real symmetric matrices (Axxelson, 1980) by neglecting the imaginary part of the diagonal term. This approach can not be followed here as the coefficient matrix \mathbf{C} is not symmetric.



Furthermore, the equation (4.58), required for generation of Jacobian matrix, has the same coefficient matrix as equation (4.33). In case of matrix solvers based on direct methods, the already existing LU decomposition of matrix \mathbf{C} can be reused. Whereas in other methods, the whole procedure is to be done afresh each time. All these points justified the use of direct method for solving the forward problem.

4.5.2 Inverse matrix solver

The EM inverse problem, in matrix form, is stated in equation (3.45). On account of the finite and erroneous data, the problem is ill-posed and need be regularised for obtaining an approximate solution. The problem, in general, is either overdetermined or underdetermined, depending upon the number of observations and parameters. For such cases, ridge-regressed least square or minimum norm estimators are used. These solutions are

$$\Delta \mathbf{P} = (\mathbf{J}^H \mathbf{J} + \lambda^2 \mathbf{I})^{-1} \mathbf{J}^H \Delta \mathbf{R} \quad \dots(4.69)$$

$$\text{and } \Delta \mathbf{P} = \mathbf{J}^H (\mathbf{J}^H \mathbf{J} + \lambda^2 \mathbf{I})^{-1} \Delta \mathbf{R} \quad \dots(4.70)$$

To obtain least square or minimum norm solution, the matrix \mathbf{J} should be evaluated before hand using equation (4.58). Since the inverse matrix equation (3.45) is to be solved only for single right hand side, semi-iterative methods can be used instead of the direct ones. Due to real data which is invariably erroneous, the resulting system of governing equations will be inconsistent. Therefore, only an approximate solution can be sought. This means that inaccuracy in the estimation of unknown parameters within a prescribed error range can be tolerated and this can be more efficiently achieved through iterative or semi-iterative methods. But when solved using direct or iterative methods the equation (4.33) is to be solved as many times as the number of blocks in the inversion domain, for each inversion iteration. In case of CGM, on the other hand, one avoids the explicit construction of \mathbf{J} . Instead only the product of \mathbf{J} or of its Hermitian with a given vector need be known. It is so because the coefficient matrix appears only in the product of the search vector \mathbf{P} with itself. Hence, the equation (4.33) is to be solved only twice for each inversion iteration.

Most of the literature on CGM has only dealt with the case of a real, symmetric and positive definite matrix (Reid, 1971). However, the system of equation (3.45) is complex. As a result, it is solved using the complex Bi-Conjugate Gradient Method (BCGM) where matrix \mathbf{J} or its Hermitian appears only in their product with the search

vector \mathbf{q} (Jacobs, 1986). Since resistivity is a real quantity, only the real part of the correction vector $\Delta\mathbf{P}$ is retained. The irregular behaviour of convergence is observed in BCGM. Moreover, the obtained solution does not reflect the true behaviour of resistivity. Hence, a way out has been found to recast the equation (3.45) into real form and the regular steps of BCGM are modified to solve this equation for an equivalent real system. The complex matrix and the right hand side are broken up into their real and imaginary parts and the equation (3.45) is written as

$$(\mathbf{J}_r + i\mathbf{J}_i) \Delta\mathbf{P} = (\Delta\mathbf{R}_r + i\mathbf{R}_i), \quad \dots(4.71)$$

where the 'r' and 'i' subscripts denote the real and imaginary parts respectively. The equation (4.71) can be rewritten as

$$\begin{pmatrix} \mathbf{J}_r \\ \mathbf{J}_i \end{pmatrix} \Delta\mathbf{P} = \begin{pmatrix} \Delta\mathbf{R}_r \\ \Delta\mathbf{R}_i \end{pmatrix}$$

or $\mathbf{J}_c \Delta\mathbf{P} = \mathbf{R}_c \quad \dots(4.72)$

where subscript 'c' indicates complex quantity. The obtained solution, correction vector $\Delta\mathbf{P}$, is real. There is no need of preconditioning as the system converges in two or three iterations. The basic steps of BCGM are discussed in Appendix 2. The inverse problem solution is obtained using BCGM to solve the matrix equation $\mathbf{Ax} = \mathbf{b}$, with the coefficient matrix \mathbf{A} and the right hand side vector \mathbf{b} defined for the two estimators given by equation (4.69) or (4.70), as

For least square

$$\mathbf{A} = (\mathbf{J}_c^H \mathbf{J}_c + \lambda^2 \mathbf{I})$$

$$\text{and } \mathbf{b} = \mathbf{J}_c^H \Delta\mathbf{R}_c$$

For minimum norm

$$\mathbf{A} = (\mathbf{J}_c \mathbf{J}_c^H + \lambda^2 \mathbf{I})$$

$$\text{and } \mathbf{b} = \Delta\mathbf{R}_c .$$

For minimum norm estimator, the solution vector \mathbf{x} is multiplied by \mathbf{J}_c^H to get the estimate. Hence, for solving above equations the product $(\mathbf{J}_c^H \mathbf{J}_c) \mathbf{q}$ or $(\mathbf{J}_c \mathbf{J}_c^H) \mathbf{q}$ is required. These can be computed as described below. Rewriting equation (4.58) in real and imaginary parts as

$$(\mathbf{C}_r + i\mathbf{C}_i) (\mathbf{J}_r + i\mathbf{J}_i) = \mathbf{Y}_r + i\mathbf{Y}_i. \quad \dots(4.73)$$

Splitting equation (4.73) into two equations corresponding to real and imaginary parts

$$C_r J_r - C_i J_i = Y_r \quad \dots(4.74a)$$

and

$$C_i J_r + C_r J_i = Y_i. \quad \dots(4.74b)$$

Above equations of real and imaginary parts can be combined and written in matrix form as

$$\begin{pmatrix} C_r & -C_i \\ C_i & C_r \end{pmatrix} \begin{pmatrix} J_r \\ J_i \end{pmatrix} = \begin{pmatrix} Y_r \\ Y_i \end{pmatrix}$$

or

$$C_c J_c = Y_c. \quad \dots(4.75)$$

Multiply equation (4.75) with an arbitrary vector q

$$C_c J_c q = Y_c q \quad \dots(4.76)$$

or

$$J_c q = C_c^{-1} Y_c q. \quad \dots(4.77)$$

Similarly, taking Hermitian of equation (4.75) as

$$J_c^H C_c^H = Y_c^H \quad \dots(4.78)$$

or

$$J_c^H = Y_c^H (C_c^H)^{-1} \quad \dots(4.79)$$

and multiplying it with an arbitrary vector q we get

$$J_c^H q = Y_c^H (C_c^H)^{-1} q. \quad \dots(4.80)$$

For each inverse problem iteration, the equation (4.33) is solved with as many right hand sides as the number of blocks in case of direct methods while in case of BCGM it is solved twice for each conjugate gradient iteration. Hence, BCGM scores over direct method as long as the number of iterations needed for convergence is less than half the number of blocks in inverted model. Further, BCGM is preferred to other iterative matrix solvers by virtue of its faster convergence rate.

The solution of forward problem, generation of Jacobian and the solution of inverse problem constitutes one iteration of the quasi-linear inversion.

4.6 Solution of the inverse problem

In inverse problem there are two levels of iterations. The outer loop is on the iterations of quasi-linearization, whereas the inner loop is on the iterations of the BCGM used to obtain the parameter correction vector.

The obtained correction vector $\Delta \mathbf{P}$ is added to the initial guess of parameter vector \mathbf{P}^0 from equation (3.48). Since P_j is related to ρ_j from equation (4.56), the equation (3.48) gets modified

$$\rho_j = \rho_j^0 \exp(\Delta P_j) \quad \dots(4.81)$$

The logarithmic parametrization works well for larger changes in the model parameter resulting from larger dynamic range in the signals and therefore it stabilizes the inversion procedure. The updated parameter vector \mathbf{P} is used as initial guess for the next iteration. After each iteration the solution is checked for convergence. The convergence is checked on two counts, the degree of improvement in the parameter vector and the level of fit. For fit, the computed response of the model is compared with the observed one and the computed root mean square (rms) error is then compared with a preassigned threshold value. The inversion process stops when either the convergence is achieved, or the rms error is greater than that of previous iteration or when the iteration number exceeds a given limit. The obtained model is accepted as one of the possible solution of the inverse problem.

4.7 Closure

The FDM having simple mathematics and easy implementation is preferred over other numerical methods for solving EM inverse problem. The direct matrix solver is chosen for solving forward matrix equation while conjugate gradient method for inverse matrix equation. The algorithm **EM2INV**, where the different aspects of finite difference implementation have been programmed, is discussed in Chapter 5.

CHAPTER 5

DEVELOPMENT OF ALGORITHM - *EM2INV*

5.1 General

The ultimate goal of any EM inversion algorithm is to find an optimum resistivity model by employing a cost-effective technique. The usage of EM methods is limited on account of their insufficient data inversion capabilities. Therefore, in the present research work, an effort has been made to develop an efficient 2-D EM data inversion algorithm **EM2INV**, by numerically implementing the forward and inverse formulations discussed in Chapter 4.

5.2 Background

The survey of literature on EM data inversion had revealed that, in 1993, the bulk of quantitative interpretation was carried out using 1-D inversion algorithms. Even today, the multidimensional data inversion is carried out through stacking of results obtained using 1-D inversion algorithm (Fischer et al., 1981; Constable et al., 1987; Agarwal et al., 1993). For EMSLAB, one of the most significant experiment of EM data procurement and analysis (EMSLAB, 1988), the trial and error forward modelling was used for quantitative interpretation of 3-D data (Wannamaker et al., 1989b). Jiracek et al. (1989), however, did use the 2-D inversion algorithm of Rodi et al. (1984) for inversion of the same data.

The 2-D inversion algorithms are appearing in literature since late seventies, e.g. Weidelt (1975b), Jupp & Vozoff (1977), Rodi et al. (1984), Pek (1985), Sasaki (1987), deGroot-Hedlin & Constable (1990), Oldenburg (1990), Smith & Booker (1991), Oldenburg & Ellis (1993), Yamane et al. (1996). Rapid Relaxation Inversion (RRI)

scheme of Smith & Booker (1991) iteratively improves the 1-D inversion result whereas the generalized RRI of Yamane et al. (1996) is based on a localized 2-D analysis. Isolated attempts of 3-D data inversion have also been reported, e.g. by Mackie & Madden (1993b). Although results of these inversion algorithms are available in literature, yet these are in restricted circulation. After critical assessment of all the available alternatives, it was concluded that there still exists a dire need of development of an efficient 2-D inversion algorithm for EM data.

The Finite Difference Method (FDM) was chosen as the numerical technique for modelling and inversion, primarily because of its simplicity and also because of its exhaustive presentation by Brewitt-Taylor & Weaver (1976). Like any major exercise, the algorithm **EM2INV** was also developed in various stages.

5.3 Sequence of development

The present research work, spanning over a period of more than three years, started with the development of a primitive algorithm which implemented simple boundary conditions and modelled simple geometries. During the course of time, the different versions of inversion algorithm were developed. Some features of these intermediate versions have survived in the final version, while others have been dropped out. It must be emphasized here that some of the failures helped us in learning lessons which, in turn, led to the improvements in the algorithm. The outcome of this thorough and extensive research is the 2-D EM data inversion algorithm, **EM2INV**. In order to give a flavour of the circuitous route of development, the various versions of algorithm are briefly discussed.

5.3.1 Version I

The foundation of present research work is the paper of Brewitt-Taylor & Weaver(1976) which described the finite difference modelling of 2-D induction problems through the EM Boundary Value Problem (BVP) comprising the governing Helmholtz equations and simple Dirichlet boundary conditions. Electromagnetic BVP is solved, using finite difference method, for the magnetic and/or electric field components. Resulting finite difference coefficient matrix is complex, symmetric and pentadiagonal. The non-linear EM problem is quasi-linearized for solution of the inverse problem. To start with, the algorithm was developed for profiling and subsequently it was modified for sounding data.

The Gaussian elimination method, exploiting the banded structure of coefficient matrix, was used for solving the forward as well as inverse matrix equation. The Jacobian matrix **J** was generated explicitly and stored. This means that for each inversion iteration, the forward matrix equation was to be solved for as many right hand sides as the number of blocks. The direct matrix solver, where the original Lower triangular and Upper triangular (LU) decomposition was reused every time, was considered more efficient for this purpose.

It was realized that inspite of being based on FDM recommendations the manually generated grid was not optimized as simplest Dirichlet boundary conditions were used. Although the algorithm version I was saving computation time in generation of Jacobian matrix by using LU decomposition of the forward direct matrix solver, yet the overall time taken in solving the inverse problem was quite large. The explicit computation and storage of Jacobian matrix accounted for a major share of computer time requirements.

For improving efficiency of the algorithm, an iterative method was employed to solve the forward matrix equation in the algorithm version II.

5.3.2 Version II

The Alternating Direction Implicit Scheme (ADIS), an iterative scheme, was used for solving forward problem. In ADIS, the 2-D forward problem was partitioned to two 1-D problems, each of which resulted in tridiagonal FDM coefficient matrices. The 2-D problem was solved, iteratively by solving the 1-D problem in two directions, alternatively in each iteration. This resulted in a significantly fast forward algorithm. However, it was discovered that large number of inversion iterations, increased the total computation time. The interpolated field at interior nodes using boundary field values was also used as initial guess for faster convergence. For some cases the algorithm was faster than the version I but on the whole the inference in this regard was inconclusive. Therefore, an alternate iterative method was tried in version III.

5.3.3 Version III

The structure of complex coefficient matrix was judiciously exploited in this version of the algorithm (Rastogi et al., 1994). A glance at equation (4.33) reveals that the complex coefficient matrix **C** can be partitioned as the following sum of two real submatrices

$$C = A + iD. \quad \dots(5.1)$$

In equation (5.1), **A** is a real, symmetric and pentadiagonal matrix depending only on the grid geometry, while **D** is a real diagonal matrix that depends on both, conductivity structure and grid geometry. Using this decomposition, equation (4.33) was written as

$$(A + iD)F = S \quad \dots(5.2)$$

to set up the following iterative relation for evaluation of field values **F**

$$F = A^{-1}S - iA^{-1}DF \quad \dots(5.3)$$

Throughout the inversion process there is no change in grid geometry, therefore, the matrix **A** remains unchanged. This implies that **A** need be evaluated and LU decomposed only once. However, due to updating of block resistivities after each inversion iteration, the diagonal matrix **D** changes and needs reevaluation of the second term of equation (5.3) each time.

This scheme was implemented in the version III of the algorithm. The modified algorithm scored over the previous one but it was constrained by following limitations:

- (1) The algorithm worked only for the E-polarization.
- (2) The grid spacings had to be uniform within the inversion domain to assign equal weights to the elements of diagonal matrix **D**, which were weighted average of conductivities of the surrounding four blocks at a particular node. However, outside this domain it was non-uniform.
- (3) The matrix **D** was treated as a perturbation in **A**. Therefore, to achieve convergence in matrix solution the small grid spacing must be chosen. This constrained the choice of test model size due to limitations of computer memory.

To improve convergence for large grid spacings, the relaxation was also introduced but it did not lead to much improvement. Although the algorithm was successfully tried on initial models, yet it was found to be inefficient for large models.

5.3.4 Version IV

Around this time we came across the papers of Mackie & Madden (1993a, 1993b) on 3-D modelling and inversion using Conjugate Gradient Method (CGM). They highlighted the advantages of CGM over other matrix solvers, especially for inverse matrix equation as it dispenses with the explicit Jacobian computation. Inspired by their

work, we incorporated CGM in our inversion algorithm also. Mackie & Madden (1993a) worked with an approximate real problem, neglecting imaginary component, whereas we preferred to work with complex inverse matrix equation and therefore used Bi-Conjugate Gradient Method (BCGM). In the process we developed our own subprogram for BCGM. The convergence rate of BCGM was dependent on the coefficient matrix, in particular, on the number of distinct eigenvalues and their spread. Fewer the numbers of distinct eigenvalues, lesser numbers of steps were needed to obtain the solution (Jennings, 1977). Although the explicit generation of \mathbf{J} was avoided, yet the uniformly distributed eigenvalues of FDM coefficient matrix resulted in large number of iterations for convergence. Hence, preconditioning, an algebraic procedure to redistribute eigenvalues, was used so that the modified coefficient matrix had clustered eigenvalues. The matrix was symmetric but it was not Hermitian as the diagonal elements were complex. The incomplete Cholesky decomposition was implemented in BCGM as FDM coefficient matrix was also a M-matrix (Meijerink & van der Vorst, 1977). This modification resulted in faster convergence.

During the testing of version IV, it was observed that the rate of convergence of BCGM was sensitive to the ratio of grid spacing to skin depth. Smaller this ratio, faster was the convergence. However, the economy of BCGM was offset by the increase in time of individual iteration due to the larger grid size. In view of this trade-off, the multigrid procedure was devised and implemented in the next version.

5.3.5 Version V

The multigrid procedure and multilevel inversion were implemented in version IV of the 2-D inversion algorithm (Rastogi et al., 1997).

Starting with a coarse grid and an initial guess model the problem is solved in a number of steps in the multigrid procedure (McCormick, 1987). In subsequent steps, the grid is refined and the last obtained coarse grid solution is interpolated for its use as initial guess for the refined grid. The strategy is followed till the preassigned grid refinement is achieved. The inversion being an iterative procedure, the initial guess for each refined grid, provided by the solution of previous grid, is closer to the solution than the one originally guessed and this results in faster convergence and it drastically reduced computation time.

For further improvement of the inversion quality, the multilevel inversion was attempted. From the first inverted result the top-level block resistivities are fixed and

the inversion exercise is repeated with the reduced inversion domain, comprising the remaining levels. This is done till the last level resistivities are finally estimated. In subsequent iterations, the number of unknown blocks kept on reducing and thus enhanced the convergence rate.

Besides the error free synthetic data, the inversion algorithm was also tested for synthetic data with 5% Gaussian noise and modified for sounding data. The problems faced with this version were due to the large domain of study which yielded large grid sizes.

5.3.6 Version VI

The final version of inversion algorithm **EM2INV** was achieved after the forward program was modified by incorporating features like automatic grid generator and the integral and asymptotic boundary conditions. The skeletons of subprograms for these purposes were adapted from the program fr2d.for of Weaver (1995). Now an optimal FDM grid, based on standard thumb rules, is generated. The exceptionally large extent of model domain is reduced by imposing integral boundary conditions on the horizontal and asymptotic boundary conditions on the vertical boundaries of the domain. These modifications result in FDM coefficient matrix which instead of a pentadiagonal structure has only a block tridiagonal structure. Loss in sparsity structure of coefficient matrix is, however, made up by the economy in grid size. This change in structure forced us to forgo BCGM and use the direct matrix solver for the forward problem. The Gaussian elimination method is used for forward matrix equation where the inverse of each block submatrix is obtained using Gauss-Jordan method. These block inverses are stored and used for solving the forward matrix equation for multiple right hand sides during Jacobian based computations.

The inverse matrix equation is still solved using BCGM because of its special feature of circumventing explicit computation of Jacobian matrix. The splitting into real and imaginary parts has been implemented using the BCGM. The forward matrix equation is solved only twice for each BCGM iteration. In addition to this, the Jacobian matrix need not be stored. These savings in generation and storage of Jacobian economize the computer time. Further, this saving in each BCGM iteration reduces the time of each inversion iteration and, in turn, of overall inversion procedure. The salient features of the final algorithm **EM2INV** are discussed next.

5.4 Salient features

Besides the matrix solvers, various measures are taken to enhance the efficiency and versatility of the algorithm **EM2INV**. Since the algorithm has a compact modular structure, a subroutine can be plugged in or taken out easily without affecting the remaining program. The special features result in a cost effective algorithm providing good quality inversion. The various features, depending on whether they enhance versatility or efficiency, are categorized in two groups and discussed in that order below.

5.4.1 Versatility features

The versatility of an algorithm ascertains its applicability in diverse situations. Different versatility features of inversion algorithm **EM2INV** pertain to types of response functions, sounding data and noisy synthetic data.

5.4.1.1 Response functions

The algorithm **EM2INV** can be used for 2-D inversion of MT as well as GDS data. For response functions like impedance, induction vector or apparent resistivity, the transformation matrices are computed using the corresponding field component for B- or E-polarization. These transformation matrices together with the Jacobian matrix $J_x^{E,B}$, corresponding to the main field component, then lead to the Jacobians for response functions given by equations (4.63), (4.65) and (4.67). The transformation matrices are computed in subroutines **BDERIV** or **EDERIV**, whereas subroutine **RESMAT** is called for respective Jacobian based computations.

Further, for synthetic exercises, the inversion of different field components for the B- and E- polarizations can also be performed.

5.4.1.2 Sounding data

The development of **EM2INV** was initiated with single frequency inversion using the optimal grid generated by the grid generator routine during each inversion iteration. Subsequently, the algorithm was modified for sounding enabling inversion of data over a frequency range. Since the grid size is frequency-dependent, the grid generation rules are in terms of skin depth. The change in frequency results in grid changes. The different grid for various frequencies will give rise to different number of unknowns, i.e. resistivities of blocks within the inversion domain. To keep these number of blocks fixed, superblock notion, discussed later, has been devised.

5.4.1.3 Source term

The program is so structured that initially the computations are carried out in terms of secondary fields. Later on, for the total field computations, the secondary fields are added to the primary fields. Therefore, in order to incorporate the source effect only a subroutine, computing the response of primary layered earth model in presence of source, is to be added in lieu of the existing **ONEDF** subroutine which computes 1-D field due to a plane wave source.

5.4.1.4 Gaussian noise

In order to simulate erroneous characteristic of real data, the synthetic data is corrupted with Gaussian noise. The function **RAND** is used for generating the noise for a given signal to noise ratio. It generates mean, unit variance random noise following Gaussian distribution.

5.4.1.5 Field and synthetic data

The inversion algorithm **EM2INV** can handle both field and synthetic data. For synthetic models, first the forward response is generated, next, if desired, corrupted with noise and then inverted.

5.4.2 Efficiency features

Efficiency is a measure of how much saving has been achieved in computer time and memory to obtain a solution of given quality. In this respect, several notions and computational techniques have been employed.

5.4.2.1 Superblock

During the implementation of sounding data in the algorithm **EM2INV**, the ticklish problem was how to fix the number of blocks with unknown resistivity for all the grids of given frequencies. In order to keep this number of blocks constant throughout the procedure, inversion was tried using the same grid for all frequencies. The choice of this single frequency grid is crucial. The usage of the grid corresponding to the lowest, an optimal intermediate or the highest frequency resulted in inaccurate results as the response for other frequencies was erroneous. The errors were quite significant and therefore, for all frequencies of the given range, same grid cannot be used. Moreover, the small horizontal extent of highest frequency grid was too restricted for other lower frequencies.

As a result a frequency, considered ideal for tapping the target, is selected from the given frequency range. The choice of this ideal frequency is governed by the characteristics of the observed response and the expected target. The blocks within the inversion domain, corresponding to the grid of this frequency, are termed as 'superblocks'. The superblocks, for standard frequency, are generated in the starting of the inversion process. Later on, the grids are generated for other frequencies with the inversion domain defined in such a manner that there exist grid lines corresponding to the superblocks boundaries. If the generated grid is finer than the standard grid, a few of its blocks are merged to form a superblock. As a result, the number of blocks to be inverted remains constant throughout the inversion procedure. For example superblocks formed by merging four subblocks are shown in Fig. 5.1. The superblock notion results in reduction of Jacobian matrix size. This reduction in number of blocks, in most of the cases, converts the minimum norm problem to a least square one.

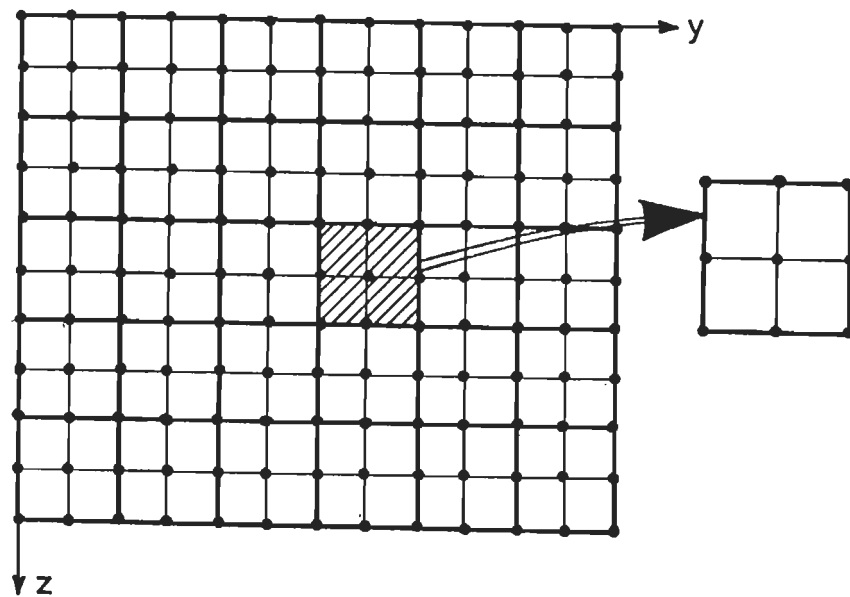


Fig. 5.1 Finite difference grid and nodes to demonstrate superblock notion. Thick lines represent boundaries of superblocks formed by merging four subblocks.

For Jacobian matrix based computations the equation (3.49) is solved, where the derivative of FDM matrix contains only four non-zero terms with respect to a particular block resistivity. If a superblock is having more than one subblock, it is associated with more than four nodes, thereby reducing the sparsity of \mathbf{J} . These computations, depending upon the number of subblocks and of the associated nodes, are carried out in subroutine **RHSMAT**. The superblock notion is implemented through subroutines **SUPBLK**, **RHSV**, **RHSMAT**, **INVDOM**.

5.4.2.2 Grid generator

The FDM grid should be designed according to certain basic thumb rules. The grid generator, **GRIDYZ** adapted from fr2d.for of Weaver (1995), generates an optimal grid for a given frequency. By doing so, not only the manual labour is saved but it also leads to more accurate results as accuracy of finite difference algorithm depends on grid spacings.

5.4.2.3 Logarithm of resistivity

Logarithm of resistivity is used as unknown variable in the algorithm. It removes the bias against the choice of conductivity or resistivity and ensures a positive value of resistivity.

5.4.2.4 Interpolation matrix

The observation points, in general, do not coincide with the grid points and therefore, the response has to be interpolated. For obtaining the response at observation points, an interpolation matrix, I_p , of order $n_{obs} \times n_y$ is computed where n_{obs} and n_y are the number of observation and grid points in y direction respectively. Linear interpolation has been used for this purpose.

During each inversion iteration, the interpolation matrix is computed only once. Instead of storing the full matrix only the weights and the column positions of non-zero elements in each row are stored. The product of interpolation matrix with the grid response vector gives the desired interpolated vector.

5.4.2.5 Bi-Conjugate gradient method

The inverse matrix equation (4.58) is solved using the bi-conjugate gradient method. This particular choice of matrix solver is governed by the fact that BCGM does not need explicit computation of Jacobian matrix. All it needs is the product of this matrix or its Hermitian with a vector and compute Jacobian matrix explicitly (see section 4.5). Moreover, for each inversion iteration the forward matrix equation (4.33) is solved only twice, in contrast to other matrix solvers where it has to be solved as many times as is the number of blocks. So, till the number of iterations is less than half the number of blocks, the BCGM will be more efficient than other methods.

5.4.2.6 Finite domain boundary conditions

Instead of imposing Dirichlet boundary conditions at sufficiently far placed boundaries, the horizontal and vertical extent of domain is restricted by imposing the

asymptotic and integral boundary conditions on vertical and horizontal domain boundaries respectively. These boundary conditions not only result in grid economy but also yields more accurate results.

5.5 Description of algorithm

The algorithm **EM2INV**, based on the finite difference formulation, is developed for inversion of 2-D geoelectromagnetic data. It comprises 6120 lines, 42 subroutines and 3 function subprograms. It employs 14 integer, 12 complex and 22 real arrays. The 14 common statements, defined in main program, exchange information between various subprograms. The program works in double precision arithmetic. In order to control dimension overflows, various checks with error and stop messages are inserted in the program. The arrays are initialized and reused to optimize the memory requirements. The description and salient features of inversion algorithm are highlighted in Fig. 5.2.

In total nine I/O units are opened in the main program. The parameter and data controls are read from the file **EM.DAT**. The two scratch files are used for buffer storage. The remaining six output files are used for outputs in different formats. The documentation and the input requirements of **EM2INV** for various modes, along with the corresponding input and output files, are given in Appendix 3.

5.5.1 Structure

The main module of the inversion algorithm **EM2INV** provides the infrastructure and the run controls. It can be partitioned into two basic modules, i.e. Forward and Inverse modules. The main program gets the control parameters by calling the subroutine **DTCTRL** and then decides to which module it should get directed to. Two operational subroutines **FWDSOL** and **INVSOL** constitute the forward and inverse modules respectively. Flow chart of the main program is given in Fig. 5.3.

The parameters read in **DTCTRL** are **nprnt**, **ninv**, **nert**, **npol**, **ncond** and **nper**. The frequency/period, whose grid is chosen as the standard, is termed as **jfq**. The choice of base field component is governed by **ntype**. The ω and μ values for different periods are computed and stored in arrays **aomega** and **aomu** respectively. The control parameters, their purpose(s) and the numerical values for different options are listed in Table 5.1.

EM2INV	- 6,120 Lines
Main Program	476 Lines
Subroutines (34+8')	- 5,551 Lines
Functions (2+1')	- 84 Lines
* Adapted from various programs	

METHODOLOGY

Finite Difference Method.
Quasi-linearized inversion.
Bi-Conjugate Gradient matrix solver.

FORWARD MODELLING

EFFICIENCY FEATURES

- **Automatic grid generation.**
- **Asymptotic boundary conditions** on vertical boundaries.
- **Integral boundary conditions** on horizontal boundaries.
- **Gaussian elimination**, direct matrix solver.

VERSATILITY FEATURES

- **Response functions** for MT and GDS data.
- **Gaussian noise.**
- **Profiling and Sounding** data.

DATA INVERSION

EFFICIENCY FEATURES

- **Jacobian matrix not** explicitly computed.
- **Ridge-regressed** estimators.
- **Superblock inversion.**
- **Logarithm** of resistivity.
- **Interpolation** matrix.

VERSATILITY FEATURES

- **Field/Synthetic** data.
- **Profiling and Sounding** data.
- **Transformation matrices** for response functions.

Fig. 5.2 EM2INV, the inversion algorithm at a glance.

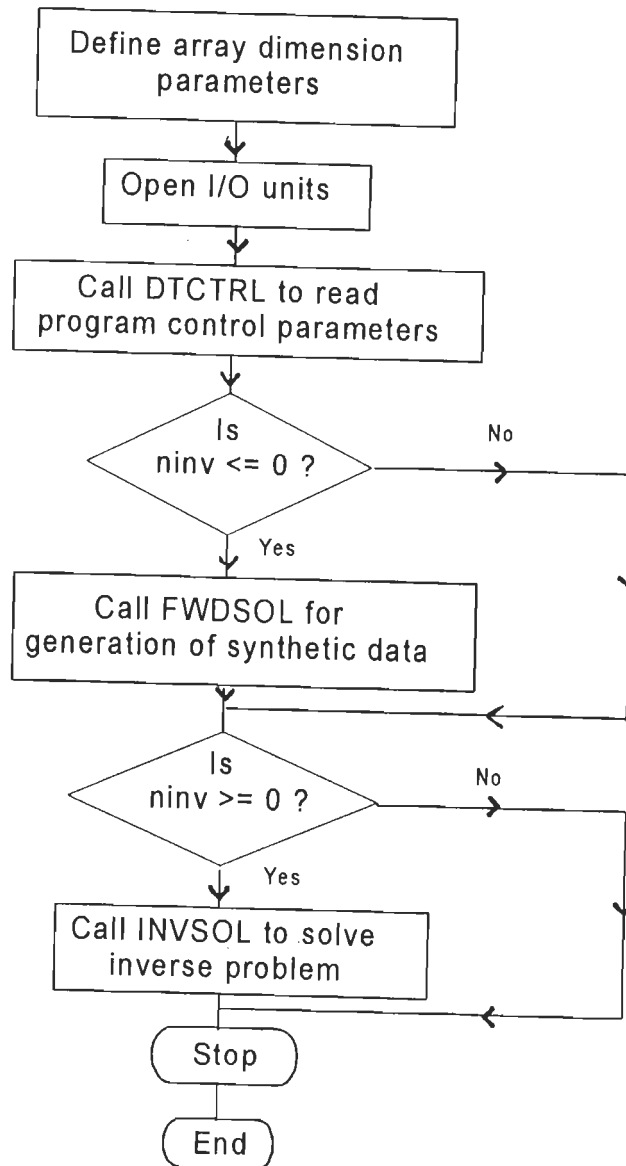


Fig. 5.3 Flow chart of the main program of algorithm EM2INV.

Table 5.1 Description of **EM2INV** control parameters

Parameter	What it controls	Values	Description
nprnt	Output of EM2INV	0	For final iteration
		1	For each inversion iteration
		2	For each inversion & BCGM iteration
		3	Detailed results
ninv	Problem type, i.e. forward or inverse	-1	Only forward
		0	Both forward & inverse
		1	Only inverse
nert	Noise to be added in the synthetic response	-1	Noise free
		0	Gaussian noise
npol	Mode of polarization	0	B-polarization
		1	E-polarization
nder	Order of differences whose norm is minimizes in regression estimator	0	Minimum norm
		1	Occam's inversion
ncond	Indicates parameter data type	0	Conductivity
		1	Resistivity
ntype	Response type	1	B_x or E_x
		2	B_y or E_y
		3	B_z
		4	ρ_{yx} or ρ_{xy}
		5	Z_{yx} or Z_{xy}
		6	I_{zy}

5.5.2 Subprograms of **EM2INV**

Out of the 45 subprograms of the inversion algorithm **EM2INV**, 30 are developed by us, 10 are adapted from Weaver's program fr2d.for and the remaining 5 are borrowed from the literature. The subprograms, categorized as forward subprograms or inversion subprograms according to the module in which these are called, are discussed below one by one. Grid parameters and other run environment parameters used in subprograms are described in Table 5.2.

Table 5.2 Brief description of grid parameters used in **EM2INV**

Parameter	Description
ny	Number of nodes in y- direction
nz	Number of nodes in z- direction
nyz2 = (ny-2) x (nz-2)	Number of internal nodes
nyzc = nyz2 + 2(ny-2)	Number of unknown field values
nper	Number of time periods
nobs	Total number of observation points for a given period
nobp = nper * nobs	Total number of observation points for all time periods
nbl	Number of superblocks in inversion domain
mnter	Minimum number of inversion iterations after which convergence is checked
mxter	Maximum number of inversion iterations
eps	Convergence threshold for inversion
mni	Minimum number of BCGM iterations after which convergence is checked
mxi	Maximum number of BCGM iterations
epi	Convergence threshold for BCGM
aps	Regression parameter
jy	Running index of node in y- direction
kz	Running index of node in z- direction
jfq	Index for standard frequency
ifq	Running index for general frequency

5.5.2.1 Forward subprograms

The forward subprograms are called in the forward module **FWDSOL**, which is called for model response generation. For this purpose, the input data and other parameters are read in the subroutine **DTFWD**. The subroutine **RESPONSE** is called to compute the response for a given frequency. In order to simulate real data, the random noise can also be added by calling **ERRADD** (Fig. 5.4). The tree of various subprograms, in the order they are called in **FWDSOL**, is shown in Fig. 5.5. A list of various subprograms along with their purpose, the subroutines these are called in and subroutine they call is given in Table 5.3 for completeness.

Development of algorithm

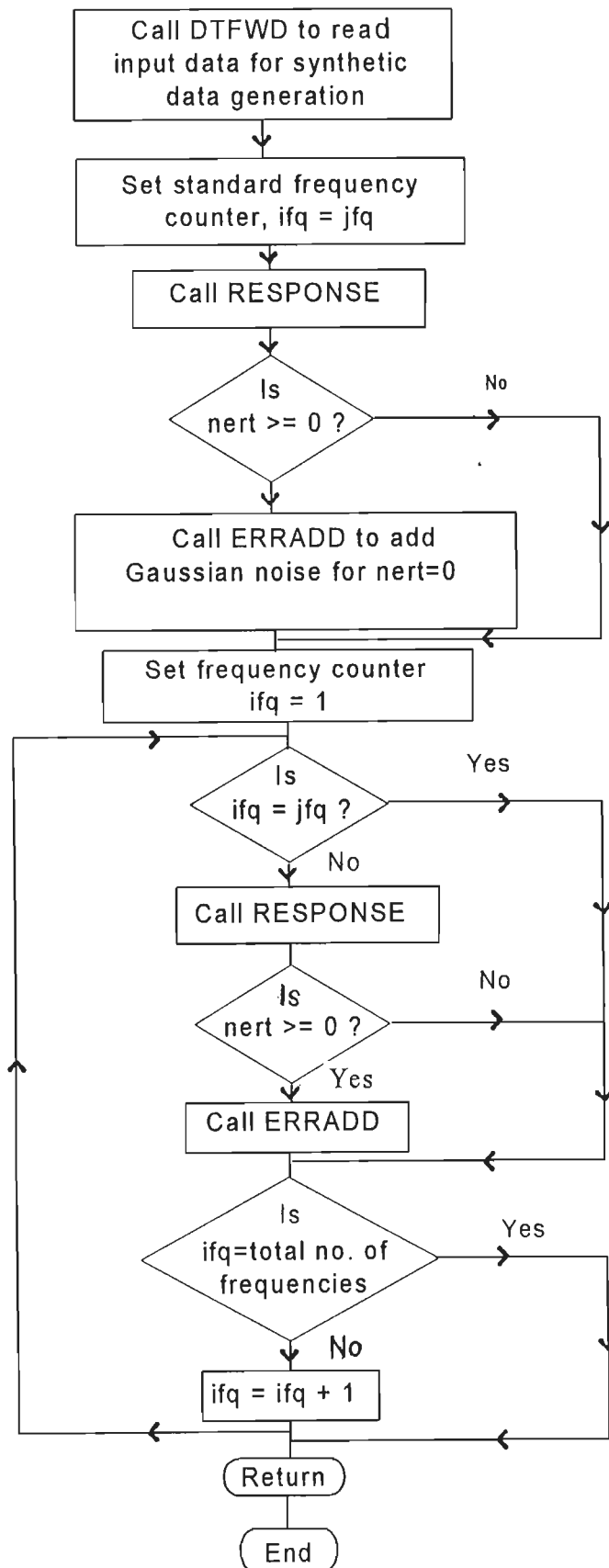


Fig. 5.4 Flow chart of subroutine FWDSOL.

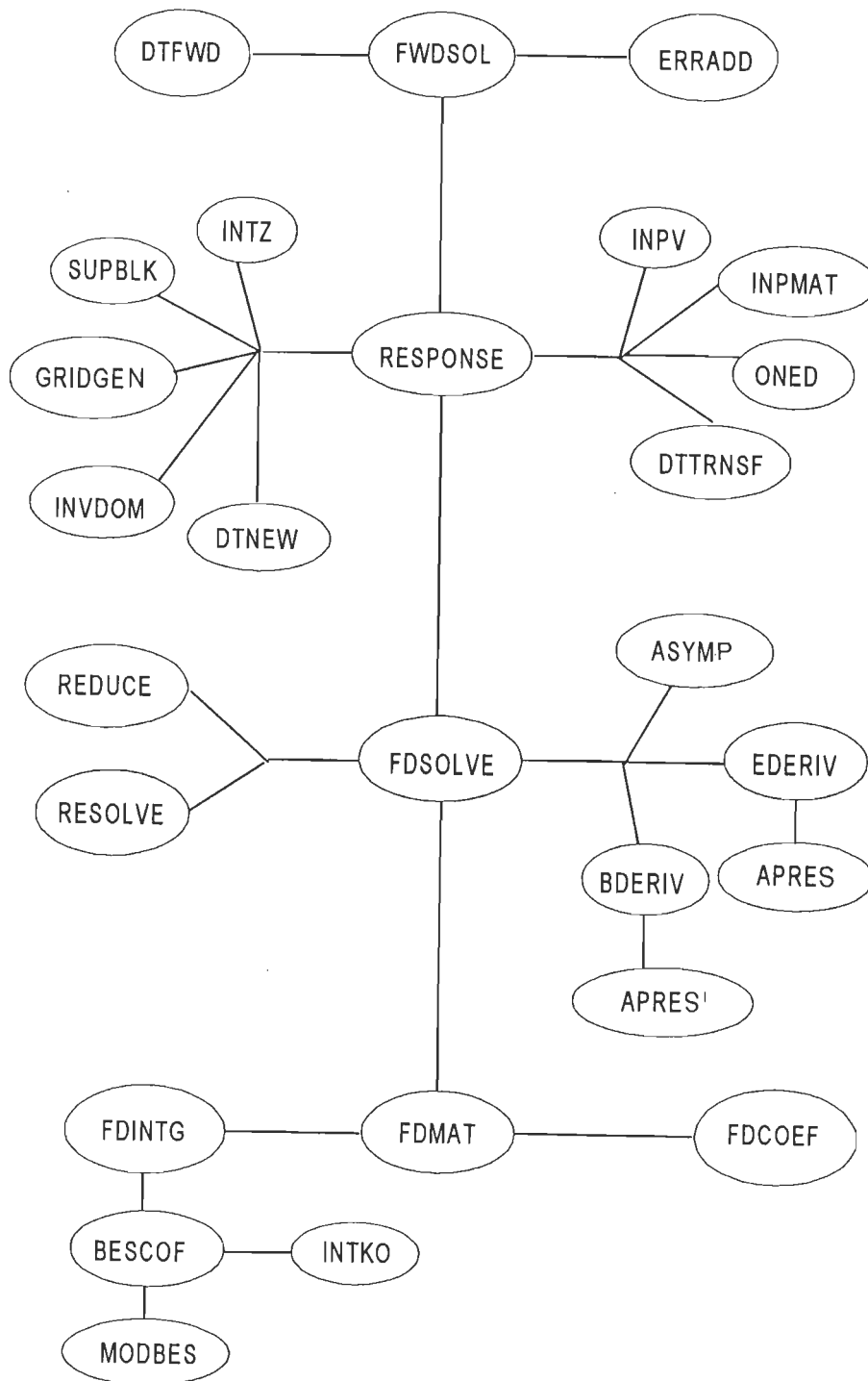


Fig. 5.5 Tree of subprograms called in subroutine FWDSOL.

Table 5.3 Various forward subprograms and their purpose(s)

Subprogram	Purpose	Called by	Calls
APRES	Computes apparent resistivity and phase of impedance	BDERIV EDERIV	x
ASYMP	Convert obtained secondary field values to total field values Computes asymptotic boundary conditions for E-polarization	FDMAT	x
BESCOF	Computes bottom integral boundary condition coefficients involving Bessel functions	FDMAT	BESVV BESWW INTKO MODBES
BESVV	Computes zeroth order modified Bessel functions	BESCOF	x
BESWW	Computes first order modified Bessel functions	BESCOF	x
BDERIV	Computes derived field components and response functions for B- polarization	FWDSOL	APRES
DTFWD	Reads input for synthetic data generation	FWDSOL	x
DTRNSF	Transfers grid information to(from) global from(to) local arrays	RESPONSE	x
EDERIV	Computes derived field components and response functions for E-polarization	FWDSOL	APRES
ERRADD	Adds random noise to synthetic response	FWDSOL	RAND
FDCOEF	Calculates FDM coefficient submatrix for internal nodes	FDMAT	x
FDINTG	Calculates top and bottom block matrices of coefficient matrix for integral boundary conditions	FDMAT	BESCOF
FDMAT	Generates entire FDM coefficient matrix	RESPONSE	FDCOEF FDINTG

Table 5.3 Contd.

FDSOLVE	Solve forward matrix equation (4.33)	RESPONSE	INTZ FDMAT REDUCE RESOLVE ASYMP EDERIV BDERIV
FWDSOL	Computes forward response of a model for given frequencies	Main	DTFWD RESPONSE ERRADD
GRIDGEN	Controls optimal grid generation	RESPONSE	SORT GRIDYZ RNDOFF
GRIDYZ	Generates optimal grid lines in y- or z- direction	GRIDGEN	x
INPMAT	Define interpolation matrix by computing and storing weights and column positions	RESPONSE	x
INPV	Computes product of interpolation matrix or its transpose with a vector	RESPONSE	x
INTKO	Computes integral over modified Bessel function	BESCOF	x
INTZ	Initializes an array to zero	FWDSOL INVSOL	x
MODBES	Calculates zeroth and first order modified Bessel functions of second kind	BESCOF	x
MAXMZ	Finds maximum magnitude component of a vector	INVSOL	x
ONEDF	Computes 1-D field values at left and right grid boundaries	RESPONSE	x
RAND	Generates random numbers	ERRADD	x
REDUCE	Computes inverse of each block matrix Reduce block tridiagonal matrix to upper bidiagonal matrix using Gauss-Jordan method	FDMAT	x
RESOLVE	Reduces the right hand side and obtains solution by backsubstitution	FDMAT	x

Table 5.3 Contd.

RESPONSE	Computes model response for single frequency	FWDSOL INVSOL	INTZ GRIDGEN INVDOM SUPBLK DTNEW DTTRNSF ONEDF FDSOLVE INPMAT INPV
RNDOFF	Rounds off grid spacings	GRIDGEN	x
SORT	Sorts out grid spacings in increasing order	GRIDGEN	x

Few important forward subprograms are briefly described here.

Subroutine **DTFWD** is called only for synthetic problems where the forward response is to be computed for data generation. Here the data is read in two parts. Firstly, it reads in arrays **cy**, **cz** the y, z coordinates of constant resistivity subregions and in arrays **dy**, **dz** the spacings. The resistivity or conductivity is read in array **res**. The scaling factor for grid spacing values, **scale**, is read later. The second set is read only when random noise is to be added to the computed response. The number of data points, **neran**, where noise is to be added and the percentage of noise level **rns** are read. If noise is not to be added at all points then use arrays **ierr** and **aerr** location and percentage of noise level for the selected point are additionally read.

Subroutine **RESPONSE** computes the model response for single frequency. Its operations include FDM grid generation, 1-D field computations and the model response computations. First, **GRIDGEN** is called for grid generation. In case of an inverse problem, the subroutines **DTNEW**, **INVDOM** and **SUPBLK**, described under inversion subprograms, are also called. The relevant grid information is stored into global arrays by calling **DTTRNSF**. The subroutine **ONEDF** next computes 1-D boundary field. Finally, the **FDMSOLVE** is called for computing the model response. If the observation points are not grid points then the response is interpolated by calling **INPOL** and **INPV** as shown in flow chart 5.6.

Subroutine **GRIDGEN**, adapted from Weaver's program fr2d.for, is called for optimal grid generation. The model coordinates and resistivity/conductivity read in

DTFWD and/or **DTINV** are used as input. The grid lines are generated in y - and z -directions one after the other in three steps. The subroutines **SORT**, **GRIDYZ** and **RNDOFF** are called for sorting the input coordinate data in increasing order, for grid generation and for rounding off grid spacings.

Subroutine **FDSOLVE** computes the unknown field values at surface/internal nodes for a given model and mode of polarization. For this purpose, the coefficient matrix elements are generated by calling the subroutine **FDMAT**. It may be stressed here that the coefficient matrix is generated for each horizontal grid line and the resulting block matrices are reduced to upper bidiagonal form and the reduction is complete. The solution is obtained by calling **RESOLVE**. For inverse problem the Hermitian of FDM coefficient matrix is also reduced and stored. The final solution comprises the secondary field values at nodes. These field values are converted to total field values by adding primary field in **ASYMP**. For E-polarization the asymptotic boundary conditions are employed to modify the field values at first and last nodes of the top interface. Once the base field component, corresponding to polarization mode, is computed the other field components can be derived using **BDERIV** or **EDERIV** as shown in flow chart 5.7.

Subroutine **REDUCE** is called for reducing the FDM block tridiagonal coefficient matrix to an upper bidiagonal block matrix during the solution of forward matrix equation (4.33). It is so programmed as to exploit the block diagonal structure of coefficient matrix. The reduction is carried out in two steps. The first step is to compute the inverse of diagonal subblock using Gauss-Jordan method while the second step is to reduce the corresponding block row of FDM matrix. The block matrix inverses are written on records and stored in buffer.

Subroutine **RESOLVE** reduces the right hand side of equation (4.58) and performs backsubstitution to obtain the solution. For backsubstitution, it reads the record from buffer one by one to retrieve the inverse of block matrix.

Subroutine **INPMAT** generates an interpolation matrix for interpolating a given vector when the observation points do not coincide with the grid nodes. The size of interpolation matrix is $n_{obs} \times n_y$. In place of storing the full matrix only the value **wt** and the column positions, **ipcol**, of non-zero elements are stored. If grid is smaller than the observation profile, the field is taken as 1-D for the points to the left of the first grid point or to the right of the last grid point.

Development of algorithm

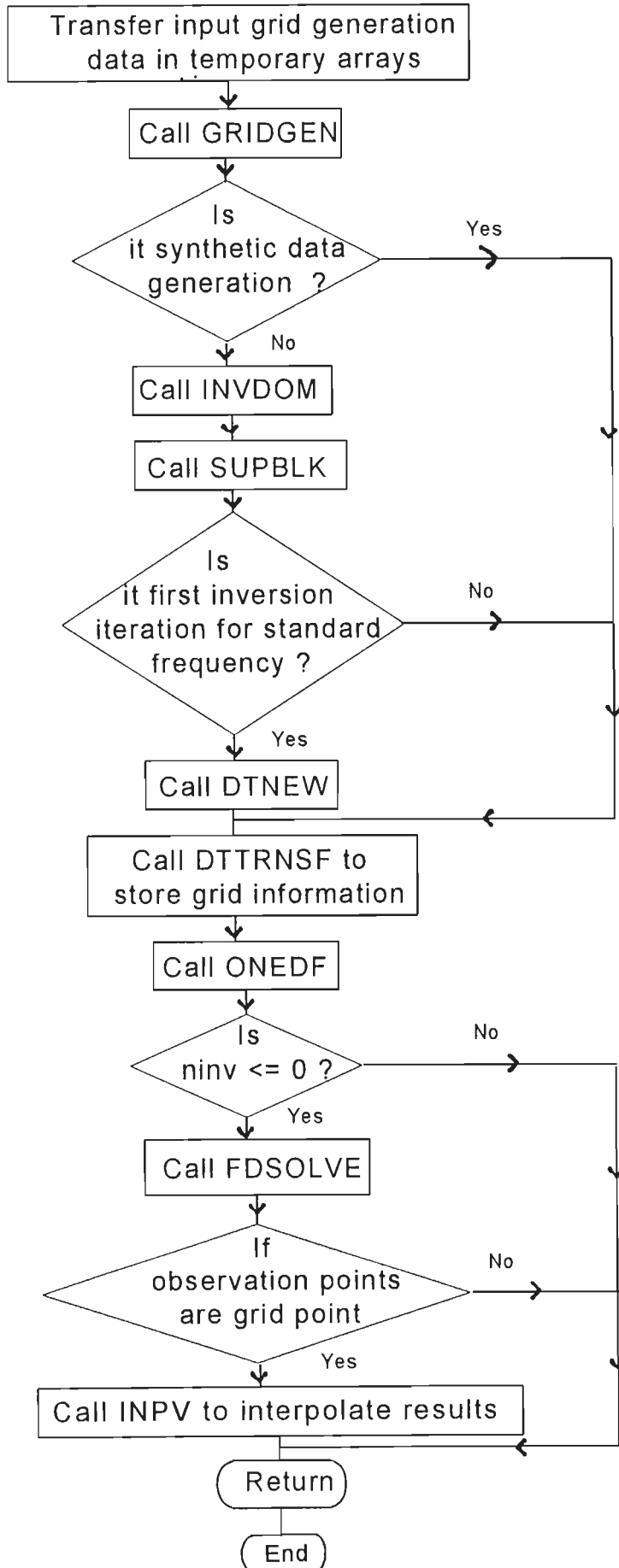
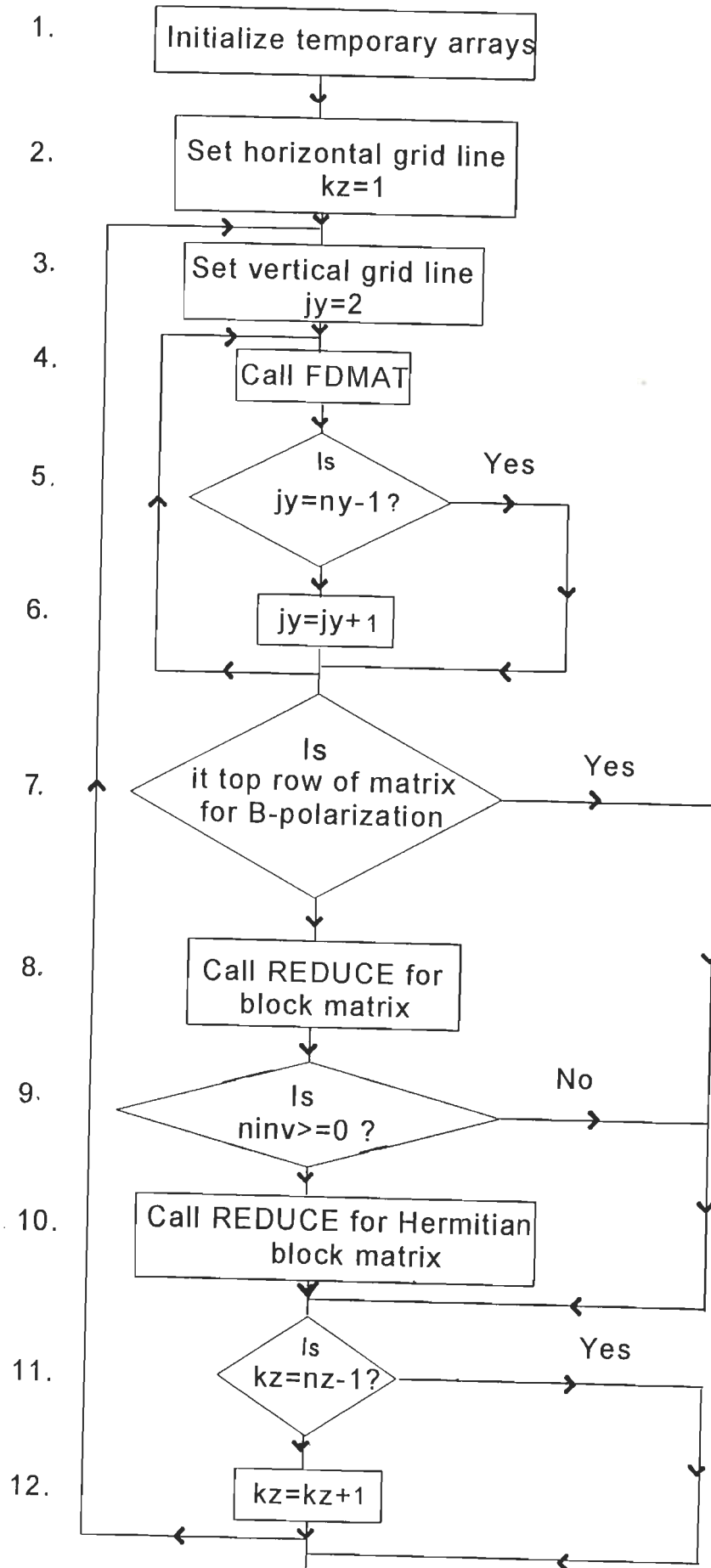


Fig. 5.6 Flow chart of subroutine **RESPONSE**.

Development of algorithm



To Step 13

Fig. 5.7 Contd.

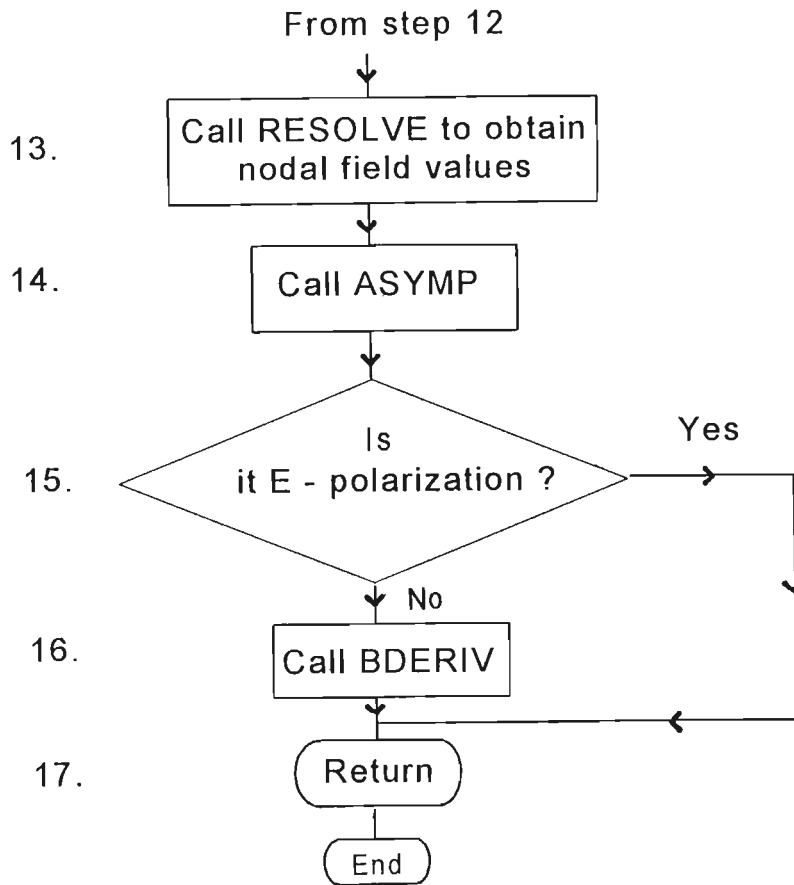


Fig. 5.7 Flow chart of subroutine **FDSOLVE**.

Subroutine **ERRADD** is called to simulate realistic field response by adding given levels of random noise to synthetic data through the control parameter **nerf**. The Gaussian noise can be added at all or selected data points as desired. It is possible to add random noise with zero mean and unit variance, having Gaussian (**nerf**>0) distribution. The function **RAND**, used for this purpose, was adapted from Stearns & David (1988). With this option, noise-free response (**nerf**=0) of a model can be compared with response(s) computed with different noise levels.

5.5.2.2 Inversion subprograms

The inversion subprograms are used in inversion module **INVSOL** which is called for computation of inverse problem solution. If observation points are not grid points then inverse matrix equation gets modified as

$$K\Delta P = \Delta R \quad \dots(5.4)$$

where matrix **K**, the modified Jacobian, is

$$K = I_p J. \quad \dots(5.5)$$

In equation (5.5), I_p is the interpolation matrix which is identity when grid points are the observation points. For reading the input data pertaining to the initial guess model, the inversion domain geometry and other inversion parameters, the subprogram **DTINV** is called. For each inversion iteration, first the model response and the right hand side of matrix equation (4.58) are computed for standard frequency by calling the subprograms **RESPONSE** and **RHSMAT** respectively. Subsequently, the superblocks are defined and the response and right hand sides are generated for other frequencies. The misfit between the observed and computed response is expressed in terms of root mean square (rms) error and the convergence is checked. The flow chart and the tree of subprograms used in **INVSOL** are given in flow charts 5.8 and 5.9 respectively. A brief description of inversion subprograms, along with their purpose(s), subroutines they are called in and subroutines they call, is given in Table 5.4. The important inversion subprograms are also discussed in brief.

Table 5.4 Various inversion subprograms and their purpose(s)

Subprogram	Purpose	Called by	Calls
CGINV	Solves inverse matrix equation (5.4) using BCGM	INVSOL	DTRNSF JDELT JHDELR NORM
DTINV	Reads input data for initial guess model, inversion control parameters and field data, if necessary	INVSOL	x
DTNEW	Modifies original input grid generation data	RESPONSE	x
INVDOM	Identifies grid blocks bounding the inversion domain	RESPONSE	x
INVSOL	Inverts the given/generated data	Main	DTINV RESPONSE RHSMAT CGINV DTNEW

Table 5.4 Contd.

JCBV	Performs Jacobian based calculations for various response functions using transformation matrices	CGINV JDELT JHDELR	INPV
JDELT	Computes product of Jacobian matrix with a vector	CGINV	JCBV RESOLVE RHSV OUTMAT
JHDELR	Computes product of Hermitian of Jacobian matrix with a vector	CGINV	JCBV RESOLVE RHSV OUTMAT
NORM	Computes inner product of a vector with its complex conjugate	CGINV	x
OUTMAT	Computes product of derivative of transformation matrix with a vector for outcropping body	CGINV JHDELR JDELT	INPV
RESMAT	Computes transformation matrices for derived field components and response functions	RHSMAT	x
RHSMAT	Computes right hand side of equation (4.58) for Jacobian based computations	INVSOL	RESMAT
RHSV	Computes product of right hand side matrix or its Hermitian with a vector	CGINV JDELT JHDELR	INPV
SUPBLK	Computes number of subblocks in each superblock, for a given grid	RESPONSE	x

In subroutine **DTINV** first the parameters of the initial guess model, on the basis of observed response, are read. Next, the iteration and convergence parameters **mnter**, **mxter**, **eps** and **mni**, **mxi**, **epi** are read for inversion and the BCGM iterations respectively. The inversion domain is chosen to encompass the inhomogeneity. The left and right corner coordinates of inversion domain **ylc** and **ync** and the top and bottom corner coordinates **zuc** and **zdc** are read. The **rhoin**, the initial guess of resistivity, within the inhomogeneity is read. The permissible range of resistivity values,

identified on the basis of thumb rules, is read. The **romn** and **romx** are the minimum and maximum values. The **aps** is the Marquardt parameter. In the end, for field problem, field data - **nobs**, the number of observation points, **yobs** their y- coordinates and **resp**, the response value - is read.

Subroutine **INVDOM** is called to define inversion domain for the inverse problem. The number of blocks for which resistivities are to be inverted is calculated. For the standard grid, these blocks define the superblocks and the initial guess of resistivity is transferred to these blocks.

Subroutine **SUPBLK** is called for defining the number of subblocks in each superblock for a given frequency. For standard frequency each superblock has only one subblock. The number of subblocks is stored separately for the y- and z- directions.

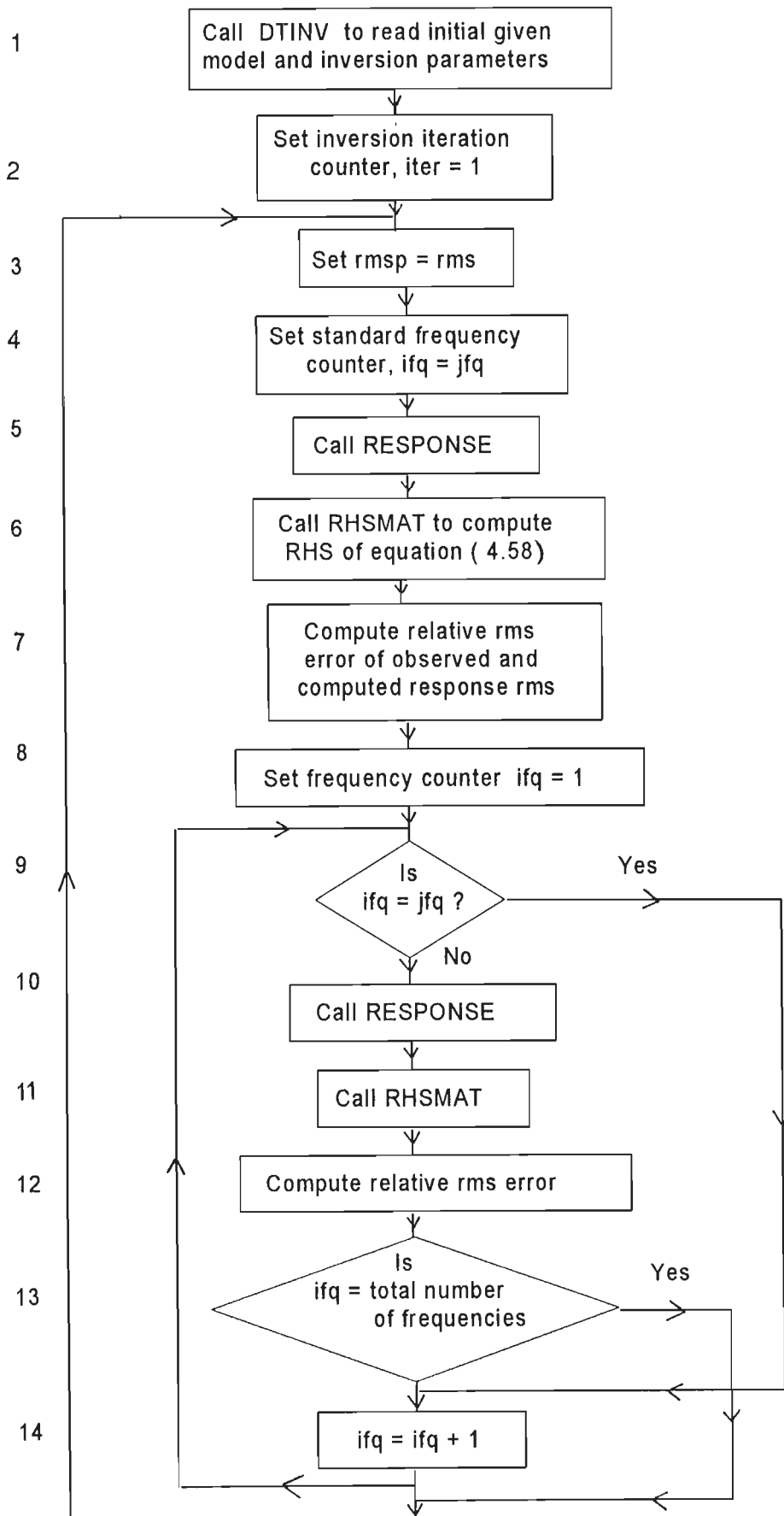
In subroutine **DTNEW** the grid lines within the inversion domain of the standard grid are used for modifying the original input grid generation data for other frequencies. The modified grid input data is used for generating grid at other frequencies to ensure grid lines at superblock boundaries.

Subroutine **DTTRNSF** stores in (retrieves from) the necessary grid information and related parameters global arrays from (into) local arrays. The choice of transfer from global to local or vice-versa is governed by a counter. The number of records needed to store the reduced FDM coefficient matrix is calculated in accordance with the given buffer size.

Subroutine **RHSMAT** is called for the right hand side matrix of equation (4.58) which is needed for Jacobian based computations. It is the product of field vector with the coefficient matrix derivative with respect to resistivity parameter. Its flow chart is shown in Fig. 5.10.

If a superblock is having one subblock, only four nodes are associated with it. As a result the derivative of coefficient matrix has sparse structure with only four terms being non-zero in each row. As the number of subblocks in a superblock increases, so does the number of associated nodes. Therefore, the derivative of matrix is calculated accordingly. This right hand side matrix is stored for each frequency. The subroutine **RESMAT** is called for Jacobian of derived field components and response functions.

Development of algorithm



To Step 15

Fig. 5.8 Contd.

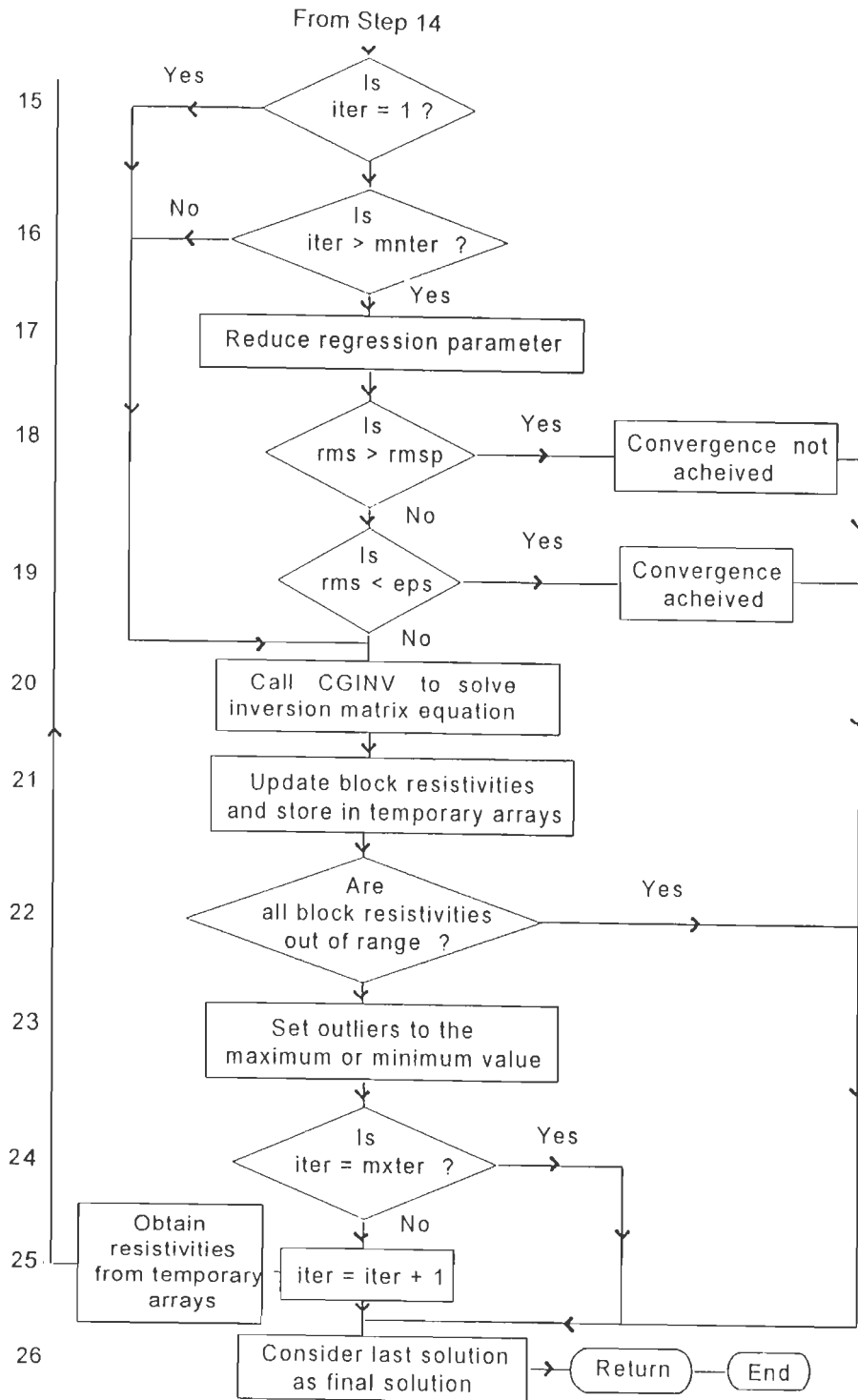


Fig. 5.8 Flow chart of subroutine **INVSOL**.

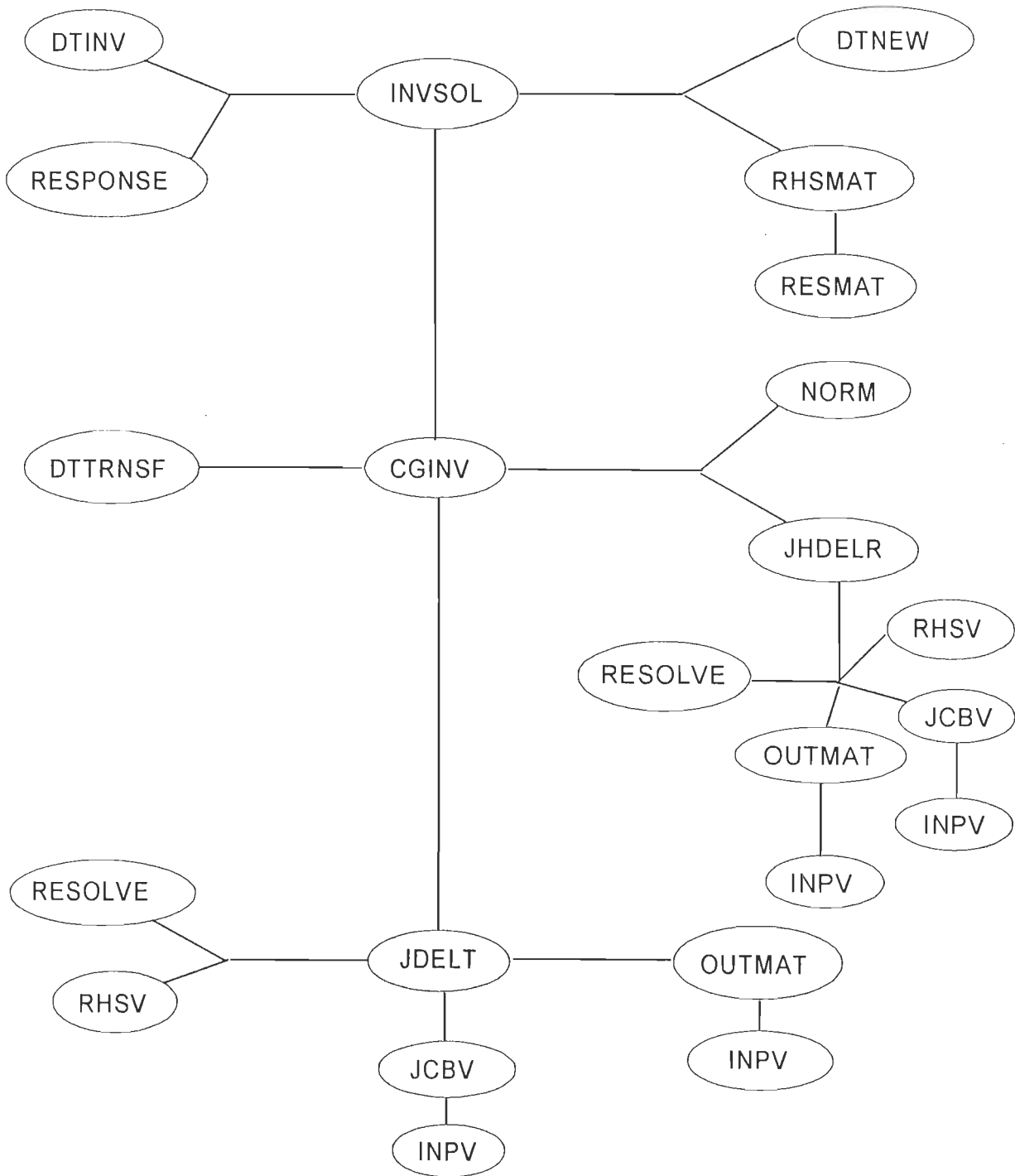


Fig. 5.9 Tree of subprograms called in subroutine **INVSOL**.

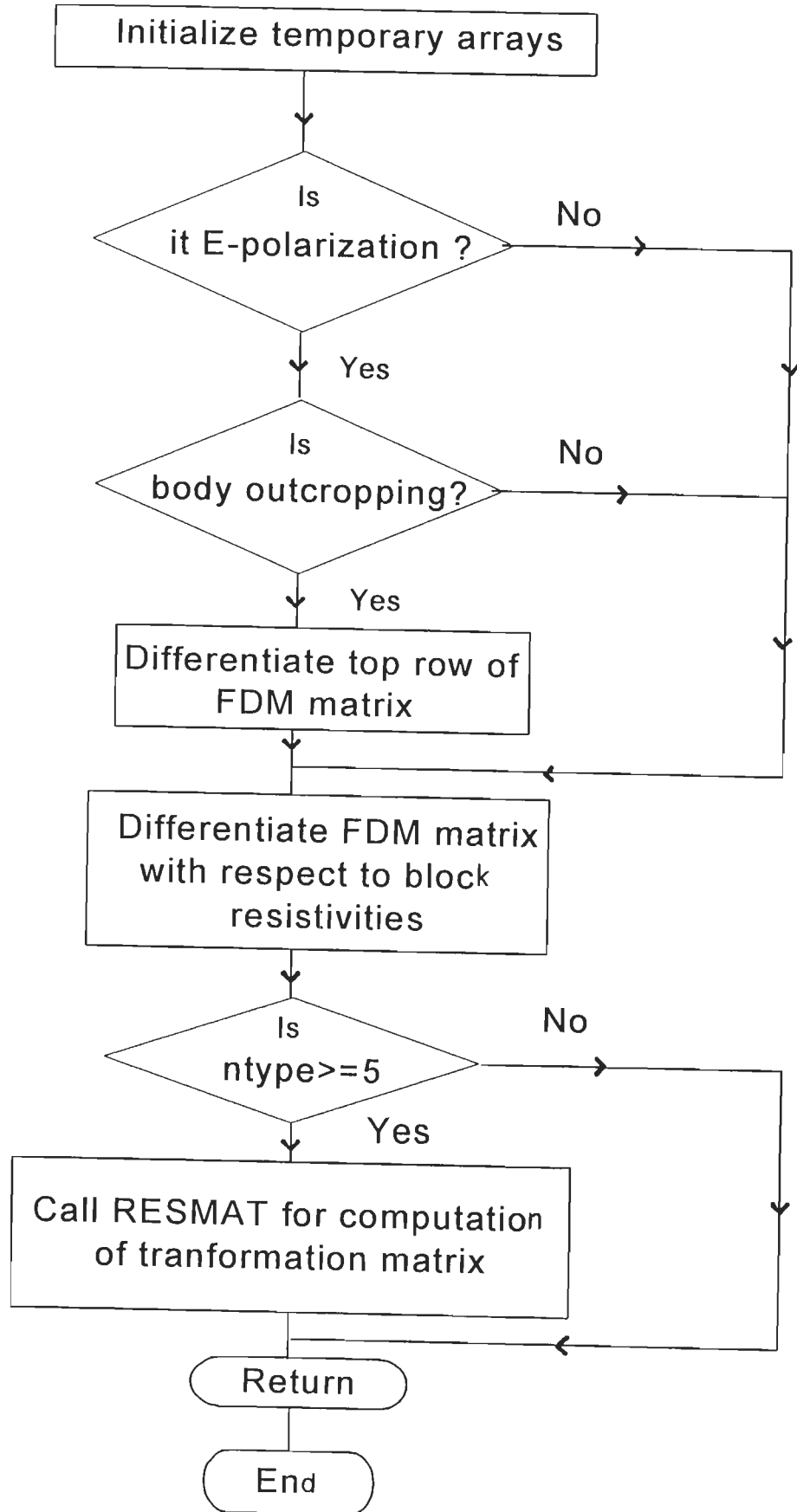


Fig. 5.10 Flow chart of subroutine RHSMAT.

In subroutine **RESMAT** the transformation matrices for field derivatives and response functions are computed in subprograms **BDERIV** and **EDERIV** for B- and E-polarization respectively. These matrices are generally banded with maximum of four diagonals which are stored in four vectors. According to the response type, i.e. impedance or induction vector, the transformation matrices are updated in **RESMAT** (Fig. 5.11).

Subroutine **CGINV** solves the inverse matrix equation using bi-conjugate gradient matrix solver which is implemented through splitting of real and imaginary parts. The counter, **invtr**, is defined as -1, 0 and 1 for least square, exact and minimum norm inverses respectively. According to the counter **invtr** the product of matrices are computed. The basic steps for obtaining these inverses are discussed below.

Least square solution

The least square solution of inverse problem can be written as

$$\Delta P = (K^H K + \lambda^2 I)^{-1} K^H \Delta R. \quad \dots(5.6)$$

First the product $K^H \Delta R$ is computed, from equation (5.5), as

$$V_1 = K^H \Delta R = J^H I_p^T \Delta R. \quad \dots(5.7)$$

For the product of Hermitian of Jacobian matrix with a vector subroutine **JHDELR** is called. The least square inverse is now found out iteratively. The product KV_1 is computed using equation (5.5) as

$$V_2 = KV_1 = I_p J V_1 \quad \dots(5.8)$$

and then

$$V_3 = K^H V_2 \quad \dots(5.9)$$

is computed. For each iteration, the products KV_1 and $K^H V_2$ are computed and subroutines **JDELT** and **JHDELR** are called for this purpose. Since we are seeking the ridge regressed solution, $\lambda^2 V_1$ is added to the final product V_3 . The iterative process is continued till convergence is achieved.

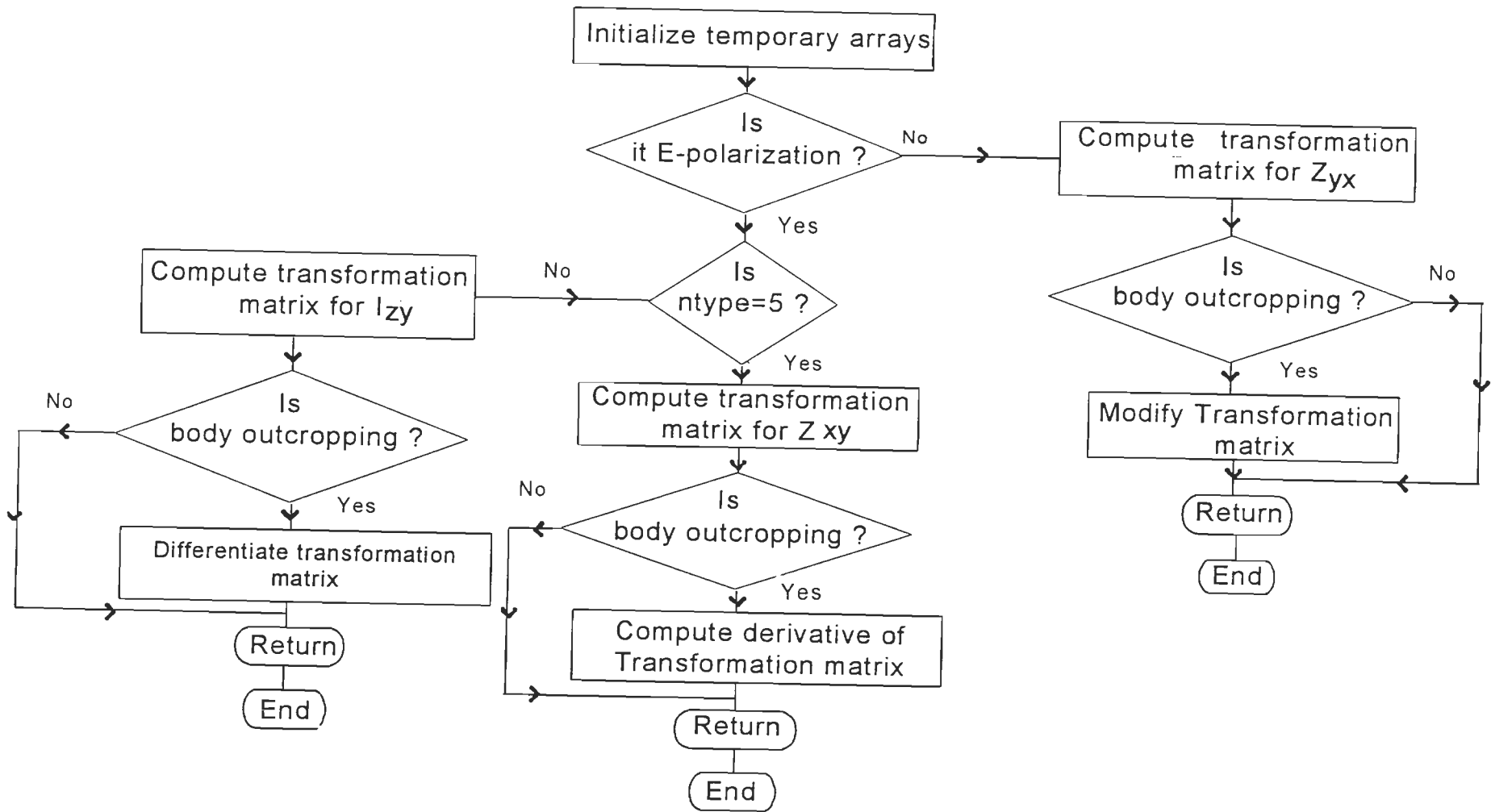


Fig. 5.11 Flow chart of subroutine RESMAT.

Minimum norm solution

$$\Delta P = K^H (KK^H + \lambda^2 I)^{-1} \Delta R. \quad \dots(5.10)$$

Unlike least square solution, the iterations are set in the starting itself. The product $V_1 = K^H \Delta R$ and $V_2 = K \Delta R$ are computed using equations (5.7) and (5.8) and subroutines **JHDEL**R and **JDEL**T are called for each BCGM iteration. For ridge-regressed solution, $\lambda^2 \Delta R$ is added to the product V_2 . Once convergence is achieved the final solution, $V_3 = K^H V_2$, is obtained by calling **JDEL**R. The various steps of **CGINV** are shown in flow chart 5.12.

The product of generalized Jacobian with a vector, given in equation (4.68), is obtained as

$$J_R \Delta R = Q \Delta R + T J_x \Delta R. \quad \dots(5.11)$$

where matrix $Q = T^H F$. In terms of modified Jacobian equation (vide equation 4.77) the equation (5.11) becomes

$$K \Delta R = I_p J_R \Delta R = I_p Q \Delta R + I_p T (C)^{-1} Y \Delta R. \quad \dots(5.12)$$

The first term is computed only for outcropping body by calling subroutine **OUTMAT**. For second term, the subroutine **RHSV** is called for the product of right hand side matrix with a vector $Y \Delta R$. After this product **RESOLVE** is called for solution $(C)^{-1} Y \Delta R$. Lastly for computation of the final product the subroutine **JCBV** is called. The flow chart of subroutine **JDEL**T is given in Fig. 5.13.

Analogous to subroutine **JDEL**T, subroutine **JHDEL**R is called for product of Hermitian of Jacobian with a vector as

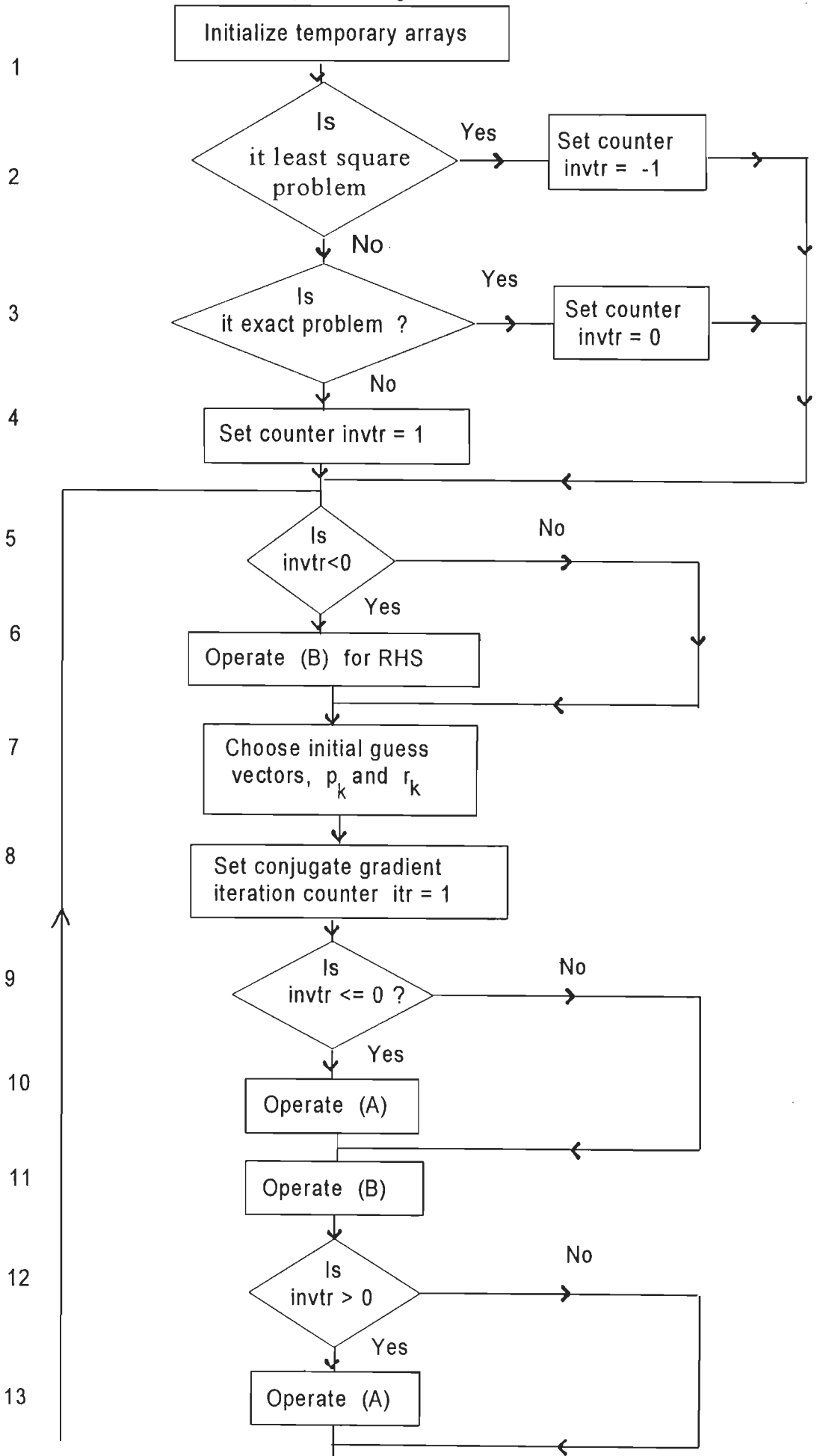
$$J_R^H \Delta R = Q^H \Delta R + J_x^H T^H \Delta R. \quad \dots(5.13)$$

In terms of modified Jacobian K the equation (5.14) can be written as

$$K^H \Delta R = J_R^H I_p^T \Delta R = Q^H I_p^T \Delta R + Y^H (C^H)^{-1} I_p^T \Delta R. \quad \dots(5.14)$$

If body is outcropping the subroutine **OUTMAT** is called for the first term which is zero otherwise. Here the order of computations for second term are reversed, in comparison to that of **JDEL**T. First the Jacobian is modified according to the response type by calling **JCBV**, then **RESOLVE** is called for solution $(C^H)^{-1} I_p^T \Delta R$ and finally **RHSV** is called as shown in flow chart 5.14.

Development of algorithm



To Step 14

Fig. 5.12 Contd.

Development of algorithm

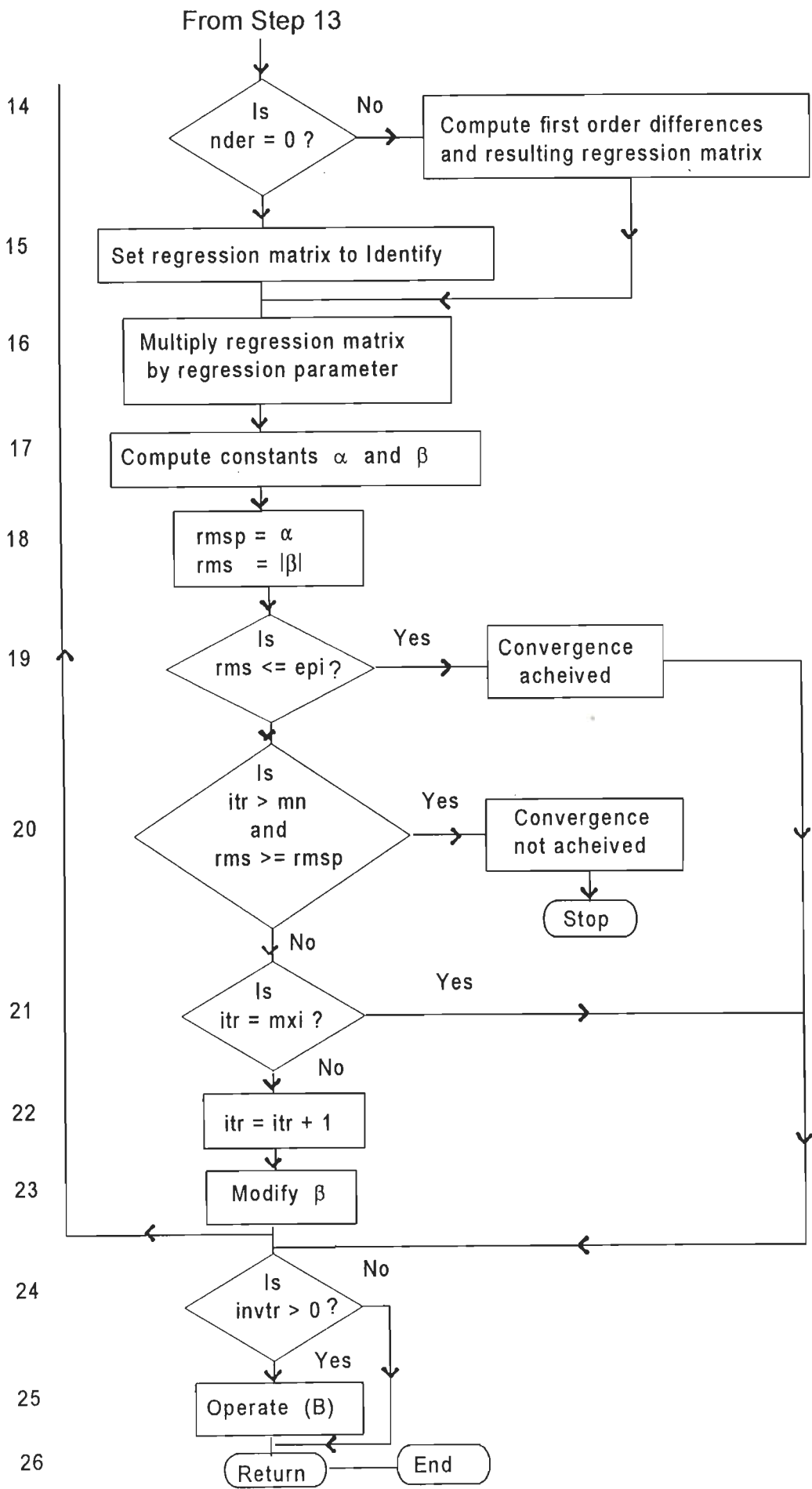


Fig. 5.12 Contd.

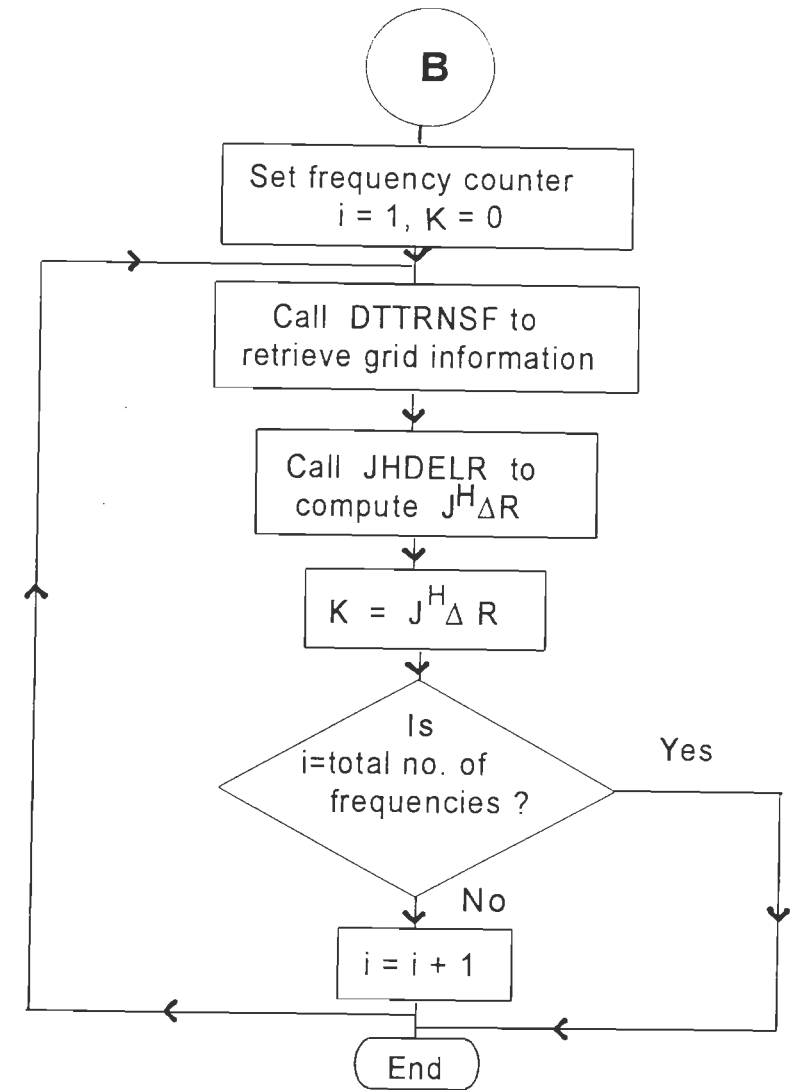
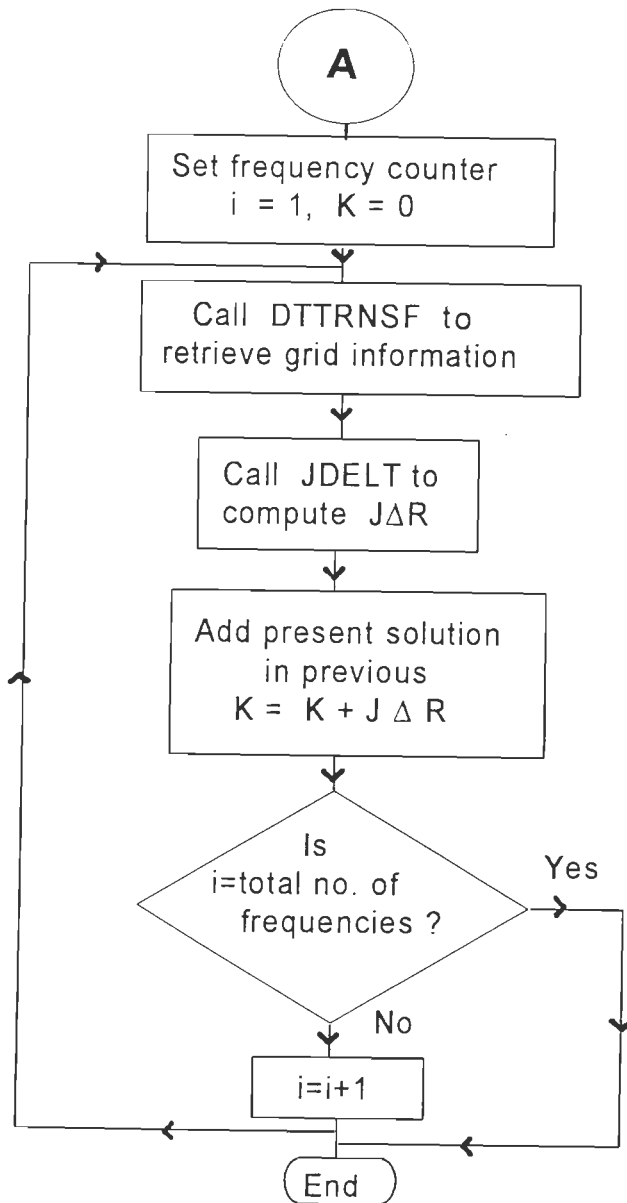


Fig. 5.12 Flow chart of subroutine CGINV.

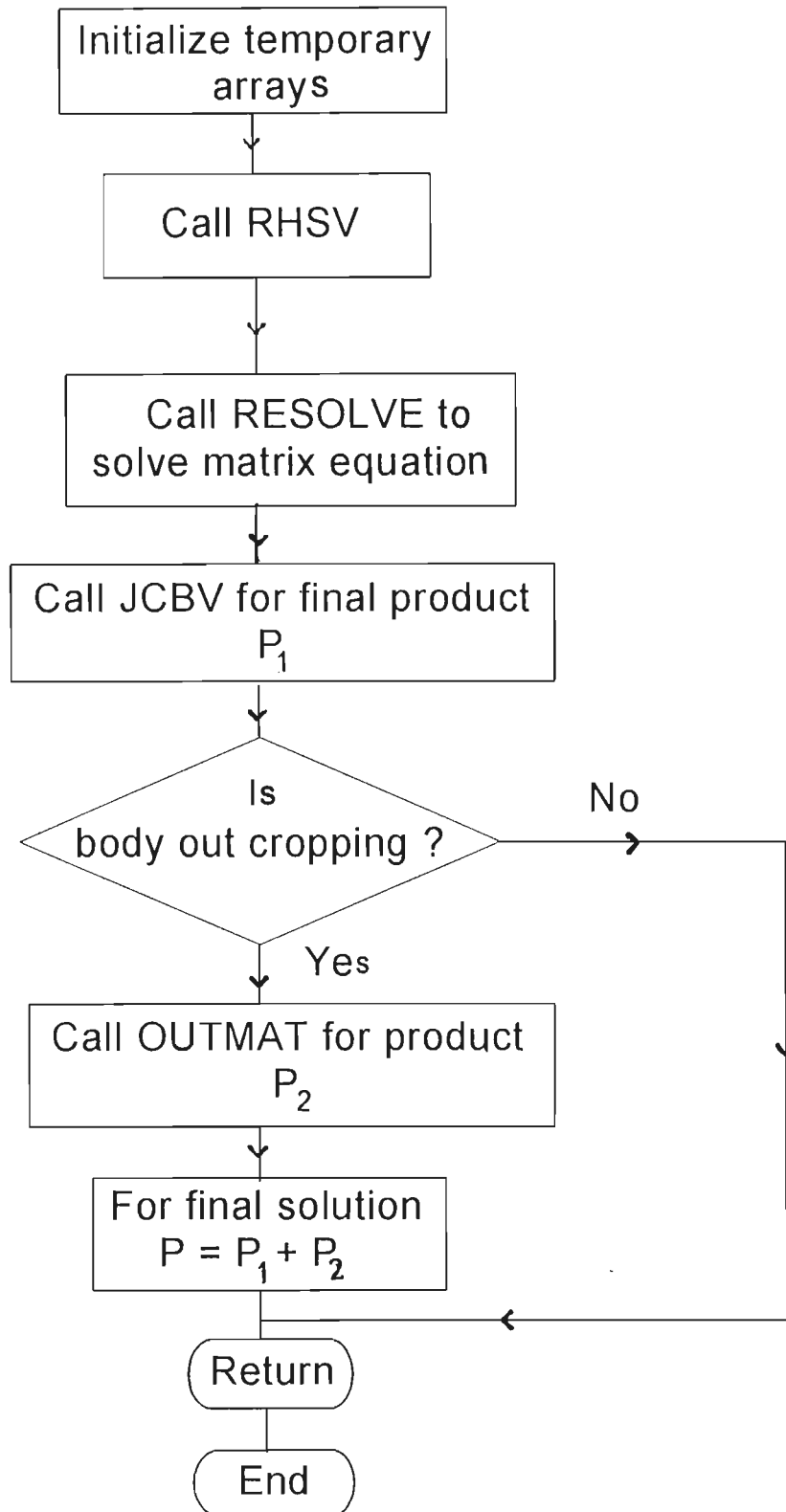


Fig. 5.13 Flow chart of subroutine JDELT.

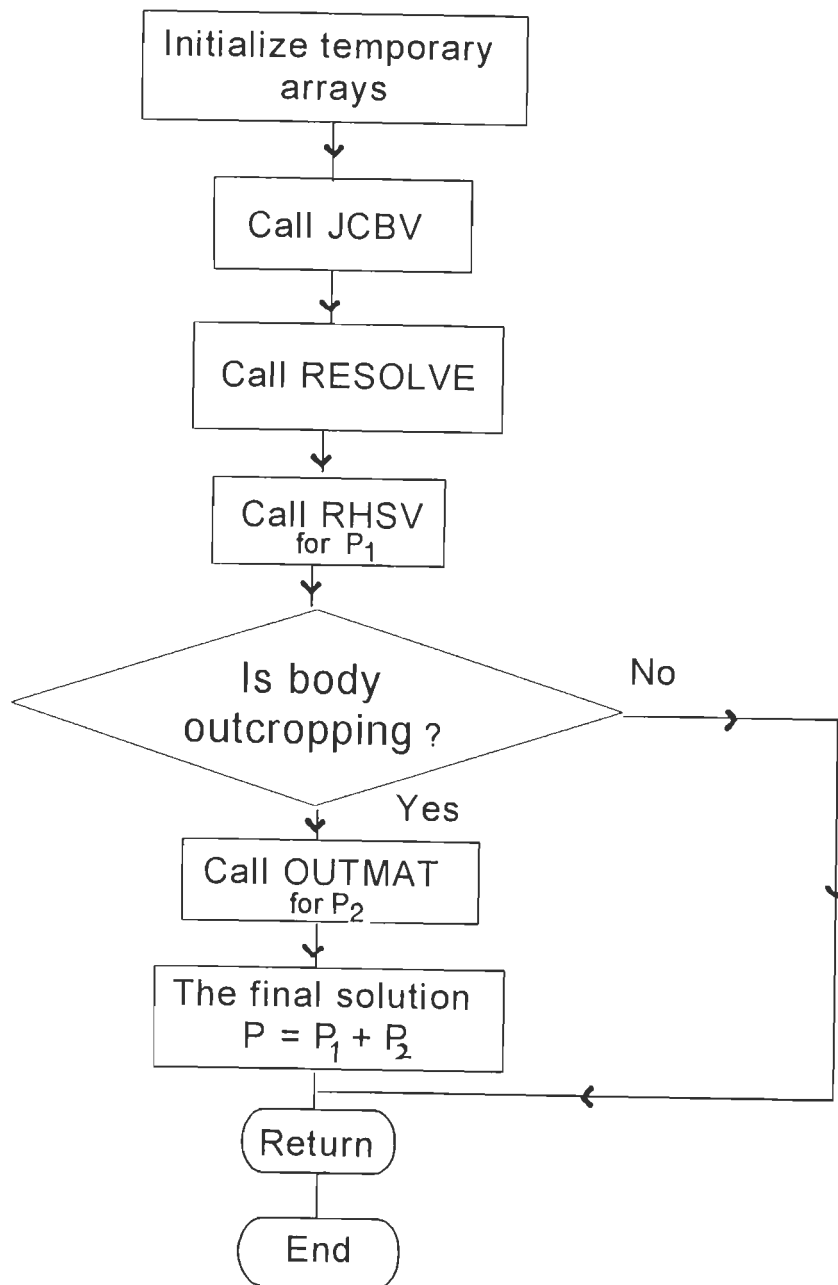


Fig. 5.14 Flow chart of subroutine JHDELR.

5.6 Computing environments

EM2INV is an efficient and versatile algorithm. However, it is in place here to list hardware as well as software limitations under which it was developed.

5.6.1. Hardware limitations

The algorithm is written in FORTRAN 77. It is developed and debugged on an IBM compatible EISA based PC-486 machine with 32 MB RAM and 383 MB hard disk. The SVR 4.0 version of Unix operating system and F78 FORTRAN compiler are used. The various dimension control parameters and their maximum values used in **EM2INV** are given in Table 5.5.

Table 5.5 Description and values of dimension control parameters

Parameter	Description	Value
mxbl	Maximum number of blocks in inversion domain	100
mxdy	Maximum number of nodes in y- direction	90
mxdz	Maximum number of nodes in z- direction	60
mxpr	Maximum number of time periods/frequencies	15
mxsb	Maximum number of nodes in a superblock	50
mxyy	Maximum size of block matrix, mxdy x mxdy	8100
mxyz	Maximum size of FDM coefficient matrix, mxdy x mxdz	5400
nersiz	Maximum size of buffer	4000
nesiz	Maximum size of buffer in bytes, 16 x nersiz	64000

5.6.2. Software limitations

Since algorithm **EM2INV** is based on quasi-linearization it needs judicious choice of convergence criterion. The use of regularised estimators makes the choice of regression parameter crucial. The inherent equivalence ambiguity is also present. In its present version, the inversion domain should encompass all the inhomogeneities. As a result the algorithm is found to be more efficient for confined targets.

5.7 Closure

The developed inversion algorithm **EM2INV** for 2-D EM data is the final result of through research. Its validity and applicability are tested through various theoretical exercises designed especially for this purpose. The experiment design exercises and inferences drawn from these are discussed in Chapter 6.

ALGORITHM TESTING AND EXPERIMENT DESIGN EXERCISES

6.1 General

Once a software is developed, it is essential to ascertain its accuracy and evaluate its efficiency. Every aspect of the algorithm **EM2INV** is checked by designing exercises of diverse nature. The accuracy is established through these exercises and reproduction of published results. The applicability of the algorithm is illustrated via various theoretical experiment design exercises of practical significance. For understanding the relationship between various model parameters and the computed responses, experiments for forward algorithm have been especially devised. The results of these experiments help in setting up the guidelines that can be used for successful inversion of real data. Some important findings of this whole process are presented here.

6.2 Validation of EM2INV

EM2INV, being a quasi-linearized algorithm solves the forward problem a number of times. Therefore, the forward algorithm has to be validated first.

6.2.1 Forward algorithm

First the mesh convergence and no contrast tests are performed and then the published results of certain models have been reproduced for validation. Since the development of our algorithm was started with the paper by Brewitt-Taylor & Weaver (BW) (1976), their model is used for these tests. This model comprises a 500 x 500 m² square target of resistivity 0.1 ohm-m, buried at a depth of 100 m, in a half-space of 1 ohm-m (Fig. 6.1a). The Dirichlet boundary conditions are imposed at the domain boundaries and the BW grid comprises 41 x 41 nodes. Horizontally the body is located

at the centre of the grid. The real and imaginary parts of electric field, E_x , at grid points are plotted against horizontal distance and found to be in good agreement as shown in Fig. 6.1b and c respectively.

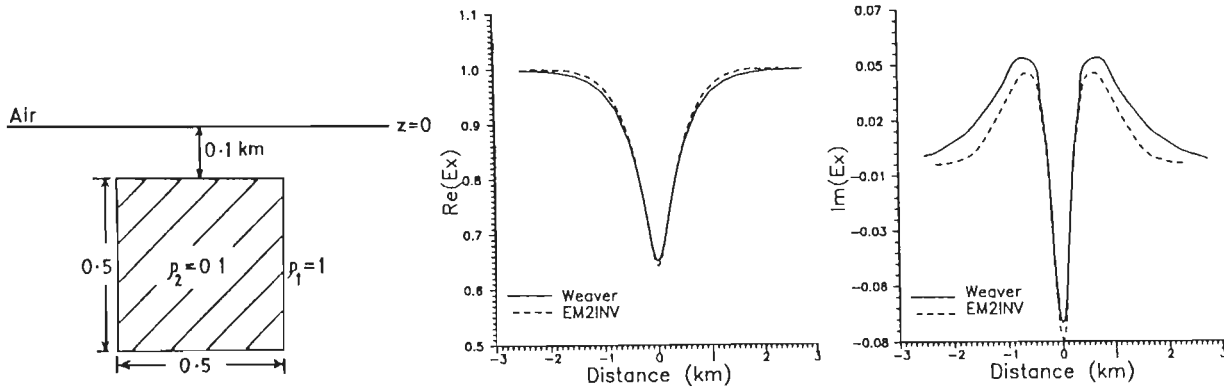


Fig. 6.1 The BW model (a), the real (b) and imaginary (c) components of electric field for E-polarization.

6.2.1.1 Mesh convergence test

Mesh convergence test is of crucial importance for proving the efficacy of any numerical field algorithm. The accuracy of finite difference method depends on grid spacings of the mesh (Chen & Fung, 1989).

For mesh convergence study, the comparison between various coarser and finer versions of BW grid, along with the optimal grid used by **EM2INV**, has been made. The mesh spacings which are four and two times of the original grid spacings result in the coarser grids of 11 x 11 and 21 x 21 nodes, respectively, whereas the finer 81 x 81 nodes grid is obtained when spacings are reduced by half. The size of **EM2INV** grid, generated by automatic grid generator, **GRIDYZ**, is 31 x 12. The real and imaginary components of the electric field for all these grids along with those of original grid are presented in Fig. 6.2. These plots exhibit results of higher accuracy of with the finer grid. Further, the improvement in accuracy becomes smaller and the results converges to a limit, the true solution. After this the further refinement of optimal grid does not improve the results at all. The reduction in size of the optimal grid renders significant reduction in computation time.

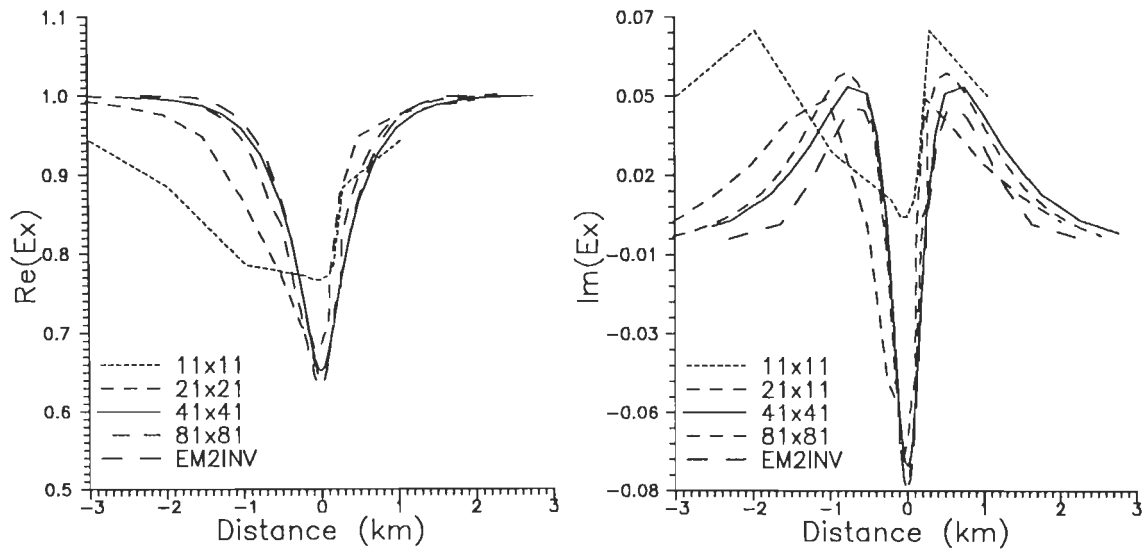


Fig. 6.2 Mesh convergence test: The real and imaginary components of electric field of BW model computed using five different grids having 11 x 11, 21 x 21, 41 x 41 (BW), 81 x 81 and 31 x 12 (optimal grid) nodes.

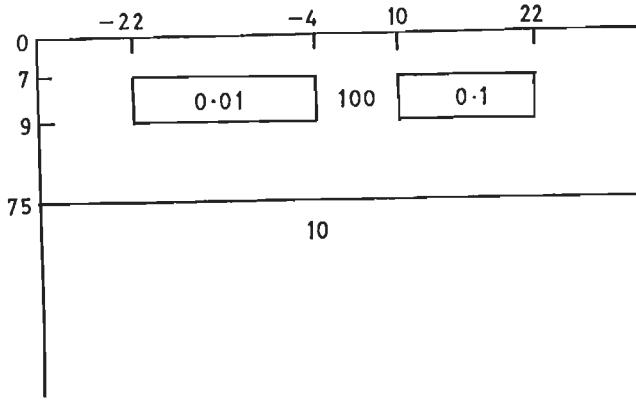
6.2.1.2 No contrast study

Another test conducted on the algorithm **EM2INV** is to verify the convergence of the buried target response to that of a half-space when the resistivity contrast is reduced to 1. The resistivity of the rectangular target of BW model is modified to 0.9 ohm-m for this test. The impedances for the two polarizations are computed and found to be identical within computational errors.

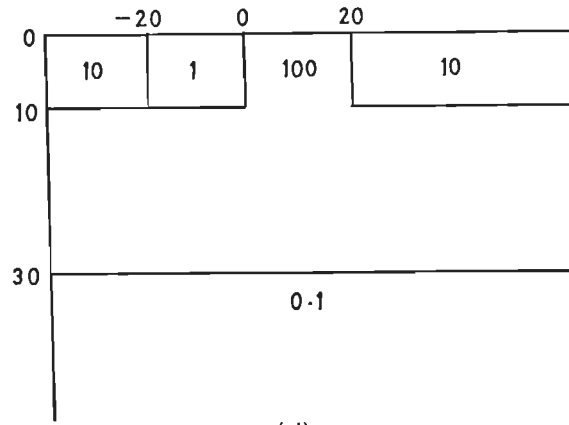
6.2.1.3 Reproduction of published results

The comparison of results obtained by the developed algorithm with the published ones is an important aspect of validation. After reproducing the results of BW model, to gain more confidence, the forward results of **EM2INV** were matched for the models taken from the report of an international project on comparison of modelling methods for EM induction problems (Zhdanov et al., 1990). In this report the results of different numerical methods used by various workers are compiled. Here, however, only for two models the results of **EM2INV** along with those of other modelling techniques are presented.

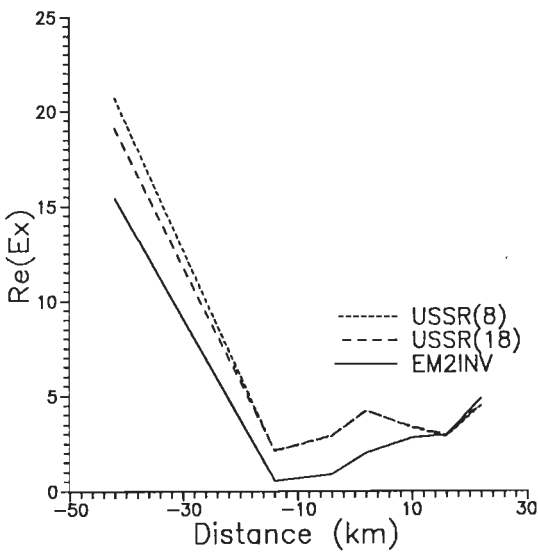
The first model (Fig. 6.3a) is a two-layer one with the layers having resistivities 100 and 10 ohm-m. Two conductive blocks of resistivities 0.01 and 0.1 ohm-m are embedded at a depth of 7 km, in the first resistive layer. The second model (Fig. 6.3d) has 10 km thick inhomogeneities outcropping in the top layer. The real components



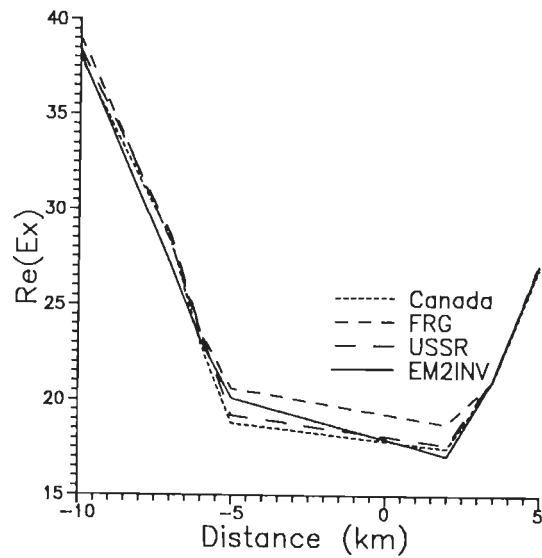
(a)



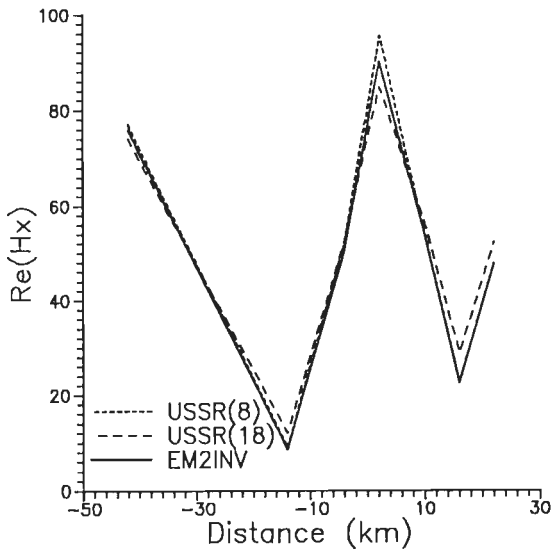
(d)



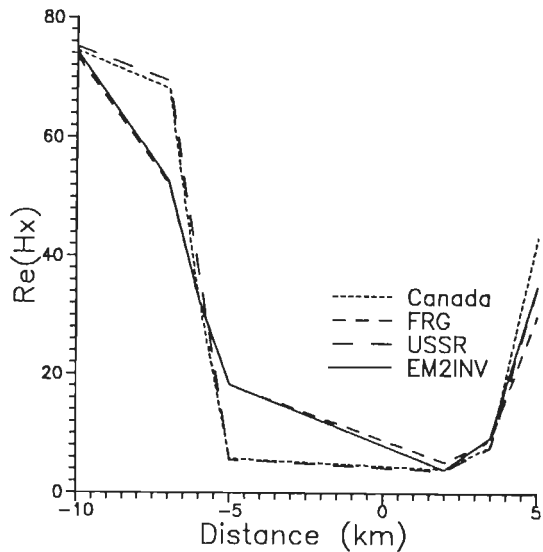
(b)



(e)



(c)



(f)

Fig. 6.3 The two models chosen from report of Zhdanov et al., (1990) (a,d). Comparison of **EM2INV** results with some of the results given in report (b,c) and (e, f) are plots of real parts of E_x and H_x for the two models respectively.

of base electric field, E_x , and magnetic field, H_x , are computed for these models at periods 1000 s and 100 s respectively. The **EM2INV** results, E_x and H_x , are compared in Figs. 6.3b and e and Figs. 6.3c and f for the two models respectively.

6.2.2 Inversion algorithm

The validity of inversion computations has been checked by inverting the synthetic responses and comparing the results with the true model responses. Subsequently, the stability of **EM2INV** has been established by inverting the synthetic responses corrupted with random Gaussian noise.

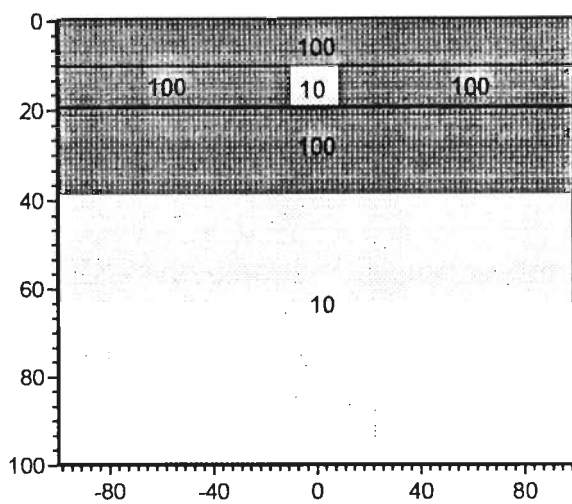
6.2.2.1 Inversion of synthetic responses

The synthetic conductive block model of Agarwal et al. (1993) has been chosen for illustration. The model comprises a block of width 20 km, thickness 10 km and resistivity 10 ohm-m. It is embedded in a medium of 100 ohm-m resistivity with its top surface at a depth of 10 km. The first layer, which is 40 km thick, is underlain by a conductive layer of 10 ohm-m. The horizontal extent of the model ranges from -100 to 100 km, whereas its vertical extent is 100 km. The model, along with its parameters and geometry, is displayed in Fig. 6.4a. On the basis of forward response, an inversion domain of resistivity 40 ohm-m, ranging from -30 to 30 km in horizontal direction and 5 to 25 km in vertical direction, has been identified.

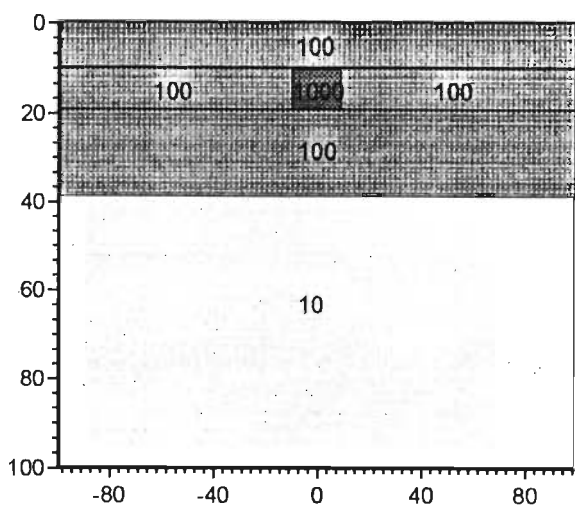
Since the body is sensed best at period 80 s the E-polarization impedance, Z_{xy} , computed at this period has been inverted. The detailed inversion results are shown in Fig. 6.5. Both the real and imaginary components of the impedance of inverted model fit those of the true model (Fig. 6.5a). The root mean square (rms) error of inversion is continuously decreasing with increasing iteration number (Fig. 6.5b) and this signifies acceptable inversion quality. The resistivity contours (in ohm-m) within the inversion domain of final model are plotted in Fig. 6.5c. The top horizontal and the vertical boundaries of the body are well resolved, whereas the bottom horizontal boundary can be inferred reasonably well.

6.2.2.2 Check on stability

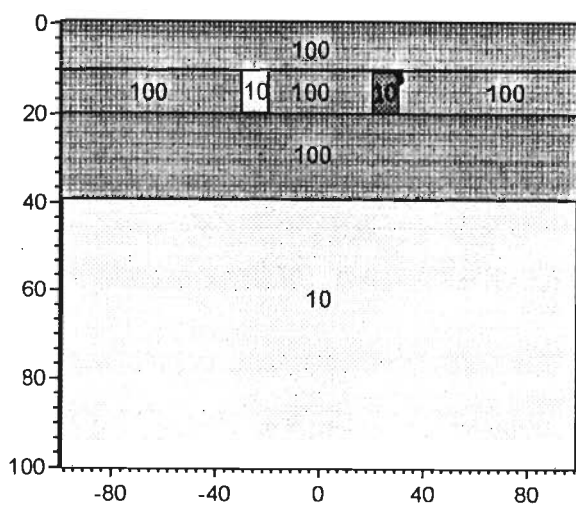
The stability has been checked through inversion of noisy data. In order to simulate real data the random Gaussian noise of different signal to noise ratio has been added to the synthetic response before carrying out the inversion. The addition



(a)



(b)



(c)

Fig. 6.4 The models studied - (a) the conductive block model, (b) the resistive block model and (c) the model having both conductive and resistive blocks.

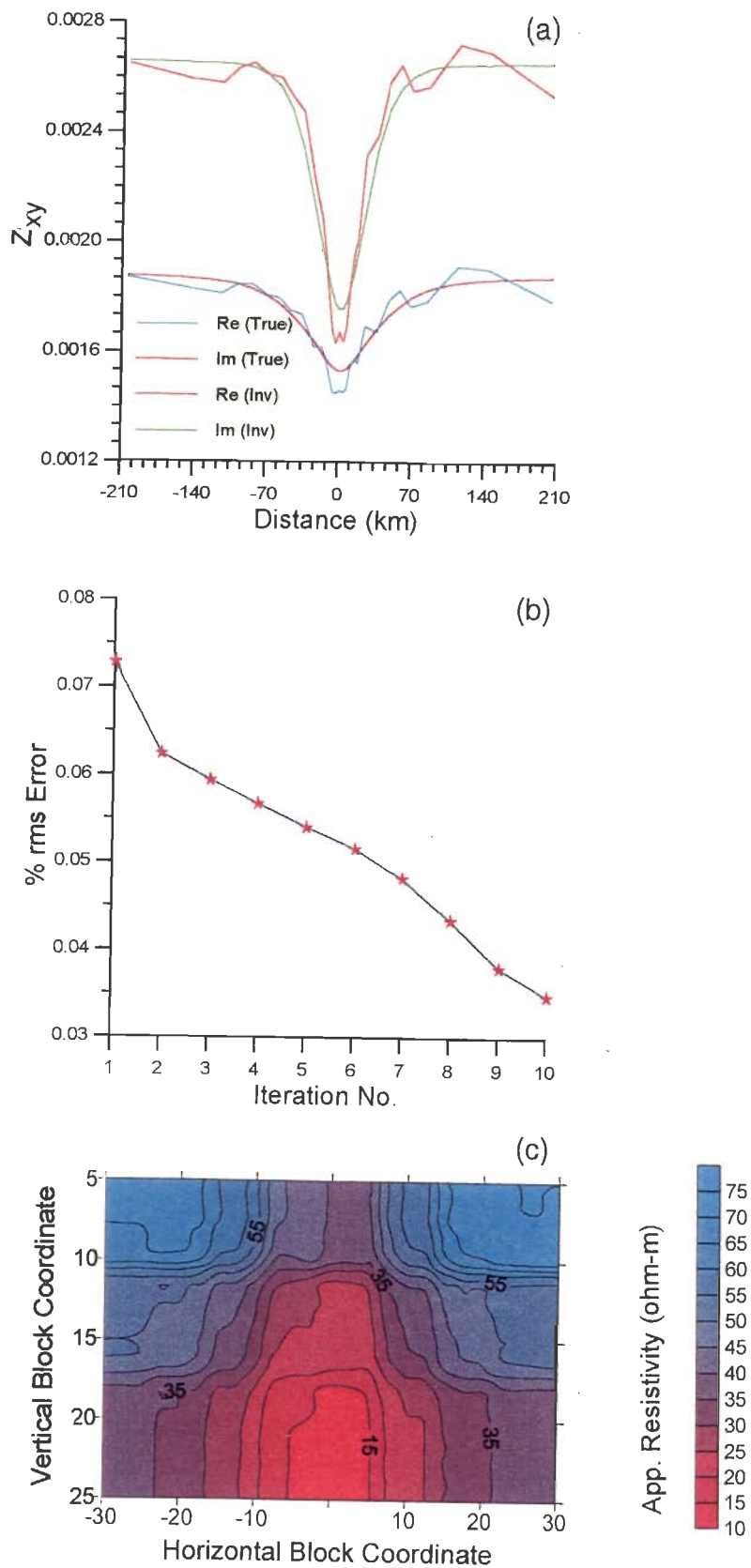


Fig. 6.5 Inversion of Z_{xy} response of the conductive block model - (a) the comparison of responses of true and inverted models, (b) convergence of rms error in inversion and (c) resistivity contour plots over the inversion domain.

of noise results in high frequency oscillations into the otherwise smooth response curve. Inversions of the corrupted Z_{xy} responses of the conductive block model have been carried out. It has been observed that the quality of inverted model is acceptable as long as the noise level is lower than or equal to 5%. The inversion algorithm **EM2INV** is, therefore, robust and can tolerate noise up to 5% level.

The inversion results for noise free, 2% and 5% Gaussian noise cases are shown in Fig. 6.6. The results illustrate the comparison of true and inverted model responses (Figs. 6.6a-c), resistivity contours of inverted models (Figs. 6.6d-f) and convergence of rms error of inversion (Figs. 6.6g-i) for the three cases.

6.3 Experiment design exercises

The algorithm **EM2INV** has been employed to study the nature of forward and inverse problems. In this process the forward response generation as well as data inversion capabilities of algorithm are not only rigorously tested but also enhanced. For this purpose, several design exercises have been set up. Since the initial guess model for inversion has to be obtained from observed anomaly, the forward experiments aim at studying the impact of model parameters on forward responses, whereas the inversion experiments aim at gauging the inversion quality under different situations. These experiments help in improving quality of inversion and also in planning of data procurement.

For these studies the theoretical models chosen from literature (Agarwal et al., 1993) are - a conductive block, a resistive block and a conductive and resistive block pair buried in a two-layer earth. The conductive block model has already been described in section 6.2.2.1.

The resistive block model is similar to the conductive one except that the block resistivity is now 1000 ohm-m in place of 10 ohm-m (Fig. 6.4b). In the third model, which has both conductive and resistive blocks, the two blocks of width 10 km, thickness 10 km having resistivities 10 and 1000 ohm-m, respectively, are buried in the host of 100 ohm-m. The separation between these two blocks is 40 km (Fig. 6.4c). The conductive block, resistive block and conductive and resistive block pair models are referred to as model 1, model 2 and model 3 in the text respectively. Model 1 has been used more frequently for undertaking the design exercises.

6.3.1 Experiments on forward algorithm

The algorithm, like any other inversion algorithm possess the capability to generate the forward response for various types of synthetic models. In order to develop thumb rules, which can be used to derive information about the initial guess model, a set of apparent resistivity vs distance curves, for a given set of model parameters, are generated for B- and E-polarization.

The parameters studied in case of models 1 and 2 are the resistivity contrast between the block and host and the depth of burial to the top of the block. In model 3, the parameters studied are the resistivity contrast between the two blocks and the horizontal separation between them. During experiment, only the parameter under study is allowed to vary keeping rest of the parameters fixed. The different values of host and block resistivity contrast ratio, used for response computation, are 2, 5, 10, 100 and 1000 for model 1 and 10, 50 and 100 for model 2. The depth of burials are (in km) - 0 (outcropping body), 10, 30, 40 and 50. The separation values taken between the two blocks of model 3 are (in km) - 0, 10, 20, 30 and 40. As the body is sensed best at period 80 s, all these responses are generated for this period.

Different parameter sets can result in similar responses. Therefore, a preliminary discriminant analysis to plan guidelines for estimation of target resistivity and size has been attempted. Although concrete quantitative rules could not be derived, yet the qualitative inferences, based on these forward responses, have been drawn and are discussed.

6.3.1.1 Effect of resistivity contrast

For B- and E-polarization, the apparent resistivity curves for different contrast ratios are generated for models 1 and 2 for a given depth of burial and for model 3 for a given separation value. These plots are shown for B- and E- polarizations, respectively, in Figs. 6.7 - 6.8 for model 1, in Figs. 6.9 - 6.10 for model 2 and in Figs. 6.11 - 6.12 for model 3. The base models are retained with the change in desired parameter.

According to these plots the anomaly peak sharpens with increase in resistivity contrast ratio. But this sharpness is perceptible only up to a certain depth of burial beyond which even a large contrast ratio does not help in detecting the body. For the

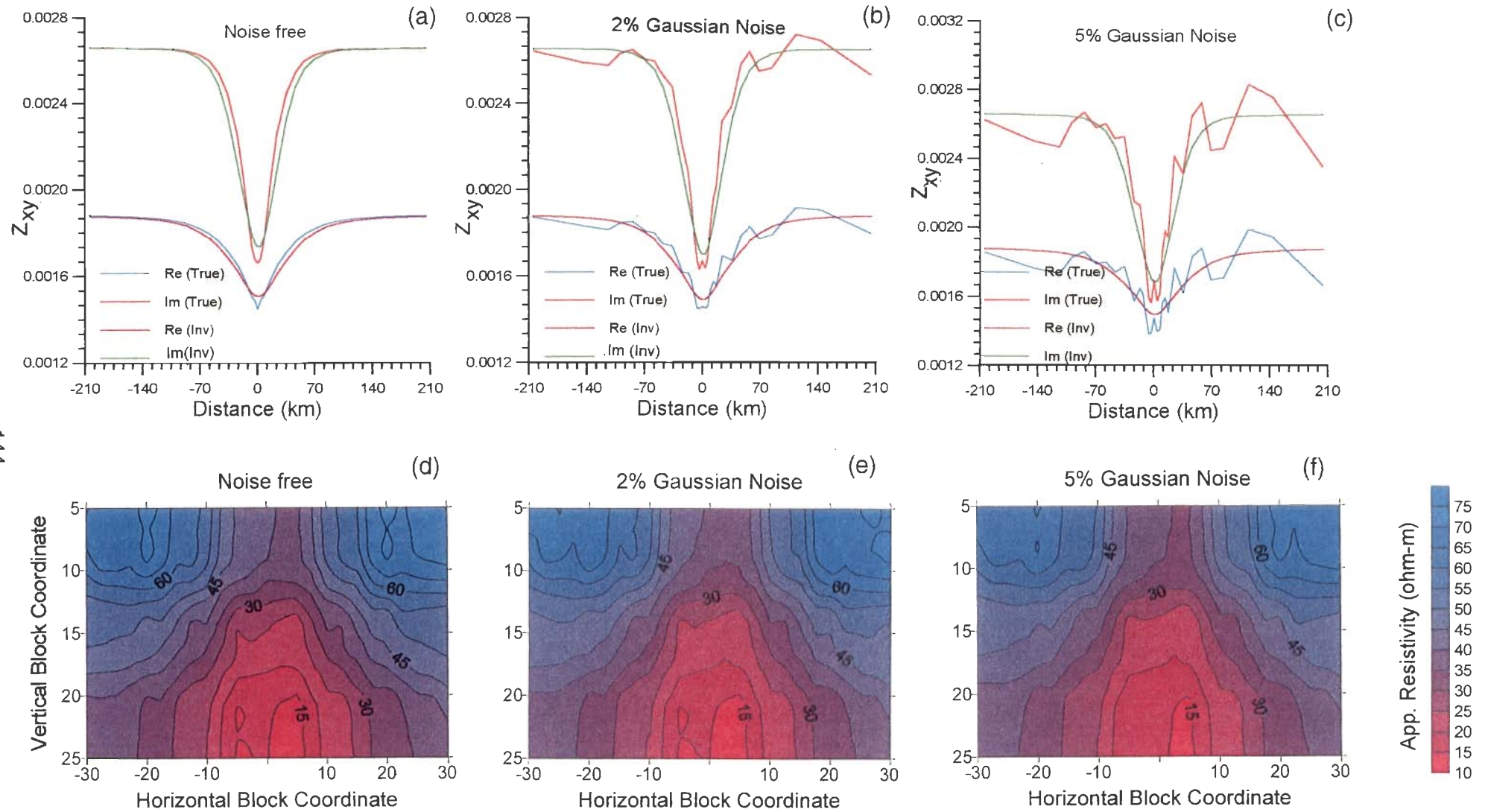


Fig. 6.6 Contd.

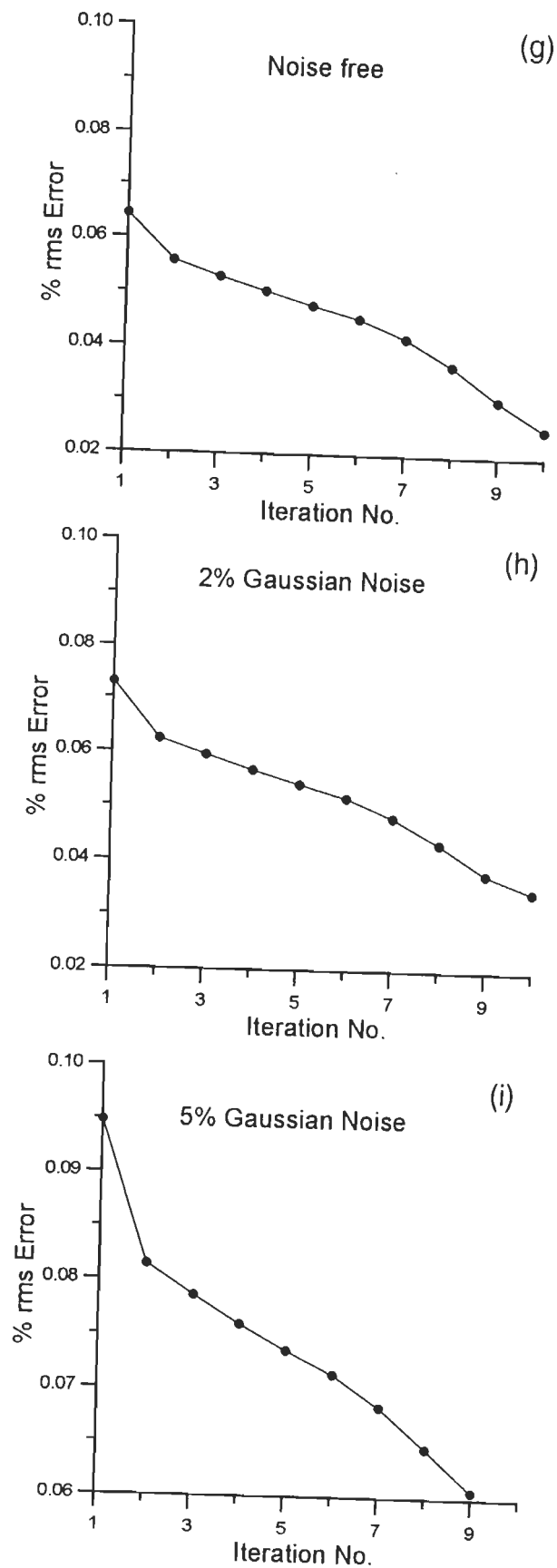


Fig. 6.6 Inversion of synthetic Z_{xy} data for conductive block model with increasing random noise. The comparisons of true and inverted model responses for (a) noise free, (b) 2% noise and (c) 5% noise. Parts (d) - (f) show the contours of resistivity (in ohm-m) within inversion domain while (g) - (i) show the convergence of rms error in inversion for noise free, 2% and 5% noise respectively.

same contrast ratio, the magnitude of anomaly is greater for the conductive block in comparison to that of the resistive block. The conductive block is sensed better by E-polarization (Fig. 6.8) whereas the resistive block is by B-polarization (Fig. 6.9). The responses of model 3 clearly support this observation, as ρ_{xy} curves do not reflect the presence of resistive block at all and merge into half-space values (Fig. 6.12).

6.3.1.2 Impact of depth of burial

This study has been performed only on models 1 and 2. The apparent resistivities are computed at different depths of burial for a given resistivity contrast ratio. These response curves for B- and E- polarizations are given in Figs. 6.13 - 6.14 for model 1 and in Fig. 6.15 for model 2 respectively.

It has been observed that due to attenuation of signal the magnitude of anomaly decreases with increase in depth of burial. The study reveals that for burial depths greater than 30 km one cannot infer any information about the body as anomalies are almost flat. The outcropping body is distinct in B-polarization responses due to the sudden jump in ρ_{yx} values at the edges, which helps in estimating the horizontal extent of the body as represented in Fig. 6.13 and Figs. 6.15a-c.

6.3.1.3 Effect of separation between two bodies

For different separation values the apparent resistivities, ρ_{yx} and ρ_{xy} , of model 3 are computed for a fixed contrast ratio. The effect of separation between two blocks is reflected better in ρ_{yx} plots (Fig 6.16) than in ρ_{xy} plots (Fig. 6.17). For ρ_{xy} , this effect is perceptible only when the block is conductive in comparison to the host (Figs. 6.17a and 6.17b). As the block becomes resistive the response curves become almost similar for different separation values.

6.3.2 Experiments on inversion algorithm

The inversion algorithm **EM2INV** is a versatile algorithm and can be used to invert various response functions. In addition, the profiling as well as sounding data can be inverted. Numerous factors like choice of response function, mode of polarization, number of periods used for inversion, spread of observation points individually or jointly, affect the quality of inversion. In order to study their influence, some theoretical experiments have been designed which further establish the efficacy of **EM2INV**.

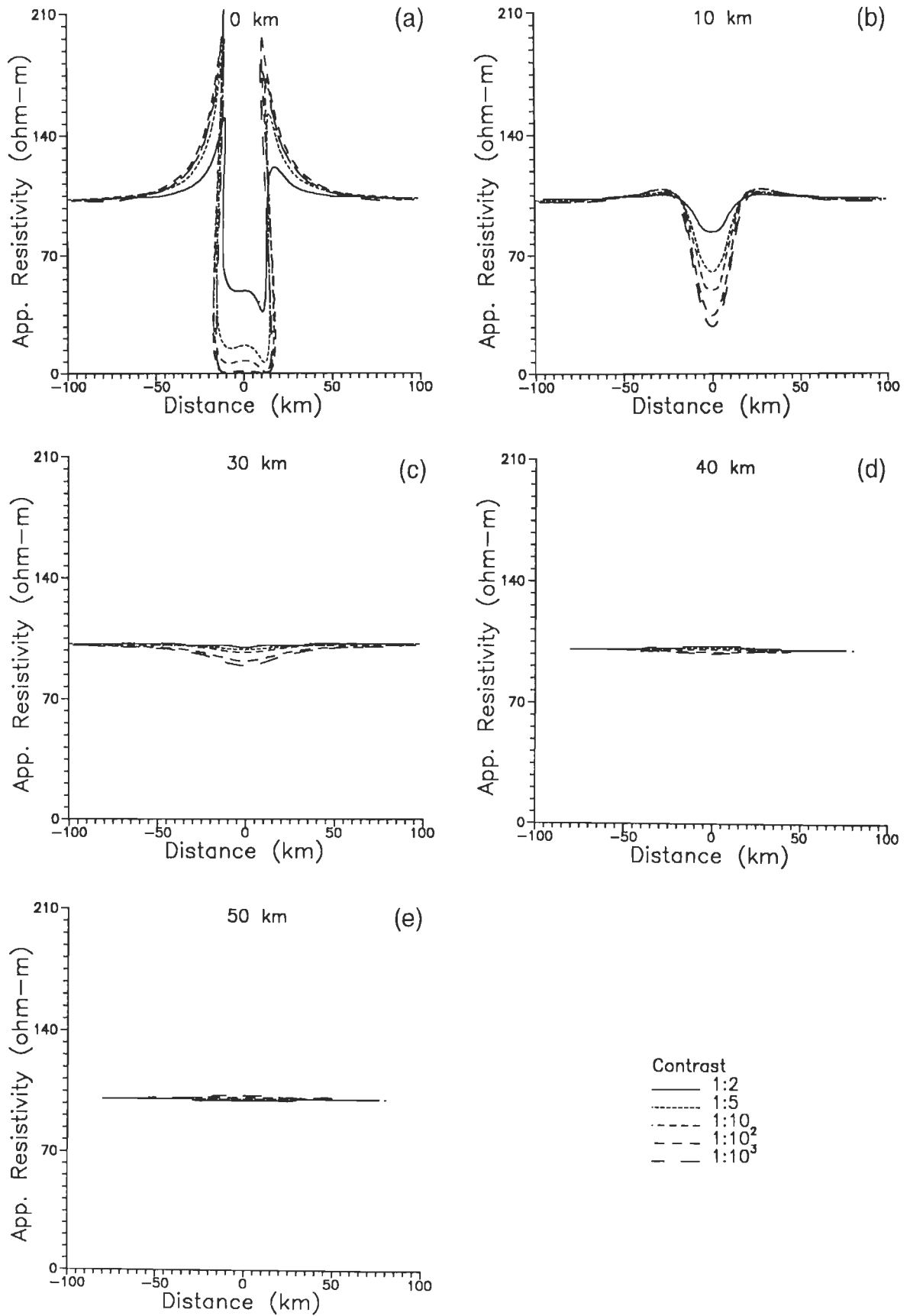


Fig. 6.7 Impact of resistivity contrast on ρ_{yx} of model 1 for a given depth of burial. Plots (a), (b), (c), (d) and (e) correspond to 0, 10, 30, 40 and 50 km burial depth respectively.

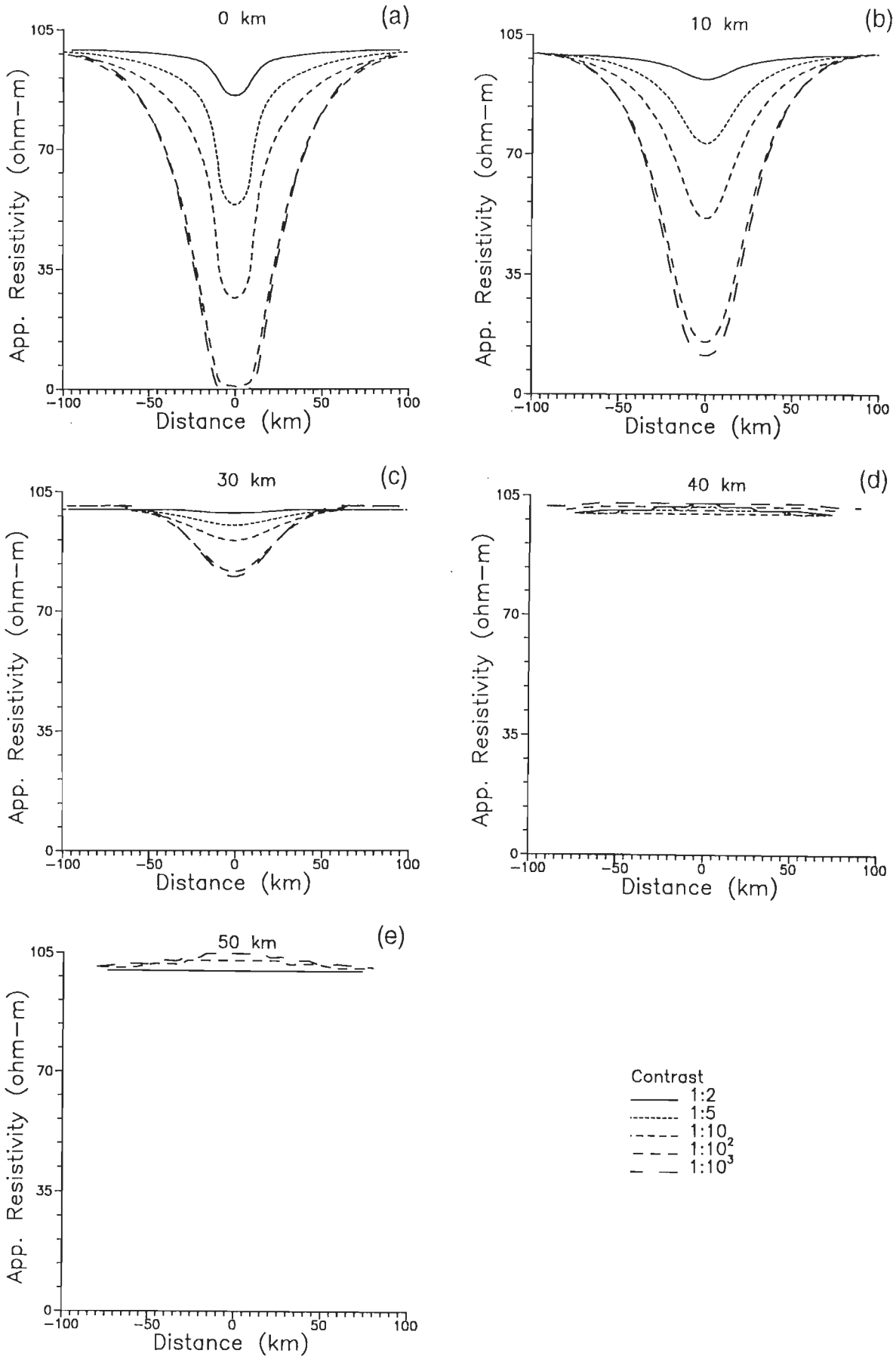


Fig. 6.8 Same as Fig. 6.7 but for ρ_{xy} .

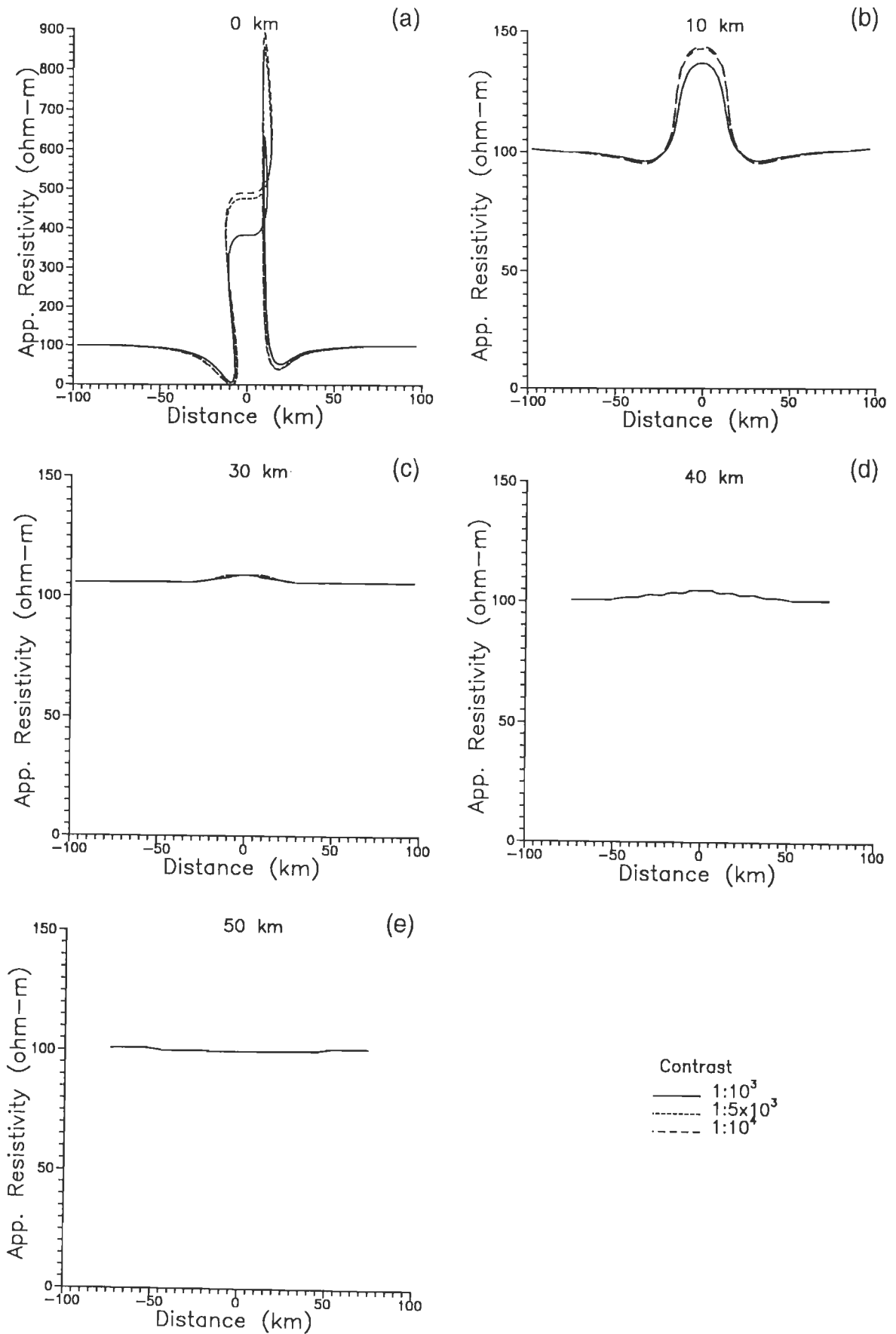


Fig. 6.9 Same as Fig. 6.7 but for model 2.

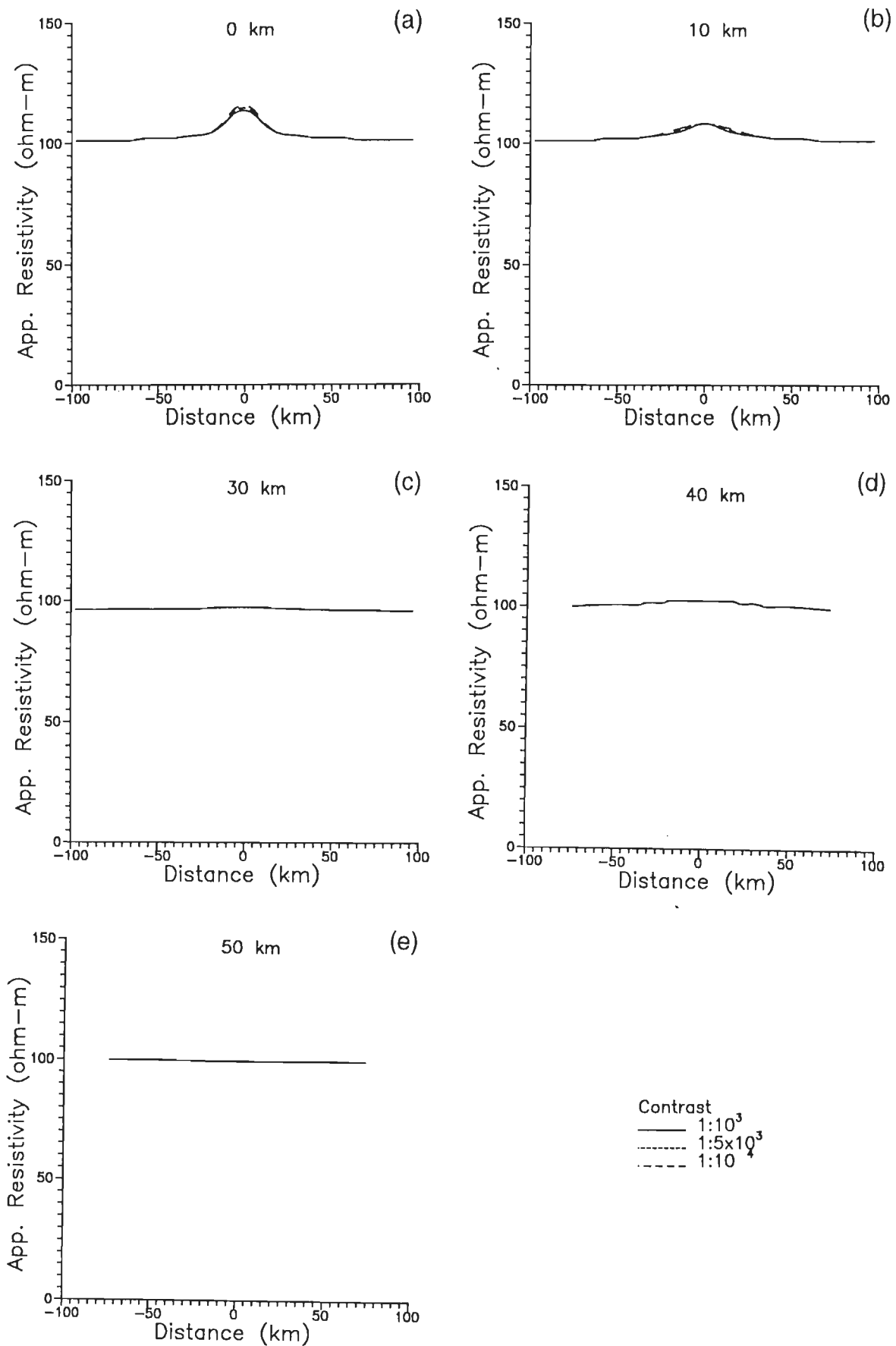


Fig. 6.10 Same as Fig. 6.9 for ρ_{xy} plots.

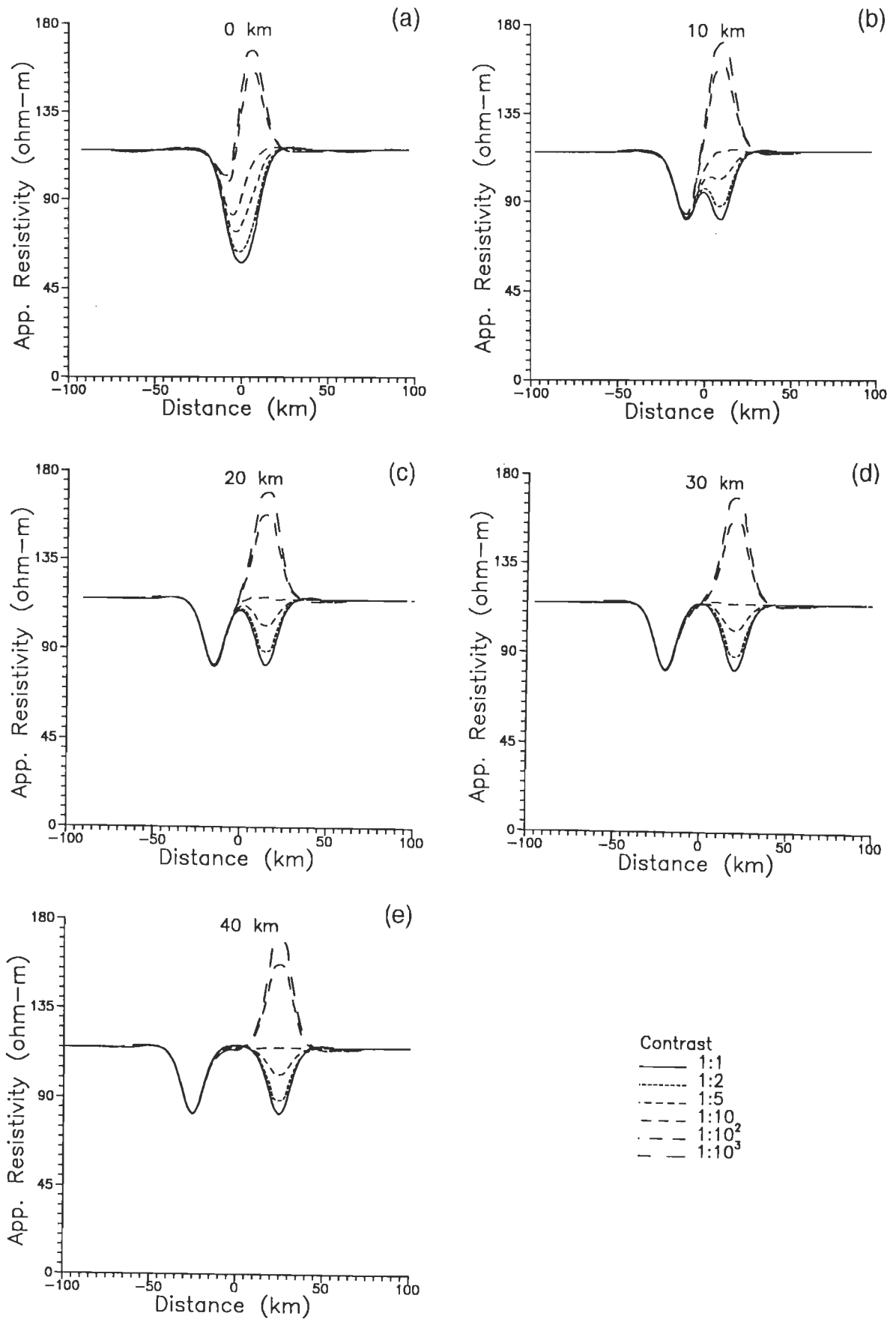


Fig. 6.11 Impact of resistivity contrast on ρ_{yx} of model 3 for a given separation value. Plots (a), (b), (c), (d) and (e) correspond to 0, 10, 20, 30, and 40 km separation.

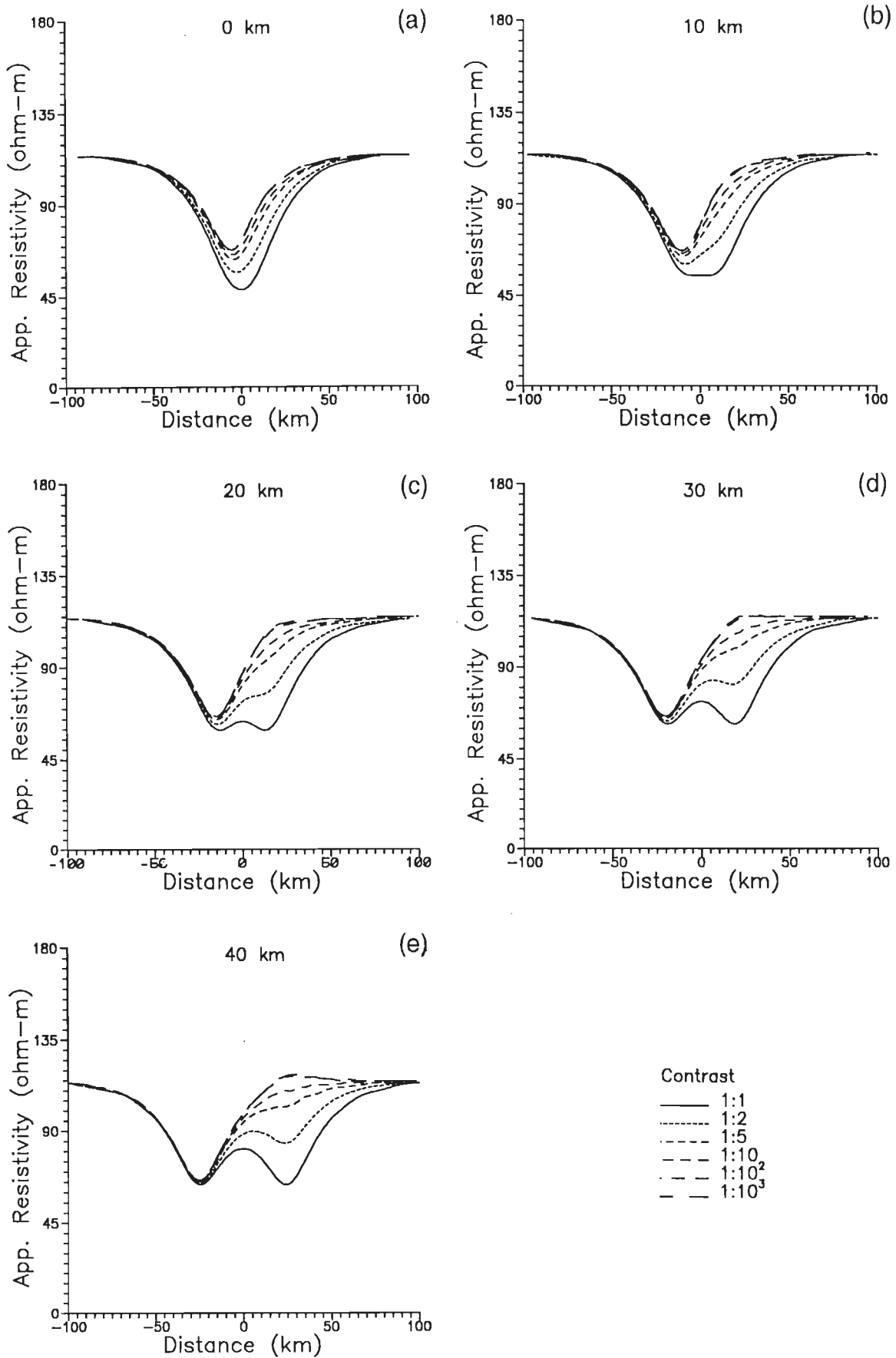


Fig. 6.12 Same as Fig. 6.11 for ρ_{xy} .

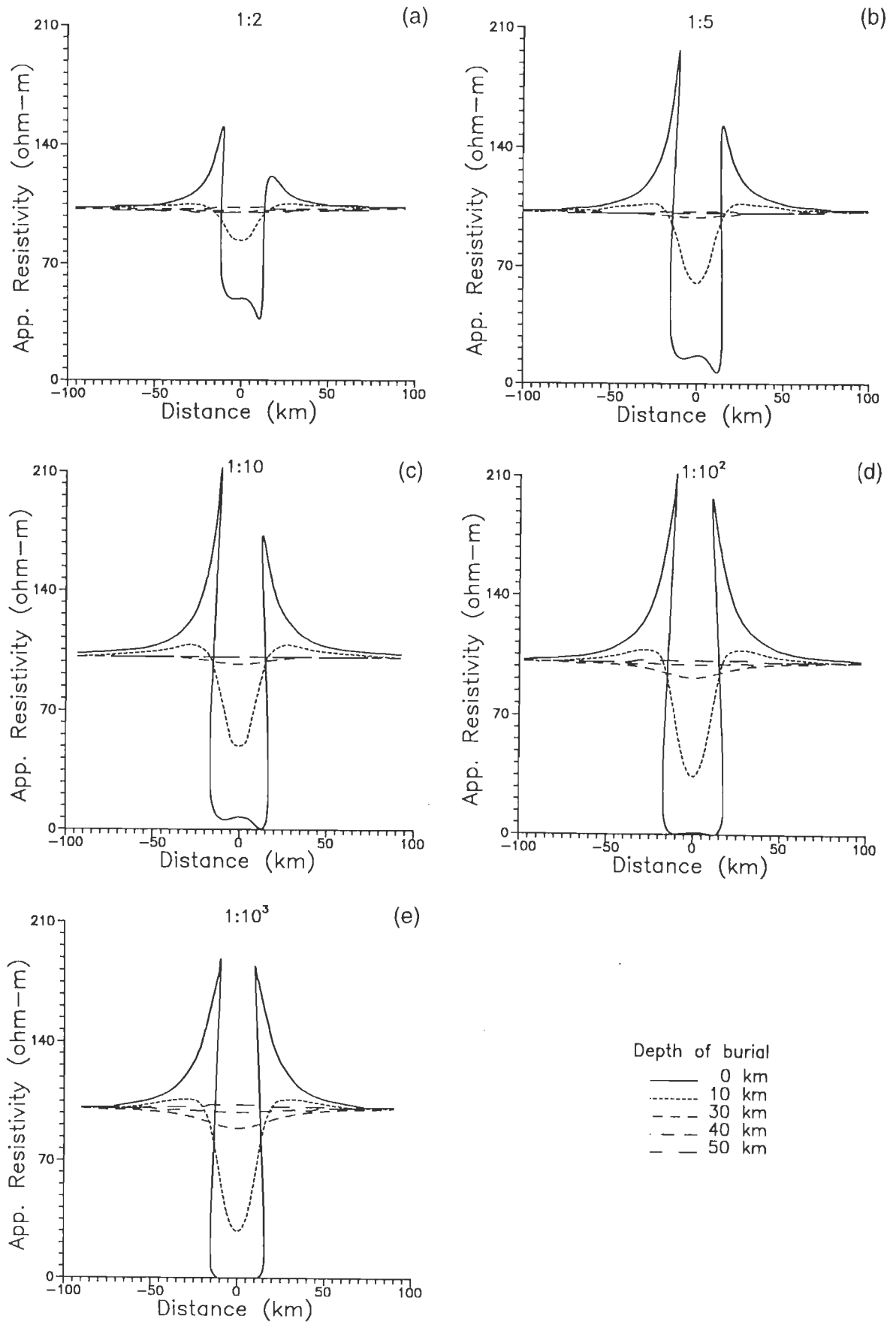


Fig. 6.13 Variation in ρ_{yx} of model 1 with change in depth of burial for a given resistivity contrast ratio. Plots (a), (b), (c), (d) and (e) are for resistivity contrasts 2, 5, 10, 100 and 1000 respectively.

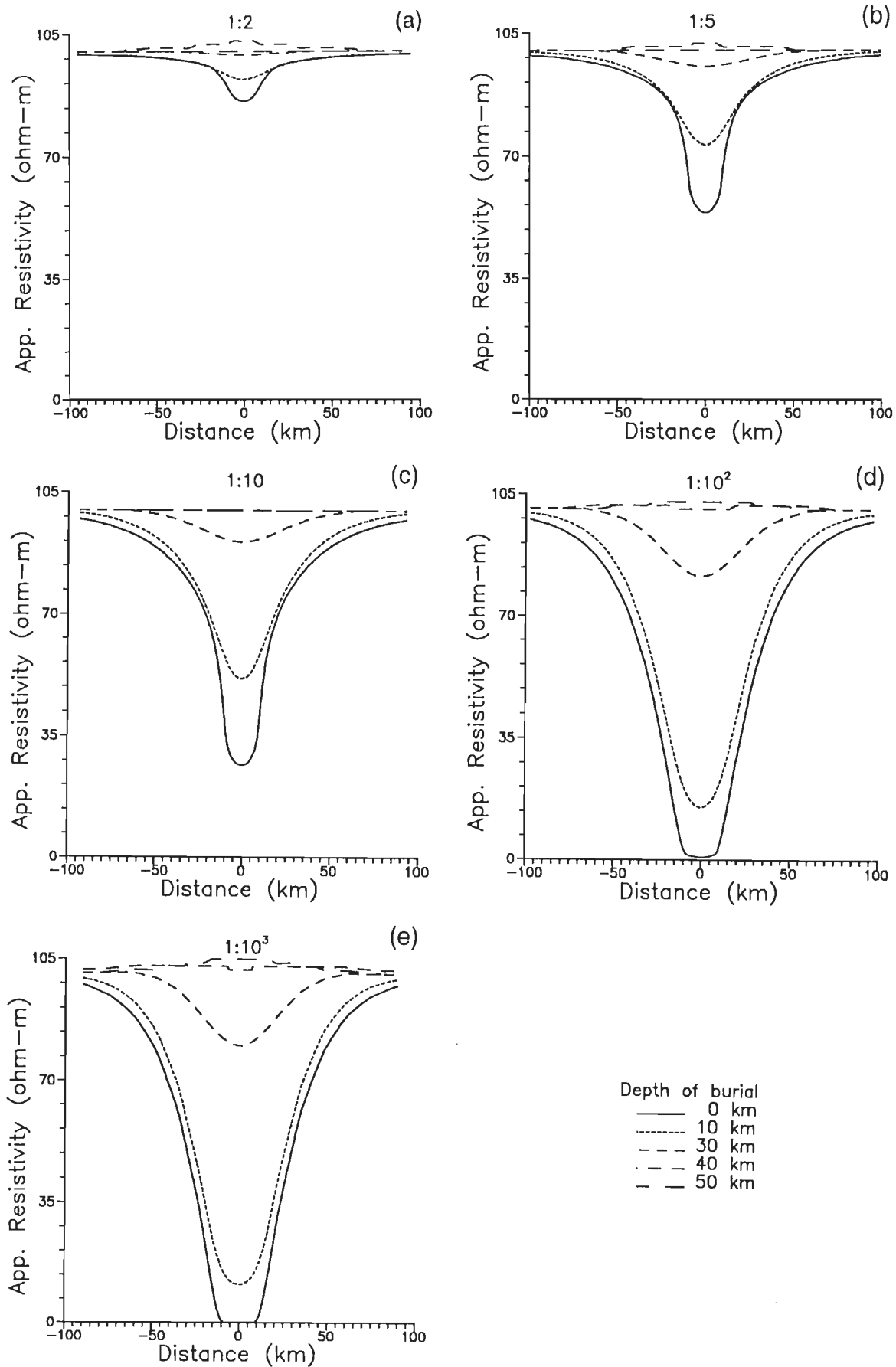


Fig. 6.14 Same as Fig. 6.13 but for ρ_{xy} .

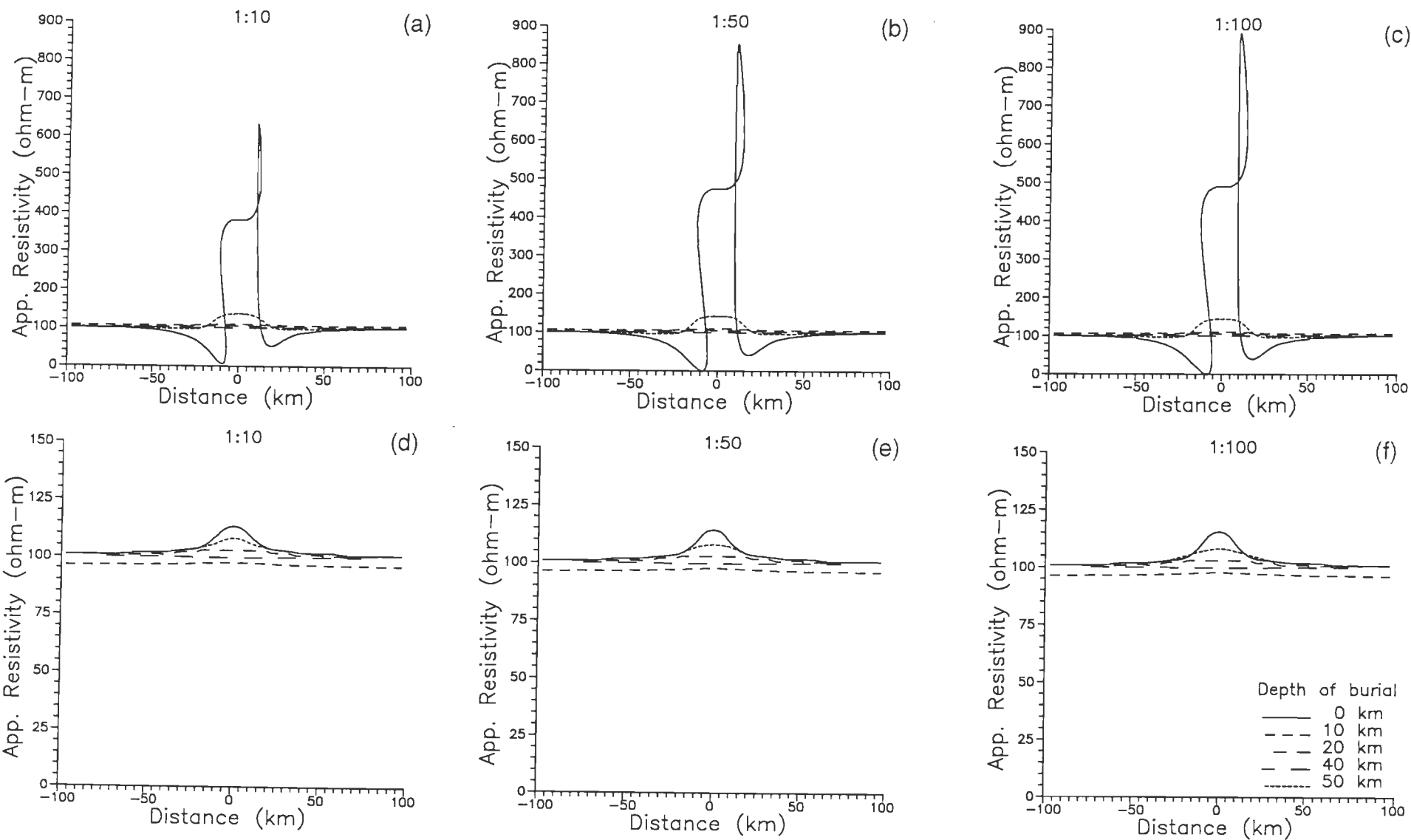


Fig. 6.15 Variation in ρ_{yx} (a,b,c) and ρ_{xy} (d,e,f) for model 2 for resistivity contrast ratio 10, 50 and 100.

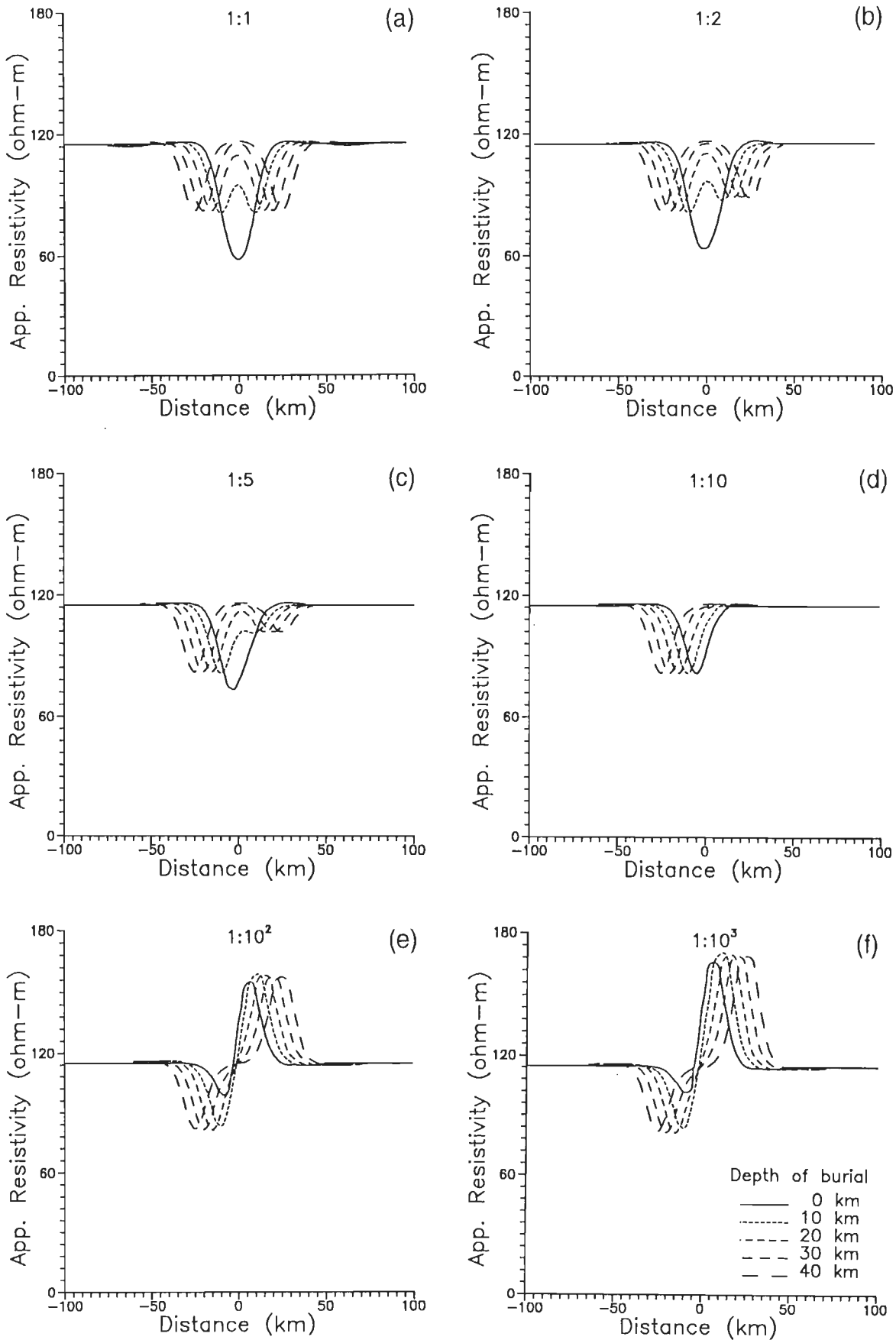


Fig. 6.16 Effect of the variation in separation between the two blocks of model 3 on ρ_{yx} for resistivity contrast ratios 1, 2, 5, 10, 100 and 1000 shown respectively in (a), (b), (c), (d), (e) and (f).

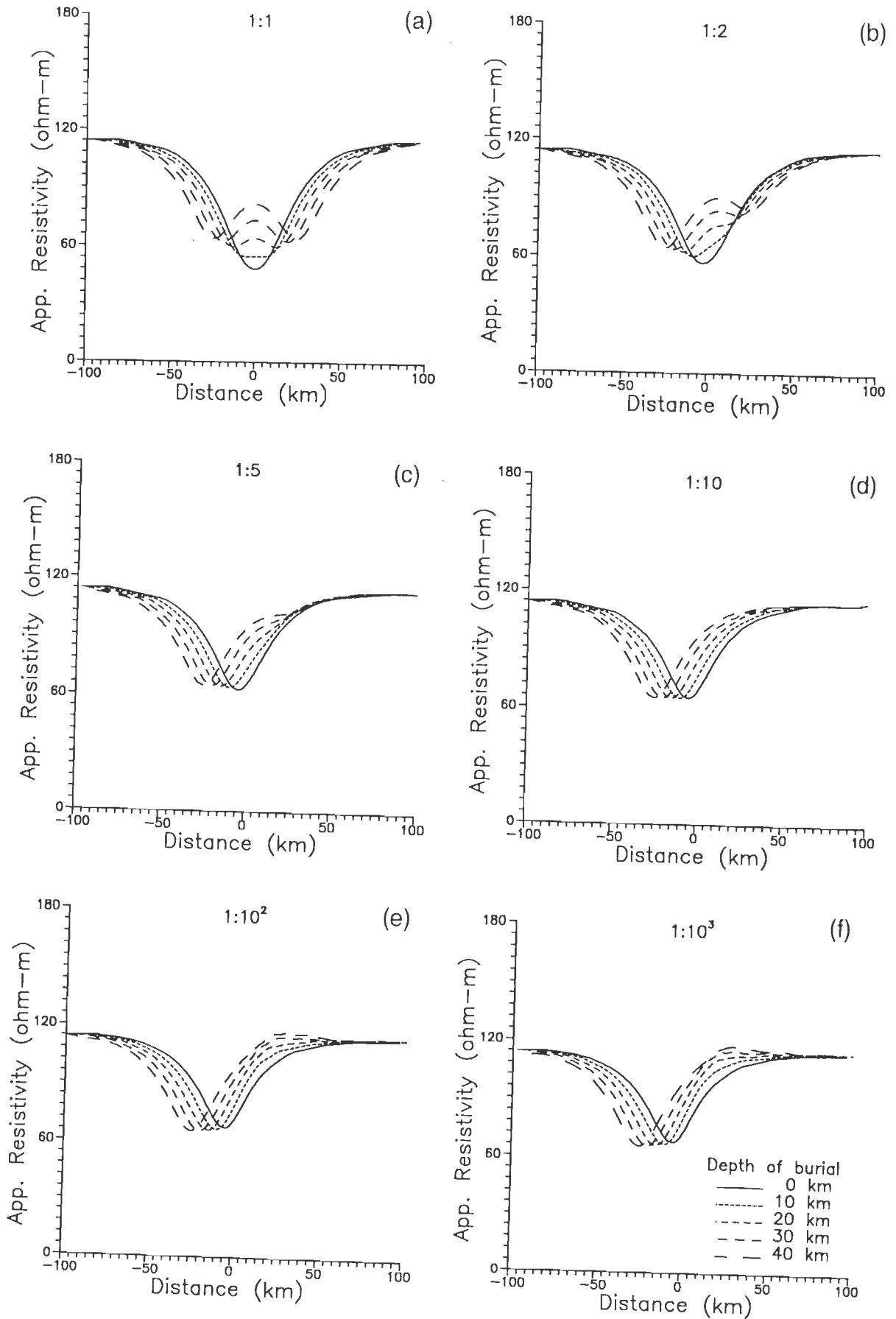


Fig. 6.17 Same as Fig. 6.16 but for ρ_{xy} .

These exercises are conducted on simple models with synthetically generated 'experimental' data. Models 1 and 2, the conductive block model and the resistive block model, respectively, are used for this purpose. Apart from using the *a priori* information about 1-D layered earth models, the better initial guess models, which provide a rough idea about the body, are constructed on the basis of forward anomalies. For the chosen models, the inversion domain encompassing the true body ranges from -30 to 30 km horizontally and 5 to 25 km vertically. The assumed resistivities of inversion domains for models 1 and 2 are 40 and 500 ohm-m respectively.

The grids used to invert data are different from the ones used in forward computations. Agarwal et. al (1993) have used 15 periods (in s) - 2, 3, 5, 8, 10, 15, 20, 40, 80, 160, 320, 640, 1280, 2560 and 5120, for generation of synthetic responses. Since during inversion periods smaller than 10 s result in large numerical grids which cannot be handled on available facility, only 11 periods, starting from 10 s to 5120 s, are used here.

The choice of standard frequency is crucial because the inversion domain blocks of its grid are used as superblocks in subsequent inversion iterations. For its selection, the single frequency inversion at each period(frequency) of the given range has been carried out. Since the inversion of response computed at period 80 s is good and economic, this particular period is taken for standard frequency. The 31 grid points of standard frequency grid, extending from -204 km to 204 km, are used as observation points for inversion. The observation points are (in km) - -204, -144, -114, -99.3, -84.3, -69.3, -58, -46.7, -35.5, -24.2, -17.1, -13.6, -10, -6.6, -3.3, 0, 3.3, 6.6, 10, 17.1, 24.2, 35.5, 46.7, 58, 69.3, 84.3, 99.3, 114, 144, 204. The optimum value of Marquardt parameter used, is 0.1. The minimum and maximum limits of resistivity values are, respectively, 1-100 ohm-m and 100-5,000 ohm-m for models 1 and 2 respectively. Before 2-D inversion, the computed responses are corrupted with 2% random Gaussian noise to simulate erroneous nature of real data. The experiments performed and their important results are discussed here.

6.3.2.1 Relative Performances of response functions

The impedance and the induction vector, the response functions of MT and GDS methods respectively, can be inverted using **EM2INV**. In order to analyse the

relative performance of impedance Z_{xy} with the induction vector I_{zy} these responses are computed at standard frequency for model 1 and then inverted. Fig. 6.18 shows the detailed inversion results. It is clear that the responses from inverted model fit the true Z_{xy} and I_{zy} response (Figs. 6.18a and b). In spite of greater % rms error in inversion of MT data (Fig. 6.18e), it estimates the body resistivity better than that estimated by GDS data. Moreover, it also resolves the exact depth of burial while the GDS data demarcates the horizontal extent of body better. The sudden change in resistivity gradient is reflected in the form of dense contours (Figs. 6.18c and d). The lower end of the body cannot be resolved by any of the responses.

Thus, the results of this experiment support the fact that the MT response is better for estimating vertical position and the extent of the body while the GDS response is better for horizontal variations.

6.3.2.2 Inversion quality for B- and E- polarizations

The MT data is available in both modes of polarization. If data for both polarizations, B- as well as E-, are given then the question arises as which one to prefer. A study which investigates and compares the inversion quality for these two modes of polarization, on conductive and resistive model, has been carried out.

The responses of models 1 and 2 for the B- and E- polarizations are generated for the standard frequency and then inverted as shown in Figs. 6.19 and 6.20. The inversion of Z_{xy} data images the body better (Fig. 6.19d) than that of Z_{yx} data (Fig. 6.19c) for model 1 which is conductive in nature. Especially the top level of body is distinct in resistivity contour plots of the inverted model. In contrast to this, the inversion results for resistive model (Fig. 6.20), indicates superior inversion of Z_{yx} response, as the body gets shifted upwards in inversion of Z_{xy} response. The lower end of the body is not clear in either mode of the polarization for any model. The lateral boundaries are well imaged by inversion of Z_{yx} response for both the models as indicated in Figs. 6.19c and 6.20c. This is in accordance with the charge accumulation on the boundaries. The % rms errors in inversion for the two models are shown in Figs. 6.19e and 6.20e respectively.

The results of the above mentioned study indicates that the conductive bodies are better resolved by inversion of E-polarization data while the resistive bodies by inversion of B-polarization data.

6.3.2.3 Efficacy of single and multifrequency inversion

The different depth levels of inhomogeneity can be tapped by controlling the choice of frequencies which, in turn, control the penetration depth. Generally, the large number of frequencies are used as a means for improving the resolution. This results in overall increase of computation time that is linearly proportional to the number of frequencies used. A theoretical exercise that demonstrates the impact of the number of frequencies used for inversion on the quality of inversion has been devised. It also identifies the minimum number of frequencies necessary for performing efficient inversion. The experimental results are demonstrated through inversion of Z_{xy} responses of model 1.

Initially, the model response generated at the standard frequency is inverted using all observation points. In subsequent steps, the number of frequencies have been increased one by one. The period, lying on either side of the standard frequency, is selected from the given range, i.e. 10 s to 5120 s. The procedure is repeated till all the frequencies of the range are included and inversion is carried out for each step.

Here only the selected inversion results, i.e. performed using single (80 s), three (40, 60 and 80 s) and six (20, 40, 80, 160, 320 and 640 s) frequencies are displayed in Fig. 6.21 for comparison. Figs. 6.21a and b are graphical displays of the corresponding % rms error plots and computation timings of algorithm for three cases. It has been observed that with increase in the number of frequencies, there is no remarkable difference in respective inversion results (Figs. 6.21c-e). Though this increase in number of frequencies used for inversion continuously decreases the % rms error but at significant increase in computing time. Hence, in lieu of economic viability the single frequency inversion is preferred to the multifrequency one.

We conclude from these results that if the extent of profile length is large enough to tap the target, then increase in number of frequencies does not improve the inversion quality.

6.3.2.4 Minimum number of observation points

Besides the frequency, the spread of observation points also controls the penetration depth. Larger the spread deeper will be the penetration. Next, an experiment, analogous to the previous one, which aimed at finding out the minimum number of observation points needed for good quality inversion has been carried out.

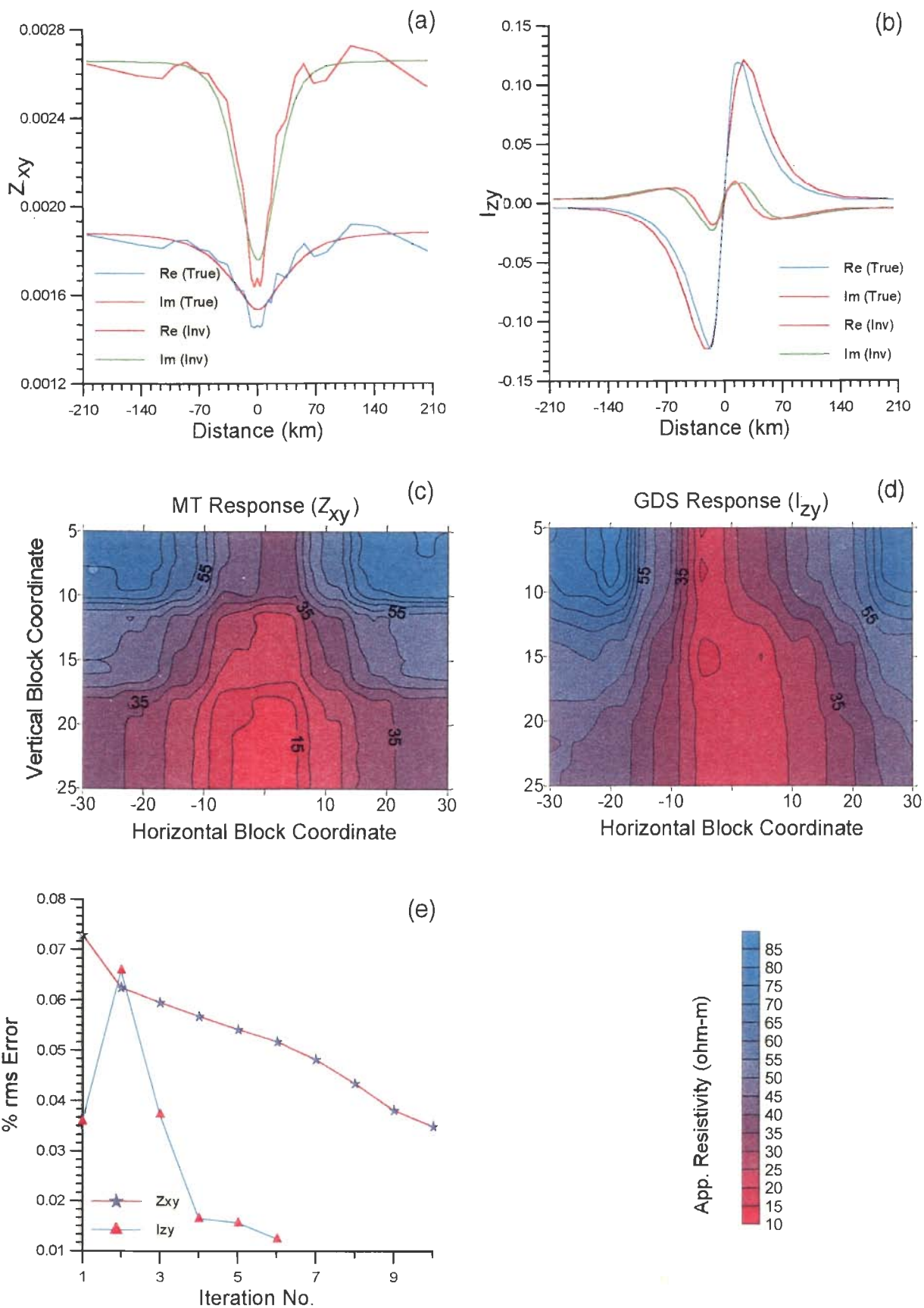


Fig. 6.18 The inversion quality of MT and GDS responses. The comparison of true and inverted model responses for (a) MT and (b) GDS responses; (c) and (d) present the obtained resistivity contours (in ohm-m); (e) the % rms errors during inversion.

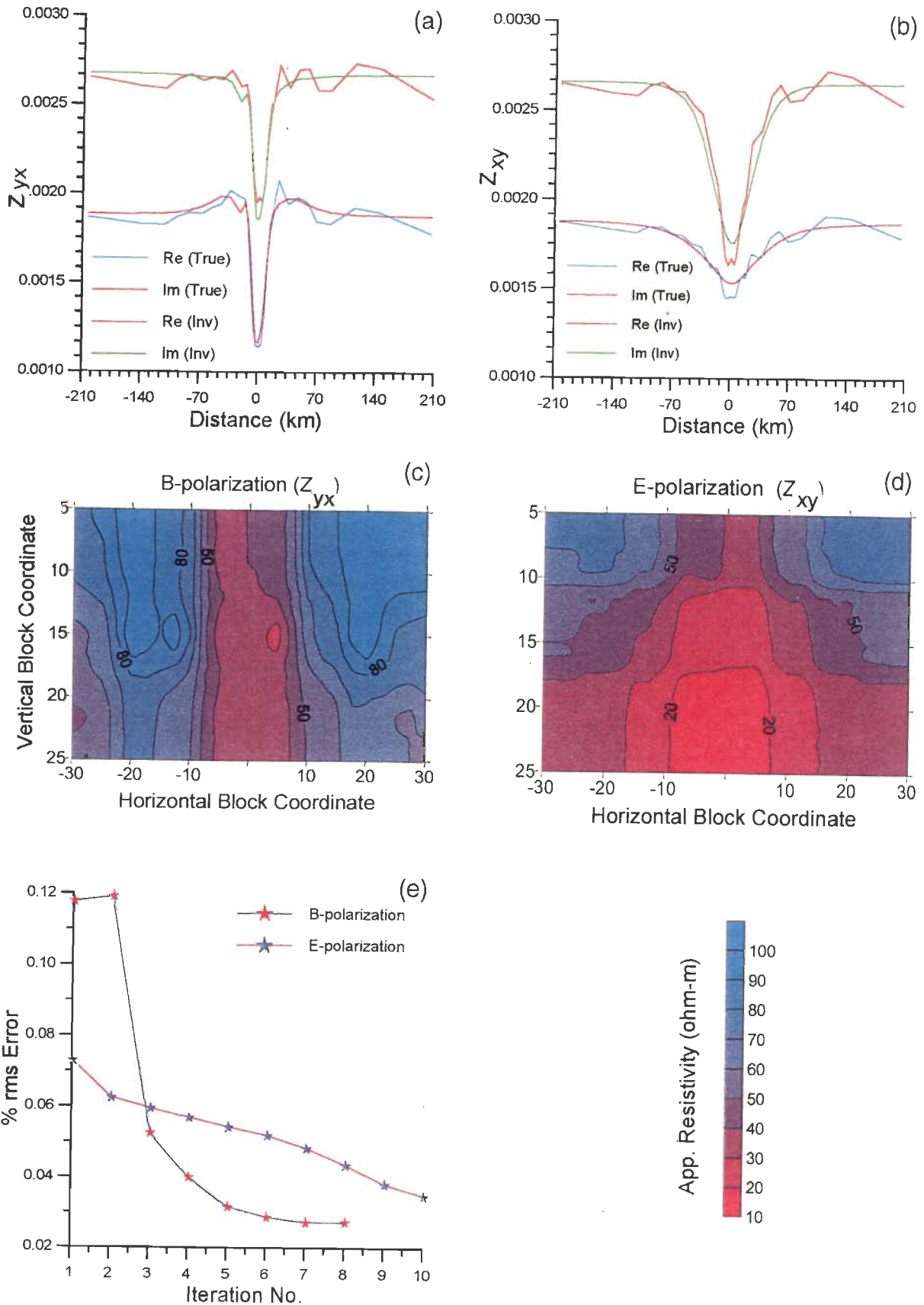


Fig. 6.19 Inversion quality for two modes of polarization for model 1. The Z_{yx} and Z_{xy} responses of true and inverted model are shown in (a) and (b) respectively; the resistivity contours of inverted model for the two polarizations are contoured in (c) and (d); (e) shows the % rms errors during inversion.

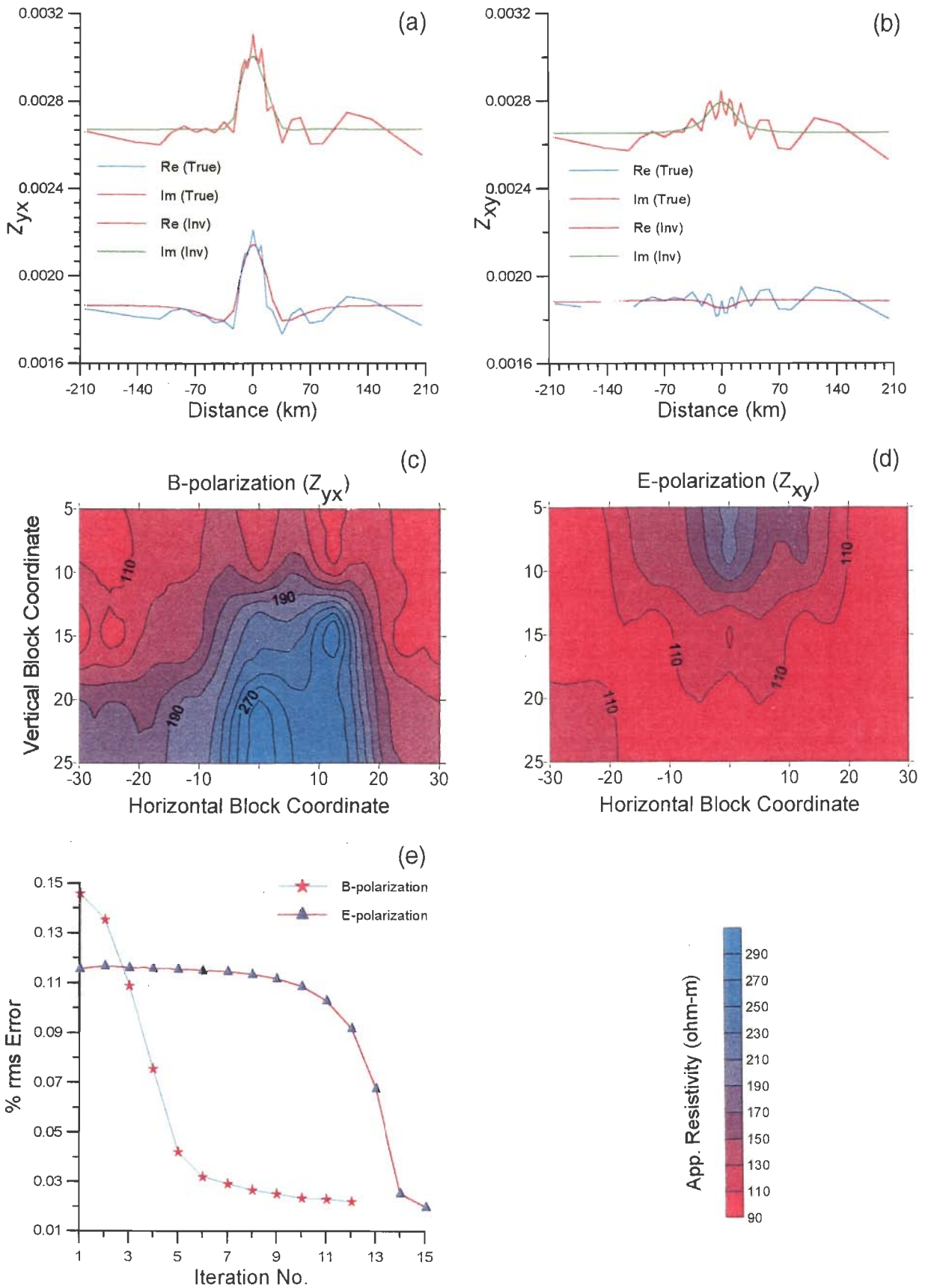


Fig. 6.20 Same as Fig. 6.19 but for model 2.

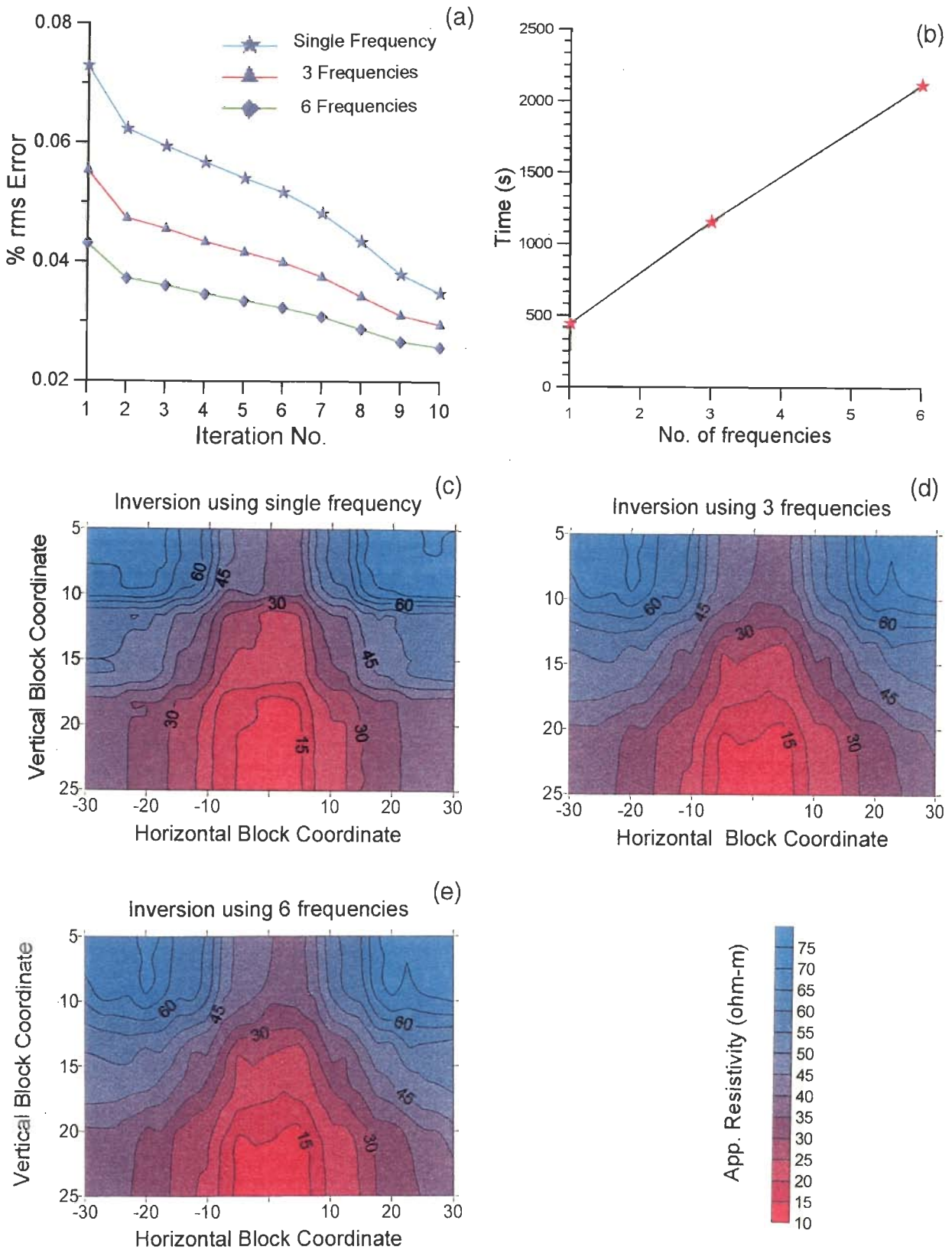


Fig. 6.21 The results of inversion performed using 1, 3 and 6 frequencies - (a) the % rms errors during inversion, (b) the CPU run time of algorithm for the three cases, (c), (d) and (e) show the obtained resistivity contours (in ohm-m) within the inversion domain for 1, 3 and 6 frequencies.

Initially all the 31 observation points, extending from -204 to 204 km, are used for inversion of impedance Z_{xy} , computed at standard frequency. Gradually two observation points, one on each flank have been removed till only one observation point, the central point of the profile, is left. If the set of frequencies used is not able to invert the data properly then another frequency is added.

The inversion results using 31, 19, 5 and 1 observation points are given in Fig. 6.22. The periods (in s) used for inversion are 80 for 31 points, 80 and 160 for 19 points, 80, 160, 320 and 640 for 5 points and 80, 160, 320, 640 and 1280 for single observation point. The profile for standard frequency (in km) extends from -204 to 204, -58 to 58, -6.6 to 6.6 and zero length, respectively, for 31, 19, 5 and 1 observation points.

The body is best resolved when inversion is performed using 31 observation points (Fig. 6.22a) but even when very few, i.e. 5 or 1 observation points, are used for inversion it helps in deciphering the approximate model. The most interesting result is when inversion is carried out using only one observation point (Fig. 6.22e). These results illustrate that even a single observation point of profile contains significant information about the body and can yield approximate model when used for inversion. The result highlights the applicability of 2-D inversion in comparison to 1-D one, where the point inversion provides only a layered earth model.

6.4 Closure

After validation and exhaustive testing of the inversion algorithm **EM2INV**, through theoretical experiments, its applicability has been established. For this, data inversion exercises and feasibility studies are carried out on synthetic as well as on field data as discussed in Chapter 7.

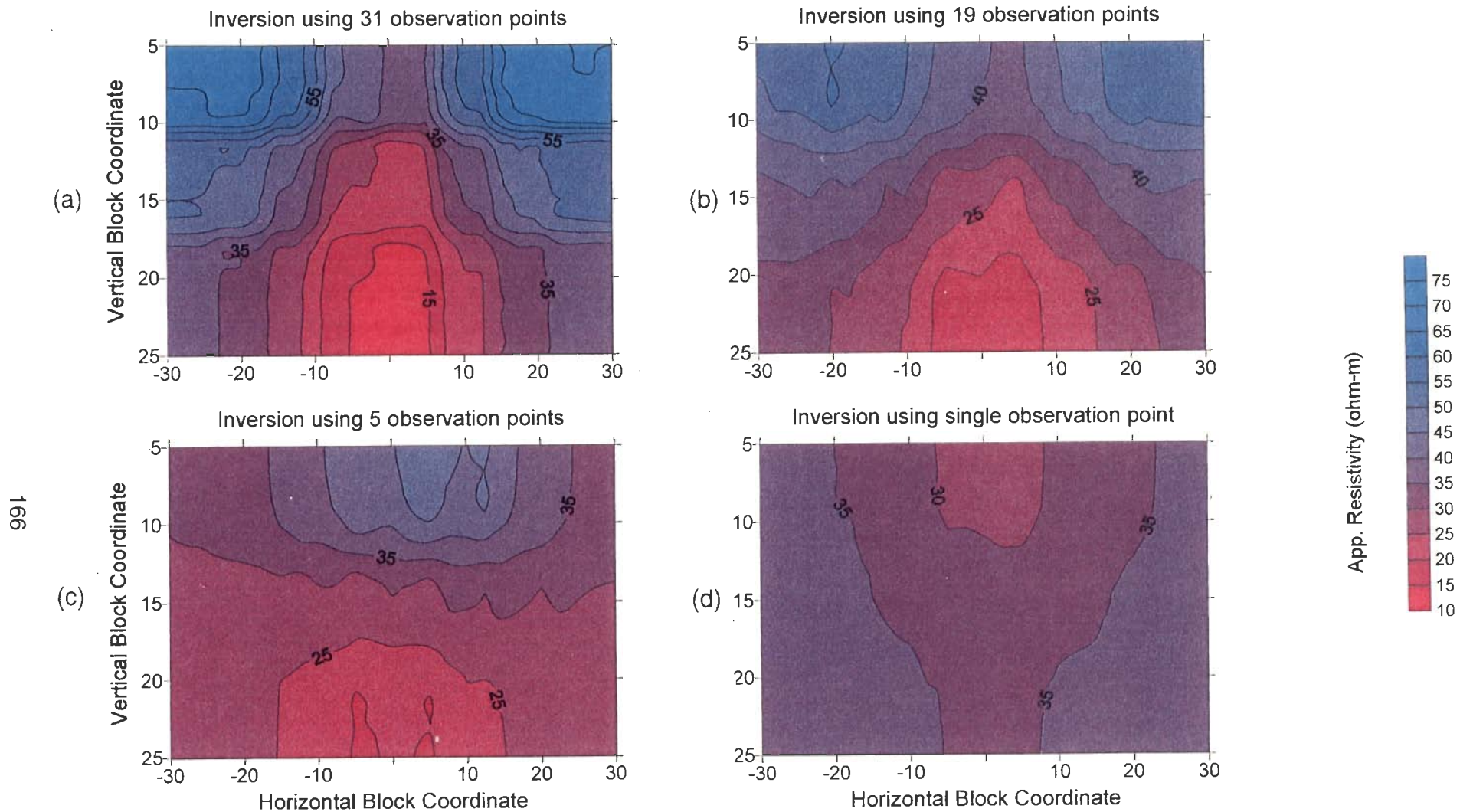


Fig. 6.22 Impact of spread of observation points on inversion quality - (a), (b), (c) and (d) show the inverted resistivity contours when 31, 19, 5 and 1 points are used for inversion.

RESULTS AND DISCUSSIONS**7.1 General**

The experiment design exercises of diversified nature using synthetic data, discussed in the Chapter 6, validate the inversion algorithm **EM2INV**. However, an algorithm cannot be used confidently unless it is tested on a large number of synthetic data sets and field data. The inversion related studies reported here are categorized, depending upon the nature of models and data, into three classes based on (i) purely synthetic data, (ii) data derived from models based on field studies and (iii) purely field data. A summary of different models, used for inversion studies, and their description is given in Table 7.1.

Table 7.1 Various models chosen for testing of **EM2INV**

Model	Type of response	Source	Model description
Horst	MT (synthetic)	Agarwal et al. (1993)	Conductive block of 10 ohm-m buried in host of 1000 ohm-m.
Conductive block	MT (synthetic)	Agarwal et al. (1993)	Conductive block of 10 ohm-m buried in a layered earth.
Resistive block	MT(synthetic)	Agarwal et al. (1993)	Resistive block of 1000 ohm-m buried in a layered earth.
Conductive and resistive block pair	MT (synthetic)	Agarwal et al. (1993)	Conductive and resistive blocks of 10 and 1000 ohm-m buried in a layered earth.

Table 7.1 Contd.

Sedimentary basin	MT (synthetic)	Madden & Mackie (1989)	Conducting basin of 5 ohm-m buried in half-space of 300 ohm-m.
Transverse structure	GDS (field study based)	Arora & Mahashabde (1987)	Asthenospheric ridge of 2 ohm-m at a depth of 15 km.
Trans Himalayan conductor	GDS (field study based and field)	Arora (1990)	Two blocks of 3 ohm-m embedded in a layered earth.
Graben structure	MT (field study based)	Peeples & Rankin (1973)	Conductive graben of 15 ohm-m in resistive host of 400 ohm-m.
COPROD2	MT (field)	Jones (1988)	NACP anomaly

A 2-D model can be obtained using 2-D inversion scheme and also through stacked results of 1-D inversion. The results and inferences drawn from these studies are presented here.

7.2 Inversion of synthetic data

The algorithm **EM2INV** is first tested on several data sets derived from synthetic models. The basic structures, commonly encountered during exploration or solid earth studies, are horst, sill, dyke, faulted block, conductive block, resistive block, salt dome, sedimentary basin etc. The two-dimensional models, representing the geologically meaningful situations, have been selected through a comprehensive literature survey. Various workers, Patra & Mallick (1980), Pek (1985), Madden & Mackie (1989), Oldenburg (1990), Zhdanov et al. (1990), Smith & Booker (1991), Agarwal et al. (1993), have given simple 2-D geophysical models. These models have been used as standard test of several 2-D inversion schemes (Pek, 1985; deGroot-Hedlin & Constable, 1990; Oldenburg, 1990; Smith & Booker, 1991; Agarwal et al., 1993). Agarwal et al. (1993) have not only described the basic models but have also presented their 2-D models based on stacked 1-D inversion results.

The models selected for the present study are horst, a resistive block, a conductive block and conductive resistive block pair, embedded in a two-layer earth (Agarwal et al., 1993) and the sedimentary basin model (Madden & Mackie, 1989).

A study, to ascertain whether the obtained 1-D stacked models can be improved further by 2-D inversion or not, has been conducted on the models picked up from Agarwal et al. (1993). As a result the inversion has become a two step procedure. In the first step, the 1-D inversion of a chosen model is carried out at each observation point for given time periods and then the obtained inverted models are stacked together to derive a starting 2-D model. In the second step, this starting model is used for 2-D inversion to obtain a final model. The Straightforward Inversion Scheme (SIS) has been used for the first step (Gupta et al., 1996) while for the second step **EM2INV** is used. Being linear, the SIS is a non-iterative scheme and it dispenses with the choice of an initial guess model. However, it requires the number of layers in the model and the constant layer thickness units of layer skin depth. The number of layers assumed for the present inversion are, in general, 100. For **EM2INV**, the inversion domain encompassing the true body, and its resistivity is defined on the basis of derived 1-D stacked model.

The forward responses, computed for the given period range at specified observation points and corrupted with 2% Gaussian noise, are used as data for SIS. In contrast, for **EM2INV**, only the significant periods at which the body is better sensed are used for efficient inversion. For a general model, where responses are to be computed at 9 observation points and for 6 periods, the CPU time for SIS is about 120s for one observation point, i.e. 1080 s for obtaining the stacked model. For **EM2INV**, which uses all the observation points but only 2 periods the CPU time is about 816 s.

The graphical display of the basic results is divided into two sets (i) 2-D pseudosections, with depth rather than period on vertical axis, derived from SIS inversion and (ii) the resistivity contour plots (in ohm-m) within the inversion domain of the 2-D model obtained from **EM2INV**. In most of the cases the convergence has been achieved in 10-12 iterations. However, in the basin model the convergence is achieved in 16 iterations. The computed results agree to observed results within 2% of rms error. In SIS the regression parameter ϵ^2 is taken as 0.02 for 2% Gaussian noise. The chosen models and their inversion results are presented here.

7.2.1 Horst model

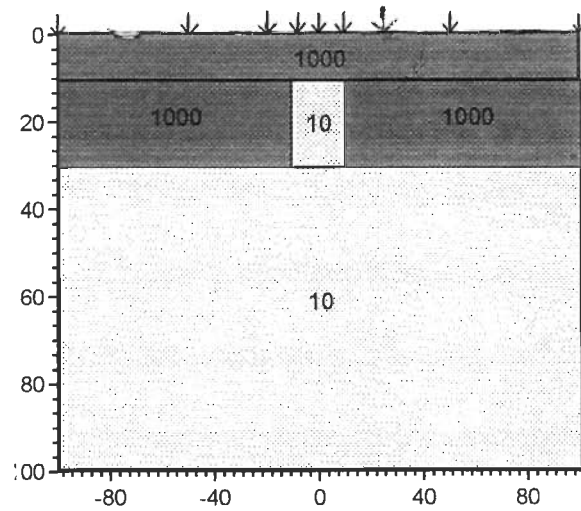
This simple geophysical model can be regarded as an upwelling of upper-mantle material into the crust. The resistivities of the crust and mantle are taken as 1000 ohm-m and 10 ohm-m respectively, the thickness and width of the horst are 20 km each, and the crust-mantle boundary is at a depth of 30 km (Fig. 7.1a).

The SIS 1-D inversion is carried out for B- and E- polarizations using six periods (in s) - 2, 10, 50, 200, 1000 and 5000 and at the nine sites (in km) -100, -50, -25, -10, 0, 10, 25, 50 and 100 while the **EM2INV** 2-D inversion employs only two periods 50 s and 200 s. From the SIS derived model, the inversion domain identified lies between -20 to 20 km and 5 to 30 km in horizontal and vertical directions, respectively, and its resistivity is 30 ohm-m. In Fig. 7.1, the inversion results indicate that the horst has been imaged well. Directly over the anomaly, the apparent resistivity value is fairly accurately recovered from Z_{xy} response but it is much less in comparison to that recovered from Z_{yx} which gives far too large a value. It is concluded that the horizontal extent is better resolved in case of B-polarization (Fig. 7.1b) while the localization of the boundaries in the vertical direction as well as the resistivity estimates have been better resolved in case of E-polarization (Fig. 7.1c). The inversion results shown in parts of Figs. 7.1d and e support the above view and highlight the superior quality of 2-D inversion.

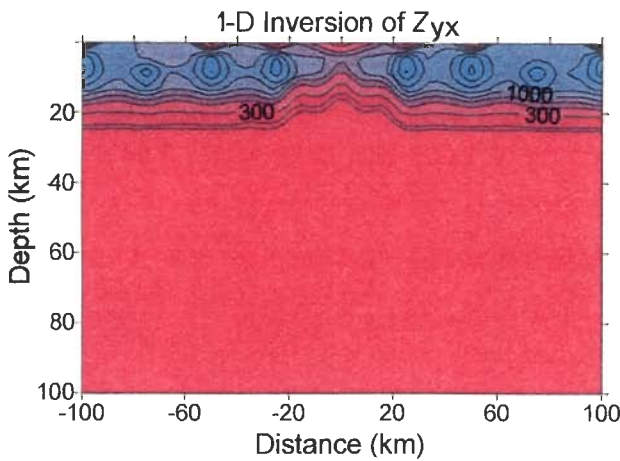
7.2.2 Resistive block model

The resistive block model, already discussed in section 6.3, is described here again for clarity. A block of width 20 km, thickness 10 km and resistivity 1000 ohm-m is embedded, with its top surface at a depth of 10 km, in a crust of 100 ohm-m resistivity (Fig. 7.2a). The crust mantle boundary is at a depth of 40 km and the mantle resistivity is 10 ohm-m. The responses for SIS are generated for 15 periods (in s) - 2, 3, 5, 8, 10, 15, 20, 40, 80, 160, 320, 640, 1280, 2560, 5120 at the 15 sites (in km) - 100, -75, -50, -30, -20, -10, -5, 0, 5, 10, 20, 30, 50, 75 and 100. In contrast, for **EM2INV** the inversion has been carried out using only two periods, 80 s and 160 s. On the basis of the 1-D stacked models the inversion domain, with resistivity 150 ohm-m, has been demarcated from -20 to 20 km in horizontal and 5 to 25 km in vertical direction.

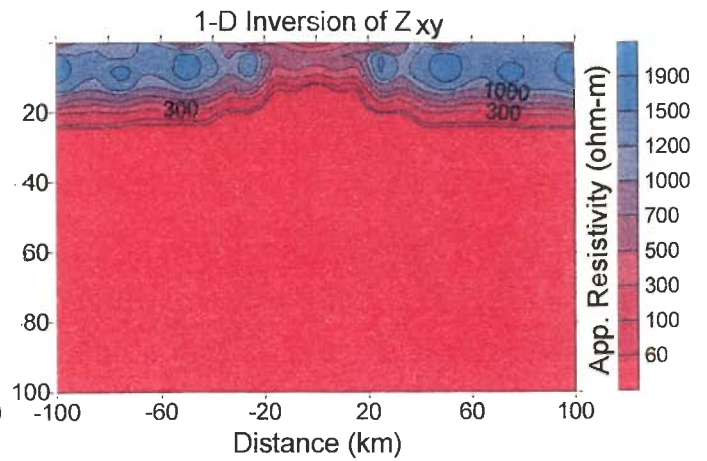
Fig. 7.2 exhibits the pseudosections of 1-D stacked model along with the resistivity contours, within the specified inversion domain of the model, obtained from 2-D inversion. A comparison of the inversions of Z_{yx} and Z_{xy} responses in Figs. 7.2b and c demonstrates the better quality of Z_{yx} inversion than that of Z_{xy} . It is interesting to observe that these features get more pronounced in 2-D inversion results and horizontal dimensions and depth of burial of the block are determined correctly. The block resistivity has been fairly well reproduced in Z_{yx} inversion (Fig. 7.2d).



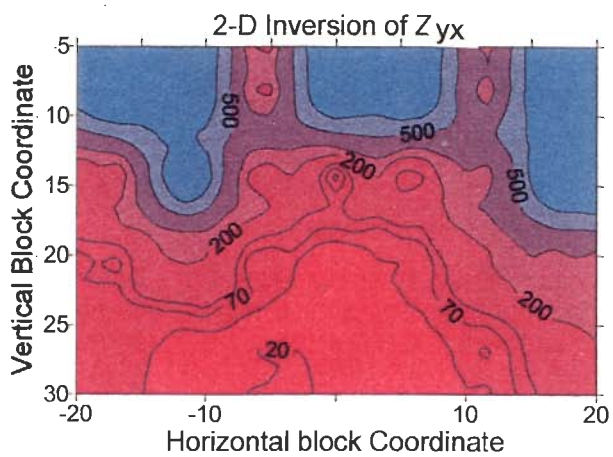
(a)



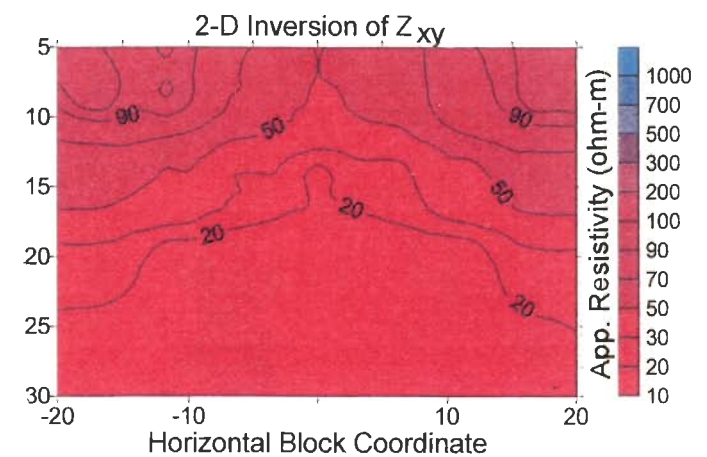
(b)



(c)

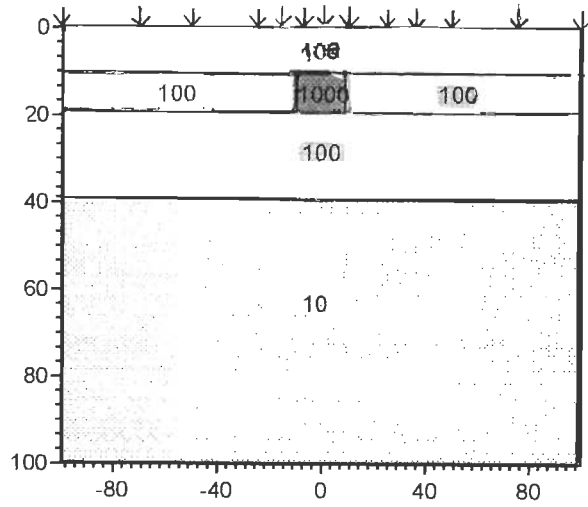


(d)

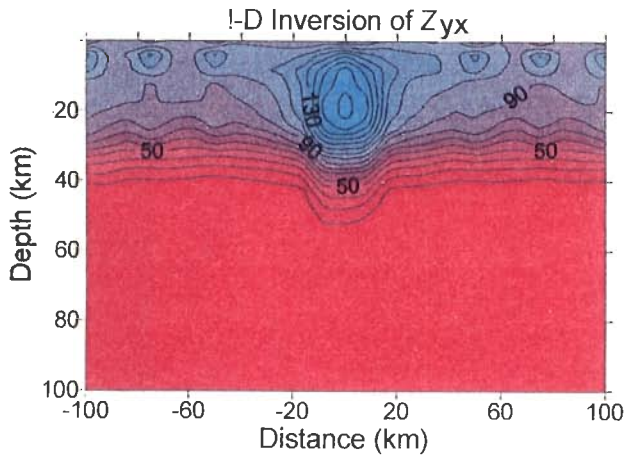


(e)

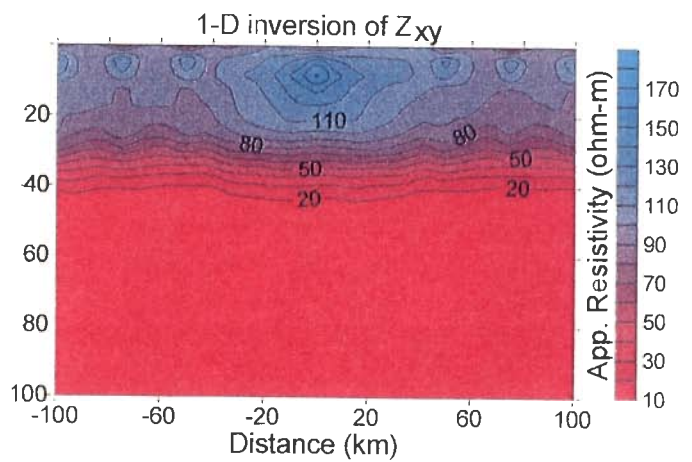
Fig. 7.1 (a) Horst model with positions of observation points marked on the horizontal axis by arrows; (b) and (c) the pseudosections obtained from SIS for the B and E-polarizations; (d) and (e) resistivity contour plots of model obtained from EM2INV for both B and E-polarizations.



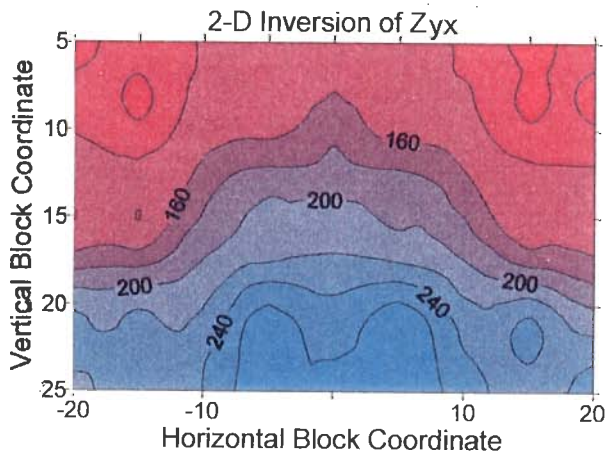
(a)



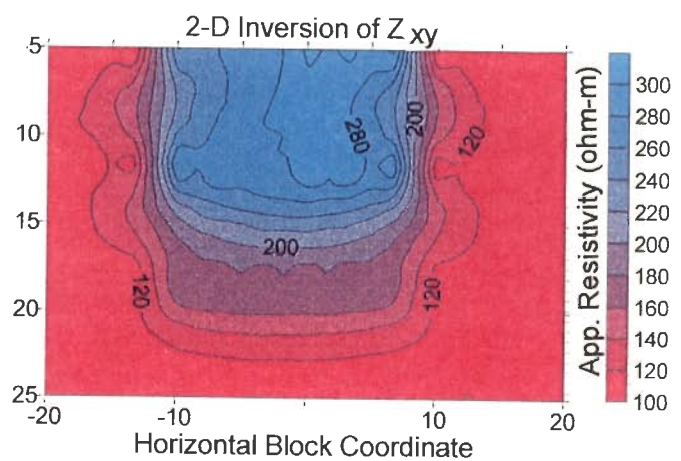
(b)



(c)



(d)



(e)

Fig. 7.2 As in Fig. 7.1 but for the resistive block model.

7.2.3 Conductive block model

This model is identical to the resistive one except that the block having resistivity 10 ohm-m is now more conductive than its host crustal layer (Fig. 7.3a). The data is generated for the same periods and observation points as in the case of resistive block model for both SIS and **EM2INV** inversions. For **EM2INV**, however, the guessed resistivity of the inversion domain is 30 ohm-m.

Being the conductive model, the block and the underlying structure are more accurately revealed by 1-D inversion of Z_{xy} response than of Z_{yx} , as is evident from Figs. 7.3b and c. In Z_{yx} inversion the lateral boundaries are better imaged, however, the block being elongated in vertical direction. The remaining Figs. 7.3d and e present the resistivity contour plots within the inversion domain of final 2-D model where the high density of contours due to sudden change in resistivity value signifies the presence of boundary.

7.2.4 Conductive and resistive block pair model

The two isolated blocks discussed in the previous two sections are brought together in this model, having a distance of 40 km between them (Fig. 7.4a).

The responses for SIS and **EM2INV** have been calculated for the same periods as before, but the number of sites is increased to 19 specifically (in km) -100, -75, -50, -40, -35, -30, -25, -20, -10, 0, 10, 20, 25, 30, 35, 40, 50, 75 and 100, to cover the full width of the region containing the anomalous bodies. The domain used for 2-D inversion ranges from -40 to 40 km in horizontal and 10 to 25 km in vertical direction. Since the inversion of starting model with variable depth of burial does not succeed, the exact burial depth of blocks has been taken. The assumed resistivities of inversion domain are 150 and 30 ohm-m, respectively, for Z_{yx} and Z_{xy} inversions.

The basic inversion results, pseudosections and resistivity contours, resulting from 1-D and 2-D inversions, respectively, are shown in Fig. 7.4. For the block pair model, the results turn out to be similar to single block models (Figs. 7.2 and 7.3). The Z_{yx} inversion indicates the presence of resistive block in a better manner (Figs. 7.4b and d), whereas the Z_{xy} inversion reproduces conductive block more prominently (Figs. 7.4c and e). Figs. 7.4d and e present the 2-D resistivity contour plots and further support this observation by giving better estimates of resistivities and, in turn, better 2-D models. This shows that the results of B- and E- polarizations are complimentary to each other and can be used for estimating the comprehensive true model.

7.2.5 Sedimentary basin model

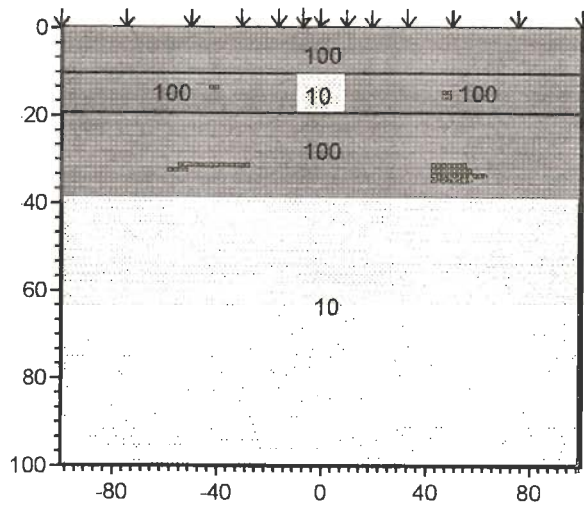
The inversion of the response of a simple basin model, used by Madden & Mackie (1989), has been performed directly using **EM2INV**. Fig. 7.5a portrays the 2-D model with a 2:1 vertical exaggeration. The conductive basin of 5 ohm-m resistivity is buried in a resistive host of 300 ohm-m. A numerical value 9999 ohm-m is assigned to the highly resistive basement.

Since the model is conductive, as expected, the inversion of Z_{xy} response scored over that of Z_{yx} response. Moreover, in this particular case the inversion results of Z_{yx} responses are not very satisfactory. Hence, results only for the Z_{xy} response are presented. The forward response has been computed for period 10 s and inversion has been carried out using all the grid points as observation points. Based on *a priori* information of 1-D model and forward anomaly, the inversion domain has been assumed from -7 to 7 km and 0 to 9 km respectively in the horizontal and vertical directions with the assumed resistivity being 100 ohm-m. The misfit between the true and inverted response, the resistivity contour plots and the % rms error plot are shown in Figs. 7.5b, c and d respectively. The response of the inverted model matches with the Z_{xy} response. The inverted model is able to identify the bottom boundary of the basin. Being Z_{xy} inversion, the resistivity is underestimated in the inverted model (Fig. 7.5c). The % rms error is high in the first iteration. As soon as the true parameter values are approached in subsequent iterations, the error estimates get reduced and convergence is achieved after few more iterations (Fig. 7.5d).

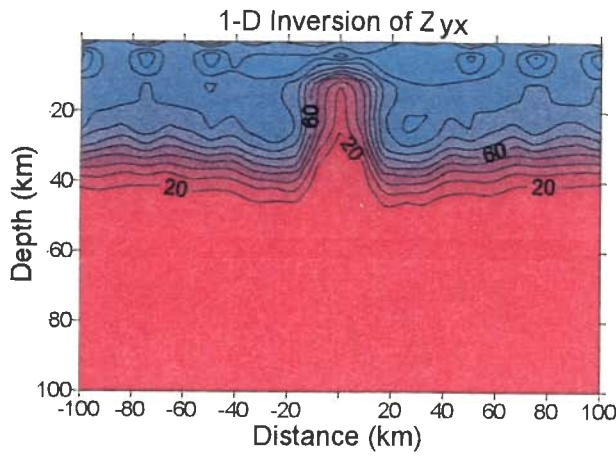
7.3 Inversion of data derived from field studies based models

Further test of the algorithm for simulating geologically interesting and real features has been carried out on models based on field studies. These model were obtained using trial and error method of forward modelling by various investigators. The following discussion presents a summary of basic results of investigating the efficacy of **EM2INV**.

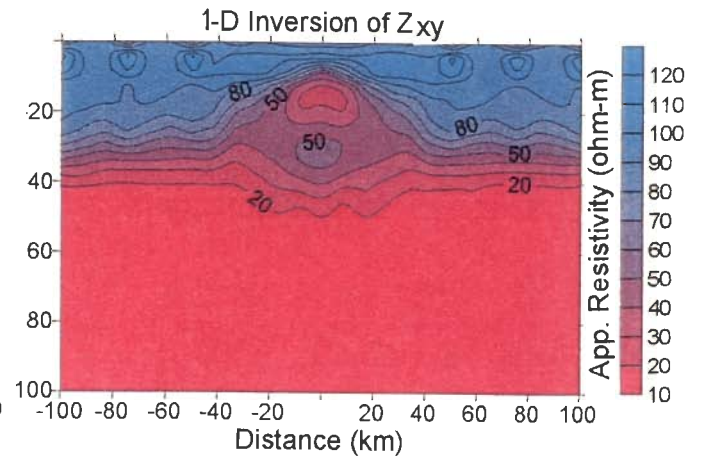
The field studies conducted for MT and GDS have been chosen from the literature. Two sets of GDS data (Arora & Mahashabde, 1987; Arora, 1990) and one set of MT data (Peeples & Rankin, 1973) have been considered. In order to assess the quality of inversion, the computed responses have been inverted and the inverted models are compared with the original models. The plot of % rms error vs iteration number graphically displays the convergence of the inversion. Finally, the inverted model resistivity contour plots (in ohm-m) within the inversion domain are presented.



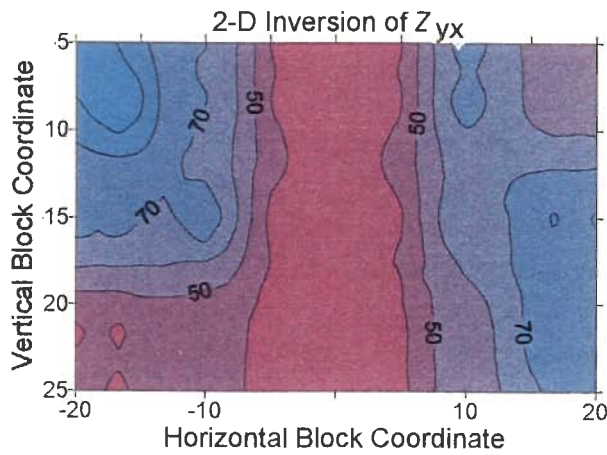
(a)



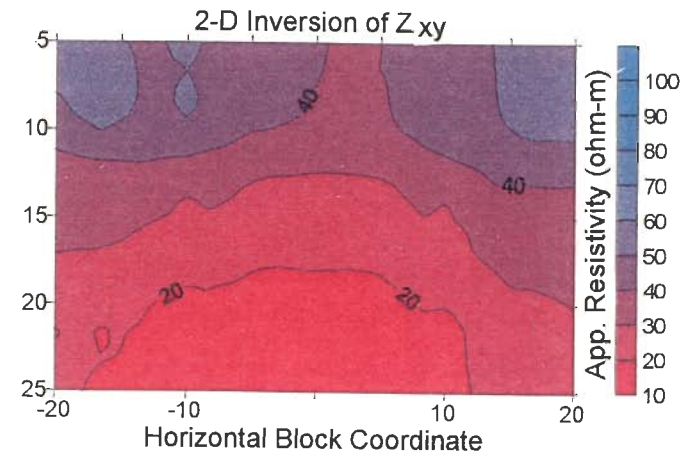
(b)



(c)

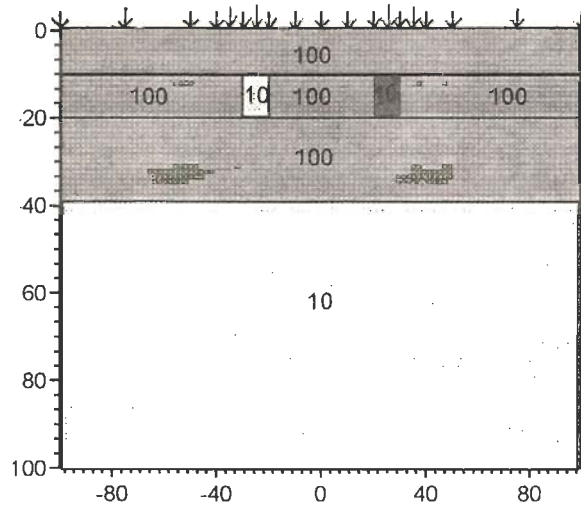


(d)

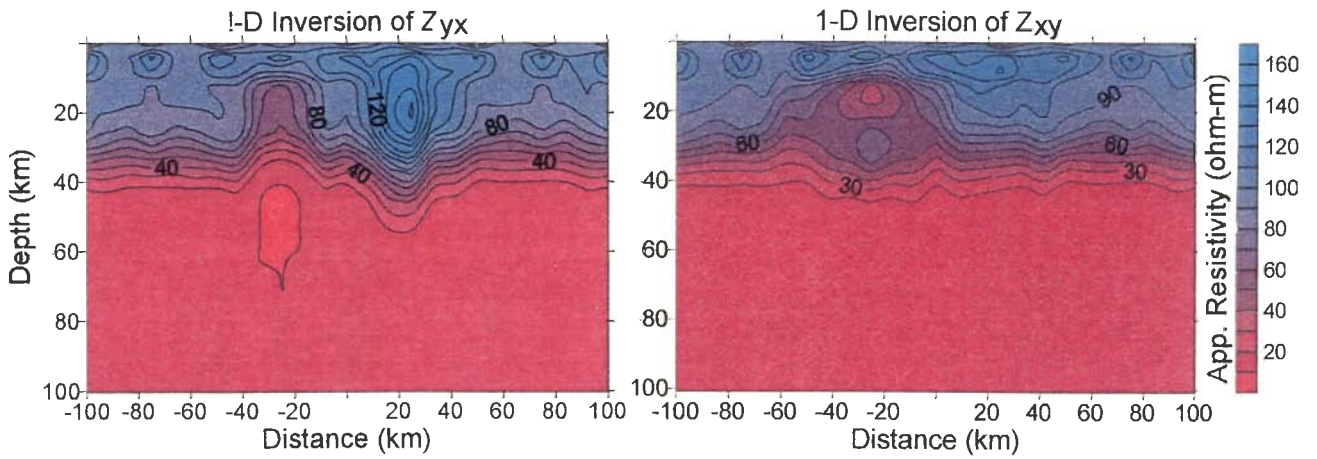


(e)

Fig. 7.3 As in Fig. 7.1 but for the conductive block model.

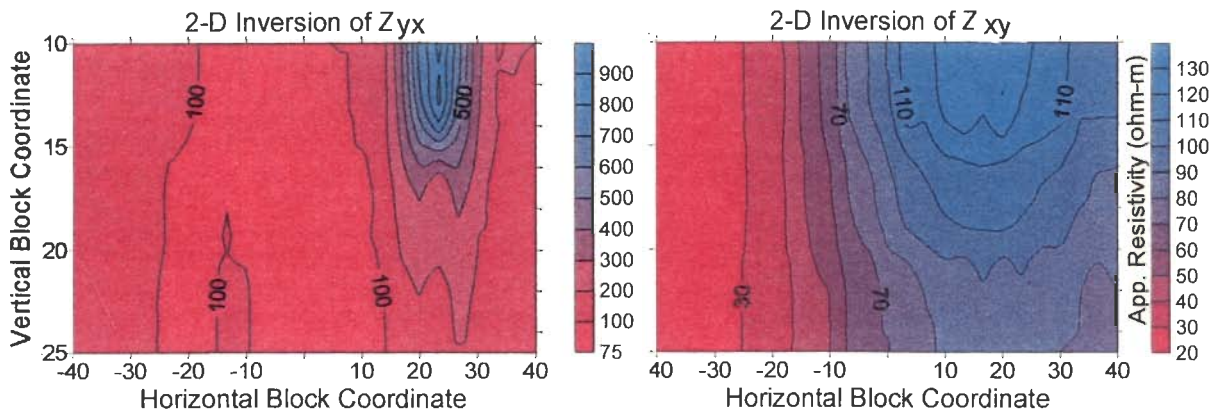


(a)



(b)

(c)



(d)

(e)

Fig. 7.4 As in Fig. 7.1 but for the conductive and resistive block model.

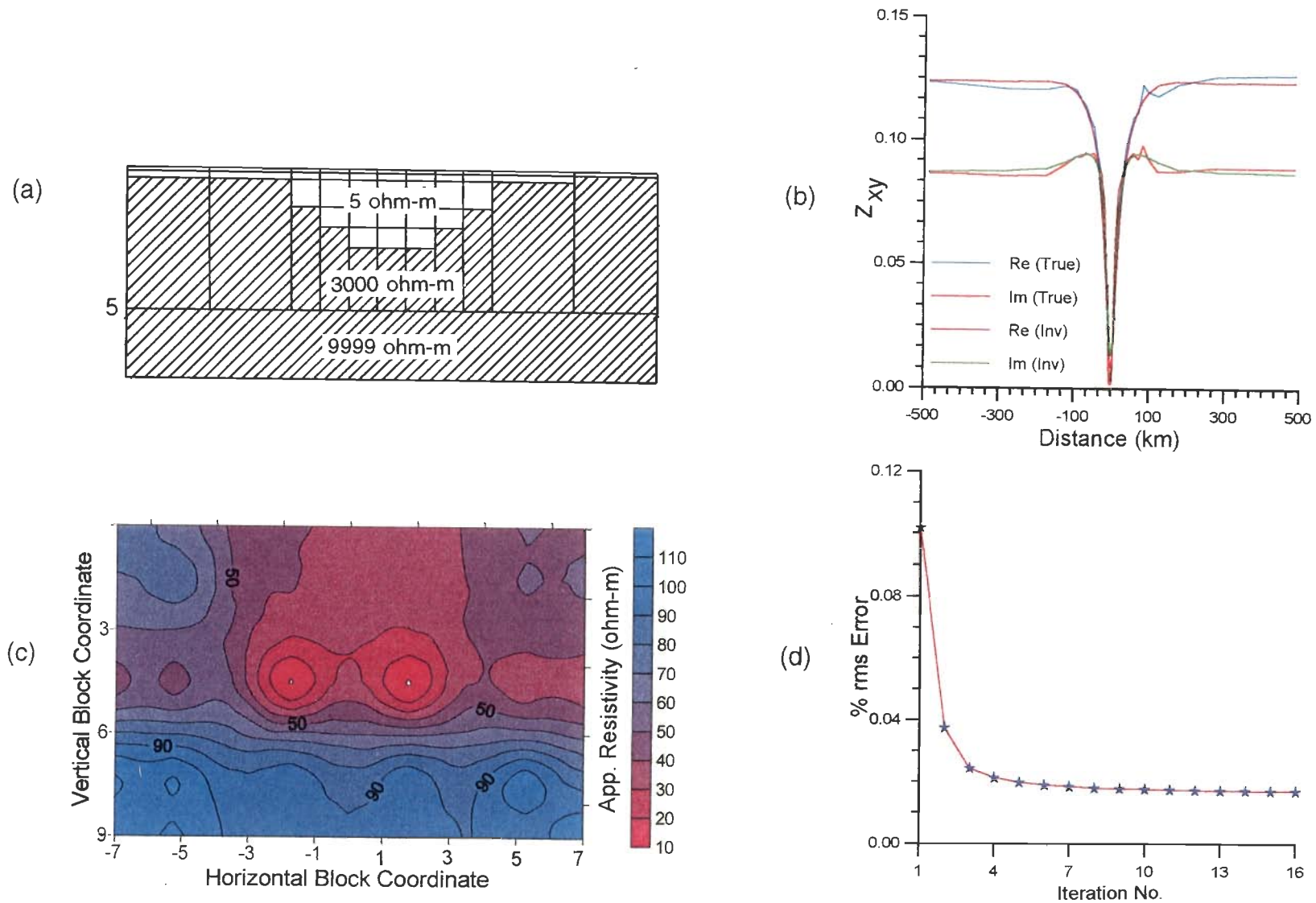


Fig. 7.5 (a) Sedimentary basin model with 2:1 vertical exaggeration (after Madden & Mackie, 1989). (b) Comparison of true and computed Z_{xy} response. (c) Resistivity contour plots of inverted models obtained from inversion of Z_{xy} response. (d) Convergence of the inversion iterations for inverted model.

7.3.1 Transverse conductive structure

The 1979 and 1984 magnetometer array studies over northwest India led to the discovery of a major conductivity structure across the Ganga basin in the foothills of the Himalayas (Lilley et al., 1981; Arora & Mahashabde, 1987). An examination of data for period 46 min resulted in the estimation of the position, orientation and extent of the structure.

In above mentioned study, the conductivity structure is modelled using the 2-D formulation of Jones & Pascoe (1971). On the basis of numerical modelling results, Arora & Mahashabde (1987) found that the observed induction pattern for 46 min along the lesser Himalayas belt, could be explained by asthenospheric ridge, about 45 km wide with its top at a depth of 15 km and a resistivity of 2 ohm-m (Fig. 7.6a). The profile with station locations is displayed on top of the model. The observed GDS response, both real and imaginary components, are shown in Fig. 7.6b.

During validity check of model, when computed and observed responses were compared for period 46 min, it was found that the computed result totally differ from the observed one. Singh & Pedersen (1988) also claimed that the response reported is not compatible with the observations. It appears that there was something inherently wrong with the response computations carried out by Arora & Mahashabde (1987) otherwise such a drastic difference in forward response is not possible at all. It is interesting to note that this fact was accepted by Arora (1990) wherein he has attributed to improperly chosen grid dimensions.

The possible changes in the model by keeping the forward response unchanged have also been attempted. The change in lithosphere resistivity, from 10,000 ohm-m to 1,000 ohm-m, resulted in almost the same anomaly. Even when the top layer resistivity is reduced to 100 ohm-m the results do not seem to be affected much.

Next, 2-D inversion of the proposed model response using **EM2INV** has been performed. The extent of the grid for period 46 min ranges from -14,000 km to 11,300 km, whereas the sites are located from -90 to 130 km (Fig. 7.6a). Since the 7 station data has been used in deriving the field model the GDS response of initial guess model has also been computed at these points. The inversion domain has been identified from -40 to 40 km and 15 to 100 km in horizontal and vertical directions

respectively. The attempts to invert data with 7 observation points and single frequency failed miserably and the convergence is not achieved for any of the models tried. This means that the data is insufficient for unconstrained 2-D inversion. To overcome this problem of limited *a priori* information, inversion has been attempted by increasing the number of observation points by adding points gradually on the left and right flanks of the profile till the convergence is achieved.

This exercise identified 19 observation points with the extent ranging from -250 to 200 km as the minimum number of data points needed for successful inversion. The inversion using the initial guess model with variable depth of burial could not succeed as it is difficult to derive vertical information from single period data. As a result, the initial guess model with exact vertical extent has been taken. Besides, the inversion has also been performed using all the 40 grid points as observation points. The % rms error for 19 and 40 observation points is .015 and .01 respectively. Figs. 7.6c and d indicate the excellent agreement between the observed and computed GDS response curves for both the real and imaginary components. Since the GDS resolves the lateral variations, the edges of the ridge have been recovered in the resistivity contours within specified inversion domain. Increase in data points results in further refinement of the estimated model as is evident from Figs. 7.6e and f plotted, respectively, for 19 and 40 observation points.

7.3.2 Trans Himalayan conductor

The highly differing responses, obtained by Arora & Mahashabde (1987) and Singh & Pedersen (1988) or **EM2INV** for a given model, may be an artifact of the inadequate choice of grid dimensions (Arora, 1990). Furthermore, the accuracy of the computed response depends on both the size and uniformity of the grid adopted in numerical modelling. Chamalaun et al. (1987) have discussed about the factors contributing to the non-uniqueness of the proposed models. The uncertainty, which arises due to the large station spacing, resulted in a poor definition of the observed response profile which ultimately determines the model parameters and their interpretation. The more realistic constraints on the best fitting model can be provided by comparing the responses over a wide range of frequencies. In addition, the denser network of stations need be considered to define depth and boundaries of conductive bodies and the shape parameters of the conductor.

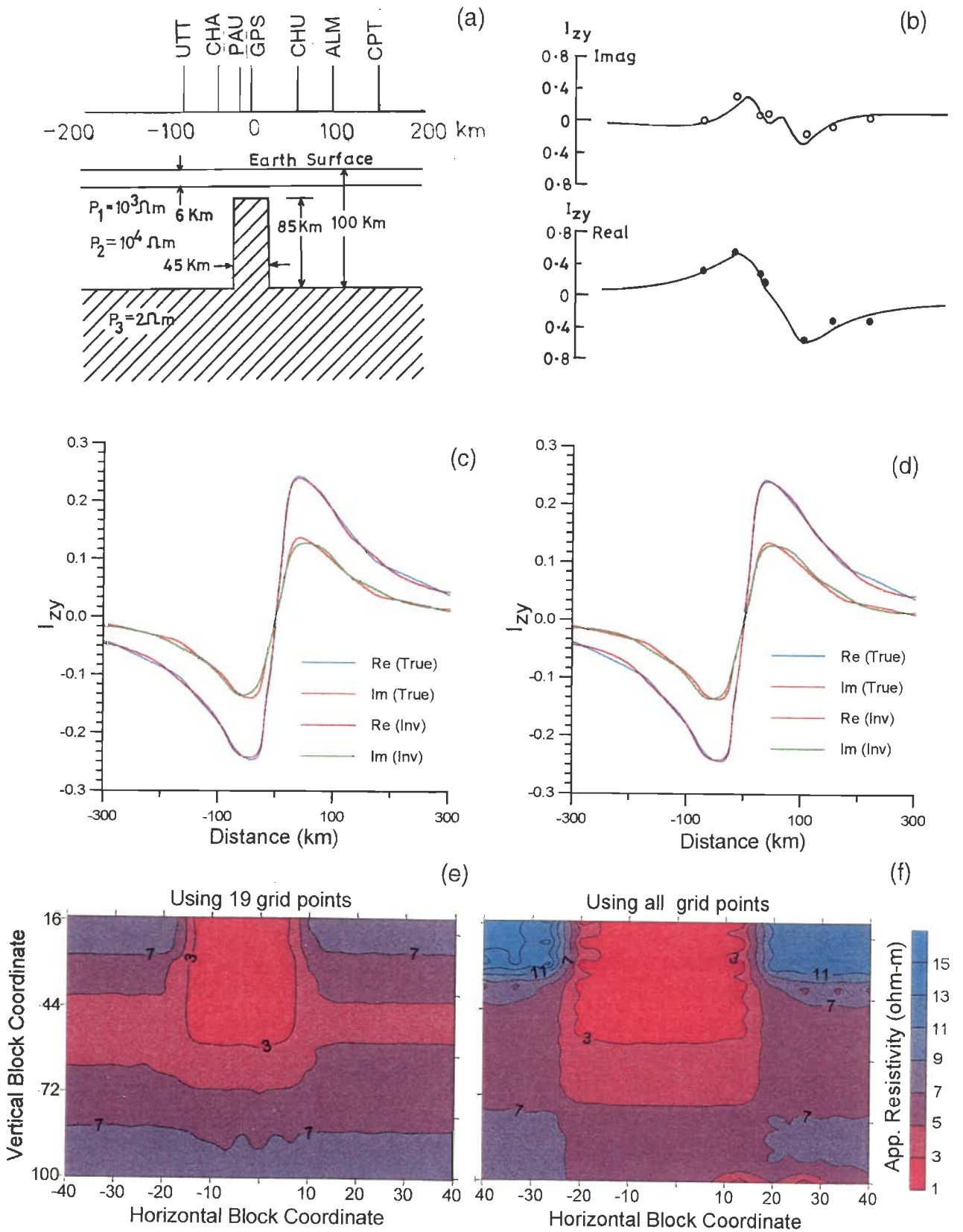


Fig. 7.6 (a) Proposed model for the conductor striking across the Himalayas (after Arora & Mahashabde, 1987). (b) The real and imaginary parts of the observed GDS response. (c) and (d) The real and imaginary parts of GDS responses for two cases are compared with the computed model response. (e) and (f) The resistivity contours of inverted model within the inversion domain for the two cases.

Being aligned transverse to the Himalayan mountains, the conductive structure has been named 'Trans Himalayan' conductor (Arora, 1990). The location sites of magnetometers together with the principal tectonic features of the region are discussed in detail by Arora (1990, 1993).

Arora (1990) found that real part of GDS responses at periods 46, 62 and 82 min could be reproduced by induction response of two tabular blocks of 3 ohm-m as shown in Fig. 7.7a. The left block is approximated to have a width of 25 km, a thickness of 12 km with its top at a depth of 8 km. The right block with its top at a depth of 12 km is approximated to have a width of 38 km and thickness of 18 km. The inclusion of a surface conducting layer of thickness 2-3 km simulating conducting sediments of 15 ohm-m in the Indo-Gangetic plains, improves the fit for the real part of the anomaly (Arora, 1993). The reliability of the proposed model was tested by comparing real part of the observed and calculated responses at three periods using 2-D FDM modelling approach of Brewitt-Taylor & Weaver (1976).

The computed synthetic responses of the proposed model at periods 46, 62 and 82 min have been inverted. For **EM2INV**, the inversion domain has been identified as ranging from -40 to 60 km in horizontal and 5 to 35 km in vertical directions. The resistivity is assumed to be 15 ohm-m. The inversion has been performed using 12 sites as observation points. The convergence is achieved in 6 iterations and the continuous decrease in misfit with iteration number indicates the good quality of inversion. Though individual block boundaries are not clear yet the side boundaries, which distinguish the block from the host are distinct in resistivity contours plotted for the inversion domain in Fig. 7.7c. Fig. 7.7d displays the goodness of fit between real parts of the observed (blue curve) and computed (pink curve) responses at the three periods; the sites are marked on the horizontal axis.

7.3.3 Graben structure

Peebles & Rankin (1973) conducted a field MT study for the buried graben in the Western Canadian sedimentary basin, flanked on the north-east by the Canadian shield. The basin comprises low resistivity sediments overlying the more resistive basement. Measurements of the data, on twenty locations along two profiles, were made in the period range 10 s to 1000 s to determine sedimentary and crustal resistivities for this region. The details of data procurement, analysis and interpretation are discussed in detail by Peebles & Rankin (1973).

Peeples & Rankin (1973) proposed a 2-D model for the graben on the basis of transmission surface analogy technique of Madden & Thompson (1965) and Swift (1967). The tensor apparent resistivity curves which are rotated into the principal directions of resistivity for the six selected recording locations, along a traverse across the strike of the structure, has been used as data for modelling. Their model consists of a low density fill layer of 15 ohm-m embedded in the resistive host of 400 ohm-m. The graben structure is overlain by a layer of 8 ohm-m low resistive sediments as represented in Fig. 7.8a. The horizontal line at the top of the model shows the location of stations across the MT profile.

The 1-D layered earth model has been assumed as the initial guess for carrying out 2-D inversion using **EM2INV**. For this purpose, the inversion domain considered, ranges from 30 to 120 km and 3 to 12 km in horizontal and vertical directions respectively. Further, the three periods 10 s, 40 s and 50 s have been used for inversion. Figs. 7.8b, c and d exhibit the rms error plot along with resistivity contour plots of inverted model for both the B- and E-polarization responses. Although the Z_{xy} response has taken large number of inversion iterations in comparison to Z_{yx} response, yet the % rms error is still smaller for Z_{xy} as shown in Fig 7.8b. The conductive graben structure, as expected, is recovered better by Z_{xy} response (Fig. 7.8d).

7.4 Inversion of field data

After gaining confidence with the successful inversion of synthetic data derived from theoretical and field study based models, an attempt has been made to invert the field data using **EM2INV**. For this purpose, the 2-D inversion of the GDS data of Trans Himalayan conductor and COPROD2 MT data have been undertaken.

7.4.1 Trans Himalayan conductor data

The proposed model of Trans Himalayan conductor (Fig. 7.7a) and other relevant details have already been discussed in section 7.3.2. Field data was recorded only at 12 observation points (in km) : -180, -90, -80, -50, -40, -10, 0, 55, 90, 100, 140 and 180 for periods 46, 62 and 82 min. Only real component of observations, induction vector, is available. The domain used for inversion and its resistivity is identical to the synthetic exercise carried out in section 7.3.2. This implies that inversion domain of 10 ohm-m ranges from -40 to 60 km and 5 to 35 km in horizontal and vertical directions respectively.

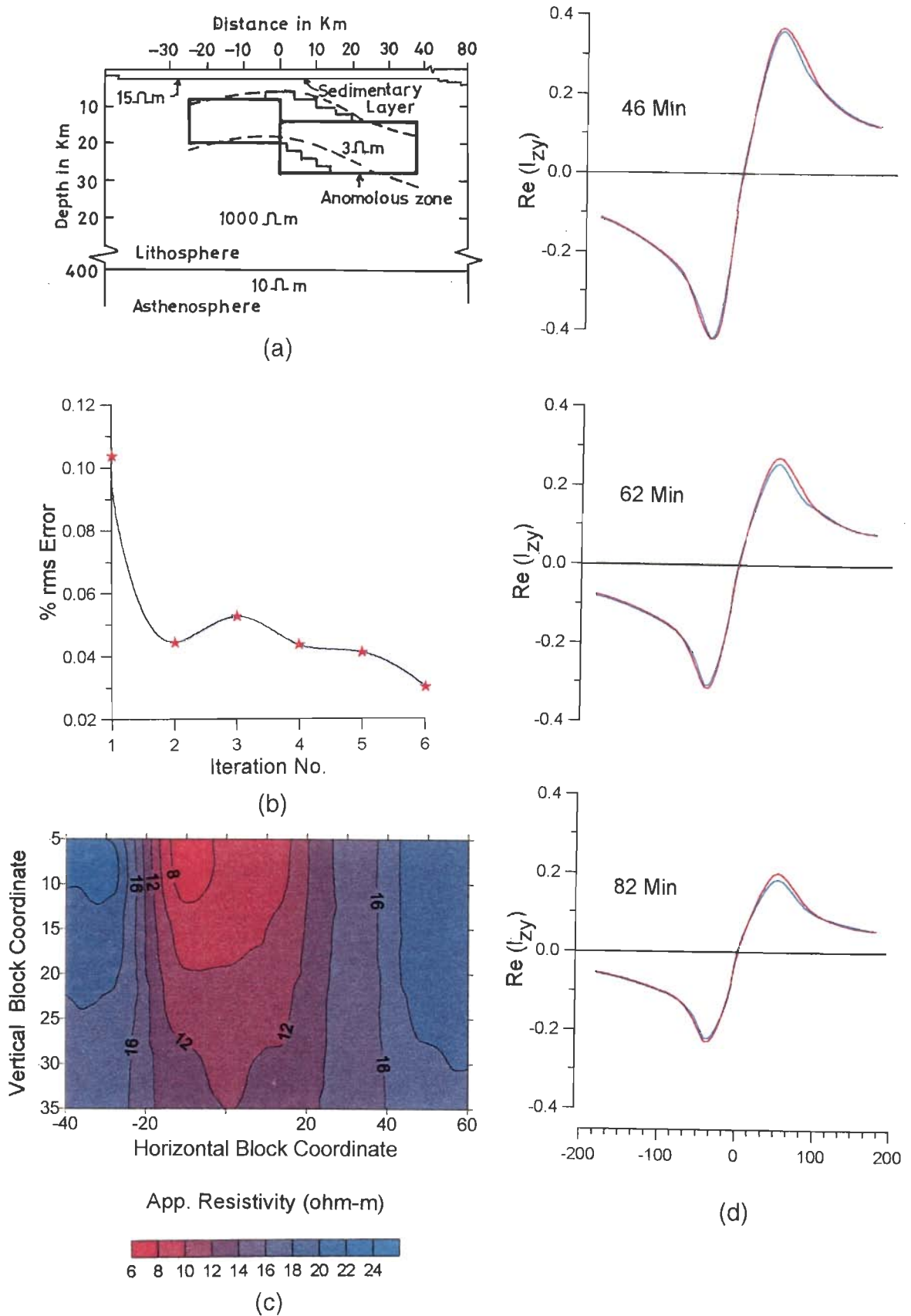


Fig. 7.7 (a) Proposed geoelectrical model for the Trans-Himalayan conductor (after Arora, 1990). (b) % rms error plot representing convergence. (c) Resistivity contours of the real part of GDS response of the inverted model within inversion domain. (d) Comparison of the real part of GDS response of the true model with the computed one for three periods.

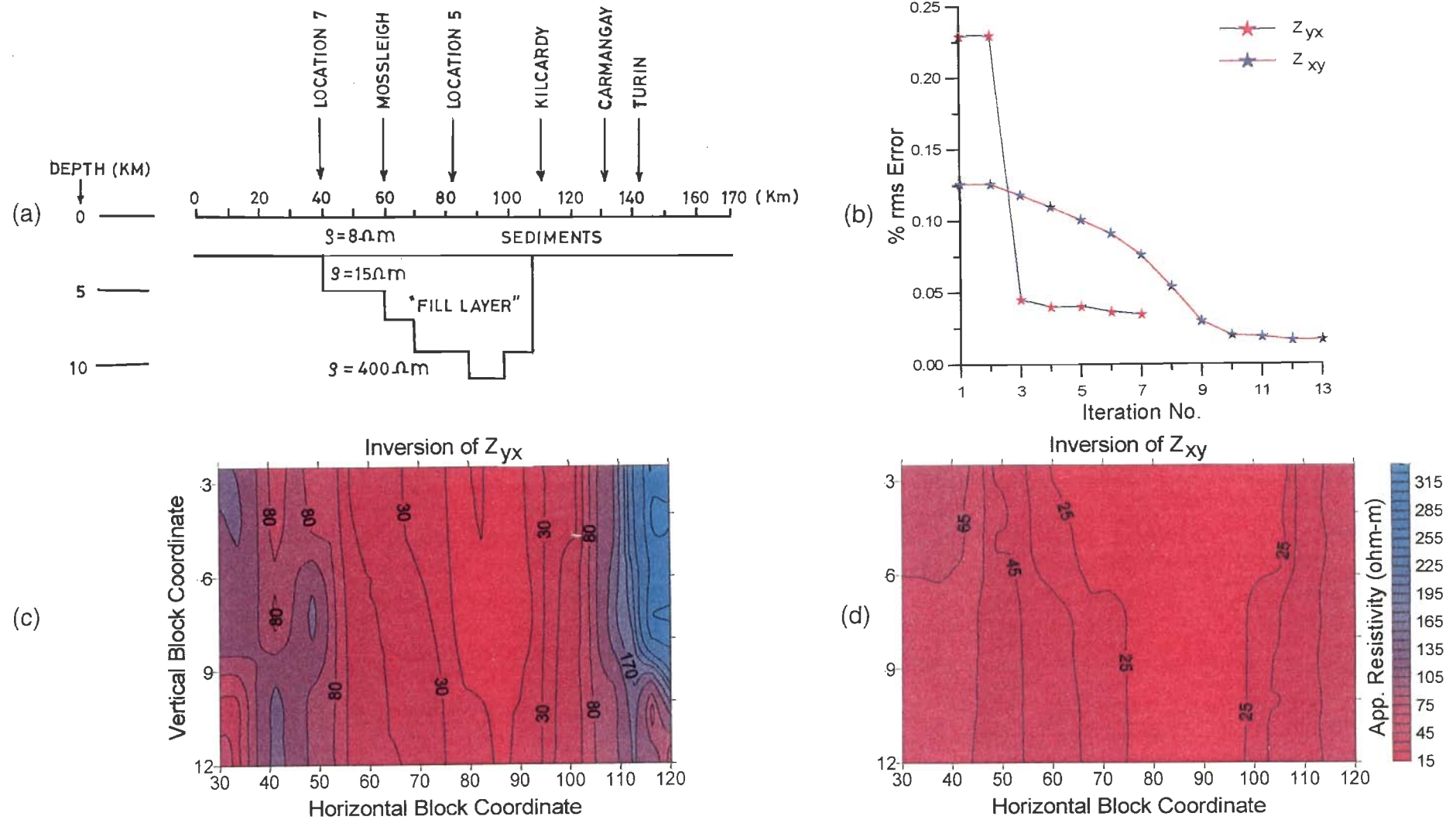


Fig. 7.8 (a) Proposed graben model based on the MT field study (after Peebles & Rankin, 1973). (b) Comparison of convergence of % rms error for Z_{yx} and Z_{xy} inversions. (c) and (d) Resistivity contour plots within the inversion domain for Z_{yx} and Z_{xy} responses respectively.

Comparison of real components of the inverted model responses with observations is shown in Fig. 7.9a for 3 periods where observation sites are shown in the bottom part of the figure. The error bars of the observations are marked by dots. Fig. 7.9b presents % rms error of inversion. The rms error and number of iterations have increased in comparison to that of synthetic exercise (Fig. 7.7b). The resistivity contours within inversion domain of the inverted model are plotted in part c of Fig. 7.9. Here too the lateral boundaries of the blocks have been recovered.

7.4.2 COPROD2 data

The MT data, recorded along a profile across the Phanerozoic Williston Basin in south Saskatchewan, Canada, have been corrected for static shifts (Jones, 1988). Jones & Craven (1990) had performed 1-D Occam's inversion by trial and error 2-D forward modelling while Nong et al. (1993) used Rapid relaxation inversion scheme for this purpose. On the basis of data analysis Jones & Craven (1990) had suggested two prominent conductivity anomalies - (i) the North American Central Plains (NACP) anomaly, with its centre in the array and top surface at a depth of 10 km reaching possibly to the base of crust and, (ii) the Thompson Belt (TOBE) anomaly to the east of the survey area, with its top surface virtually at the base of sediments and having a width of about 5 km. Since the two anomalies are separated by more than 100 km, these can be studied independently. Moreover, it is not feasible to investigate both these anomalies together because of the constraints on the grid dimensions imposed by the available computer memory.

In this section, only the inversion of NACP anomaly, the larger one, has been reported. The reduced data set (COPROD2R), covering the NACP anomaly, at the 20 sites has been taken from Agarwal et al. (1993). The sites selected are located at positions -113.5, -100.9, -93.0, -84.6, -74.4, -64.9, -55.7, -45.8, -35.0, -25.9, -14.6, -5.9, 4.9, 22.8, 41.8, 54.5, 64.2, 79.5, 96.2 and 117.3 km.

The strategy used for inversion of synthetic models, which is a two step process, has been followed for field data too (see section 7.1). First the separate 1-D inversions using SIS at various MT sites of the array have been performed. The 1-D inverted results of all observation points are then stacked to derive a pseudosection. The derived model is used as a starting model for **EM2INV**.

Agarwal & Weaver (1993) have obtained the final model using automatic 1-D inversion scheme (Weaver & Agarwal, 1993). Since the model is obtained through minimum number of columns by the data it is called the 'least blocked' model. Their

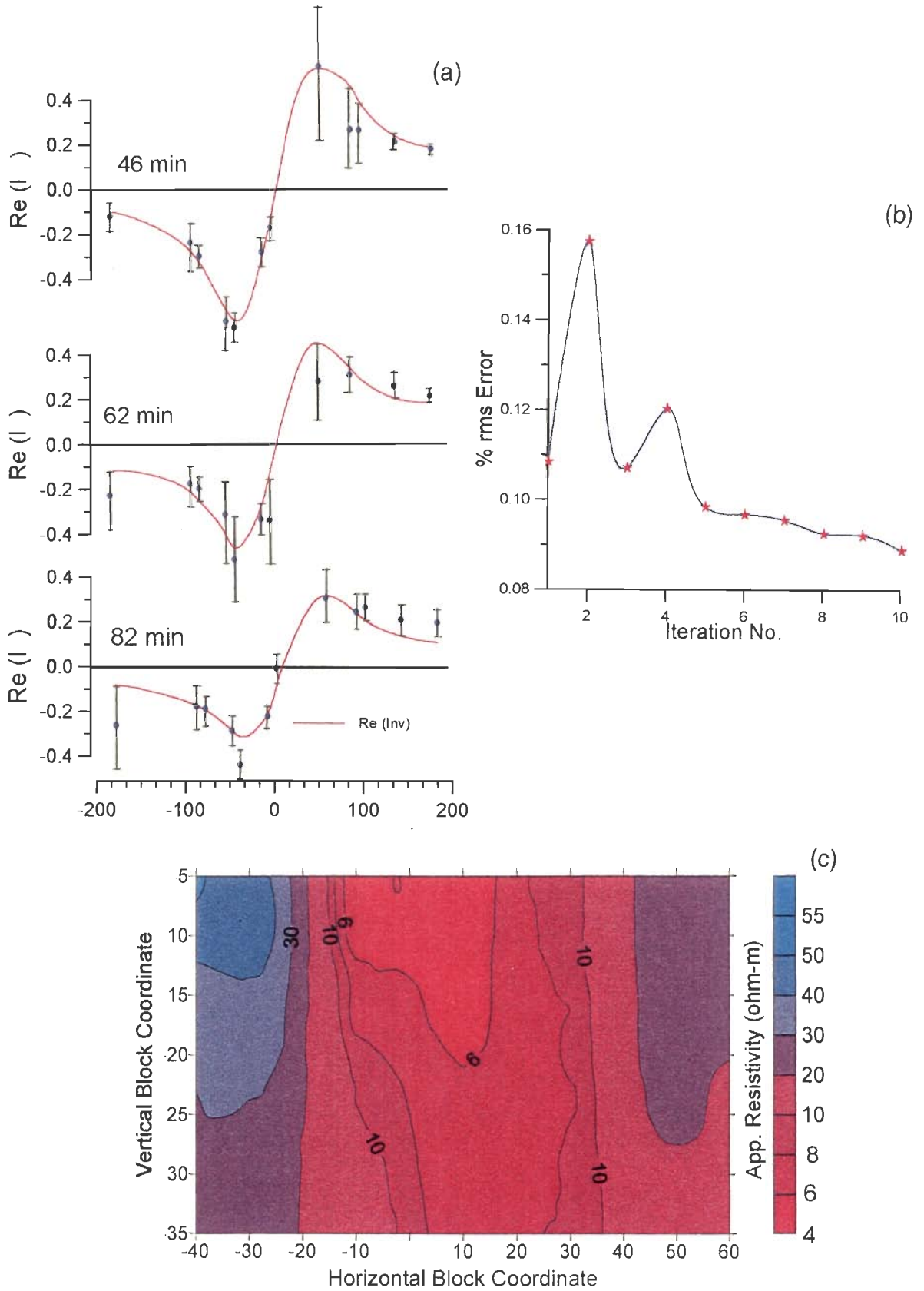


Fig. 7.9 (a) Comparison of real part of inverted GDS response of Trans Himalayan conductor model with the observations for three periods. (b) Convergence plot of % rms error of inversion. (c) The resistivity contours of the inverted model within the inversion domain.

final model, a 4 column one, has been obtained using data of sites -100.9, -14.6, -5.9 and 117.3 at seven periods 10.7, 21.3, 42.7, 85.3, 170.7, 341.3 and 682.7 s (Agarwal et al., 1993). For SIS, initially the apparent resistivity and phase of field data has been converted to impedance data and used for inversion. The regression parameter ϵ^2 is taken as 0.05 assuming 5% noise while the number of layers are assumed to be 100 with $\alpha = 0.2$. Since the NACP anomaly is conductive, the E-polarization gives better model than B-polarization. Hence, the 1-D inversion has been performed only for E-polarization. The pseudosection, constructed by assembling 1-D inversion results, is shown in Fig. 7.10a, whereas the model derived from it is displayed in Fig. 7.10b. The thickness (3 km) and the resistivity (3 ohm-m) of the Palaeozoic sedimentary layer at the surface are well resolved. The model is terminated at a fixed depth of 60 km by a uniform half-space. The inversion domain ranging from -113 to 118 km and 3 to 60 km in horizontal and vertical directions with resistivity 50 ohm-m, derived from the model shown in Fig. 7.10b, is used as the starting model for 2-D inversion carried out for the same locations and 5 periods, i.e. 21.3, 42.7, 85.3, 170.7 and 341.3 s. Fig. 7.11a exhibits the resistivity contours within the inversion domain of the final model. It shows that the low resistivity NACP anomaly is situated in the centre extending from 84 km left to 35 km right of the centre. Below 20 km, the lower crust to the left of anomaly is much more resistive than that to the right. A close scrutiny of Fig. 7.11a reveals that the resistivity range is too large to accommodate the finer details of the middle conductive structure. As a result the solution domain has been divided vertically into two parts to increase the resolution of the resistivity plot. The first part, which extends from 3 to 20 km, is shown in Fig. 7.11b. Since the resistive structure on the extreme right of the lower crust (Fig. 7.11a) is well resolved it is not included in the second part which extends from -84 to 118 km in horizontal and 20 to 60 km in vertical direction. The model obtained by us is similar to the one obtained by Agarwal et al. (1993) except that the resistivity values of the surrounding crust are very high in their case.

7.5 Closure

The inverted models obtained by **EM2INV**, under various categories, are in broad agreement with the true or published models. The critical analysis of inversion results of exercises discussed above reveals that 2-D inversion does improve the model estimate in comparison to the 1-D stacked model.

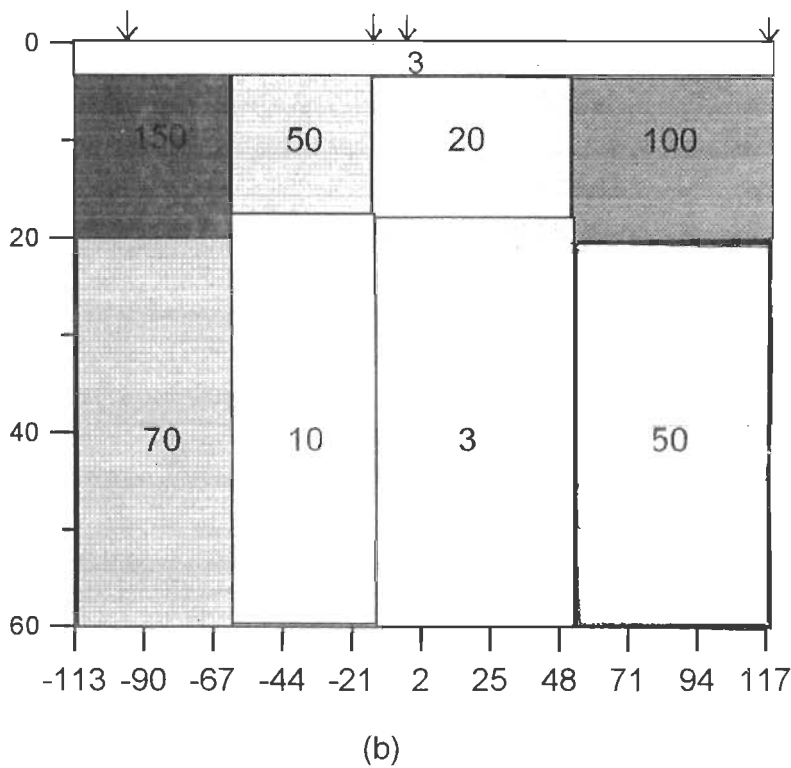
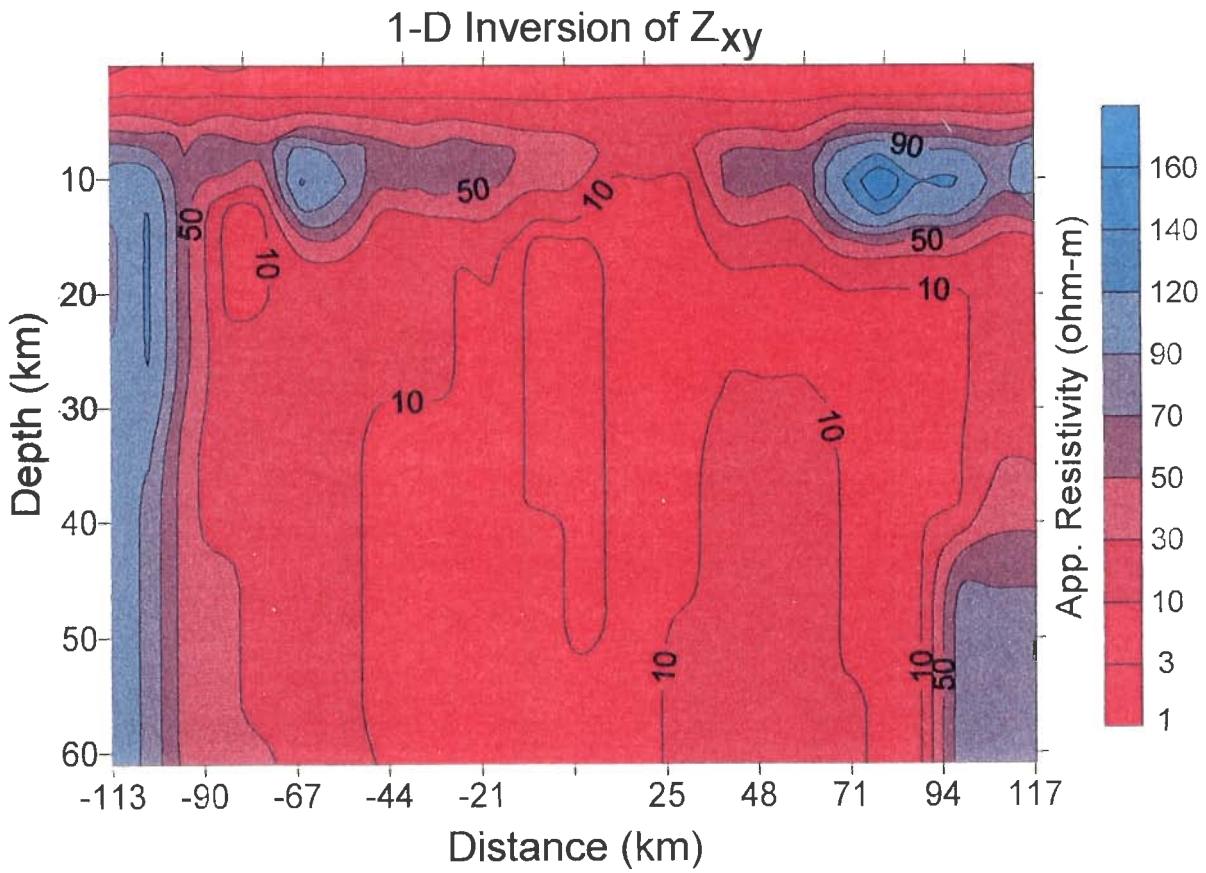


Fig. 7.10 (a) The pseudosection obtained from 1-D SIS inversions of the Z_{xy} responses at the 4 sites of the COPROD2R data. (b) The 2-D starting model, obtained from the pseudosection, the sites are indicated by the arrows.

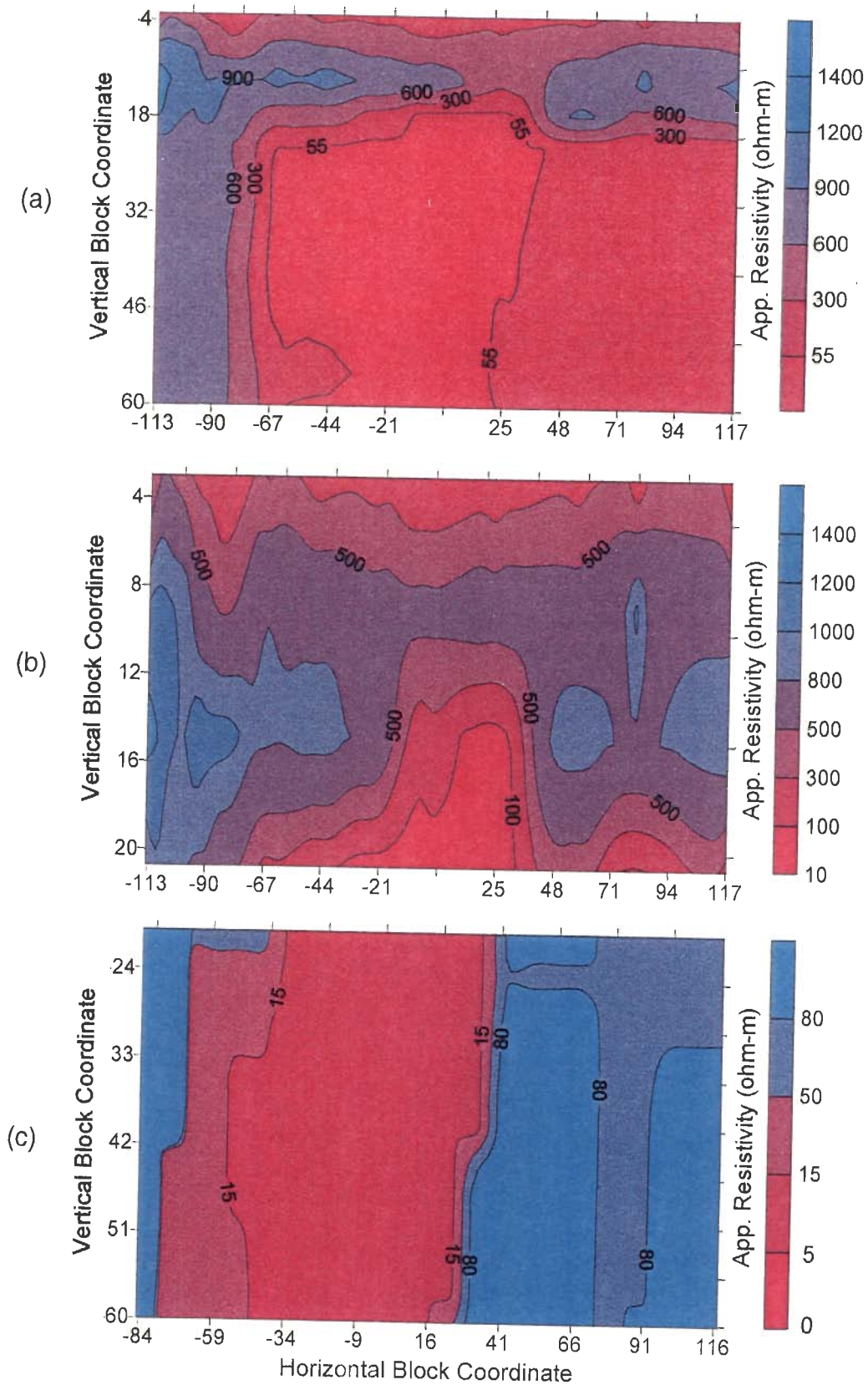


Fig. 7.11 Resistivity contours of Z_{xy} response within domain of inversion of the NACP model, obtained after 2-D inversion, for ; (a) complete inversion domain ranging from -113 to 118 km in horizontal and 3 to 60 km in vertical direction, (b) top portion of domain extending from 3 to 20 km in vertical direction and (c) a section of domain extending from -84 to 118 km in horizontal and 20 to 60 km in vertical direction.

CONCLUSIONS AND SUGGESTIONS

8.1 Concluding remarks

The algorithm **EM2INV**, developed in this thesis, is an efficient and reliable software package for inversion of 2-D geoelectromagnetic data. The algorithm has been as rigorously and comprehensively tested as was possible within the limited time frame of this study and available computing facility. All the studies conducted to investigate the efficacy of this algorithm yielded encouraging results. The comparison of the results of **EM2INV** with those obtained using other algorithms highlighted efficiency of the algorithm. This justified a qualified faith in the algorithm, **EM2INV**. However, there exists a scope for further studies on this algorithm. Primarily from results of design exercises and inversion studies using different types of data sets, the following conclusions have been drawn which are listed under achievements and limitations of the algorithm.

8.1.1 Achievements of the algorithm

The present study helps in setting up the guidelines for data procurement and enhances the inversion quality optimally as discussed below :

1. Choice of time periods, employed for observations, should not only be constrained by skin depth criterion but also by the spread of observation points, i.e. length of profile. If profile length is sufficiently large then increase in number of periods does not improve the inversion quality.
2. For a wide spectrum of frequencies even a single observation point on the profile contains significant information about inhomogeneity. 2-D inversion of such a data set does yield an approximate model.
3. The inversion of MT data provides better estimates of vertical variations in inhomogeneities, whereas GDS data deciphers the horizontal variations better.

4. The conductive and resistive bodies are better resolved by inversion of E- and B-polarization responses respectively.
5. The localization of vertical boundaries is better achieved by inversion of B-polarization data in comparison to E-polarization one which is good in demarcating the horizontal boundaries.
6. The inverted resistivity values are over estimated in B-polarization data, in comparison to that obtained in E-polarization data.
7. An initial guess model derived from 1-D stacked results substantially improves the inversion quality in comparison to the one using the guess model constructed on the basis of 2-D forward anomaly.

8.1.2 Limitations of the algorithm

The limitations of algorithm **EM2INV** identified during its testing are :

1. Since **EM2INV** is based on quasi-linearization, it has all the pitfalls of a quasi-linearized procedure, such as necessity of a close initial guess model and choice of a judicious convergence criterion.
2. Presently, the algorithm can be used only for a plane wave source, i.e. natural sources, however, its modular structure permits replacement of the present 1-D field computation routine by subroutines written for other sources.
3. Although the algorithm can handle large variations in horizontal direction, yet it is sensitive to the vertical extent of inversion domain.
4. In its present form, the algorithm is so programmed that it can have only one inversion domain with single resistivity. As a result the initial guess model sometimes is a gross approximation of true model. This can be modified in subsequent versions.

8.2 Suggestions for future work

The present thesis has turned out to be an exploratory effort during which a computer program **EM2INV** as been developed with an aim to enable quantitative interpretation of 2-D EM data. However, for better understanding of the complex nature of the EM inverse problem, detailed studies on certain aspects of the problem will be performed. There exists significant scope for further development, which may possibly be carried out on the following lines :

1. The displacement current term can be incorporated for extension of algorithm to shallow exploration geophysics problems.

2. Automatic grid generator should be refined to incorporate generation of staggered grid (Mackie et al., 1993; Weaver, 1994; Smith, 1996a, 1996b; Weaver et al., 1996).
3. Significant improvement in matrix equation solver routine is possible. It is suggested that the upcoming versions of conjugate gradient matrix solver (Sarkar et al., 1988; Ashby et al., 1990) should be tried.
4. The weighting matrices for error norm and solution norm computations should be designed for better noise models and for smooth/compact inversion.
5. Joint inversion of B- and E-polarization data can be performed for better resolution of a problem having resistive as well as conductive structure.
6. Frequency stepping can be used for upgradation of the algorithm to a time domain inversion algorithm.
7. For better understanding of the complex electromagnetic field variations the algorithm can be extended to a 3-D environment.
8. In order to reduce the high requirements of computer time and storage the possibility of pipelining and parallel processing approaches will have to be considered (Hjelt, 1989; MacDonald & Agarwal, 1994).

REFERENCES

- Adam, A., Vanyan, L.L., Varlamov, D.A., Yegorov, I.V., Shilovski, A.P. and Shilovski, P.P., 1982. Depth of crustal conducting layer and asthenosphere in the Pannonian Basin determined by magnetotelluric method. *Phys. Earth Planet. Int.*, **28**: 251-260.
- Agarwal, A.K., Poll, H.E. and Weaver, J.T., 1993. One- and two-dimensional inversion of magnetotelluric data in continental regions. *Phys. Earth Planet. Int.*, **81**: 155-176.
- Agarwal, A.K. and Weaver, J.T., 1993. Inversion of the COPROD2 data by a method of modelling. *J. Geomag. Geoelectr.*, **45**: 969-983.
- Aminzadeh, F., 1987. Pattern recognition and image processing. Geophysical Press, London, Vol. 20: 568 pp.
- Aprea, C., Booker, J.R. and Smith, J.T., 1990. Accurate finite difference approximations for discrete boundaries with arbitrary geometry. Unpublished poster presentation, 10th Workshop on EM induction in the Earth, Ensenada, Mexico.
- Arora, B.R., 1990. Magnetometer array studies in India: Present status, data interpretation and assessment of numerical modelling results. *Proc. Indian Acad. Sci.*, **99**: 693-716.
- Arora, B.R., 1993. Implications of electrical conductivity structures in the tectonic framework of northwest India. *Current Science*, **64**: 848-855.
- Arora, B.R. and Mahashabde, M.V., 1987. A transverse conductive structure in the northwest Himalaya. *Phys. Earth Planet. Int.*, **45**: 119-127.
- Arora, B.R. and Singh, B.P., 1992. Geomagnetic and geoelectric investigations for seismicity and seismotectonics of the Himalaya region. *Mem. Geol. Soc. India*, **23**: 223-263.
- Ashby, S.F., Manteuffel, T.A. and Saylor, P.E., 1990. A taxonomy for conjugate gradient methods. *SIAM. J. Numer. Anal.*, **27**: 1542-1568.
- Axxelson, O., 1980. Conjugate gradient type methods for unsymmetric and inconsistent system of linear equations. *Linear Algebra Appl.*, **29**: 1-16.

- Backus, G.E. and Gilbert, J.E., 1967. Numerical applications of a formalism for geophysical inverse problems. *Geophys. J. Roy. Astr. Soc.*, **13**: 247-276.
- Backus, G.E. and Gilbert, J.E., 1970. Uniqueness in the inversion of inaccurate gross earth data. *Phil. Trans. Roy. Soc. London*, **266**: 123-192.
- Bailey, R.C., 1970. Inversion of the geomagnetic induction problem. *Proc. Roy. Soc.*, **315**: 185-194.
- Bazinet, R. and Legault, J., 1985. Scalar audiomagnetotellurics: a tool in the evaluation of nuclear waste disposal sites. Expanded abstracts, Annual meeting of the Soc. Expl. Geophys., **55**: 149-150.
- Beamish, D. and Banks, R.J., 1983. Geomagnetic variation anomalies in northern England: processing and presentation of data from a non-simultaneous array. *Geophys. J. Roy. Astr. Soc.*, **75**: 513-539.
- Berdichevsky, M.N. and Zhdanov, M.S., 1984. Advanced theory of deep geomagnetic sounding. Elsevier, Amsterdam, 408 pp.
- Bernard, J., Vachette, C. and Valla, P., 1990. Deep groundwater survey with audio-magnetotelluric soundings. Expanded abstracts, Annual meeting of the Soc. Expl. Geophys., **60**: 528-531.
- Brewitt-Taylor, C.R. and Weaver, J.T., 1976. On the finite difference solution of two-dimensional induction problems. *Geophys. J. Roy. Astr. Soc.*, **47**: 375-396.
- Brown, C., 1994. Tectonic interpretation of regional conductivity anomalies. *Surv. Geophys.*, **15**: 123-157.
- Cagniard, L., 1953. Basic theory of the magnetotelluric method of geophysical prospecting. *Geophysics*, **18**: 605-635.
- Cantwell, T., 1960. Detection and analysis of low frequency magnetotelluric signal. Ph.D. Thesis, Dept. of Geol. and Geophysics, M.I.T., Cambridge, Mass.
- Chamalaun, F.M. and McKnight, J.D., 1993. A New Zealand wide magnetometer study. *J. Geomag. Geoelectr.*, **45**: 741-759.
- Chamalaun, F.H., Prasad, S.N., Lilley, F.E.M., Srivastava, B.J., Singh, B.P. and Arora, B.R., 1987. On the interpretation of the distinctive pattern of geomagnetic induction observed in northwest India. *Tectonophysics*, **140**: 247-255.
- Chave, A.D., 1990. Seafloor electromagnetic exploration methods in Gorga Ridge, a seafloor spreading centre in the United States exclusive economic zone. Edited by R. McMurray, Springer-Verlag, New York, 191-199.

- Chave, A.D. and Cox, C.S., 1983. Electromagnetic induction by ocean currents and the conductivity of the oceanic lithosphere. *J. Geomag. Geoelectr.*, **35**: 491-499.
- Chen, P.F. and Fung, P.C.W., 1989. A mesh convergence test for the finite difference method in three-dimensional electromagnetic modelling. *Chinese J. Geophys.*, **32**: 569-573.
- Chouteau, M., Krivochieva, S., Castillo, R.R., Gonzale Moran, T. and Jouanne V., 1994. Study of the Santa Clara aquifer system (Mexico Basin) using magnetotelluric soundings. *J. Appl. Geophys.*, **31**: 85-106.
- Christopherson, K.R., 1990. Applications of magnetotelluric to petroleum exploration in Papua New Guniea. Proc. of first PMG petroleum convention, Port Moresby, 63-71.
- Coggon, J.H., 1971. Electromagnetic and electrical modelling by the finite element method. *Geophysics*, **36**: 132-155.
- Constable, S.C., 1990. Marine electromagnetic induction studies. *Surv. Geophys.*, **11**: 303-327.
- Constable, S.C., Hoversten, M., Morrison, F. and Orange, A., 1994. Seafloor magnetotellurics for petroleum exploration (abstract). 3rd circular and proceedings of 12th Workshop on Electromagnetic induction in the Earth, Brest, France.
- Constable, S.C., Parker, R.L. and Constable, C.G., 1987. Occam's inversion: a practical algorithm for generating smooth models from EM sounding data. *Geophysics*, **52**: 289-300.
- deGroot-Hedlin, C.D. and Constable, S.C., 1990, Occam's inversion to generate smooth, two-dimensional models from magnetotelluric data: *Geophysics*, **55**: 1613-1624.
- Devijver, P.A. and Kittler, J.V., Eds., 1987. Pattern recognition theory and applications. Springer, Berlin.
- Dosso, S.E. and Oldenburg, D.W., 1991. Magnetic appraisal using simulated annealing. *Geophys. J. Int.*, **99**: 483-495.
- Doucet, D. and Pham Van Ngoc, 1984. Generalisation et optimisation de la methode des differences finies pour la modelisation en magnetotellurique. *Geophys. Prospect.*, **32**: 292-316.

- Duda, R.O. and Hart, P.E., 1973. Pattern classification and scene analysis. John Wiley and Sons, Inc., New York.
- EMSLAB, 1988. The EMSLAB electromagnetic sounding experiment. *Eos. Trans. AGU*, **69**: 89-99.
- EMSLAB, 1989. Special issue of *Journal of Geophysical Research* devoted to the EMSLAB experiment (14 papers). *J. Geophys. Res.*, **94**: 14093-14283.
- Engquist, B. and Majda, A., 1977. Absorbing boundary conditions for the numerical simulation of the waves. *Math. Comp.*, **31**: 629-651.
- ERCEUGT Group, 1992. An electrical resistivity crustal section from the Alps to the Baltic sea (central segment of the EGT). *Tectonophysics*, **207**: 123-139.
- Erdelyi, A., (Ed.), 1954. Tables of integral transforms. Vols. I and II, McGraw-Hill, New York.
- Ernst, T., Jankowski, J., Rozluski, C. and Teisseyre, R., 1993. Analysis of the electromagnetic field recorded in the Friuli seismic zone, Northeast Italy. *Tectonophysics*, **224**: 141-148.
- Fainberg, E.B., 1980. Electromagnetic induction in the world ocean. *Geophys. Surv.*, **4**: 157-172.
- Filloux, J.H., 1981. Magnetotelluric exploration of the north Pacific: progress report and preliminary soundings near a spreading ridge. *Phys. Earth Planet. Int.*, **25**: 187-195.
- Fischer, G., Schnegg, P.A., Peguiron, M. and Le Qquang, B.V., 1981. An analytic one-dimensional magnetotelluric inversion scheme. *Geophys. J. Roy. Astr. Soc.*, **67**: 257-278.
- Forsythe, G.E. and Wasow, W.R., 1964. Finite difference method for partial differential equations. Wiley, New York, 444 pp.
- Goldberg, D.E., 1989. Genetic algorithm in search, optimisation and machine learning. Addison-Wesley.
- Golub, G.H. and Van Loan, C.F., 1983. Matrix computations. John Hopkins Univ. Press.
- Gough, D.I., 1992. Electromagnetic exploration for fluids in the earth's crust. *Earth Sci. Rev.*, **323**: 3-28.
- Grant, F.S. and West, G.F., 1965. Interpretation theory in applied geophysics. McGraw-Hill Book Company, New York, 584 pp.
- Gupta, G., Gokaran, S. and Singh, B.P., 1993. High frequency magnetotelluric soundings between Mohand and Ramnagar in northwestern Himalaya. *J.*

- Himalayan. Geol., **4**: 271-278.
- Gupta, P.K., Niwas, S. and Gaur, V.K., 1996. Straightforward inversion scheme (SIS) for one dimensional magnetotelluric data. Proc. Indian Acad. Sci., December issue.
- Hadamard, J.V., 1932. Le probleme de cauchy et les equations aux dirives partielles linearies hyperboliques. Hermann, Paris.
- Heinson, G.S., White, A., Law, L.K., Hamano, Y., Utada, H., Yukutake, T., Segawa, J. and Toh, H., 1993. EMRIDGE: the electromagnetic investigations of the Juan de Fuca Ridge. Mar. Geophys. Res., **15**: 77-100.
- Hestenes, M.R. and Stiefel, E., 1952. Methods of conjugate gradients for solving linear systems. J. Res. Nat. Bureau Stand., **49**: 409-436.
- Hibbs, R.D. and Jones, F.W., 1976. The calculation of perturbation and induction arrows for a there-dimensional conductivity model and dipole source fields. PAGEOPH, **114**: 997-1008.
- Hildebrand, F.B., 1974. Introduction to numerical analysis, Tata-McGraw Hill, New Delhi, 669 pp.
- Hjelt, S.E., 1988. Regional electromagnetic studies in the 80's. Surv. Geophys., **9**: 349-387.
- Hjelt, S.E., 1989. Parallel processing and geophysical inversion (some abstract thoughts). Paper presented at the MOFTIG Meeting, Uppsala, Sweden, 11-13: 1989.
- Hjelt, S.E., 1992. Pragmatic inversion of geophysical data. Springer - Verlag, Berlin, 262 pp.
- Hjelt, S.E. and Korja, T., 1993. Lithospheric and upper mantle structure, results of electromagnetic soundings in Europe. Phys. Earth Planet. Int., **79**: 137-178.
- Hobbs, B.A., 1992. Terminology and symbols for use in studies of electromagnetic induction. Surv. Geophys., **13**: 489-515.
- Hohmann, G.W., 1971. Electromagnetic scattering by conductors in the earth near a line source of current. Geophysics, **36**: 101-131.
- Hohmann, G.W., 1975. Three-dimensional induced polarization and electromagnetic modelling. Geophysics, **40**: 309-324.
- Hohmann, G.W., 1987. Numerical models for electromagnetic methods of geophysics. In: Electromagnetic methods in applied geophysics, Vol. I, M.N. Nabighian (Ed.), Soc. Expl. Geophys., 313-364.

- Hohmann, G.W. and Raiche, A.P., 1988. Inversion of controlled source electromagnetic data. In: *Electromagnetic methods in applied geophysics*, Vol. I, M.N. Nabighian (Ed.), Soc. Expl. Geophys., 469-505.
- Honkura, Y., Niblett, E.R. and Kurtz, R.D., 1977. Preliminary study of the use of magnetotelluric fields for earthquake prediction. *Acta. Geod. Geophys. Montan.*, **12**: 33-36.
- Honkura, Y., Oshiman, N. and Matsushima, M., 1994. Monitoring of the changes in the electric and magnetic fields in a seismically active area in the Izu Peninsula, Japan (abstract). 3rd circular and proceedings of 12th Workshop on Electromagnetic induction in the Earth, Brest, France.
- Hoover, D.B., Long, C.L. and Senterfit, R.M., 1978. Some results from audiomagnetotelluric investigations in geothermal areas. *Geophysics*, **43**: 1501-1514.
- Hutton, R., 1976. Induction studies in the rifts and the other active region. *Acta. Geod. Geophys. Montan.*, **11**: 347-376.
- Ingham, M.R., 1994. A magnetotelluric and magnetovariational traverse across the New Zealand subduction zone. *Geophys. J.*, **92**: 495-504.
- Ingham, M., 1996. Magnetotelluric soundings across the South Island of New Zealand: electrical structure associated with the orogen of the Southern Alps, 1996. *Geophys. J. Int.*, **124**: 134-148.
- Jackson, D.D., 1972. Interpretation of inaccurate, insufficient and inconsistent data. *Geophys. J. Roy. Astr. Soc.*, **20**: 97-110.
- Jackson, D.D., 1979. The use of a priori data to resolve non-uniqueness in linear inversion. *Geophys. J. Roy. Astr. Soc.*, **57**: 137-157.
- Jackson, J.D., 1975. *Classical electrodynamics*. John Wiley and Sons, New York.
- Jacobs, D.A.H., 1981a. The exploitation of sparsity by iterative methods. In: *Sparse matrices and their uses*, Ian S. Duff (Ed.), Springer-Verlag, 191-221.
- Jacobs, D.A.H., 1981b. Preconditioned conjugate gradient algorithm for solving finite difference system. In: *Sparse matrices and their uses*. Ian S. Duff (Ed.), Springer-Verlag, 509-535.
- Jacobs, D.A.H., 1986. A generalization of the conjugate gradient method to solve complex system. *IMA. J. Numer. Anal.*, **6**: 447-452.
- Jennings, A., 1977. Influence of eigenvalue spectrum on the convergence rate of the conjugate gradient method. *J. Inst. Math. Its Appl.*, **20**: 61-72.
- Jiracek, G.R., Curtis, J.H., Ramirez, J., Martinez, M. and Romo, J., 1989. Two-

- dimensional magnetotelluric inversion of the EMSLAB Lincoln line. *J. Geophys. Res.*, **94**: 14145-14152.
- Jones, A.G., 1988. Static-shift of magnetotelluric data and its removal in a sedimentary basin environment. *Geophysics*, **53**: 967-978.
- Jones, A.G., 1993. Electromagnetic images of modern and ancient subduction zones. *Tectonophysics*, **219**: 29-46.
- Jones, A.G. and Craven, J.A., 1990. The North American Central Plains conductivity anomaly and its correlation with gravity, magnetic, seismic and heat flow data in Saskatchewan, Canada. *Phys. Earth Planet. Int.*, **63**: 169-194.
- Jones, A.G. and Dumas, A., 1993. Electromagnetic image of a volcanic zone. *Phys. Earth Planet. Int.*, **81**: 289-314.
- Jones, A.G. and Haak, V., (Eds.) 1993. The VRS Hutton Symposium: EM studies in the continents. *Phys. Earth Planet. Int.*, **81**: 1-325.
- Jones, A.G. and Hutton, V.R.S., 1979. A multi-station magnetotelluric study in southern Scotland-II. Monte-carlo inversion of the data and its geophysical and tectonic implications. *Geophys. J. Roy. Astr. Soc.*, **56**: 351-368.
- Jones, F.W., 1974. The perturbations of geomagnetic fields by two-dimensional and three-dimensional conductivity inhomogeneities. *PAGEOPH*, **112**: 793-800.
- Jones, F.W. and Pascoe, L.J., 1971. A general computer program to determine the perturbation of alternating electric currents in a two-dimensional model of a region of uniform conductivity with an embedded inhomogeneity. *Geophys. J. Roy. Astr. Soc.*, **24**: 3-30.
- Jones, F.W. and Pascoe, L.J., 1972. The perturbation of alternating geomagnetic fields by three-dimensional conductivity inhomogeneities. *Geophys. J. Roy. Astr. Soc.*, **27**: 479-485.
- Jones, F.W. and Price, A.T., 1970. The perturbation of alternating geomagnetic fields by conductivity anomalies. *Geophys. J. Roy. Astr. Soc.*, **20**: 317-334.
- Jones, F.W. and Price, A.T., 1971. Geomagnetic effects of sloping and shelving discontinuities of earth conductivity. *Geophysics*, **36**: 58-66.
- Jones, F.W. and Thomson, D.J., 1974. A discussion of the finite difference method in computer modeling of electrical conductivity structures. A reply to the discussion by Williamson, Hewlett and Tammemagi. *Geophys. J. Roy. Astr. Soc.*, **37**: 537-544.
- Jupp, D.L.B. and Vozoff, K., 1977. Two dimensional magnetotelluric inversion. *Geophys. J. Roy. Astr. Soc.*, **50**: 333-352.

References

- Kaufman, A.A. and Keller, G.V., 1981. The magnetotelluric sounding method. Elsevier, Amsterdam, 594 pp.
- Kaufman, A.A. and Keller, G.V., 1983. Frequency and transient soundings. Elsevier, Amsterdam, 685 pp.
- Keller, G.V. and Frischknecht, F.C., 1966. Electrical method of geophysical prospecting. Pergamon Press, New York, 519 pp.
- Kershaw, D.S., 1978. The incomplete Cholesky-conjugate gradient method for the iterative solution of systems of linear equations. *J. Comput. Phys.*, **26**: 43-65.
- Koziar, A. and Strangway, D.W., 1978. Permafrost mapping by audiofrequency magnetotellurics. *Can. J. Earth Sci.*, **15**: 1539-1546.
- Kuvshinov, A.V., Pankratov, O.V. and Singer, B.Sh., 1990. The effect of the oceans and sedimentary cover on global magnetovariational field distribution. *PAGEOPH*, **134**: 533-540.
- Kunetz, G., 1972. Processing and interpretation of magnetotelluric soundings. *Geophysics*, **37**: 1005-1021.
- Kurtz, R.D., Delaurier, J.M. and Gupta, J.C., 1986. A magnetotelluric study across Vancouver island detects the subducting Juan de Fuca plate. *Nature*, **321**: 596-599.
- Lakanen, 1986. Scalar audiomagnetotelluric applied to base metal exploration in Finland. *Geophysics*, **51**: 1628-1646.
- Lawson, C.L. and Hanson, D.J., 1974. Solving least squares problem. Prentice Hall, Englewood Cliffs, New Jersey.
- Lee, K.H., Pridmore, D.F. and Morrison, H.F., 1981. A hybrid three-dimensional electromagnetic modelling scheme. *Geophysics*, **46**: 796-805.
- Lilley, F.E.M., 1993. Electromagnetic induction studies on the ocean floor, geophysics down under. *Newsletter*, **17**: Geol. Soc. of Australia: 14-20.
- Lilley, F.E.M., Singh, B.P., Arora, B.R., Srivastava, B.J., Prasad, S.N. and Sloane, M.N., 1981. A magnetotelluric array study in northwest India. *Phys. Earth Planet. Int.*, **25**: 232-240.
- Lines, L.R. and Jones, F.W., 1973a. The perturbation of alternating geomagnetic fields by an island near a coastline. *Can. J. Earth Sci.*, **10**: 510-518.
- Lines, L.R. and Jones, F.W., 1973b. The perturbation of alternating geomagnetic fields by three dimensional island structures. *Geophys. J. Roy. Astr. Soc.*, **32**: 133-154.

References

- Livelybrooks, D., 1993. Program 3D feem: a multidimensional electromagnetic finite element model. *Geophys. J. Int.*, **114**: 443-458.
- Livelybrooks, D., Mareschal, M., Blais, E. and Smith, J.T., 1996. Magnetotelluric delineation of the Trillabelle massive sulfide body in Sudbury, Ontario. *Geophysics*, **61**: 971- 986.
- Loewenthal, D., 1975. Theoretical uniqueness of the magnetotelluric inverse problem for equal penetration discretizable models. *Geophys. J. Roy. Astr. Soc.*, **43**: 897-903.
- MacDonald, K.J. and Agarwal, A.K., 1994. Two and three dimensional induction modelling on massively parallel supercomputers (abstract). 3rd circular and proceedings of 12th workshop on electromagnetic induction in the earth, Brest, France.
- Mackie, R.L., Bennett, B.R. and Madden, T.R., 1988. Long-period magnetotelluric measurements near the central California coast: a land locked view of the conductivity structure under the Pacific Ocean. *Geophys. J.*, **95**: 181-194.
- Mackie, R.L. and Madden, T.R., 1993a. Conjugate direction relaxation solutions for 3-D magnetotelluric modeling. *Geophysics*, **58**: 1052-1057.
- Mackie, R.L., and Madden, T.R., 1993b. Three-dimensional magnetotelluric inversion using conjugate gradients. *Geophys. J. Int.*, **115**: 215-229.
- Mackie, R.L., Madden, T.R. and Wannamaker, P.E., 1993. Three-dimensional magnetotelluric modeling using difference equations- Theory and comparisons to integral equation solutions. *Geophysics*, **58**: 215-226.
- Mackie, R.L., Smith, J.T. and Madden T.R., 1994. Three-dimensional electromagnetic modeling using finite difference equations: The magnetotelluric example. *Radio Science*, **29**: 923-935.
- Madden, T.R. and Mackie, R.L., 1989. Three-dimensional magnetotelluric modeling and inversion. *Proc. IEEE*, **77**: 318-333.
- Madden, T.R. and Swift, C.M., 1969. Magnetotelluric studies of the electrical conductivity structure of the crust and upper mantle. In: *The earth's crust and upper mantle*, P.J. Hart (Ed.), A.G.U. Monograph, **13**: 469-479.
- Madden, T.R. and Thompson, 1965. Low frequency electromagnetic oscillations of the earth ionosphere cavity. *Rev. Geophys.*, **3**: 211.
- Marquardt, D.W., 1970. Generalized inverses, ridge regression, biased linear estimation, and nonlinear estimation. *Technometrics*, **12**: 591-612.
- McCormick, S.F., (Ed.), 1987. *Multigrid methods*. Soc. Ind. Appl. Math.

References

- McNeill, J.D., 1990. Use of electromagnetic methods for groundwater studies. In: Geotechnical and Environmental geophysics, Review and Tutorial, S.H. Ward (Ed.), Soc. Expl. Geophys., **1**: 191-218.
- Meijerink, J.A. and van der Vorst, H.A., 1977. An iterative solution method for linear systems of which the coefficient matrix is a symmetric M-matrix. Math. Comp., **31**: 148-162.
- Meju, M.A., 1994. Geophysical data analysis: Understanding inverse problem theory and practice. Soc. Expl. Geophys., Course Notes Series, Vol. 6, 296 pp.
- Menke, W., 1984. Geophysical data analysis: Discrete inverse theory. Academic Press, Inc., Orlando, 260 pp.
- Miller, E.K., 1988. A selective survey of computational electromagnetics. IEEE. Trans. Antenn. Propag. **36**: 1281-1305.
- Mitchell, A.R. and Griffiths, D.F., 1980. The finite difference method in partial differential equations. Wiley.
- Mitra, R., 1973. Computer techniques for electromagnetics. Pergamon, New York.
- Mitra, R., 1975. Numerical and asymptotic techniques in electromagnetics. Springer-Verlag, New York.
- Mogi, T., 1996. Three-dimensional modeling of magnetotelluric data using finite element method. J. App. Geophys., **35**: 185-189.
- Morgan, M.A., (Ed.), 1990. Finite element and finite difference methods in electromagnetic scattering. Elsevier, New York.
- Morse, P.M. and Feshbach, H., 1953. Methods of theoretical physics. McGraw-Hill Book Co., Inc., Tokyo.
- Nabighian, M.N., (Ed.), 1988. Electromagnetic methods in applied geophysics, Vol. I, Theory. Soc. Expl. Geophys., 528 pp.
- Nabighian, M.N., (Ed.), 1991. Electromagnetic methods in applied geophysics, Vol. II, Applications. Soc. Expl. Geophys., 992 pp.
- Nong, Wr., Booker, J.R. and Smith, J.T., 1993. Rapid two-dimensional inversion of COPROD2 data. J. Geomag. Geoelectr., **45**: 1073-1087.
- Oldenburg, D.W., 1979. One dimensional inversion of natural source magnetotelluric observations. Geophysics, **44**: 1218-1244.
- Oldenburg, D.W., 1984. An introduction to linear inverse theory. IEEE Trans. Geosc. and Remote Sensing, **GE-22**: 665-674.
- Oldenburg, D.W., 1990. Inversion of electromagnetic data: An overview of new

- techniques. *Geophys. Surv.*, **11**: 231-270.
- Oldenburg, D.W. and Ellis, R.G., 1993. Efficient inversion of magnetotelluric data in two dimensions. *Phys. Earth Planet. Int.*, **81**: 177-200.
- Oldenburg, D.W., 1994. Practical strategies for the solution of large scale electromagnetic inverse problems. *Radio Science*, **29**: 1081-1099.
- Orange, A.S., 1989. Magnetotelluric exploration for hydrocarbons. *Proc. IEEE*, **77**: 287-316.
- Palaz, I., 1986. Artificial intelligence: Expert systems for exploration. *Geophysics: The leading edge of exploration*, **5**: 60-64.
- Palshin, N.A., 1988. Deep sea floor magnetotelluric soundings in northeastern Pacific (in Russian). *Tikhookeanskaya geologia*, **6**: 95-99.
- Palshin, N.A., 1994. Oceanic electromagnetic studies: a review. Review paper. 3rd circular and proceedings of 12th Workshop on Electromagnetic induction in the Earth, Brest, France: 159-177.
- Park, S.K., 1994. Precursors to earthquakes: Seismoelectromagnetic signals. Review paper. 3rd circular and proceedings of 12th Workshop on Electromagnetic induction in the Earth, Brest, France: 179-190.
- Park, S.K., Johnston, M.J.S., Madden, T.R., Morgan, F.D. and Morrison, H.F., 1993. Electromagnetic precursors to earthquakes in ULF band: a review of observations and mechanisms. *Rev. Geophys.*, **31**: 117-132.
- Park, S.K., Orange, A.S. and Madden, T.R., 1983. Effects of three-dimensional structure on magnetotelluric sounding curves. *Geophysics*, **48**: 1402-1405.
- Parker, R.L., 1977. Understanding inverse theory. *Annu. Rev. Earth Planet. Sci.*, **5**: 35-64.
- Parker, R.L., 1980. The inverse problem of electromagnetic induction: Existence and construction of solutions based upon incomplete data. *J. Geophys. Res.*, **85**: 4421-4428.
- Parker, R.L., 1983. The magnetotelluric inverse problem. *Geophys. Surv.*, **6**: 5-25.
- Parker, R.L. and Whaler, K.A., 1981. Numerical methods for establishing solutions to the inverse problem of electromagnetic induction. *J. Geophys. Res.*, **86**: 9574-9584.
- Parrot, M. and Johnston, M.J.S. (Eds.), 1993. Seismoelectromagnetic effects. *Phys. Earth Planet. Int.*, **75**: 1-315.

References

- Pascoe, L.J. and Jones, F.W., 1972. Boundary conditions and calculations of surface values for the general two-dimensional electromagnetic induction problem. *Geophys. J. Roy. Astr. Soc.*, **27**: 179-193.
- Patra, H.P. and Mallick, K., 1980. *Geosounding principles, 2: Time-varying geoelectric soundings*. Elsevier, Amsterdam, 419 pp.
- Patrick, F.W. and Bostick, F.X. Jr., 1969. *Magnetotelluric modelling technique*. Rep. 59, Elec. Geophys. Res. Lab., University of Texas, Austin.
- Pedersen, J. and Hermance, J.F., 1986. Least square inversion of one dimensional magnetotelluric data: An assessment of procedures employed by Brown University. *Surv. Geophys.*, **8**: 187-231.
- Peebles, W. and Rankin, D., 1973. A magnetotelluric study in the Western Canadian sedimentary basin. *PAGEOPH*, **102**: 134-147.
- Pek, J., 1985. Linearization methods of interpreting magnetotelluric and magnetic variation data. *Travaux Inst. Geophys. Acad. Tcheosl. Sci.*, No. **609**: 199-326.
- Pellerin, L., Johnston, J.M. and Hohmann, G.W., 1996. A numerical evaluation of electromagnetic methods in geothermal exploration. *Geophysics*, **61**: 121-130.
- Porstendorfer, G., 1975. *Principles of magnetotelluric prospecting*. Borntraeger, Berlin.
- Poulton, M.W., Sternberg, B.K. and Glass, C.E., 1992. Neural network pattern recognition of subsurface images. *J. App. Geophys.*, **29**: 21-36.
- Prelat, A.E., 1977. Discriminant analysis as a method of predicting mineral occurrence potentials in Central Norway. *Math. Geol.*, **9**: 341-367.
- Raiche, A.P., 1974. An integral equation approach to three-dimensional modeling. *Geophys. J. Roy. Astr. Soc.*, **36**: 363-376.
- Raiche, A., 1991. A pattern recognition approach to geophysical inversion using neural nets. *Geophys. J. Int.*, **105**: 629-648.
- Rao, C.R. and Mitra, S.K., 1971. *Generalized inverse of matrices and its applications*. Wiley, New York.
- Rao, K.P., Saraf, P.D. and Mallick, K., 1996. Magnetotelluric modelling of the cretaceous sedimentary formation in Krishna-Godavari Basin. *Jour. Assoc. Expl. Geophys., India*, **27**: 1-10.
- Rastogi, A., Gupta, P.K. and Niwas, S., 1994. Inversion of two-dimensional EM data using finite difference method. Unpublished poster presentation. 3rd circular and proceedings of 12th Workshop on Electromagnetic induction in the Earth, Brest, France.

- Rastogi, A., Gupta, P.K. and Niwas, S., 1997. Multigrid inversion of two-dimensional EM data using bi-conjugate gradient method. *Jour. Assoc. Expl. Geophys., India*, January issue.
- Reddy, C.D. and Arora, B.R., 1993. Quantitative interpretation of geomagnetic induction response across the thrust zones of the Himalaya along the Ganga-Yamuna Valley. *J. Geomag. Geoelectr.*, **45**, 775-785.
- Reddy, I.K. and Rankin, D., 1972. On the interpretation of magnetotelluric data in the plains of Alberta. *Can. J. Earth Sci.*, **9**: 514-527.
- Reddy, I.K. and Rankin, D., 1973. Magnetotelluric response of a two-dimensional sloping contact by finite element method. *Pure Appl. Geophys.*, **105**: 847-857.
- Reddy, I.K., Rankin, D. and Phillips, R.J., 1977. Three-dimensional modelling in magnetotelluric and magnetic variational sounding. *Geophys. J. Roy. Astr. Soc.*, **51**: 313-325.
- Reid, J.K., 1971. On the method of conjugate gradients for the solution of large sparse systems of equations. In: *Proceedings of the conference on large sparse sets of linear equations*, J.K. Reid (Ed.), Academic Press, 231-254.
- Rikitake, T., 1961. Sq and ocean. *J. Geophys. Res.*, **66**: 3245-3254.
- Rikitake, T., 1966. *Electromagnetism and the earth's interior*. Elsevier, Amsterdam, 308 pp.
- Rikitake, T., 1976. *Earthquake predictions*. Elsevier, Amsterdam, 357 pp.
- Ripley, B.D., 1996. *Pattern recognition and neural networks*. Cambridge Univ. Press, Cambridge, 403 pp.
- Rodi, W.L., Swanger, H.J. and Minster, J.B., 1984. ESP/MT: An interactive system for two-dimensional magnetotelluric interpretation (abstract). *Geophysics*, **46**: 611.
- Rokityansky, I.I., 1982. *Goelectromagnetic investigations of the earth's crust and mantle*. Springer-Verlag, Berlin, 381 pp.
- Roy, K.K., Rao, C.K. and Chattopadhyay, A., 1989. Magnetotelluric survey across Singhbhum granite batholith. *Proc. Indian Acad. Sci.*, **98**: 147-165.
- Rozluski, C.P. and Yukutake, T., 1993. Preliminary analysis of magnetotelluric and seismic activity in the Chubu district, Japan. *Acta. Geophys. Polonica*, **41**: 17-26.
- Sabatier, P.C., 1974. Remarks on approximation methods in geophysical inverse problem. *Proc. Roy. Soc. London, Ser A* **337**: 49-71.

References

- Sarkar, T.K., (Ed.), 1991. Application of conjugate gradient method to electromagnetic and signal analysis. Elsevier Science Publ. Co., Inc.
- Sarkar, T. K., Siarkiewicz, K. R. and Stratton, R. F., 1981a. Survey of numerical methods for solution of large system of linear equations for electromagnetic field problems, *IEEE Trans. Antennas Propagat.* **AP-29**: 847-856.
- Sarkar, T.K., Weiner, D.D. and Jain, V.K., 1981b. Some mathematical considerations in dealing with the inverse problem. *IEEE Trans. Antennas Propagat.*, **AP-29**: 373-379.
- Sarkar, T.K., Yang, X. and Arvas, E., 1988. A limited survey of various conjugate gradient methods for solving complex matrix equations arising in electromagnetic wave interactions. *Wave Motion*, **10**: 527-546.
- Sasaki, Y., 1989. Two-dimensional joint inversion of magnetotelluric and dipole-dipole resistivity data, *Geophysics*, **50**: 254-262.
- Schmucker, U., 1970. Anomalies of geomagnetic variations in the Southwestern United States. *Bull. Scripps Inst. Oceanogr.*, **13**: 1-165.
- Schultz, A., Everett, M.E., Pritchard, G. and Smith, J.T., 1994. Nonlinear optimisation strategies in electromagnetic inversion (abstract). 3rd circular and proceedings of 12th Workshop on Electromagnetic induction in the Earth, Brest, France.
- Singh, B.P., 1980. Geomagnetic sounding of conductivity anomalies in the lower crust and upper most mantle. *Geophys. Surv.*, **4**: 71-87.
- Singh, R.P. and Pedersen, L.B., 1988. A transverse conductive structure in the northwest Himalaya by BR Arora and MV Mahashabde. *Phys. Earth Planet. Int.*, **53**: 177-179.
- Singh, R.P., Kant, Y. and Rastogi, A., 1992. Magnetotelluric soundings in Indo-Gangetic plains and Himalayan foothills region. *Indian. J. Pet. Geol.*, **1**: 258-271.
- Smith, J.T., 1996a. Conservative modeling of 3-D electromagnetic fields, Part I: Properties and error analysis. *Geophysics*, **61**: 1308-1318.
- Smith, J.T., 1996b. Conservative modeling of 3-D electromagnetic fields, Part II: Biconjugate gradient solution and an accelerator. *Geophysics*, **61**: 1319-1324.
- Smith, J.T. and Booker, J.R., 1991. Rapid inversion of two- and three-dimensional magnetotelluric data. *J. Geophys. Res.*, **96**: 3905-3922.
- Smythe, W.R., 1950. Static and dynamic electricity. McGraw-Hill Book Co., Inc., Tokyo, 616 pp.
- Stanley, W.D., 1984. Tectonic study of Cascade range and Columbia Plateau in

- Washington State based upon magnetotelluric sounding. *J. Geophys. Res.*, **89**: 4447-4460.
- Stanley, W.D., Saad, A.R. and Ohofugi, W., 1985. Regional magnetotelluric surveys in hydrocarbon exploration, Parana basin, Brazil. *AAPG Bull.*, **69**: 346-360.
- Stearns, S.D. and David, R.A., 1988. Signal processing algorithms. Prentice Hall, Inc., Englewood Cliffs, New Jersey.
- Strangway, D.W., Swift, C.M. Jr. and Holmar, R.C., 1973. The application of audiofrequency magnetotelluric (AMT) to mineral exploration. *Geophysics*, **38**: 1159-1175.
- Stratton, J.A., 1941. Electromagnetic theory. McGraw-Hill Book Co., Inc., Tokyo.
- Swift, C.M. Jr., 1967. A magnetotelluric investigation of an electrical conductivity anomaly in the southwestern United States, Ph.D Dissertation, Geophysics Laboratory, M.I.T., Cambridge.
- Taflove, A., 1995. Computational electrodynamics: The finite-differentiation time-domain method. Artech House, Inc., Norwood, 599 pp.
- Takeda, M., 1991. Electric currents in the ocean induced by the geomagnetic Sq field and their effect on the estimation of mantle conductivity. *Geophys. J. Int.*, **104**: 381-385.
- Tarantola, A., 1987. Inverse problem theory: Methods for data fitting and model parameter estimation. Elsevier Science Publishers, 613 pp.
- Tarits, P., 1992. Electromagnetic studies of global geodynamic processes. Review papers of 11th Workshop on Electromagnetic induction in the Earth, Wellington, New Zealand, 1-23.
- Tikhonov, A.N., 1950. On investigation of electrical characteristics of deep strata of Earth's crust (in Russian). *Dokl. Acad. Nauk USSR*, **73**: 295-297.
- Tikhonov, A.N. and Arsenin, V.Y., 1977. Solution of ill-posed problems. V.H. Winston and Sons, 258 pp.
- Ting, S.C. and Hohmann, G.W., 1981. Integral equation modelling of three-dimensional magnetotelluric response. *Geophysics*, **46**: 182-197.
- Travis, B.J. and Chave A.D., 1989. A moving finite element method for magnetotelluric modelling. *Phys. Earth Planet. Int.*, **53**: 432-443.
- Treitel, S., Lines, L.R. and Ruckgaber, G., 1993. Geophysical inversion and applications. *Soc. Expl. Geophys.*, 142 pp.
- Twomey, S., 1977. Introduction to the mathematics of inversion in remote sensing and

indirect measurements. *Developments in Geomathematics 3*, Elsevier Scientific Publishing Company, Amsterdam.

- Vanyan, L.L. and Palshin, N.A., 1990. Near-shore effects in T-soundings (in Russian). *Izvestiya Akademii nauk USSR, Seriya Fizika Zemli*, **4**: 83-89.
- Vozoff, K., 1972. The magnetotelluric method in the exploration of sedimentary basins. *Geophysics*, **37**: 98-141.
- Vozoff, K., 1990. Magnetotellurics: Principles and practices. *Proc. Indian Acad. Sci.*, **99**: 441-471.
- Vozoff, K., 1991. The magnetotelluric method. In: *Electromagnetic methods in applied geophysics*, Vol.2, M.N. Nabighian (Ed.), Soc. Expl. Geophys., 641-671.
- Vozoff, K., Holcomb, H.L. and Holliday, J., 1982. Audio frequency magnetotellurics - a deep electromagnetic method for groundwater evaluation. Australian Water Resources Council, Technical paper, Research project 78/97, Australian Government Publishing Service.
- Wait, J.R., 1982. *Geo-Electromagnetism*. Academic Press Inc., New York.
- Wannamaker, P.E., 1991. Advances in three-dimensional magnetotelluric modeling using integral equations. *Geophysics*, **56**: 1716-1728.
- Wannamaker, P.E., Hohmann, G.W. and San Filippo W.A., 1984a. Electromagnetic modeling of three-dimensional bodies in layered earths using integral equations. *Geophysics*, **49**: 60-74.
- Wannamaker, P.E., Hohmann, G.W. and Ward, S.H., 1984b. Magnetotelluric responses of three-dimensional bodies in layered earths. *Geophysics*, **49**: 1517-1533.
- Wannamaker, P.E., Stodt, J.A. and Rijo, L., 1987. A stable finite element for two-dimensional magnetotelluric modelling. *Geophys. J. Roy. Astr. Soc.*, **88**: 277-296.
- Wannamaker, P.E., Booker, J.R., Filloux, J.H., Jones, A.G., Jiracek, G.R., Chave, A.D., Tarits, P., Waff, H.S., Egbert, G.D., Young, C.T., Stodt, J.A., Martinez, M., Law, L.K., Yukutake, T., Segawa, J.S., White, A. and Green, A.W. Jr., 1989a. Magnetotelluric observations across the Juan de Fuca subduction system in the EMSLAB project. *J. Geophys. Res.*, **94**: 14111-14126.
- Wannamaker, P.E., Booker, J.R., Jones, A.G., Chave, A.D., Filloux, J.H., Waff, H.S. and Law, L.K., 1989b. Resistivity cross section through the Juan de Fuca subduction system and its tectonic implications. *J. Geophys. Res.*, **94**: 14127-14144.
- Ward, S.H., 1967. Electromagnetic theory for geophysical application. In: *Mining*

References

- Geophysics, Vol. II, Chap II, Part A, Soc. Expl. Geophys., Tulsa, Oklahoma, 10-196.
- Ward, S.H. and Fraser, D.C., 1967. Electromagnetic theory for geophysical application. In: Mining Geophysics, Vol. II, Chap II, Part B, Soc. Expl. Geophys., Tulsa, Oklahoma.
- Ward, S.H. and Hohmann, G.H., 1988. Electromagnetic theory for geophysical application. In: Electromagnetic methods in applied geophysics, Vol. 1, M.N. Nabighian (Ed.), Soc. Expl. Geophys., 131-311.
- Weaver, J.T., 1994. Mathematical methods for geo-electromagnetic induction. Research Studies Press, Taunton, 316 pp.
- Weaver, J.T., 1995. Personal Communication.
- Weaver, J.T. and Agarwal, A.K., 1993. Automatic one-dimensional inversion of magnetotelluric data by the method of modelling. *Geophys. J. Int.*, **112**: 115-123.
- Weaver, J.T. and Brewitt-Taylor, C.R. 1978. Improved boundary condition for the numerical solution of E-polarization problems in geomagnetic induction. *Geophys. J. Roy. Astr. Soc.*, **54**: 309-317.
- Weaver, J.T., Pu, X.H. and Agarwal, A.K., 1996. Improved methods for solving for the magnetic field in E-polarization induction problems with fixed and staggered grids. *Geophys. J. Int.*, **126**: 437-446.
- Weidelt, P., 1972. The inverse problem of geomagnetic induction. *Zeit. fur Geophysik*, **38**: 257-289.
- Weidelt, P., 1975a. Electromagnetic induction in three-dimensional structures. *J. Geophys.*, **41**: 85-109.
- Weidelt, P., 1975b, Inversion of two-dimensional conductivity structures. *Phys. Earth Planet. Int.*, **10**: 282-291.
- Whittall, K.P., 1986. Inversion of magnetotelluric data using localized conductivity constraints. *Geophysics*, **51**: 1603-1607.
- Whittall, K.P. and Oldenburg, D.W., 1992. Inversion of magnetotelluric data for a one-dimensional conductivity. *Geophysics Monograph series*, No. 5, D.V. Fitterman (Ed.), Soc. Expl. Geophys., Tulsa, Oklahoma.
- Williamson, K., Hewlett, C. and Tammemagi, H.Y., 1974. Computer modelling of electrical conductivity structures. *Geophys. J. Roy. Astr. Soc.*, **37**: 533-536.
- Wright, J.A., 1970. Anisotropic apparent resistivities arising from two-dimensional structures. *Can. J. Earth Sci.*, **7**: 527-531.

References

- Wright, P.M., Ward, S.H., Ross, H.P. and West, R.C., 1985. State of art geophysical exploration for geothermal resources. *Geophysics*, **50**: 2666-2696.
- Xinghua, P., Agarwal, A.K. and Weaver, J.T., 1991. A theoretical investigation of anisotropic geoelectric structures using three-dimensional models. XX General assembly, IUGG, Vienna, Austria, IAGA Program and Abstracts, paper GAM 1.6.
- Xiong, Z., 1992. Symmetry properties of the scattering matrix in 3-D electromagnetic modelling using integral equation method. *Geophysics*, **57**: 1199-1201.
- Yamane, K., Takasugi, S. and Lee, K.H., 1996. A new magnetotelluric inversion scheme using generalized RRI. *J. App. Geophys.*, **35**: 209-213.
- Zhdanov, M.S. and Fang, S., 1996. Quasi-linear approximation in 3-D electromagnetic modeling. *Geophysics*, **61**: 646-665.
- Zhdanov, M.S., Golubev, N.G., Spichak, V.V. and Varentsov, Iv.M., 1982. The construction of effective methods for electromagnetic modelling. *Geophys. J. Roy. Astr. Soc.*, **68**: 589-607.
- Zhdanov, M.S., Varentsov, E.M., Golubev, N.G. and Kriulov, B.A., 1990. Modeling methods for electromagnetic fields. International materials project, COMMENI, Nauka, Moscow.
- Zhou, P.B., 1993. Numerical analysis of electromagnetic fields. Springer-Verlag, 406 pp.

APPENDIX 1

Derivation of Recurrence relation (2.88)

In order to understand the structure of relation (2.83), explicitly write the expressions for reflection functions $R_l(u)$ for $l = N+1$, N and $N-1$ as power series in u

$$R_{N+1}(u) = 0 = \sum_m R_{N+1,m} u^m \quad \text{with} \quad R_{N+1,m} = 0 \quad \forall m.$$

$$R_N(u) = r_N u = \sum_m R_{Nm} u^m \quad \text{with} \quad R_{N1} = r_N \quad \text{and} \quad R_{Nm} = 0 \quad \forall m > 1.$$

$$R_{N-1}(u) = \frac{R_N(u) + r_{N-1} u}{1 + R_N(u) r_{N-1}},$$

$$= u(r_N u + r_{N-1}) (1 + r_{N-1} r_N u)^{-1},$$

$$= r_{N-1} u + r_N (1 - r_{N-1}^2) \sum_{m=0}^{\infty} (-r_{N-1} r_N)^m u^{m+2},$$

$$= \sum_{m=1}^{\infty} R_{N-1,m} u^m$$

$$\text{with } R_{N-1,1} = r_{N-1} \quad \text{and} \quad R_{N-1,m} = r_N r_{N-1}^* (-r_{N-1} r_N)^{m-2} \quad \forall m > 1.$$

$$\text{Here } r_{N-1}^* = (1 - r_{N-1}^2).$$

This implies that the function $R_l(u)$ and $R_{l-1}(u)$, appearing in relation (2.83), can be expressed as

$$R_{l-1}(u) = \sum_m R_{l-1,m} u^m$$

and

$$R_l(u) = \sum R_{l,m} u^m.$$

Using these relations in equation (2.83) and cross-multiplying we get

$$\sum_{m=1}^{\infty} R_{l-1,m} u^m + r_{l-1} \sum_{m=1}^{\infty} R_{l-1,m} u^m \sum_{k=1}^{\infty} R_{l,k} u^k = \sum_{m=1}^{\infty} R_{l,m} u^{m+1} + r_{l-1} u$$

$$\text{or } (R_{l-1,1} - r_{l-1}) u + \sum_{m=2}^{\infty} [R_{l-1,m} - R_{l,m-1} + r_{l-1} \sum_{k=1}^{m-1} R_{l-1,k} R_{l,m-k}] u^m = 0$$

$$\text{or } (R_{l-1,1} - r_{l-1}) u + \sum_{m=2}^{\infty} [R_{l-1,m} - (1 - r_{l-1} R_{l-1,1}) R_{l,m-1} + r_{l-1} \sum_{k=2}^{m-1} R_{l-1,k} R_{l,m-k}] u^m = 0.$$

On equating the coefficients of various powers of u to zero as this relationship is valid for all possible values of u, we get

$$R_{l-1,1} = r_{l-1},$$

$$R_{l-1,2} = (1 - r_{l-1}^2) R_{l,1} = r_{l-1}^2 R_{l,2}$$

$$R_{l-1,m} = r_{l-1}^2 R_{l,m-1} - r_{l-1} \sum_{k=1}^{m-1} R_{l-1,k} R_{l,m-k} \quad m > 1$$

APPENDIX 2

Basic steps of Bi-conjugate gradient method to solve matrix equation $Ax = b$

To solve $Ax = b$

Start with x_0 - an initial estimate of the solution

Residual $r_0 = b - Ax_0$

Bi-residual $\hat{r}_0 = r_0^*$

Initial search vector $p_0 = r_0$

Bi- search vector $\hat{p}_0 = p_0^*$

For iteration $i = 0, 1, 2, \dots$

Step length coefficient

$$\alpha_i = \frac{(\hat{r}_i, r_i)}{(\hat{p}_i, Ap_i)}$$

New estimate $x_{i+1} = x_i + \alpha_i p_i$

New residual $r_{i+1} = r_i - \alpha_i Ap_i$

Bi-residual $\hat{r}_{i+1} = \hat{r}_i - \alpha_i A^H \hat{p}_i$

Bi-conjugacy coefficient

$$\beta_i = \frac{(A^H \hat{p}_i, r_{i+1})}{(\hat{p}_i, Ap_i)}$$

New search vector $p_{i+1} = r_{i+1} + \beta_i p_i$

Bi-search vector $\hat{p}_{i+1} = \hat{r}_{i+1} + \beta_i \hat{p}_i$

and continue until $r_{i+1} = 0$.

In above steps, H indicates Hermitian conjugate, the inner product $(x,y) = x^H y$ and $*$ denotes the complex conjugate.

APPENDIX 3

Documentation on input requirements of the inversion algorithm 'EM2INV'

- Author** : Anupma Rastogi, Department of Earth Sciences,
University of Roorkee, Roorkee - 247 667, India.
- Objective** : 2-D inversion of geoelectromagnetic data.
Different response functions can be inverted, these include
1. Induction vector for GDS
2. Impedance for MT
- Methodology** : Program uses FDM for computation of the response.
For inversion, quasi-linearized approach has been followed and
Bi-Conjugate gradient method is used for solving inverse matrix
equation. Inversion of the response is carried out with the help of the
ridge-regression method.
- Modes** : Program works in two basic modes -
1. Forward response computations for synthetic models
2. Inversion of response for data using
a. response generated from synthetic models
b. field data.
Output is two-dimensional model of resistivity distribution.
- Files** : Total nine files are opened, one for reading control parameters and
input data, six for writing outputs in different formats and remaining
two scratch files for buffer storage. The unit and unit number on which
file is opened, corresponding file name and its status are given below -

Unit & unit number	File name	Status
np1 = 1	FWD.DAT	Output file
np2 = 2	REG.DAT	- do -
np3 = 3	INV.DAT	- do -
np4 = 4	RMS.DAT	- do -
nr = 5	EM.DAT	Input file
nw = 6	EM.OUT	Output file
nu = 7	EM.RES	- do -
no = 8	-	Scratch file
nt = 9	-	- do -

(The unit numbers can be changed according to computer requirements)

- Input data** : to be read from file EM.DAT
Input 1 : nprnt, ninv, nert, nder - control parameters
nprnt = 0 for printing rms error and corrected resistivity values for final
inversion iteration.

- = 1 for printing rms error and corrected resistivity values for each inversion iteration.
- = 2 for printing rms error and corrected resistivity values for each inversion and rms error for each BCGM iteration.
- = 3 for printing detailed inversion results, 1-D solution, grid spacings, computed responses and corrected resistivity values for each inversion iteration.

ninv = -1 for forward computations only
= 0 for forward and inverse computations
= 1 for inversion to be carried out

nerf = 0 for no noise (error free)
= 1 for Gaussian noise

nder = 0 for minimum norm of the solution
= 1 for minimum norm of the first derivative

Input 2 : npol - control for polarization type

npol = 0 for B-polarization
= 1 for E-polarization

Input 3 : ncond - control for parameter type

ncond = 0 for data in conductivity
= 1 for data in resistivity

Input 4 : scale - scaling factor for spacing values

scale < 0 for scaling in terms of host skin depth
= 0 for no scaling
> 0 for scaling in terms of read factor

Input 5 : nper, jfq - number of periods and choice of standard frequency

nper - number of periods/frequencies
jfq - period/frequency for standard grid

Input 6 : (period(i), i=1,nper) - nper periods to be read (nper- cards)

Input 7 : ntype - control parameter for response type

- = 1 for E_x or B_x
- = 2 for E_y or B_y
- = 3 for B_z
- = 4 for ρ_{xy} or ρ_{yx}
- = 5 for Z_{xy} or Z_{yx}
- = 6 for I_{zy}

if (ninv. le. 0) then

Input 8 : nob - number of observation points

nobs < 0 for adding noise only at selected observation points
 = 0 for grid points are observation points
 > 0 for reading observation points and their positions

if (nobs. gt. 0) then

Input 9 : (yobs(i), i=1, nobs) - position of observation points
 (nobs-cards)

End of nobs control

End of ninv control

if (ninv.le.0) then

Read forward model

Input 10 : (cy(i), cz(i), dy(i), dz(i), res(i), i=1,mxsb)

cy - horizontal location of the left edge of each bloc (km)

cz - vertical location of the top corner of each block (km)

dy - horizontal width of each block (km)

dz - vertical depth of each block (km)

res - conductivity/resistivity of block in S/m or ohm-m respectively

5555 - indicates end of rectangular blocks in model or end of data file

if (nert. gt. 0) then

Input 11 : neran - number of observation points at which noise
 to be added

meran = abs(neran)

if (nobs. lt. 0) then

Input 12 : (ierr(i), aerr(i), i=1,meran) - points, % response
 (meran -cards)

ierr - points

aerr - % of response

else

Input 13 : rns - % noise to be added at all points

End of nobs control

End of nert control

End of ninv control

if (ninv. le. 0) then

Read initial guess model

Input 14 : (cy(i), cz(i), dy(i), dz(i), res(i), i = 1,mxsb)

cy - horizontal location of the left edge of each block (km)

cz - vertical location of the top corner of each block (km)

dy - horizontal width of each block (km)

dz - vertical depth of each block (km)

res - conductivity/resistivity of block in S/m or ohm-m respectively

5555 - indicates end of rectangular blocks in model or end of data file

**Input 15 : nind, istry - inversion domain position and counter
for inversion grid**

nind - position of inversion domain in input data
istry - counter for choice of grid for inversion
= 0 for using same grid for inversion
= 1 for using standard grid for inversion

Read iteration and convergence parameters

Input 16 : mnter, mxter, eps, deps, epsd

All parameters needed during inversion

mnter - minimum number of inversion iterations permitted
mxter - maximum number of inversion iterations permitted
eps - convergence threshold value
deps - decrement of eps
epsd - eps difference factor

Input 17 : mni, mxi, epi

All parameters needed during BCGM iterations

mni - minimum number of iterations permitted
mxi - maximum number of iterations permitted
epi - convergence threshold value

Input 18 : ylc, yrc, zuc, zdc

All parameters defining geometry of inversion domain

ylc - horizontal location of left edge
yrc - horizontal location of right edge
zuc - vertical location of top boundary
zdc - vertical location of bottom boundary

Input 19 : romn, romx, aps, daps, mnaps

**Parameters defining resistivity range and Marquardt
parameter**

romn - minimum value of resistivity
romx - maximum value of resistivity
aps - starting value of Marquardt parameter
daps - decrement of Marquardt parameter
mnaps - minimum number of iterations after which decrement starts

End of ninv control

Sample Input and Output Files of the algorithm EM2INV

Input File : EM.DAT

```

1,0,1,0          ! nprnt,ninv,nerf,nder
1                ! npol
1                ! ncond
1000.0          ! scale
1,1             ! nper,mpr
80              ! (period(i), i = 1,nper)
5               ! ntype
31              ! nobs
-204.  -144.  -114.  -99.3  -84.3  -69.30
-58.   -46.7  -35.5  -24.2  -17.1  -13.60
-10.   -6.67  -3.33   0.0   3.33   6.67
10.    13.6   17.1   24.2   35.5   46.7
58.    69.3   84.3   99.3  114.   144.
204.                                ! (yobs(i), i = 1,nobs)
-100   0    200   10   100
-100  20   200   20   100
-100  40   200   60   10
-100  10   90   10   100
10    10   90   10   100
-10   10   20   10   10      ! (cy(i), cz(i), dy(i), dz(i), res(i), i = 1,mxsb)
5555  0    0    0    0      ! indicates end of data
31
.02
-100   0    200    5   100
-100  25   200   15   100
-100  40   200   60   10
-100   5    70   20   100
30     5    70   20   100
-30    5    60   20   40      ! (cy(i), cz(i), dy(i), dz(i), res(i), i = 1,mxsb)
5555  0    0    0    0      ! indicates end of data
6,0
5,20,.001,.25,0  ! nind, istry
1,100,.05        ! mnter,mxter,eps,deps,epsd
-30,30,5,25     ! mni,mxi,epi
10,100,..2,.8,5 ! ylc,ylc,zuc,zdc
                  ! romn,romx,aps,daps,mnaps

```

Output File : EM.OUT

CONTROL PARAMETERS

** output type counter "nprnt" = 1
 ** problem type counter "ninv" = 0
 ** error control counter "nert" = 1
 ** smoothness derivative counter "nder" = 0

E- POLARIZATION, " npol " = 1
 the counter for res./cond. " ncond " = 1
 scaling factor " scale" = 1.00E+03
 no. of time periods " nper" = 1
 time period for std grid "mpr" = 1
 time periods are: 8.00E+01
 ** response type "ntype" = 5
 no. of observation points: 31

* Observation points :

-2.04E+05	-1.44E+05	-1.14E+05	-9.93E+04	-8.43E+04	-6.93E+04
-5.80E+04	-4.67E+04	-3.55E+04	-2.42E+04	-1.71E+04	-1.36E+04
-1.00E+04	-6.67E+03	-3.33E+03	0.00E+00	3.33E+03	6.67E+03
1.00E+04	1.36E+04	1.71E+04	2.42E+04	3.55E+04	4.67E+04
5.80E+04	6.93E+04	8.43E+04	9.93E+04	1.14E+05	1.44E+05
2.04E+05					

FORWARD DATA

* Add Noise in data

no. of obs. points to add noise " neran" = 31
 Noise is to be added at all points
 signal to noise ratio " rns" = 2.00E-02

period = 80.00000000000000 s
 ny 31

ypts	-204.2985139537807	-144.2774263072963	-114.2668824840541
	-99.26161054810237	-84.25633861215060	-69.25106667619883
	-57.99711272423501	-46.74315877227119	-35.48920482030736
	-24.23525086834354	-17.11762543417177	-13.55881271708589
	-10.000000000000000	-6.66666746139526	-3.333333492279053
	-2.3841857910156250E-07	3.333333015441895	6.66666269302368
	10.000000000000000	13.55881271708589	17.11762543417177
	24.23525086834354	35.48920482030736	46.74315877227119
	57.99711272423501	69.25106667619883	84.25633861215060
	99.26161054810237	114.2668824840541	144.2774263072963
	204.2985139537807		

nz 14

zpts	0.000000000000000E+00	3.333333253860474	6.66666507720947
	10.000000000000000	13.33333325386047	16.6666650772095
	20.000000000000000	23.33333325386047	26.6666650772095
	29.9999976158142	33.33333301544189	36.6666626930237
	40.000000000000000	43.55881271708589	

Grid size : ny,nz 49 18
Inversion domain block co-ordinates
jbl,jbr = 13 37
kbu,kbd = 4 13

iter = 15 rmisp = 3.3259E-02 rms = 3.5801E-02 aps =2.6844E-02
convergence not achieved after 15 iterations

Output File : EM.RES

```

-----
" EM2INV" run on Mon Dec 9 07:33:35
-----

```

```

1,0,1,0      ! nprnt,ninv,nert,nder
1            ! npol
1            ! ncond
1000.0       ! scale
1,1         ! nper,mpr
80          ! (period(i),i=1,nper)
5           ! ntype
31          ! nobs
-204. -144. -114. -99.3 -84.3 -69.30
-58.  -46.7 -35.5 -24.20 -17.1 -13.60
-10.  -6.67 -3.33  0.0   3.33  6.67
 10.  13.6  17.1  24.2  35.5  46.7
 58.  69.3  84.3  99.3 114.0 144.
204.        ! (yobs(i), i=1,nobs)
-100      0  200  10  100
-100     20  200  20  100
-100     40  200  60  10
-100     10  90  10  100
 10      10  90  10  100
-10      10  20  10  10
 5555    0   0   0   0
31        ! (cy(i), cz(i), dy(i), dz(i), res(i), i = 1,mxsb)
          ! indicates end of data
.02
-100     0  200   5  100
-100    25  200  15  100
-100    40  200  60  10
-100     5  70  20  100
 30      5  70  20  100
-30      5  60  20  40
5555     0   0   0   0
          ! (cy(i), cz(i), dy(i), dz(i), res(i), i = 1,mxsb)
          ! indicates end of data
6,0        ! nind, istdr
5,20,.001,.25,0 ! mnter,mxter,eps,deps,epsd
1,100,.05   ! mni,mxi,epi
-30,30,5,25 ! ylc,ylc,zuc,zdc
10,100,..2,.8,5 ! romn,romx,aps,daps,mnaps

```

```

Forward response for standard period      1  80.00000000000000
Grid size,nobs      31      14      31

```

Appendices

Zxy-observed

1.88E-03	2.66E-03	1.88E-03	2.66E-03	1.87E-03	2.66E-03
1.86E-03	2.65E-03	1.84E-03	2.64E-03	1.82E-03	2.63E-03
1.80E-03	2.60E-03	1.76E-03	2.55E-03	1.72E-03	2.45E-03
1.65E-03	2.26E-03	1.60E-03	2.06E-03	1.57E-03	1.95E-03
1.54E-03	1.83E-03	1.51E-03	1.74E-03	1.49E-03	1.68E-03
1.45E-03	1.67E-03	1.49E-03	1.68E-03	1.51E-03	1.74E-03
1.54E-03	1.83E-03	1.57E-03	1.95E-03	1.60E-03	2.06E-03
1.65E-03	2.26E-03	1.72E-03	2.45E-03	1.76E-03	2.55E-03
1.80E-03	2.60E-03	1.82E-03	2.63E-03	1.84E-03	2.64E-03
1.86E-03	2.65E-03	1.87E-03	2.66E-03	1.88E-03	2.66E-03
1.88E-03	2.66E-03				

** the error added synthetic anomaly

1.87E-03	2.65E-03	1.83E-03	2.59E-03	1.81E-03	2.58E-03
1.85E-03	2.64E-03	1.85E-03	2.66E-03	1.81E-03	2.61E-03
1.80E-03	2.60E-03	1.75E-03	2.53E-03	1.74E-03	2.48E-03
1.62E-03	2.22E-03	1.62E-03	2.09E-03	1.59E-03	1.97E-03
1.52E-03	1.81E-03	1.46E-03	1.68E-03	1.45E-03	1.64E-03
1.46E-03	1.68E-03	1.46E-03	1.64E-03	1.47E-03	1.69E-03
1.55E-03	1.84E-03	1.58E-03	1.96E-03	1.56E-03	2.02E-03
1.70E-03	2.32E-03	1.68E-03	2.39E-03	1.79E-03	2.59E-03
1.83E-03	2.65E-03	1.77E-03	2.56E-03	1.79E-03	2.57E-03
1.86E-03	2.65E-03	1.92E-03	2.73E-03	1.91E-03	2.70E-03
1.80E-03	2.54E-03				

Computed response for standard period 1 80.0000000000000000
 Grid size,nobs 31 9 31

Zxy-computed

1.89E-03	2.66E-03	1.88E-03	2.65E-03	1.87E-03	2.65E-03
1.86E-03	2.64E-03	1.85E-03	2.62E-03	1.83E-03	2.59E-03
1.81E-03	2.54E-03	1.79E-03	2.45E-03	1.77E-03	2.27E-03
1.75E-03	2.00E-03	1.73E-03	1.90E-03	1.72E-03	1.87E-03
1.71E-03	1.85E-03	1.71E-03	1.84E-03	1.71E-03	1.83E-03
1.71E-03	1.82E-03	1.71E-03	1.83E-03	1.71E-03	1.84E-03
1.71E-03	1.85E-03	1.72E-03	1.87E-03	1.73E-03	1.90E-03
1.75E-03	2.00E-03	1.77E-03	2.27E-03	1.79E-03	2.45E-03
1.81E-03	2.54E-03	1.83E-03	2.59E-03	1.85E-03	2.62E-03
1.86E-03	2.64E-03	1.87E-03	2.65E-03	1.88E-03	2.65E-03
1.89E-03	2.66E-03				

rho (initial guess)

4.00E+01	4.00E+01	4.00E+01	4.00E+01	4.00E+01	4.00E+01
4.00E+01	4.00E+01	4.00E+01	4.00E+01	4.00E+01	4.00E+01
4.00E+01	4.00E+01	4.00E+01	4.00E+01	4.00E+01	4.00E+01
4.00E+01	4.00E+01	4.00E+01	4.00E+01	4.00E+01	4.00E+01
44444444					
44444444					
44444444					
cginv : itr,rmsp,rms :	1	5.51E-15	1.54E-18		
Grid size,nobs	49	9	31		

```

iter = 2  rmsp = 7.2930E-02  rms = 6.9519E-02  aps =2.0000E-01

rhocorr
 3.96E+01  3.94E+01  3.90E+01  3.82E+01  3.77E+01  3.82E+01
 3.86E+01  3.92E+01  3.95E+01  3.92E+01  3.89E+01  3.82E+01
 3.79E+01  3.84E+01  3.87E+01  3.91E+01  3.95E+01  3.93E+01
 3.90E+01  3.86E+01  3.84E+01  3.87E+01  3.89E+01  3.92E+01
44433334
44433334
44433344
cginv : itr,rmsp,rms : 1  3.61E-15  2.50E-18

iter = 14  rmsp = 3.5697E-02  rms = 3.3259E-02  aps =3.3554E-02
rhocorr
 7.17E+01  7.42E+01  6.44E+01  4.22E+01  3.57E+01  5.70E+01
 7.47E+01  7.60E+01  5.09E+01  4.83E+01  3.88E+01  2.26E+01
 1.95E+01  3.47E+01  4.69E+01  5.17E+01  3.78E+01  3.32E+01
 2.55E+01  1.29E+01  1.13E+01  2.28E+01  3.14E+01  3.72E+01
67643577
54322345
33211233
cginv : itr,rmsp,rms : 1  6.34E-16  5.80E-17

iter = 15  rmsp = 3.3259E-02  rms = 3.5801E-02  aps =2.6844E-02
convergence not achieved in inversion after iter. 15
rms error = 0.4815938863325104

total time taken :
real time = 5.85E+02
user time = 1.36E+10
sys time = 0.00E+00

```

Output File : FWD.DAT

Forward Anomaly for standard time period : 80.00

y-distance (km)	real comp	imag comp
-2.0400E+02	1.8726E-03	2.6474E-03
-1.4400E+02	1.8318E-03	2.5939E-03
-1.1400E+02	1.8138E-03	2.5807E-03
-9.9300E+01	1.8460E-03	2.6356E-03
-8.4300E+01	1.8512E-03	2.6552E-03
-6.9300E+01	1.8099E-03	2.6096E-03
-5.8000E+01	1.7992E-03	2.6017E-03
-4.6700E+01	1.7548E-03	2.5343E-03
-3.5500E+01	1.7398E-03	2.4798E-03
-2.4200E+01	1.6225E-03	2.2170E-03
-1.7100E+01	1.6213E-03	2.0910E-03
-1.3600E+01	1.5882E-03	1.9713E-03
-1.0000E+01	1.5203E-03	1.8087E-03
-6.6700E+00	1.4594E-03	1.6801E-03
-3.3300E+00	1.4531E-03	1.6368E-03
0.0000E+00	1.4648E-03	1.6774E-03
3.3300E+00	1.4564E-03	1.6404E-03
6.6700E+00	1.4700E-03	1.6923E-03
1.0000E+01	1.5467E-03	1.8402E-03
1.3600E+01	1.5809E-03	1.9622E-03
1.7100E+01	1.5638E-03	2.0168E-03
2.4200E+01	1.6987E-03	2.3211E-03
3.5500E+01	1.6781E-03	2.3920E-03
4.6700E+01	1.7912E-03	2.5868E-03
5.8000E+01	1.8324E-03	2.6496E-03
6.9300E+01	1.7737E-03	2.5575E-03
8.4300E+01	1.7930E-03	2.5717E-03
9.9300E+01	1.8571E-03	2.6514E-03
1.1400E+02	1.9170E-03	2.7276E-03
1.4400E+02	1.9054E-03	2.6981E-03
2.0400E+02	1.7979E-03	2.5418E-03

Output File : REG.DAT

y- coordinate	z- coordinate	obtained resistivity
-3.0000E+01	5.0000E+00	7.1680E+01
-2.6450E+01	8.3500E+00	7.1680E+01
-3.0000E+01	1.5000E+01	5.0919E+01
-2.6450E+01	1.5000E+01	5.0919E+01
-3.0000E+01	2.1650E+01	3.7824E+01
-2.6450E+01	2.1650E+01	3.7824E+01
-2.6450E+01	2.5000E+01	3.7824E+01
-1.9350E+01	5.0000E+00	7.4247E+01
-1.9350E+01	8.3500E+00	7.4247E+01
-1.9350E+01	1.5000E+01	4.8289E+01
-1.9350E+01	2.1650E+01	3.3250E+01
-1.9350E+01	2.5000E+01	3.3250E+01
-1.2225E+01	5.0000E+00	6.4409E+01
-1.2225E+01	8.3500E+00	6.4409E+01
-1.2225E+01	1.5000E+01	3.8754E+01
-1.2225E+01	2.1650E+01	2.5461E+01
-1.2225E+01	2.5000E+01	2.5461E+01
-4.3250E+00	5.0000E+00	4.2159E+01
-4.3250E+00	8.3500E+00	4.2159E+01
-4.3250E+00	1.5000E+01	2.2647E+01
-4.3250E+00	2.1650E+01	1.2924E+01
-4.3250E+00	2.5000E+01	1.2924E+01
4.3250E+00	5.0000E+00	3.5740E+01
4.3250E+00	8.3500E+00	3.5740E+01
4.3250E+00	1.5000E+01	1.9508E+01
4.3250E+00	2.1650E+01	1.1274E+01
4.3250E+00	2.5000E+01	1.1274E+01
1.2225E+01	5.0000E+00	5.7039E+01
1.2225E+01	8.3500E+00	5.7039E+01
1.2225E+01	1.5000E+01	3.4688E+01
1.2225E+01	2.1650E+01	2.2802E+01
1.2225E+01	2.5000E+01	2.2802E+01
1.9350E+01	5.0000E+00	7.4724E+01
1.9350E+01	8.3500E+00	7.4724E+01
1.9350E+01	1.5000E+01	4.6943E+01
1.9350E+01	2.1650E+01	3.1446E+01
1.9350E+01	2.5000E+01	3.1446E+01
2.6450E+01	5.0000E+00	7.5981E+01
2.6450E+01	8.3500E+00	7.5981E+01
3.0000E+01	8.3500E+00	7.5981E+01
2.6450E+01	1.5000E+01	5.1701E+01
3.0000E+01	1.5000E+01	5.1701E+01
2.6450E+01	2.1650E+01	3.7231E+01
3.0000E+01	2.5000E+01	3.7231E+01

Output File : INV.DAT

Inverted model response for standard time period: 80.00

y-distance (km)	real comp	imag comp
-2.0400E+02	1.8795E-03	2.6596E-03
-1.4400E+02	1.8702E-03	2.6563E-03
-1.1400E+02	1.8589E-03	2.6541E-03
-9.9300E+01	1.8482E-03	2.6495E-03
-8.4300E+01	1.8310E-03	2.6383E-03
-6.9300E+01	1.8028E-03	2.6110E-03
-5.8000E+01	1.7711E-03	2.5676E-03
-4.6700E+01	1.7287E-03	2.4863E-03
-3.5500E+01	1.6770E-03	2.3426E-03
-2.4200E+01	1.6126E-03	2.1145E-03
-1.7100E+01	1.5656E-03	1.9700E-03
-1.3600E+01	1.5430E-03	1.8990E-03
-1.0000E+01	1.5219E-03	1.8294E-03
-6.6700E+00	1.5056E-03	1.7736E-03
-3.3300E+00	1.4936E-03	1.7329E-03
0.0000E+00	1.4877E-03	1.7112E-03
3.3300E+00	1.4895E-03	1.7145E-03
6.6700E+00	1.4984E-03	1.7433E-03
1.0000E+01	1.5127E-03	1.7939E-03
1.3600E+01	1.5327E-03	1.8638E-03
1.7100E+01	1.5549E-03	1.9396E-03
2.4200E+01	1.6019E-03	2.0962E-03
3.5500E+01	1.6688E-03	2.3328E-03
4.6700E+01	1.7230E-03	2.4806E-03
5.8000E+01	1.7673E-03	2.5646E-03
6.9300E+01	1.8002E-03	2.6095E-03
8.4300E+01	1.8296E-03	2.6378E-03
9.9300E+01	1.8474E-03	2.6494E-03
1.1400E+02	1.8584E-03	2.6541E-03
1.4400E+02	1.8701E-03	2.6564E-03
2.0400E+02	1.8795E-03	2.6597E-03

Output File : INV.DAT

Iteration no.	rms Error
1	7.2930E-02
2	6.9519E-02
3	6.7514E-02
4	6.2151E-02
5	6.1340E-02
6	6.0649E-02
7	5.9659E-02
8	5.8109E-02
9	5.5620E-02
10	5.1918E-02
11	4.6756E-02
12	4.0361E-02
13	3.5697E-02
14	3.3259E-02

